Flow behaviour and foaming of recycled polyolefins and nanocomposites

IPTME

Loughborough University

Flow Behaviour and Foaming of Recycled Polyolefins and Nanocomposites

by

Luís M. C. Conceição

A Doctoral thesis submitted in partial fulfilment of the requirements for the award of the degree of Doctor of Philosophy of Loughborough University

April 2007

Institute of Polymer Technology and Materials Engineering

Abstract

The flow behaviour of post-consumer recycled polyolefins, their blends and layered-silicate nanocomposites was studied by capillary rheometry and free-surface melt state elongational measurements to assess suitability for foaming applications. A novel extrusion foaming technique and a flow simulation model were developed to attempt to correlate flow and foaming behaviour. The recycled polyolefins were high-density polyethylene (HDPE), low-density polyethylene (LDPE) and polypropylene (PP) of high-molecular weight, suitable for extrusion; that also contained also paper and inorganic fillers. LDPE-PP and HDPE-PP blends were prepared in a batch mixer with and without compatibilising agents, ethylene-propylene rubber (EPR) and ethylene-propylene (EP) copolymer. Several mixing conditions (temperature, time, rotor speed) were used to modify the morphology and the flow behaviour of the blend systems. In shear flow diverse pseudoplastic index, zero shear rate viscosity and the extensional viscosities, whilst, in uniaxial extensional flow the effects of process conditions on strain energy density, elongation at break and melt modulus were detected. The melt strength of uncompatibilised LDPE-rich systems is generally higher. The use of small quantities of EPR, 2.5 and 5.0% (w/w) can further improve the rheological properties in uniaxial extension, but shear flow behaviour is virtually unchanged by the compatibilisers. EP didn't improve the extensional flow behaviour of HDPE-PP blends.

The influence of processing conditions and composition on the preparation of melt intercalated HDPE and HDPE-PP layered-silicate nanocomposites was conducted as a way of enhancing foaming behaviour; montmorillonite particles were dispersed with the aid of a compatibilising agent. Ideal mixing conditions (temperature, rotor speed and time) were determined for these nanocomposites based on rheological measurements. In HDPE nanocomposites, the melt elongation at break is reduced and the tensile modulus increased. The clay content has a significant influence on the melt tensile modulus. Wall slip behaviour appeared enhanced comparatively to

unmodified HDPE. In HDPE-PP nanocomposite blends it is possible to modify the melt tensile modulus and elongation by changing blend composition and clay dispersion morphologies.

A finite element model of capillary die flow was developed using commercial simulation software to assist the interpretation of an extrusion foaming technique. Experiments were carried out using azodicarbonamide as a blowing agent and a capillary rheometer and extruding the materials through a capillary die. Extruding at a shear rate of $300s^{-1}$ and at a temperature close to the melting point yielded the lowest foam densities; LDPE, the material with the highest melt strength and extensibility, achieved a density of 430 kg m^{-3}. Blends of HDPE-PP, LDPE-PP and HDPE-PP nanocomposites didn't show an improved foaming behaviour with densities always above 600 kg m^{-3}. Densities of 360kg m^{-3} and 500 kg m^{-3} were obtained with HDPE nanocomposites and unmodified HDPE, respectively.

Table of Contents

Acknowledgements

I would like to express my gratitude to several people that have been very important during this research.

First of all, I would like to thank my supervisor, Mr. Barry Haworth for all his support, suggestions, guidance and encouragement throughout this research period.

I would also like to thank Mr. Paul Vickers and Dr. Soran Birosca for their friendship, help, support, understanding and for all the cheerful moments.

I also wish to thank to Mr. A. J. Woolley for his invaluable help and dedication, and members of the technical staff and friends at IPTME for their support and co-operation during the course of this research.

Finally, I owe my thanks to my family and friends whose love, encouragement, patience and help made my days sunnier and cheerful.

List of Tables

List of Figures

List of Abbreviations and Symbols

ASTM	American standard test method
CBA	Chemical blowing agent
DSC	Differential Scanning Calorimetry
FTIR	Fourier transform infrared
GPC	Gel permeation Chromatography
HDPE	High-density polyethylene
LCB	Long-chain branching
LDPE	Low-density polyethylene
LLDPE	Linear low-density polyethylene
MWD	Molecular weight distribution
OIT	Oxidation induction test
PE	Polyethylene
PP	Polypropylene
PR	Reclaimed plastic
PRL	Plastics Reclamation Limited
SCB	Short-chain branching
MFR	Melt flow rate
MS	Melt strength
TGA	Thermogravimetric analysis
SEM	Scanning electron microscopy
TEM	Transmission electron microscopy
L/D	Length to diameter ratio
PTFE	Polyethylene terphtalate
σ_E	Extensional stress
ε_H	Hencky strain rate
ΔH_f^0	Heat of fusion of 100% crystalline polyethylene
η	viscosity
η_0	Zero shear rate viscosity
% RSD	% Relative Standard Deviation

1 Introduction

1.1 General Background

Plastics have become increasingly important to human society in the last few decades due to their cost and range of properties making them serious competitors to more traditional materials such as wood, glass or metals. They are so widespread that it is not difficult to find examples of their use in the automotive industry, packaging, electrical appliances and many other applications. They derive primarily from oil, which is a non-renewable resource that will get scarce in the future. Even though plastics production only uses about 4% of the total amount of oil produced worldwide annually, the continuous technological development of these materials and the growth of the markets, is leading to a higher demand. Plastic consumption has been rising steadily and is expected to grow by 70% in total until 2010,[1] as shown in Figure 1-1.

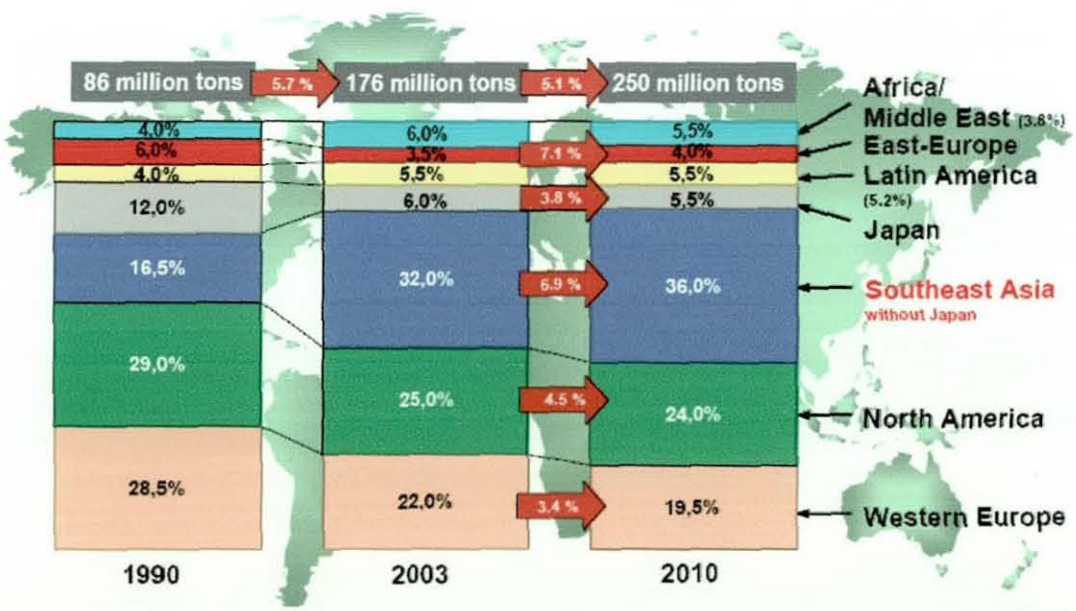

Figure 1-1 – Worldwide plastics consumption until 2003 and prediction until 2010.[1]

Although many types of plastics exist, in 2000, 68% of all plastics consumption was made up of five sorts of so called 'commodity'

thermoplastics: polyethylene (LDPE, LLDPE, HDPE); polypropylene (PP); polyvinyl chloride (PVC); polystyrene (PS and EPS) and polyethylene terphtalate (PET).[2]

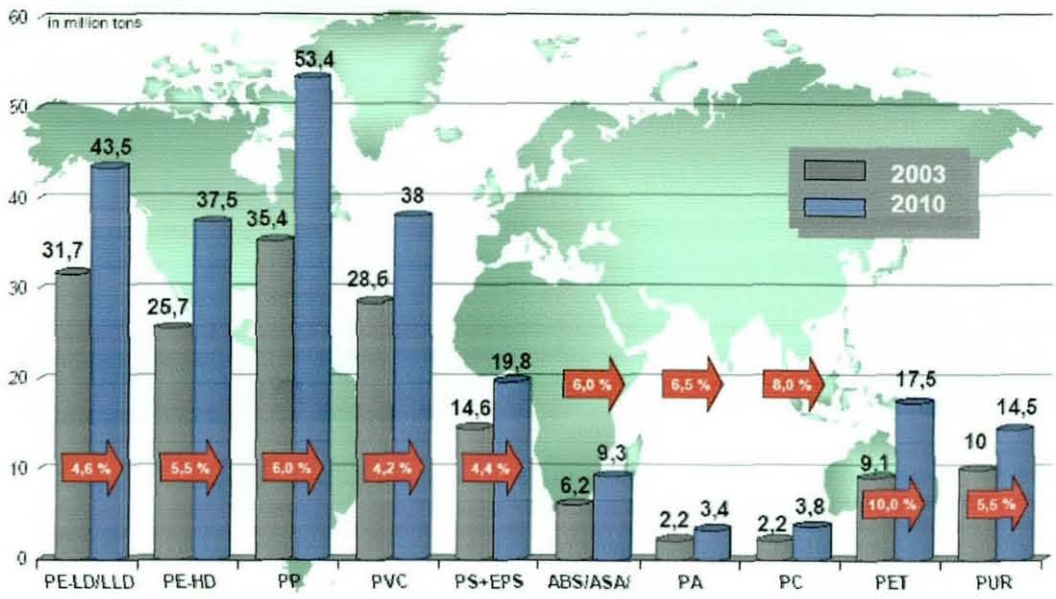

Figure 1-2 – Prediction of worldwide plastic consumption by polymer.[1]

One of the problems related to plastic consumption is their disposal and waste management. As we use more and more plastics in our lives an equivalent quantity is to be thrown away after their service life, and for some applications like packaging this lifetime is often very short. The past and current trend has usually been to landfill the plastic waste but it has been identified that this contributes 40% to the total volume of waste.[3] This creates pressure to reduce the quantity of land filled waste due to the high costs involved in building more of those sites, therefore, plastic land filling is seen less as an option. An additional environmental problem arises from the chemically stability and difficult degradation of these materials way past its normal service-use life.

In this context, recycling is obviously one answer that can satisfy both the need for increased plastic consumption and a volume reduction of plastics in the landfill sites.

There are several methods that can lead to a new use of waste plastic,[3,4] namely:

- Mechanical recycling
- Chemical recycling
- Energy recovery

Each of them has potential advantages and disadvantages. With the energy recovery method where the plastic is used as a fuel; no new use is given to the plastics and the only benefit is the energy generated. However, this can be done without any sorting, whereas with chemical recycling and mechanical recycling new products can be made. Chemical recycling involves the recovery of the monomer and tends to be more expensive than mechanical recycling but yields high quality polymers. In mechanical recycling the main option is melt reprocessing. This method usually requires prior separation, washing of the waste plastic, shredding and regeneration of polymer granules by melt compounding the flakes. The sorting and cleaning of the plastic waste is important in this method because contamination by paper fibres or other polymers can lead to inferior material properties. Recycled polymers tend to have weaker properties compared to virgin equivalents due to degradation suffered over their service life. Plastics can be separated by their chemical nature, but colour separation is not cost effective which usually leads to colour variation in batches of recycled material, which limits their future applications. Therefore applications are constantly being considered where weaker properties and colour are not so important.

Thermoplastics are a large portion of the plastic waste stream and can be mechanically recycled. One application where these materials can be used is structural foam cores for composite-based applications, because when the colour of the core sandwiched is not important and the mechanical properties are not always crucial. Being lightweight can be another important advantage as some foams have better functional properties that their bulk counterparts.

Being used in an added value product, the costs of recycling may not be prohibitively high and will be competitive with virgin resins.

Polymeric foams have been know to possess attractive properties such as low density, superior thermal insulation, excellent stiffness/weight ratio and absorption of sound, vibration and shock,[5] therefore the potential uses of such sandwich panels is wide, and could include truck panels and bodies, staging/decking, portable flooring, scaffold decks, bus floors or pallets/crates, etc.

However, to achieve this will require identification of recycled resins and/or blends with the required foamability, to produce foams with the adequate cellular structure, density, and properties for a particular application.

1.2 Specific Background

The main technical problems of plastics recycling are the potential degradation of the polymers and the lack of consistency of the raw materials.[3] Degraded polymers usually have inferior properties compared to virgin resins. They often need re-stabilisation or have their properties upgraded by blending in new resins, combining with a reinforcing phase (e.g. fillers) or incorporation of lost additives to have their service life extended. Due to the current plastic waste collection systems, sorting of mixed plastics is essential, leading unavoidably to cross-contamination of the recycled resins, so that direct use of mixed plastic would be preferable. However, as most polymers are incompatible the sortation phase is almost essential.[6]

The most common method for foaming polyolefins is the expansion method[5, 7,8] that is based upon the expansion of a gaseous phase dispersed throughout the polymer melt. The gaseous phase may be generated by separation of a dissolved gas from a volatile liquid, or by release from a chemical reaction. This expansion comprises three major steps: nucleation,

bubble growth and stabilization.[9] Foaming polyolefins is a more recent achievement compared to resins like polystyrene or polyurethane,[10] this is attributed to a narrow processing window and in linear polymers to the absence of strain-hardening behaviour under extension.[7] To enhance the polyolefins foamability it is necessary to increase their melt strength, that can be enhanced by branching, crosslinking, control of molecular weight and molecular weight distribution, blending of polymers and compatibilisation, and foaming temperature reduction.[11]

Foaming of polyolefin blends could be a way of developing foams with new properties comparatively to what has been done with non-foamed blends, and also it is expected that blending would help foaming by creating heterogeneous interfaces that lower the activation energy for bubble nucleation and lowering the crystallinity.[12] Some researchers[12, 13] have foamed blends and have pointed out that non-uniform structures may arise due to different melting points and gas solubilities, but in the successful cases some properties were better than in the non-foamed blend.[12] Blending may therefore be at the same time a solution to improve the recyclate resins foamability and ease the problem of batch inconsistency. Additionally, the use of mixed plastics will reduce sortation costs. Interestingly, it has been reported by Miller et al.[14] that a traditionally immiscible blend of HDPE/LDPE made from recycled plastics were found to be miscible, against all expectations.

Upgrading recycled polyethylene by incorporating modified nanoclays has been attempted with good results by Puttarudraiah et al.,[15] and furthermore Okamoto et al.[16] have shown that the incorporation of nanoclays in polypropylene may yield a strain-hardening effect. Nam et al.[17] have also produced intercalated PP nanocomposite foams in a batch process, while Zeng et al.[18] produced intercalated and exfoliated PS nanocomposite foams, but these are exceptions in a field largely unexplored. In this context it will be worthwhile to investigate the foaming behaviour of recycled polyolefins with possible applications in structural lightweight panels, with particular emphasis

in blends and using nanofillers, as the technology of reinforced skin (Twintex®) is already developed and therefore core research is required.

1.3 Objectives

The specific objectives of this research will be to:

- Characterize post consumer municipal waste polymers, namely, high-density polyethylene (HDPE), low-density polyethylene (LDPE) and polypropylene (PP), by Fourier Transform Infrared (FTIR), Differential Scanning Calorimetry (DSC), Gel Permeation Chromatography (GPC), and microscopy and to determine relevant fillers and/or inorganic content.
- Compare recycled materials to near-equivalent, virgin plastics, in terms of flow properties.
- Characterize chemical blowing agents using TGA and DSC.
- Prepare HDPE/PP and LDPE/PP blends by appropriate batch mixing.
- Investigate the rheological properties of recycled polyolefins, HDPE, LDPE, PP and blends of HDPE/PP, LDPE/PP, compatibilised and non-compatibilised, in shear and extensional flow, by means of capillary rheometry and a free-surface elongational uniaxial rheometer.
- Prepare and characterize polymer-clay nanocomposites by melt intercalation of commercially available clays with the recyclate polymers and two selected blend compositions with an internal mixer, and study their shear and extensional rheology.
- Produce foams of the recycled polymers, blends and nanofilled polymers by foam extrusion with chemical blowing agents.
- Use of computer aided design software, Flow 2000, to optimise foaming/processing conditions for achieving low-density foams.

2 Literature Review

2.1 Polyolefins, Blends and Nanocomposites

2.1.1 Polyolefins

Polyolefins are defined as polymers derived from olefins, of these, polyethylene and polypropylene are resins produced by a free radical polymerisation process that was first discovered at ICI in 1933.[19] Ethylene was polymerized at high pressure and temperature producing low density polyethylene. Developments in the catalyst technology gave birth to the Ziegler-Nata and chromium oxide type catalysts that allowed stereoregularity control and led to the production of linear polyethylenes, whilst more recently the discovery of metallocene or single site catalyst technology enabled a better control over the molecular weight distribution. With an adequate choice of catalyst and reactor conditions numerous polyolefins can be obtained with variations in density, branching content or molecular weight distribution. Density is generally a reflection of polyolefin linearity. The higher the density, the higher the following polymer characteristics and performance properties: (1) chain linearity, (2) stiffness, (3) tensile strength, (4) tear strength, (5) softening temperature and (6) brittleness. On the other hand, polyolefin failure properties such as impact strength, flexural strength and environmental stress crack resistance (ESRC) decrease as the polyolefin density increases.

Polyethylene is produced by polymerisation of ethylene monomer creating a long backbone with the formula $C_{2n}H_{4n+2}$ where n is the degree of polymerisation, i.e., the number of ethylene monomers polymerised to form the chain. Polyethylenes can be divided into several classes depending on density and relative content of long and short-chain branching, such as into high density, medium density, low density and linear low density polyethylene. The degree and type of chain branching strongly influences the molecular weight distribution, degree of crystallinity, lamellar

morphology, density and rheology of the polyethylenes. High-density polyethylene (HDPE) can be produced by two distinct low-pressure polymerisation methods, using either the Phillips or Ziegler catalysts. The Phillips-type catalysts (chromium oxide-based) produce medium-to-broad molecular weight distribution (MWD) resins while the Ziegler produces a much narrower MWD. HDPE consists mainly of unbranched molecules, with a low level of defects to hinder organization, allowing a high degree of crystallinity, resulting in resins of high densities ranging between 0.94-0.97 and a melting temperature of 130-135°C. LDPE is produced under high pressure (87-276 MPa) and high temperature (405-605 K) with a free radical initiator (such as peroxides and oxygen) and contains some long chain branches (LCB), which could be as long as the backbone and some short chain branches (SCB). It is produced either by a tubular or a stirred autoclave reactor. The autoclave process can produce LDPE resins having a wide range of MWD and less LCB in comparison with a tubular reactor. Long chain branching has a strong influence on MWD, and hence on resin properties such as processability, melt strength, and film optical properties. SCB's disrupt chain packing and are principally responsible for lowering the melting temperature and crystallinity of hydrocarbon polymers. LDPE is commercially available in a wide variety of molecular weight, MWD, SCB and LCB contents, and density ranges.

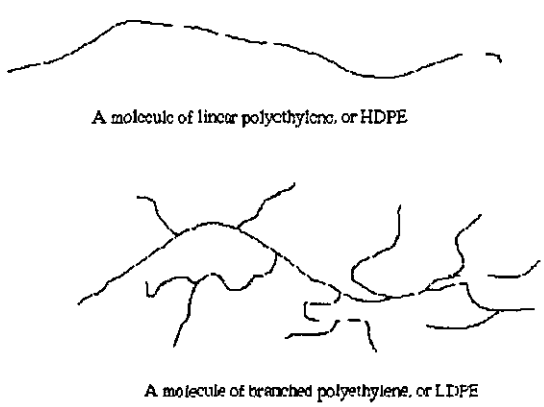

Figure 2-1 - Schematic molecular architecture of polyethylenes.[19]

Polypropylene (PP) is produced under carefully controlled heat and pressure by polymerising propylene in presence of a catalyst. The reaction can be controlled so that the orientation of the pendent methyl group attached to every other carbon are either on the same side, alternating sides or random sides of the molecule; according to this stereoregularity polypropylene is classified as atactic, isotactic and syndiotactic, respectively as shown in Figure 2-2.[20]

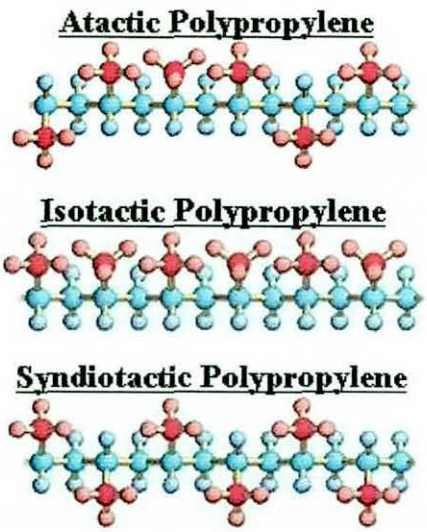

Figure 2-2 – Stereoregularity in polypropylene.

These segments are controlled by the type of catalyst and polymerization conditions, allowing manufacturers to tailor the properties of the resin. Most polymers are predominantly isotactic with small amount of atactic polymer. Isotactic polypropylene is commercially more desirable because its higher crystallinity gives increased stiffness, yield stress, flexural strength, as well as a higher melting point. Lower crystallinities are a consequence of higher molecular weight impairing the material with improved toughness, impact strength and less brittleness.[21, 22] Produced in different forms, polypropylene can be constituted only by propylene monomer or alternatively, as copolymers. Polypropylene copolymers contain one or more different types of monomers in the polymer chain. There are three types of polypropylene copolymer commonly used: (1) originally rubber, but now more typically ethylene-propylene or ethylene-propylene-diene rubber blends are used. (2) Random copolymers are produced by addition of a second monomer to

polymerisation process. (3) Block copolymers are created by sequential polymerisation of ethene and propene. The weight average molecular weight for PP generally ranges from 220,000-700,000 g/mol, with melt flow indices from less than 0.3 g/10 min. to over 1000 g/10 min. Major applications include containers and closures, fibber, cast and biaxially oriented film.[21, 23]

2.1.2 Recycled Polymers

One of the main disadvantages of using recycled polymers arises from the degradation undergone both during processing and in their service life, and due to contamination by foreign materials such as paper, metal fragments, glass and incompatible polymers, which can have a very negative impact on the performance of the new products.[24, 25] The degradation of plastics can result in structural inhomogeneties like increased unsaturation, oxidation and changes in molecular weight, despite enhanced protection from additives incorporated in the resins formulations.[24] Oxygenated structures may arise particularly due to thermal and photochemical aging, precussed by free-radicals such as peroxyls or alkoxyls, for instance. Other common recycled resin contaminants are residues of polymerisation catalysts, printing inks and pigments, residues of adhesives or even residues of fatty and oil materials. Some of the contaminants due to their catalytic or photosensitizing effects further enhance degradation reducing the stability of aged plastics. Polyolefins representing the largest constituent in municipal waste stream also suffer from these problems. In Germany, more than 60% of the household packaging consists of polyolefins, being a fraction composed mainly from HDPE bottles and LDPE film.[3] In the following sections a more detailed description of some polyolefins, namely HDPE, LDPE, LLDPE and PP, and their contaminants can be found. The most recognizable post-consumer plastic container after PET bottles is HDPE milk, juice and other household bottles, which are potentially a very consistent and highly homogeneous recycled plastic stream. Furthermore, their high consumption volume guarantees large quantities of HDPE homopolymer available for recycling. Additionally, detergent and shampoo bottles, which are made from

HDPE copolymer, are also collected and recycled in large quantities. HDPE derived from dairy and juice containers is designed for blow moulding and accordingly it has a high molecular weight, but is also tightly specified exhibiting a consistent melt flow index (MFI) and density. These dairy plastics do not suffer appreciable degradation having essentially the same rheological properties as the virgin resin.[26] Recycled HDPE contamination arises not only from other polymers such as PET and PP, but also paper and the contents of the packaging. PP contamination in HDPE comes from both injection moulded closures, as well as mistaken bottles similar to PE at collection and sorting points. Due to the low compatibility of PP and HDPE, levels of PP above 5% can lead to segregation during crystallization.[3] Furthermore, the addition of a few percent of PP to HDPE can lower its low-temperature impact strength. HDPE post-consumer milk bottles can have an unpleasant odour due to the presence of butyric acid, which can lower the tensile strength and mechanical properties due to internal plasticization/lubrication effect.[3] Highly degraded polymer, known as black spec, originating from melt reprocessing due to excess processing time, and pigments from coloured caps are also frequent. Recycled HDPE copolymer can also be contaminated with ethylene-butene copolymers used in the manufacture of detergent and household industrial chemical bottles.

LDPE recycling originates mainly from post-industrial scrap and there is only a limited proportion of recycled LDPE that can be regarded as post-consumer recyclate. A significant source of LDPE comes from pallet stretch wrap. Soil contamination can be as high as 30-40%. Furthermore, the soil can contain up to 3% iron, which is a PE prodegradant. It has been discovered that organochlorine pesticide residues can deactivate hindered amine light stabilisers. This deactivation is believed to occur as a result of hydrolysis of the pesticides to acidic species, which then react with the HALS additives. During in-service use, LDPE films can become badly degraded and form low MW oxygenated products. These low MW impurities can lead to embrittlement of the recycled polymer since low MW oxidized fractions are segregated from the melt during crystallization and concentrate at the spherulite boundaries. The majority of reclaimed PP derives from automotive

applications such as battery cases, car bumpers and dash boards, PP sacks, bottles strapping and industrial film scrap of biaxially oriented PP are other sources. One of the problems with recycling PP is maintaining the consistency of the batches; as they come in different types like homopolymer, block copolymer, random copolymers, thus presenting a wide range of melting points (160-130°C) and rheologies.[27]

2.1.3 Polyolefin Blends

Polymer blend can be used to describe a mixture of two or more polymers or copolymers. Blending different polymers is attractive because it makes it possible to obtain new material properties inexpensively, adjusted to particular applications from a limited range of polymers. Most commercial polymer blends are immiscible because of their high molecular weights and unfavourable thermodynamic interactions, thus form multiphase structures. Their properties are determined not only by the polymeric components, but also the adhesion between phases and the blend morphology that is created during mixing. This morphology is going to depend on the rheological properties of the blend components, blend composition, interfacial tension and processing conditions.[28]

2.1.3.1 Reclaimed Polyolefin Blends

Blending reclaimed polyolefins is a way, as it is with their virgin counterparts, of improving their processability or developing new combinations of properties. In reclaimed plastics another reasons are the upgrade of properties lost from degradation and exploitation of possible synergistic effects from complex matrices not found in virgin resins.

Polyethylene blends of virgin polyolefins with recycled milk bottle HDPE have been studied by Miller et al.,[29] with focus on miscibility and crystallization by thermal analysis to understand how the materials influence

each other. Not surprisingly, blends of HDPE/recycled HDPE were found to be miscible, and blends of LLDPE/recycled HDPE produced a similar result. For blends of LDPE/recycled HDPE up to about 50% HDPE phase separation was observed, a tendency that was not observed when the dominant phase was recycled HDPE, therefore it was concluded that those particular grades of polyethylene were miscible. In this study the grades of virgin polymers used were injection moulding and film blowing.

Kukaleva and Simon,[30] also with recycled milk-bottle grade HDPE, investigated the possibility of blending this material with virgin polymers to make it possible for injection moulding applications without using compatibilisers. An unexpected result was reported, namely, miscibility of the recycled HDPE with LDPE that only produced one single melting and crystallization peak in their MDSC study. This was also observed in ternary blends of recycled HDPE/LDPE/PP where only the HDPE/LDPE and PP peaks were observed. The effect on mechanical properties can be seen in Figure 2-3.

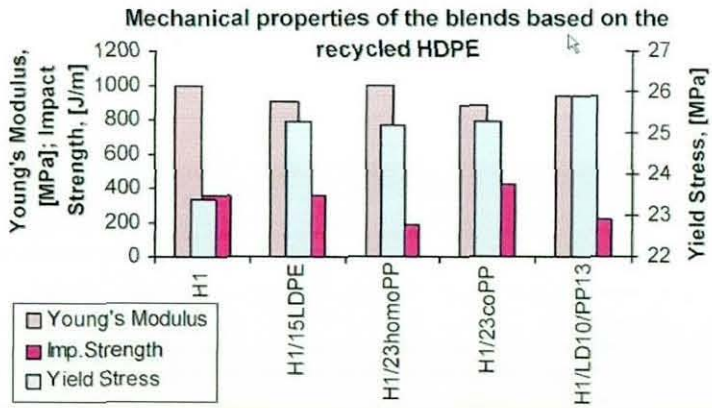

Figure 2-3 – Effect of blending LDPE and homoPP in recycled HDPE (H1).[31]

Bertin and Robin[31] studied a recycled LDPE/PP blend system with and without compatibiliser and also, a comparison between twin-screw and single-screw extrusion for blend preparation was examined. It was concluded that the dispersion obtained by twin-screw extrusion gave the blends better mechanical properties when compared with single-screw extrusion. EPDM, EPM and a new type of compatibiliser was also tested,

namely PE-g-(2-methyl-1,3- butadiene) at 5% weight, being found that mechanical properties are generally improved, such as elongation at break and Charpy impact strength.

Materials (wt.%/ wt.%)	Modulus (MPa)	Tensile strength at yield (MPa)	Tensile strength at break (MPa)	Elongation at break (%)	Charpy impact at 0 °C (kJ/m²)	Charpy impact at 20 °C (kJ/m²)
LDPE (90)/PP (10) virgin materials	205 ± 7	9.4 ± 0.1	8.4 ± 0.7	92 ± 10	15.2 ± 4.7	Partial breaking
Post-consumer material LDPE (90)/PP (10)	248 ± 9	10.0 ± 0.9	10.5 ± 1.5	383 ± 136	12.3 ± 4.3	5.3 ± 1.6
Post-consumer material LDPE (90)/PP (10)	256 ± 9	10.3 ± 0.1	12.8 ± 1.1	449 ± 50	12.6 ± 2.2	7.3 ± 0.9
Post-consumer material LDPE (90)/PP (10) – 5% EPM	228 ± 24	9.1 ± 0.2	12.3 ± 0.7	515 ± 24	Partial breaking	7.9 ± 0.8 (and 60% partial breaking)
Post-consumer material LDPE (90)/PP (10) – 5% EPDM	211 ± 15	8.9 ± 0.3	11.1 ± 0.8	469 ± 32	Partial breaking	22.5 ± 3.7 (and 45% partial breaking)
Post-consumer material LDPE (90)/PP (10) – 5% graft copolymer	240 ± 15	9.5 ± 0.2	12.5 ± 0.6	560 ± 20	Partial breaking	12.0 ± 2.5 (and 45% partial breaking)

Table 2-1 – Mechanical properties of materials after a single-screw extrusion (top) and twin-screw extrusion (bottom).[31]

2.1.4 Polyolefin Layered-Silicate Nanocomposites

Nanocomposites are a new class of composites that are particle-filled polymers for which at least one dimension is in the nanometre range.[32] These have proved to drastically improve mechanical properties, barrier properties, heat distortion temperature and flame resistance raising therefore great interest by the scientific community.[33] One of the most promising of such composite systems are hybrids based on organic polymers and inorganic clay mineral consisting of layered-silicates,[34] being the smectite type clays (e.g. montmorillonite) that have drawn most attention. The effect of these composites in the foamability of the resins and on their mechanical properties is largely unexplored, particularly in recycled polymers and blends. This section reviews the structures of layered silicate, their polymer nanocomposites and processing.

2.1.4.1 Layered-Silicates Structure

The layered silicates most commonly used in nanocomposites belong to the structural family of the 2:1 phyllosilicate. Their crystal lattice is illustrated in Figure 2-4 and consists of two-dimensional layers where a central octahedral sheet of alumina (Al_2O_3) or magnesia is fused into two external silica tetrahedra by the tip, so that the oxygen ions of the octahedral sheet also belong to the tetrahedral sheets.

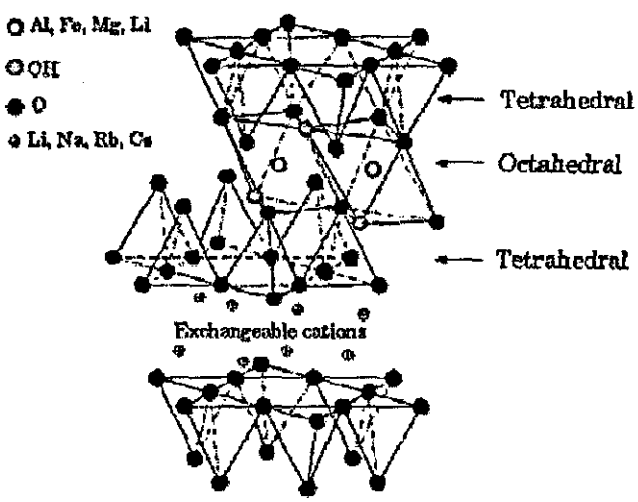

Figure 2-4 – Structure of 2:1 phyllosilicates.

The layer thickness is around 1 nm and the lateral dimensions of these layers may vary from 300 Å to several microns. Organized in stacks, these layers have a gap between them called the interlayer or gallery.[32] The forces that hold the stack are weak, thus the intercalation of small molecules is easy. However, these phyllosilicates are hydrophilic making intercalation with organic molecules difficult, unless of course, they are rendered more organophylic by modification of their structure. The most commonly used layered silicates are montmorillonite, hectorite and saponite - Table 2-2.

2:1 Phyllosilicate	General formula
Montmorillonite	$M_x(Al_{4-x}Mg_x)I_8O_{20}(OH)_4$
Hectorite	$M_x(Mg_{6-x}Li_x)Si_8O(OH)_4$
Saponite	$M_xMg_6(Si_{8-x}Al_x)O_{20}(OH)_4$

Table 2-2 –Chemical structure of some 2:1 phyllosilicates

These clays have typically a moderate negative surface charge, known as the cation exchange capacity (CEC and expresses in meq/100 g) that is greater inside the galleries.[32] When the hydrated cations are ion-exchanged with bulkier organic compounds such as alkylammoniums, it usually results in a larger interlayer spacing, a phenomenon that is also used to improve the clay capacity as an adsorbent.

2.1.4.2 Nanocomposite preparation

Nanocomposite structures depend on the nature of the layered-silicate, organic cation, polymer matrix and method of preparation[32].[32] When the polymer is unable to intercalate between silicate sheets a phase separated composite is obtained, resulting in a microcomposite. When the intercalation is successful, a nanocomposite is obtained. The nanocomposite family comprises two types of structure: the intercalated and the exfoliated. In the intercalated structure a single polymer chain is intercalated between the silicate layers, whereas if exfoliated these layers are completely and uniformly dispersed in the polymer matrix as can be seen in Figure 2-5.

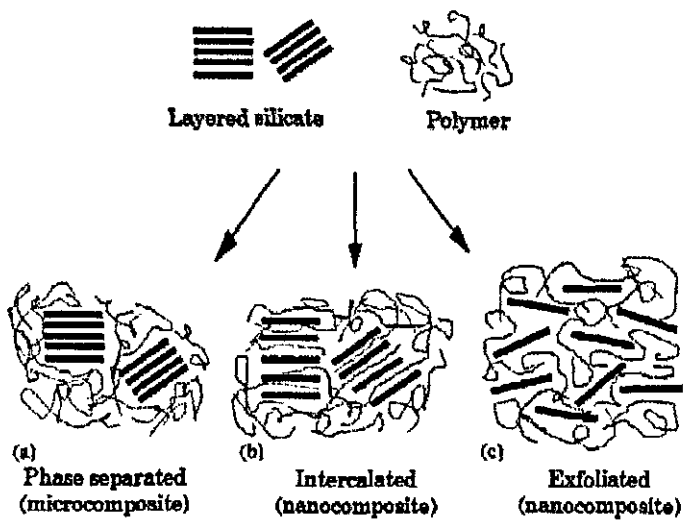

Figure 2-5 – Types of composite arising from the interaction of layered silicates and polymers: a) phase separated microcomposite; b) intercalated nanocomposite and c) *exfoliated nanocomposite*.

There are four main processes for the preparation of these nanocomposites:[32]

- *Exfoliation-adsorption*: the layered silicate is exfoliated into single layers after evaporating a solvent in which the polymer is soluble, owing to the fact that the weak forces that stack the layers together can be easily dispersed in an adequate solvent.
- *In-situ intercalative polymerisation*: in this technique, the layered silicate is swollen within the liquid monomer so as the polymer formation can occur in between the intercalated sheets.
- *Melt intercalation*: the layered silicate is mixed with the polymer matrix in the molten state. Under these conditions and if the layer surfaces are sufficiently compatible with the chosen polymer, the polymer can crawl into the interlayer space and form either an intercalated or an exfoliated nanocomposite.
- *Template synthesis*: the silicates are formed in situ in an aqueous solution containing polymer and the silicate building blocks has been widely used for synthesis of double-layer hydroxide nanocomposites. Based on self-assembly forces, the polymer aids the nucleation and growth of the inorganic host crystals and gets trapped within the layers as they grow.

2.1.4.3 Melt intercalation

2.1.4.3.1 Theoretical Models

With organically modified layered silicates it is possible to obtain nanocomposites with various degrees of polarity and chain rigidity on polycarbonates, polymethacrylates or polyolefins.[34, 35] Depending upon the characteristics of the polymer and the organically modified silicate an intercalated or exfoliated nanocomposite or a microcomposite may be obtained. These include the nature of the polymer as well as type, packing density, and size of organic modifiers on the silicate surface. Unfortunately,

current guidelines as to the optimum polymer - (OLS) combination are unsatisfactory, leading frequently to trial-and-error. In an attempt to avoid this, Vaia and Giannelis[36] proposed a lattice-based mean field theory to explain the thermodynamics behind the intercalation of a molten polymer inside a modified layered silicate. This model has the great advantage of determining analytically the effect of hybrid formation of various polymers and organically layered silicates. Starting from the free energy change per interlayer volume, ΔA_v, associated with polymer intercalation expressed as follows,

$$\Delta A_V = \Delta U_V - T\Delta S_V \qquad \textbf{2.1}$$

where ΔU_V and ΔS_V are the internal energy and entropy change per interlayer volume, and

$$\Delta U_V = \hat{\varphi}_1 \hat{\varphi}_2 \frac{1}{Q}\left(\frac{2}{h_0}\varepsilon_{sp,sa} + \frac{2}{r_2}\varepsilon_{ap}\right) \qquad \textbf{2.2}$$

$$\Delta S_V = N_A k_b\left[\Delta S_V^{chain} + \Delta S_V^{polymer}\right] = N_A k_b\left[\frac{\hat{\varphi}_2}{\nu_2}\ln(c)(\chi_S - \chi_{S0}) - \frac{\hat{\varphi}_1}{\nu_1}\left\{\frac{\pi^2}{6}\left(\frac{a_1}{h}\right)^2 + \sqrt{3}\frac{u}{\sqrt{m_1}}\frac{a_1}{h}\right\}\right] \qquad \textbf{2.3}$$

ΔS_V is expressed as the sum of the sum of the entropy change associated with the organically-modified silicate, ΔS_V^{chain}, and that the entropy change associated with the confinement of the polymer, $\Delta S_V^{polymer}$. h_0 and h are the initial and after polymer intercalation gallery height, respectively. m_i, v_i, φ_i, r_i and a_i are the number of segments per chain, molar volume per segment, the interlayer volume fraction and the radius of interaction surface, and the segment length of the ith interlayer species. u is a dimensionless excluded volume, Q is a constant near unity, and χ_S and χ_{S0} are the fractions of interlayer volume near the surface at height h and h_0, respectively, which influence the potential chain conformations. ε_{ap} represents a pair wise interaction energy per area between aliphatic chain and the surface, $\varepsilon_{sp,sa}$ =

$\varepsilon_{sp} - \varepsilon_{sp,sa}$, is the difference between the pair wise interaction energy between the aliphatic chain and the surface, ε_{sa}, and that between the polymer and the surface, ε_{sp}. A detailed derivation of this model can be found elsewhere.[36]

To confirm their theory Vaia and Giannelis[35] used polystyrene (PS) as a matrix for dispersing Li^+-fluorohectorite, saponite, and sodium montmorillonite that were accordingly modified using various ammonium cations: dioctaecylmethylammonium, octadecyltrimethyl-ammonium and a series of primary alkylammonium cations with carbon chains of 6,9-16 and 18 carbon atoms. The nanocomposites were synthesized by statically annealing (without any mixing or shearing) a pelletised intimate mix of the modified silicate in PS under a vacuum at 170°C. Under these conditions they found that for a given alkyl surfactant, increasing the cation exchange capacity from 80-120 meq/100 g allows for PS intercalation to occur. Experimental results also indicated that the outcome of polymer intercalation depends critically on silicate functionalisation and constituent interaction. It was observed that an optimal interlayer structure on the OLS, with respect to the number per area and size of the alkylammonium chains is most favourable for hybrid formation and that polymer intercalation depends on the existence of polar interaction between OLS and the polymer. They state that the hybrid formation depends on energetic factors that may be determined from the surface energies of the polymer and that the interlayer should be optimised to maximize the configurational freedom of the functionalising chains upon layer separation while maximizing potential interaction sites with the surface.[35]

In the same study they also concluded that the most successful polymers for intercalation exhibited polar character or contained Lewis-acid/base groups. Vaia et al.[35] also studied the kinetics of melt intercalation; It has been demonstrated that the accessibility of the interlayer to the polymer chains depends on the location and orientation of the crystallites within the primary particles, meaning that crystallites near the edge will be more accessible to

polymer chains than those near the centre. Polypropylene-clay hybrids were studied by Kawasumi et al.[34] Since polypropylene doesn't have any polar groups, they used two types of maleic anhydride modified oligomers with different acid values and, also montmorillonite and fluorinated mica, both intercalated with stearylammonium ion. This is different approach from a previous work[37] where they tried to use montmorillonite intercalated with distearylammonium ion to create a PP-clay hybrid resorting to PP-OH as compatibiliser. This was not entirely successful as some clay aggregates were observed. In the first study it was found that to achieve exfoliation and dispersion in the PP-MA-Mt matrix one needs to consider the intercalation capability of the oligomers in the layers and the miscibility of oligomers with PP. This came from the fact that with both clays the hybrid that exhibited more exfoliation was the one that had the PP-MA with lower acid content, which coincided with a better miscibility of the same PP-MA in PP.

2.1.4.3.2 Nanocomposite processing

Not all the studies report the use of extruders to prepare their clay-nanocomposites, which would are expected to be employed in industrial processes. To achieve a good intercalation in polymer-clay hybrids the use of twin-screw extruders is necessary most of the time, leading to a more expensive process. Therefore evaluation of single screw extruders or limiting the use twin-screw extruders to letdown operations is highly desirable. Cho et al.[38] investigated this by processing polypropylene-clay nanocomposites in a twin-screw extruder and a single-screw extruder, for which in the last case four different mixing elements were tested. Having previously prepared a organoclay concentrate masterbatch containing 50 wt.% organoclay, 25 wt.% PP-MA and 25 wt.% homo-PP, it was then let down in the single screw-extruder and in the twin-screw extruder. A comparative test where homo-PP, PP-MA and organoclay compounded in a single step was also run. Results indicated that the composites obtained from a masterbatch let down with a single screw extruder showed better dispersion and better mechanical properties than the composite obtained

from a direct compounding with a twin-screw extruder for all the mixing elements used. Moreover, the mechanical properties of the nanocomposite obtained from the single-screw extruder let down were equivalent to those of the twin-screw. The mixing section with best performance was of the dispersionary type.

The effects of processing parameters on the preparation of HDPE layered silicate composites have been reviewed by Kwak et al.[39] using a batch mixer, two different molecular weight HDPE resins, PE-MA (12% MA) and a commercially available organically modified clay (Cloisite 6A, 125 meq/100g). The major processing conditions tested on the intercalation or exfoliation behaviour were temperature, mixing time and speed. In summary, a higher operating temperature, a lower molecular weight of PE and a higher mixing speed led to a higher degree of exfoliation of the clay used. From the results, it can be generally concluded that the intensive mixing of lower molecular weight would be better for the preparation of polyethylene/clay nanocomposites.

Puttarudraiah and Goettler[33] investigated the possibility of adding value to recycled polyethylene through incorporation of nanoscale organically modified montmorillonite clay and found that this combination can generally increase the mechanical properties of these compounds, although there is a maximum for the use of PE grafted with maleic anhydride as this can degrade the properties due to lack of compatibility with the pure PE matrix.

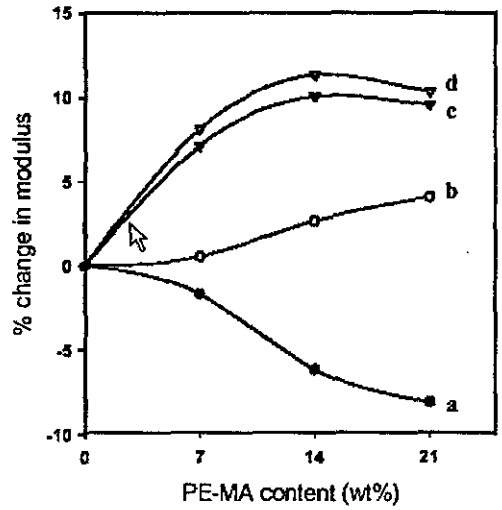

Figure 2-6 - Effect of variation of PE-MA content on moduli: clay content (a) 0%, (b) 3%, (c) 5%, (d) 7%.[39]

2.2 Rheology of Polyolefins, Blends and Nanocomposites

Understanding polymer melt rheology is essential for the design of processing methods and is also an important link between molecular structure and the end-use properties of polymers.[40] Fundamentally, it studies the responses of fluids to deformation and thrives to correlate them with molecular properties for the development of unified constitutive equations that could describe them. Since polymer melts are non-Newtonian fluids with viscoelastic properties, both elasticity and viscosity must be measured.[41] This means that under certain circumstances they will deform continuously with applied stress and show some elastic recovery from the deformation when that stress ends. From a theoretical point of view viscoelasticity is split into linear and non-linear, whether the rheological response to stress is linear or non-linear, respectively.

2.2.1 Geometry of Flow

The most relevant modes of deformation considered in rheological problems are simple shear, elongation and bulk compression. The last mode is not as relevant as the other two to most polymer processing operations only becoming important when high, near hydrostatic pressures are present, therefore it will not be discussed here.[42]

In simple shear deformation a force (F) is applied tangentially to an elemental volume, as shown in Figure 2-7, causing a relative displacement between the two layers known as shear strain (γ) defined as shown in equation 2.5. The simple shear stress (τ) is defined by equation 2.4.

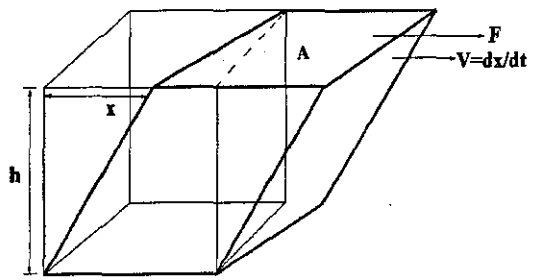

Figure 2-7 – Simple shear deformation.

$$\tau = \frac{F}{A} \qquad \textbf{2.4}$$

$$\gamma = \frac{x}{h} \qquad \textbf{2.5}$$

The rate of change of shear strain with time is the shear strain rate ($\dot{\gamma}$) given by:

$$\dot{\gamma} = \frac{1}{h}\frac{\partial x}{\partial t} = \frac{v}{h} \qquad \textbf{2.6}$$

Where,

τ – shear stress (Pa)
γ – shear strain
$\dot{\gamma}$ – shear strain rate (s^{-1})

In a simple (or uniaxial) elongational deformation the force is applied normal to the surface of the material (Figure 2-8). The simple elongational flow can be quantified using equations 2.7 and 2.8 and Figure 2-8.

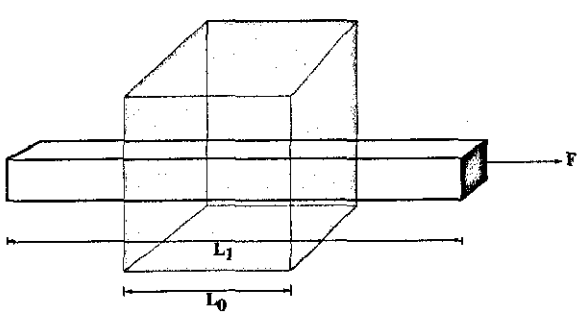

Figure 2-8 - Geometry of elongational flow.

$$\sigma_E = \frac{F}{A} \qquad 2.7$$

$$\varepsilon = \frac{L_1 - L_0}{L_0} \qquad 2.8$$

Where,

σ_E – tensile stress (N/m^2)

L_0 – original length of the sample (m)

L_1 – length at time t (m)

ε – engineering strain

Two kinds of elongational strain can be defined depending upon the ability of the material to flow. In case of an elastic material that doesn't flow like a crosslinked rubber we define an engineering strain, whilst for a polymer melt we consider often the Hencky strain to measure elongational strain as shown in equation 2.9.

$$\varepsilon_H = \int_{L_o}^{L_1} \frac{dL}{L} = \ln \frac{L_1}{L_o} \qquad 2.9$$

The instantaneous true elongational strain rate ($\dot{\varepsilon}$) can be written as shown in equation 2.10.

$$\dot{\varepsilon} = \frac{d\varepsilon_H}{dt} = \frac{1}{L_1}\frac{dL}{dt} \qquad 2.10$$

Where

ε_H – Hencky elongational strain

$\dot{\varepsilon}$ – Hencky elongational strain rate (s^{-1})

L_o – original length (m)

L_1 – immediate length before the increase of length dL (m)

2.2.2 Viscosity Models

To describe the viscoelastic responses of polymers under deformation several physical models have been proposed, but one that can be taken as a reference is the Maxwell model that proposes a dashpot in series with a spring to explain their behaviour and derive an expression relating shear stress and shear rate.[43] The differential form of the model is expressed by equation 2.11.

$$\sigma_{yx} + \lambda_0 \frac{\partial}{\partial t}\sigma_{yx} = -\eta_0 \dot{\gamma}_{yx} \qquad \textbf{2.11}$$

This model contains two parameters: η_0 and λ_0 which are, respectively, a constant viscosity and a characteristic time that is the ratio of the viscosity and elastic modulus, G_0, as expressed by equation 2.12

$$\lambda_0 = \frac{\eta_0}{G_0} \qquad \textbf{2.12}$$

As stated by Carreau,[43] in many flow situations viscoelasticity will not play an important role, and the non-Newtonian viscosity is adequate to describe the rheology of the material. Several viscosity models have been proposed, the Power-Law model probably being the most frequently used, due to its simplicity. This is given by equation 2.12

$$\eta = m\left|\dot{\gamma}\right|^{n-1} \qquad \textbf{2.12}$$

This model represents the data in the power-law region, resulting in a linear relationship in a logarithmic plot of the variables. It has two parameters *m* and *n*, being the last one a measure of departure from Newtonian behaviour, representing shear thinning in case n<1. One of the problems with this model apart from not being applicable to low deformation regions is the fact *n* dependence of *m* that clashes with the requirement of a characteristic time to describe viscoelastic behaviour; *m* has units of $Pa.s^n$.

Another popular model is the Carreau model[44] defined by equation 2.13

$$\eta = \frac{\eta_0}{\left[1 + (t_1\dot{\gamma})^2\right]^{\frac{n-1}{2}}} \qquad \textbf{2-13}$$

This model is capable of predicting the shape of the shear viscosity vs. shear rate curve in both the lower shear and high shear region, a zero shear viscosity η_0, a characteristic time t_1 and slope in the power-law region. To improve the accuracy of this model a few points from the low shear region are required.

2.2.3 Capillary Rheometry

Capillary rheometry is one the techniques that allows us to relate a shear deformation from a polymer melt to its shear stress. It derives from the Poiseuille law for capillary flow and yields two fundamental equations[44] describing apparent wall shear stress and wall shear rate:

$$\sigma = \frac{PR}{2L} \qquad \textbf{2-14}$$

$$\dot{\gamma} = \frac{4Q}{\pi R^3} \qquad \textbf{2-15}$$

Where,

σ – Apparent shear stress (Pa s)

P – pressure drop across the capillary (Pa)

R – radius of the capillary (m)

L – Length of the capillary (m)

$\dot{\gamma}$ – Apparent shear rate (s^{-1})

Q – Volumetric flow rate (m^3/s)

A detailed derivation of these equations can be found in Brydson.[45] In practice we measure the pressure drop through a capillary die and relate it to the volumetric flow rate to obtain shear rate and stress. As stated previously these equations yield only apparent rheological properties as in the derivations some assumptions that have been made do not actually hold. For example, it is assumed that the fluid is Newtonian, incompressible,[45] and the process isothermal, therefore some corrections are needed to account for such effects. Two main corrections are usually employed. One correction accounts for the fact that the pressure drop across the capillary die is not linear, being substantial at the die entrance and non-zero value at the exit. One method was proposed by Baggley, consisting of measuring the pressure drop with a series of dies of different lengths but the same radius. In practice, the greatest sensitivity is obtained by using a combination of a long die with and orifice die. After this, the true wall shear stress can be calculated using equation 2.16

$$\sigma_w = \frac{(P_L - P_0)R}{2L} \qquad \textbf{2-16}$$

Where

σ_w = true shear stress at the wall (Pa)
P_L = pressure obtained from die (Pa)
P_0 = pressure obtained from orifice die (Pa)
R = die radius (m)
L = die length (m)

Another correction that can be made derives from the fact that due to the pseudoplastic nature of the melt the assumed parabolic velocity profile in the die is actually more plug-like. This procedure is commonly known as Rabinowitsch correction and yields the following expression to determine the true shear stress:

$$\dot{\gamma}_w = \left(\frac{3n+1}{4n}\right)\frac{4Q}{\pi R^3} \qquad \textbf{2-17}$$

Where

Q = volume flow rate (m^3/s)

R = capillary radius (m)

n = power law index (from the 'apparent' flow curve)

2.2.4 Shear Behaviour of Polyolefin Melts

The behaviour of polyolefins melts under shear has been extensively studied because most polymer processing operations involve this deformation and it is much easier to study than elongation. However, this is still an area of great interest because new resins are constantly being developed either by the development of technology that can control better the molecular structure of the polymer, incorporation of additives or even blending the resins, affecting obviously their rheology. Typically, as can be seen in Figure 2-9 a polyolefin melt presents a shear constant shear viscosity in the linear viscoelastic region and thinning behaviour in the non-linear viscoelastic region.

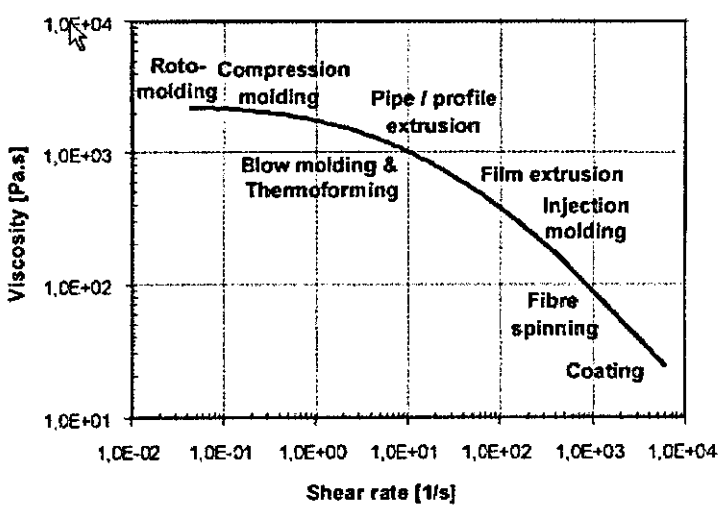

Figure 2-9 - Typical polyolefin curve – PP-homopolymer (MFI 8) at 230°C with *indication of the shear rate regions of different processing techniques*.

The effect of molecular structure was investigated by Constantin,[46] reporting on HDPE, LLDPE and LDPE. All samples, which had the same MFI but different structure and density, exhibited differences in the plot of shear

viscosity against shear strain rate; the wider the MWD the shorter the Newtonian shear viscosity (η_0) plateau. This was due to the presence of long chain branches, affecting the flow curve shapes by decreasing shear viscosity in the higher strain rate range.

Recently, Gabriel and Munstedt[47] studied the influence the of LCBs on linear viscoelastic flow properties in shear and found that for linear polyethylenes the molecular mass dependence is independent of the polydispersity of the molecular mass distribution and that the low zero shear rate viscosity of classical LDPE in comparison to linear polyethylene is a result of the high branching functionality which reduces the number of entanglements per branch. Polyethylenes with a slight degree of LBC exhibit a surprisingly high zero-shear rate viscosity in comparison to linear polyethylenes whereas the highly branched polyethylenes have a much lower viscosity compared to linear samples. Highly branched polyethylenes of broad molecular mass distribution showed a surprisingly low elasticity when compared to linear polyethylenes with an equivalent molecular mass distribution.

2.2.4.1 Polyolefin Blends

The melt flow behavior of polyethylene blends has been reviewed recently by Utracki.[48] In this work all combinations of polyethylene blends are considered, but particular emphasis is given to LLDPE blends in sequence with a previous work.[49] Dobrescu[48] has studied HDPE/LDPE blends using a capillary rheometer to find that these blends showed a strong positive deviation from the log additivity rule (eq. 2.18) and that was higher with increased viscosity ratio.

$$\log \eta = \sum W_i \log \eta_i \qquad \textbf{2-18}$$

where η is the viscosity of the blend, η_i is that of the components and W_i the weight fraction.

Alle et al.[50] studied isotactic PP/HDPE blends capillary viscosities at 180 to 210°C and the results showed a negative deviation from the log additivity rule. At the same time he studied the morphology development of the blend and reported large differences with viscosity ratios above and below 1. For systems whose viscosity ratio was lower than 1 the fluidity additivity equation[51] was found to be obeyed:

$$1/\eta = \beta_1 \sum W_i / \eta_i \qquad \textbf{2-19}$$

For a viscosity ratio larger than 1 at a concentration W_2 lower than 0.5 equation 2.1 yielded good approximation, whilst for higher PP content equation 2.2 was obeyed. Blends of PP with LDPE in plots of shear viscosity versus W_2 invariably show negative deviation to additivity rule whose magnitude varied with the method of preparation. Blends of LLDPE with other LLDPE's or LDPE may show a widely varying behavior, dependent in molecular structure, polymerization method or composition.[29]

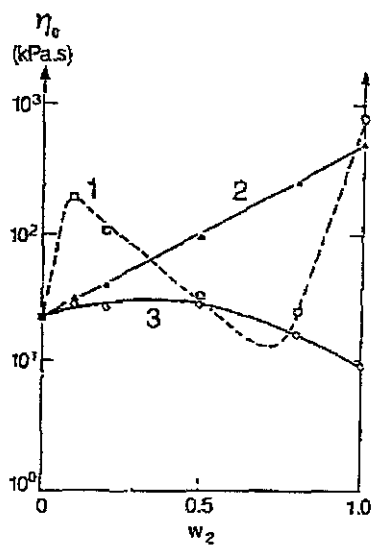

Figure 2-10 – Compositional dependence of the zero-shear viscosity for blends of LLDPE with (1) and (2) different LLDPE's, and (3) with LDPE.[48]

The rheological properties of metallocene LLDPE (m-LLDPE) with metallocene HDPE (m-HDPE) and LDPE have been studied by Liu et al.[52] m-LLDPE/m-HDPE blends obeyed a log η_0 additivity rule, with increasing viscosity with m-HDPE content, as well as the Cox-Merz rule. m-LLDPE/LDPE blends showed a non-linear large positive deviation in their η_0 log additivity rule with a maximum, which fitted very well Utracki's immiscible blend equation.[48]

2.2.4.2 Shear Flow of Filled Polymers

The addition of mineral fillers to the polymer matrix has two main targets: improving mechanical properties, mainly stiffness (modulus) and heat deflection temperature, and in case of mineral fillers and inexpensive organic fillers – also reducing the overall cost of material. Typical fillers include talc, calcium carbonate or wood fibers, for example. The rheological consequences of filler addition are most simple for the Newtonian case, where the viscosity increase can be easily formulated according to Einstein:

$$\eta = \eta_s(1 + 2.5\phi) \qquad \textbf{2.20}$$

for the dilute case where η_s is the viscosity of the suspending liquid and ϕ is the volume fraction of the solids. However, parameters of fillers/fibers are particle size and size distribution, shape factor, matrix adhesion, stability towards agglomeration, hydrophilic or hydrophobic natures, and they are not explicit in such a simple equation. Moreover, in case of viscoelastic systems, the situation is more complex, the addition of fillers here leads to a change in the relaxation time spectrum with an addition of long relaxation times resulting from particle-matrix and particle-particle interactions.[44] Generally, fillers tend to increase the viscosity of the melt,[22, 53] and many relationships have been proposed to describe this behavior. As an example, and quite simple, is the Maron-Pierce relationship that describes the effect of concentration for a variety of fillers.

$$\frac{\eta}{\eta_f} = \frac{1}{(1-(\phi/A))^2} \qquad \textbf{2.21}$$

the volume fraction of the filler is ϕ, A is the filler densest packing, η the viscosity of the pure polymer, and η_f the viscosity of the filled polymer. Kataoka et al.[54] this equation to melt filled with calcium carbonate and found it gave the best fitting when A was 0.44. As stated by Hill,[55] the addition of a rigid filler increased the non-Newtonian viscosity much more at low shear strain rates than at higher shear strain rates, which suggests the presence of a shear yield stress. This phenomenon has been verified in various filled polymer systems raising the possibility of one using the Casson equation:[44]

$$\sigma^{0.5} = \sigma_0^{0.5} + k_s\dot{\gamma}^{0.5} \qquad \textbf{2-22}$$

where k_s is a constant and σ_0 the yield stress. Dealy[44] explained that the existence of a yield stress may be related to the formation of a strongly interacting network by the suspended particles. Above the yield stress the structure breaks down and flow is dominated by the viscosity of the polymer matrix.

2.2.5 Elongational rheometry

In simple elongation the elongational viscosity, λ, is defined by

$$\lambda = \frac{\sigma_E}{\dot{\varepsilon}_H} \qquad \textbf{2-23}$$

However, only Troutonian fluids obey this expression, non-Troutonian fluids show a dependency on either stress or strain rate, depending on the controlling parameter.

$$\lambda = \lambda(\sigma_E) \text{ or } \lambda(\dot{\varepsilon}_H) \equiv \sigma_E / \dot{\varepsilon}_H$$

The most fundamental observation made by Trouton was that the zero extension rate viscosity could be related to the zero elongational strain rate. This is also known as the Trouton rule is valid for Newtonian fluids

$$\lambda_0 = 3\eta_0 \qquad \text{2-24}$$

Polymers can produce three kinds of responses to elongational deformation similarly to shear as depicted in figure Figure 2-11. In case the elongational viscosity increases with increasing tensile stress the fluid is said to have an extension stiffening behavior, whereas if the opposite occurs it is named extension thinning. When the elongational viscosity is independent of tensile stress the fluid is said to exhibit Troutonian behavior.

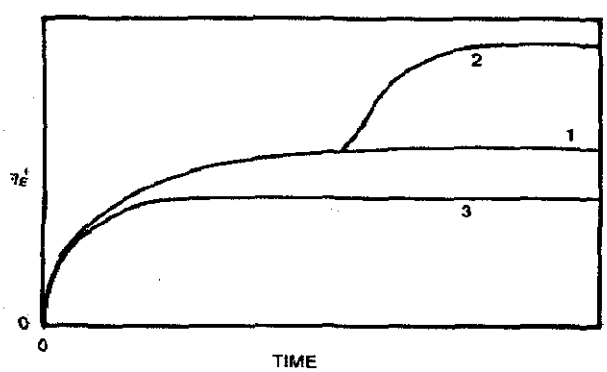

Figure 2-11 – Types of behaviour exhibited by polymeric liquids during tensile start-up flow. Curve 1 shows the response predicted by the linear theory of viscoelasticity. Curve 2 shows extension thickening (strain hardening) and curve 3 shows extension thinning.[44]

2.2.5.1 Uniaxial Elongation Rheometry

Uniaxial elongational rheometry is one of the most used techniques to determine extensional properties being either performed under controlled stress or strain rate. Several kinds of rheometer have been developed to execute the tests, that are technically more difficult develop than shear flow rheometer, namely the ones developed by Munsted and Meissner.[44] In the

Munsted equipment a sample is held vertically in an oil bath connected to a servo motor that stretches the sample and a force transducer, allowing the execution of constant strain and stress measurements. The equipment can be seen in Figure 2-12

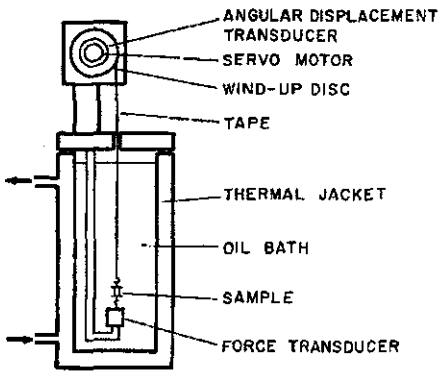

Figure 2-12 - Extensional rheometer designed by Munstedt.[44]

For the uniaxial elongational rheometer, the experimental design and data interpretation are based on the equations presented in section 2.2.1. For this kind of deformation the sample is designed to have a constant cross-sectional area (A_0) along the length (L_0) that is stretched to a total length L_t at a velocity V_t given by

$$V_t = \dot{\varepsilon}_H L_t \qquad \textbf{2-25}$$

The length of the sample increases exponentially with time while the opposite happens to the cross-sectional area as it is show in the following equations:

$$L_t = L_0 \exp(\dot{\varepsilon}_H t) \qquad \textbf{2-26}$$

$$A_t = A_0 \exp(-\dot{\varepsilon}_H t) \qquad \textbf{2-27}$$

In a constant elongational strain rate $\dot{\varepsilon}_H$ the velocity has to increase according to the displacement or sample length as can be taken from equation 2.27, and the growing tensile stress is monitored as a function of time as depicted by Figure 2-13.

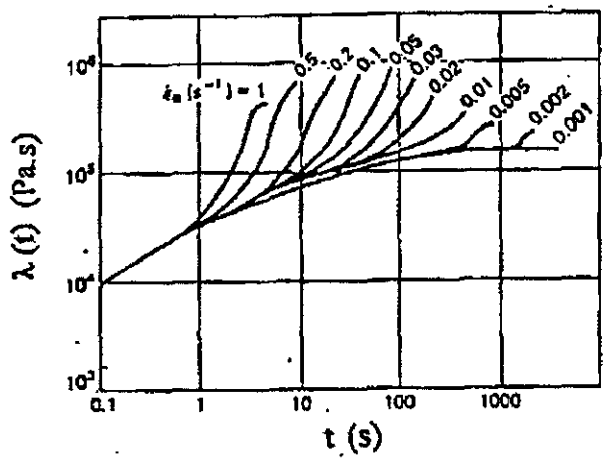

Figure 2-13 - Tensile stress growth function at various strain rates for LDPE at 150°C.[56]

If the material of interest tends toward linear viscoelastic behaviour at low elongational strain rates, the Troutonian relationship is valid and therefore

$$\lim_{\dot{\varepsilon}_H \to 0}\left[\lambda(\dot{\varepsilon}_H)\right] = 3\eta_0 \qquad \textbf{2-28}$$

When the measurements are made in the constant stress mode, the elongational strain is monitored as a function of time, and in order to obtain the elongational viscosity the applied stress is simply divided by the elongation rate. Taking advantage from the fact that in constant stress experiments the elastic response soon reaches equilibrium it is possible to define equation 2.29.

$$D(t) = D_s^0 + t/\lambda_0 \qquad \textbf{2-29}$$

where D_s^0 is the steady-state tensile compliance in the limiting case of small tensile stress and λ_0 is the zero elongational strain rate viscosity.

2.2.5.2 Converging Flow Analysis

Due to the difficulty of measuring extensional viscosities in polymer melts with conventional uniaxial rheometers Cogswell[57] after a converging flow analysis proposed an indirect method for determining extensional viscosity using the entrance pressure loss in a capillary rheometer. As melt flows from the barrel of a capillary rheometer into a die the streamlines converge, producing a strong extensional flow superposed onto a simple shear flow. Assuming that the pressure drop has two components due to shear and extension that can be calculated separately and summed to give the total pressure-loss, that shear stress is related to shear stress through a power-law, constant elongational viscosity and neglecting the Rabinowitsch procedure he derived the following formulae:

$$\sigma_e = \frac{3}{8}(n+1)P_0 \qquad \textbf{2.30}$$

$$\varepsilon_R = \ln B_0^2 \qquad \textbf{2.31}$$

$$\lambda = \frac{9}{32}\frac{(n+1)^2}{\eta}\left(\frac{P_0}{\dot{\gamma}}\right)^2 \qquad \textbf{2.22}$$

A more complicated but more rigorous analysis of contraction flow is due to Binding,[58] that makes the same assumptions of Cogswell but allows elongational viscosity to vary with deformation and doesn't neglect the Rabinowitsch procedure. Recently, Sunder and Goettfert[59] compared extensional data obtained with the Cogswell method with the Rheotens test, but included the zero length die and Bagley correction. They reported that the zero length die delivers an entrance pressure drop which is 10-100% higher than the pressure loss from the Bagley correction leading to a 60-100% higher extensional viscosity. The results obtained with the Rheotens test and the Bagley correction showed good accordance. In another study, Gotsis and Ke[60] compared the Rheotens test together with uniaxial elongation and their modification of the Binding method, using HDPE, LDPE and LLDPE as samples. They concluded that their entry flow method gave

reasonable agreement with the uniaxial extension and also that it depended on the radii of the dies and accumulated strain. The Rheotens test performed was found less reliable because the estimates obtained are affected by strain relaxation in intermediate flows which is difficult to quantify.

2.2.6 Elongational Behaviour of Polyolefin Melts

Elongational viscosity of polymer melts is an important property to be considered in processes like foaming, blow moulding or fibber spinning. Similarly to shear flow, according to the response of the material to stress it can be classified as one of three types: Troutonian behaviour when elongational viscosity is independent of elongational stress or elongational strain rate, and either tension-stiffening or tension-thinning where elongational viscosity increases or decreases respectively with increasing elongational stress or elongation strain rate.[44]

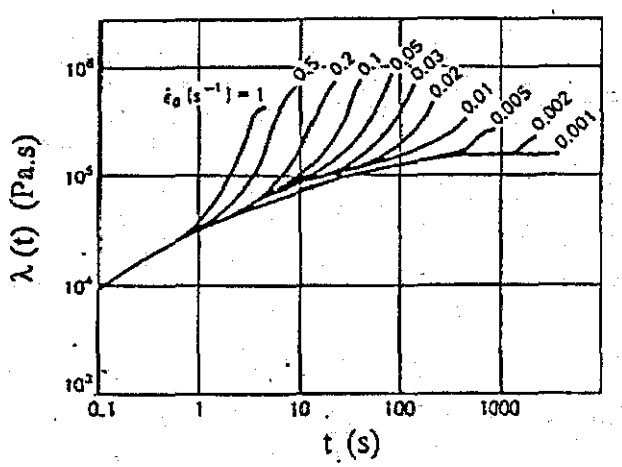

Figure 2-14 - Transient elongational viscosity-time plot of LDPE at different elongational strain rates at 150°C.[56]

Meissner[56] presented the elongational behaviour of a LDPE melt in a plot of a transient elongational viscosity versus time as determined by using the uniaxial elongational rheometer at constant strain rates from 0.001 to 1 s^{-1}. At low elongational strain rate of 0.001 s^{-1}, the LDPE behaves like a linear viscoelastic fluid, i.e., transient elongational viscosity is about $3\eta_0$. Going

from the lowest strain rate to higher elongation strain rates, transient elongational viscosity shows a rapid increase above the linear viscoelastic curve, indicating the occurrence of strain-hardening. Deviation from the linear viscoelastic curve takes place at a certain value of elongational strain (ε_H) which does not depend on the elongational strain rate.

Munsted and Laun[61] studied the influence of molecular structure on the elongational properties using a group of LDPE and another of HDPE samples with different molecular weights and molecular weight distributions. Within each group the polymer with the highest molecular weight showed the highest extensional viscosity as can be seen in Figure 2-15. The molecular weight distribution effect was accounted with a group of LDPE samples and it was found that the sample with the highest molecular weight distribution had the highest elongational viscosity, polydispersity fact that has also been observed for PS.[62, 63]

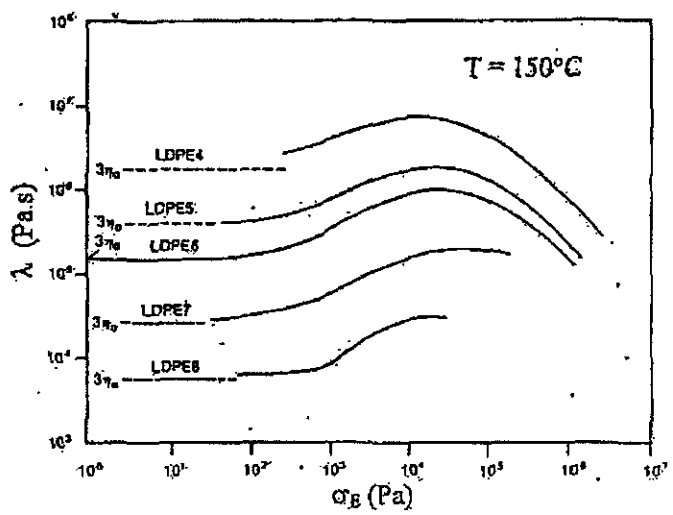

Figure 2-15 – Steady-state elongational viscosities of low density polyethylenes of different molecular weights.[61]

A comparison of the elongational flow behaviour of three PE melts at 150°C was carried out by Meissner and Hostettler.[64] Three PE melts, LDPE, LLDPE and HDPE were tested at 150°C. As seen in Figure 2-16, transient elongational viscosity, for all samples tend to follow the linear viscoelastic prediction. However, the strain-hardening for the three samples is different in

terms of magnitude and the time at which the strain-hardening take place. The LDPE starts to harden early and its transient elongational viscosity reaches a maximum value as previously observed by other workers. Both LLDPE and HDPE curves follow the liner viscoelastic values ($3\eta_0$) for longer periods and the HDPE curves deviated from $3\eta_0$ before LLDPE.

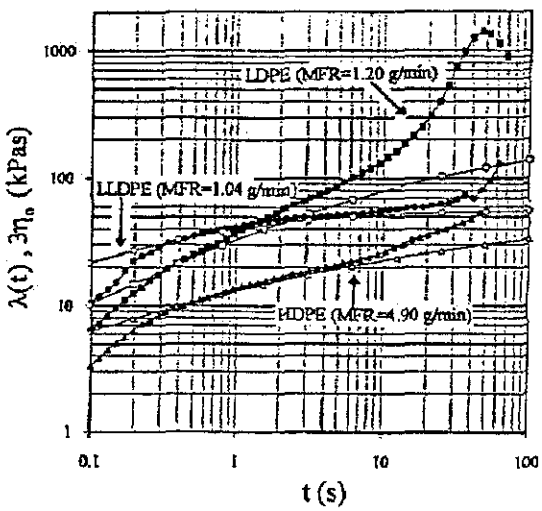

Figure 2-16 – Transient elongational viscosity of three PE melts at 150°C.[64]

Recently, Wagner et al.,[65] investigated several linear (LLDPE, HDPE, PS) and long-chain branched (LDPE, PP), with an elongational rheometer where they also applied the Molecular Stress Theory to extrapolate the steady-state elongational viscosity with success.

2.2.6.1 Polyolefin Blends

Comparatively to shear flow, not as many studies have been published regarding strictly polyolefin blends in extensional flow, exceptions can be found in the works of Utracki,[48] La Mantia and co-workers,[66] and Muller et al.[67] Utracki[48] studied LLDPE/LLDPE, LLDPE/LDPE and LLDPE/PP blends with an uniaxial rheometer at 150°C for the first two blends and 190°C for the last one. For LLDPE/LLDPE and LLDPE/LDPE blends strain-hardening effects were found, in contrast with the LLDPE/PP one where those effects were absent. When blending two types of LLDPE, strain-hardening

appeared at about 20% loading, being however more efficient the blend with low molecular weight.

La Mantia et al.[66] studied the extensional flow of HDPE/LDPE blends using the Cogswell method. The viscosities of the blends lie for all cases between those of pure polymers. However, typical features for each type of mixture were found. When the shear viscosity of LDPE is much higher than that of HDPE, all the blends show behaviour similar to that of LDPE, whereas when the shear viscosity is similar, there is a gradual change from one type of behaviour to another.

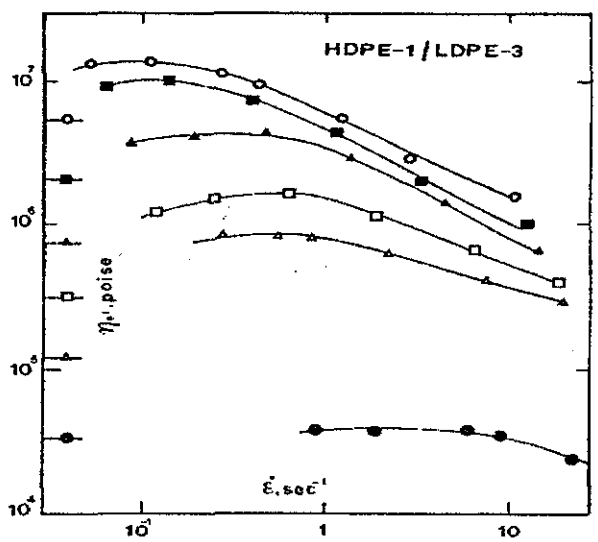

Figure 2-17 – Elongational viscosity vs. stretching rate for HDPE/LDPE (Higher MW) at 180°C.[66]

Another work using a capillary rheometer to determine extensional properties of LLDPE/LDPE blends was reported by Muller et al.[67] and also included a comparison between Cogswell and Binding methods. It was found that the rheological properties were dependant on the molecular weight of the LDPE homopolymer used. With high molecular weight LDPE though the shear viscosity wasn't substantially changed the viscosity of the blends was in almost all cases lower than pure LDPE. With a lower molecular weight LDPE the elongational viscosities were slightly higher than the value of LDPE. It was concluded that the Cogswell method overestimates the apparent extensional viscosity and predicts lowers strain rate values.

2.3 Polymer Foams

Foam can be defined as gaseous voids surrounded by a much denser continuum matrix, which is usually in a liquid or a solid phase.[5] These materials possess interesting characteristics such as lightweight, low thermal conductivity, excellent stiffness/weight ratio, and absorption of sound, vibration and shock. According to their density they can be classified as low or high density, whether it's lower than 100 kg/m^3 or higher than 600 kg/m^3, and open-celled or closed cell if we consider the cellular structure. These properties allied to the material are most important in determining the final application.

Polyolefin foams are relatively new compared to polystyrene for instance as the main industrial processes were introduced in the 1960's despite the fact the first polyethylene foaming process was patented in 1941 by Johnston using nitrogen or ammonium bicarbonate as the blowing agent.[68]

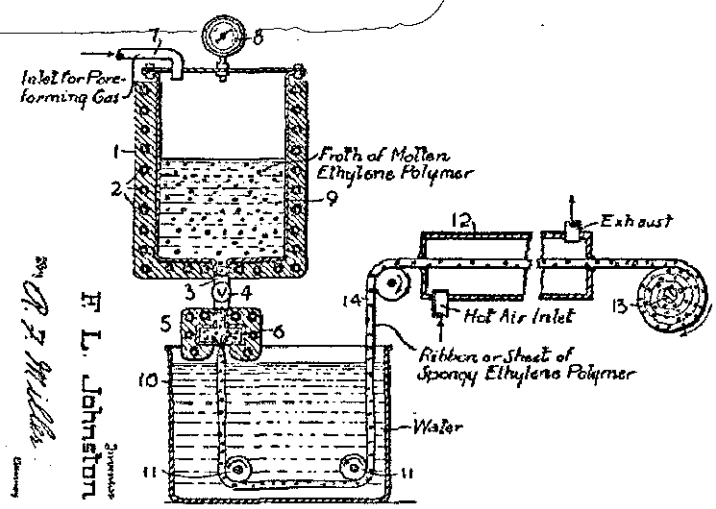

Figure 2-18 – Foamed polyethylene process (U.S. patent 2256483).[68]

These foams are generally produced by the expansion method which relies on expansion of a gaseous phase dispersed throughout the polymer melt that can be generated through the separation of a dissolved gas, vaporization of a volatile liquid, or release of gas from a chemical reaction. Regardless of gaseous phase type, also known as a blowing agent, the

expansion process comprises three major steps: nucleation, bubble growth, and stabilization. Nucleation or formation of expandable bubbles can begin within the polymer melt that has been supersaturated with the blowing agent. Once nucleated, a bubble continues to grow as the blowing agent diffuses into it. This growth will continue until the bubble stabilizes or ruptures. When cells are nucleated, the foam density decreases as the available gas molecules diffuse into the cells. The growth rate of cells is limited by the diffusion rate and stiffness of the viscoelastic properties/gas solution. As can be inferred, the rheological properties of the polymer/gas solution, diffusivity and solubility of the blowing agents are of critical importance for the foam production process development.

2.3.1 Bubble Nucleation

Polymer foams are commonly produced by expanding a supersaturated solution of gas in a polymer melt, where at a microscopic level, thermodynamic fluctuations produce clusters of gas molecules that subsequently grow or decay, depending upon whether their size was greater than a critical cluster size.[69] The phenomenon associated with the appearance of supercritical clusters is known as nucleation. Origins of a homogeneous nucleation theory can be found in the works of Gibbs[70] but numerous researchers continued its development and have included hydrodynamic and transport effects.[71] Blander and Katz[72] proposed an extension of their homogeneous nucleation model to heterogeneous nucleation. According to Gibbs,[70] a gas cluster containing n molecules, C, can be expressed as follows:

$$C(n) = Ne^{(-W(n)/kT)} \qquad \textbf{2.33}$$

where W(n) is the minimum work to sustain a bubble, N is the number of molecules per unit volume of the metastable state, and k and T are the Boltzmann constant and absolute temperature, respectively. By multiplying a frequency factor, B, the rate of nucleation can be expressed as follows:

$$J = B \cdot Ne^{(-W(n)/kT)} \qquad 2.44$$

where B is a frequency factor , N is the number of molecules per unit volume of the metastable state, W is the minimum work to get a sustainable bubble, k is the Boltzmann constant a T is the absolute temperature.

2.3.2 Bubble Growth

Bubble growth is like cell nucleation and coalescence of great importance for foaming. Historically, the models have evolved from single bubble growth models, which focused on the growth or collapse of a single bubble surrounded by an infinite sea of fluid and amount of gas available for growth to cell models. Unlike the single bubble, these account for simultaneous bubble nucleation and growth, as well as gas loss, plasticization and also, non-isothermal processes in the most sophisticated models. Due to the complexity of this subject it will not be developed here but can be found elsewhere.[8, 73] Two works worth noting are the studies from Flumerfelt et al.[69, 74] and Ramesh et al.[75]; the first proposed a model that combines nucleation and foam growth to study the effects of operating conditions on bubble growth dynamics in polymeric foams. Also, Ramesh et al.[75] that were pioneer in including, gas loss, concentrated dependent diffusion coefficient, polymer plasticization as well as temperature effects on viscosity, diffusivity and blowing agent pressure.

2.3.3 Rheology of Gas Charged Polymeric Systems

The production of thermoplastic foams is naturally linked to the rheology of the gas-polymer solution. While prior to expansion or foaming shear rheology is dominant in the ultimate stage extensional rheology is of prime importance being this knowledge necessary to develop new foams and optimise processing conditions as not all gas-polymer combinations have the

same behaviour. One aspect is that the dissolved gas has a plasticizing effect that is reflected on the processing temperature, torque on the machine and throughput, and another is that this knowledge is essential for flow simulation and use in computer assisted design software. Since not all resins are suitable for foaming, a clear understanding in terms of rheological behaviour should help design new resins and determine their influence in cellular morphology.

The measurement of rheological properties of gas-charged polymer melts cannot be accomplished with a standard rheology laboratory because it requires a pressurized system to prevent degassing. For these determinations modified apparatus and different protocols have to be used. Han et al.[76] in one study to evaluate the feasibility of determining rheological properties of gas-charged polymers verified using and extruder fitted with a cylindrical die and several pressure transducers compared the pressure profile along the die of a HDPE melt with and without a blowing agent and found that the pressure drop is not linear in the last case, which can be attributed to nucleation. The results are show in Figure 2-19.

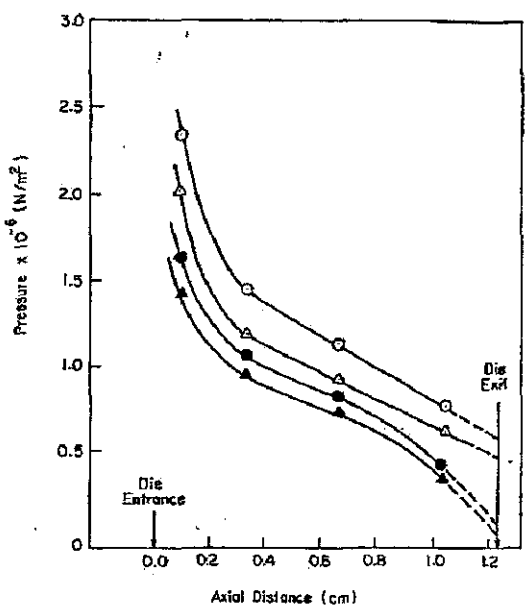

Figure 2-19 - Axial pressure profiles of HDPE (T=200°C) in extrusion through a cylindrical die, without (open symbols) and with a blowing agent (closed systems), at various apparent shear rates: (⊙,●)337.8 s^{-1}, (△,▲)249.2 s^{-1}.[77]

In such a case the expressions usually used in rheology no longer apply, and more, the problem can no longer be seen as a single phase-flow. However, the pressure profile problem was found to be correctable with a sufficiently long capillary or slit die and sufficiently high volumetric flow rates. Figure 2-19 also shows a lower pressure for the gas-polymer solutions, a typical result in these systems the gas induces plasticization of the polymer. Han and Villamizar[76] reported viscosities of gas-charged molten polymers using chemical blowing agents with PS and HDPE and it was found that for both systems, the gas-charged system had a lower apparent viscosity than the polymer alone and also verified that apparent shear viscosity decreased with increasing temperature.

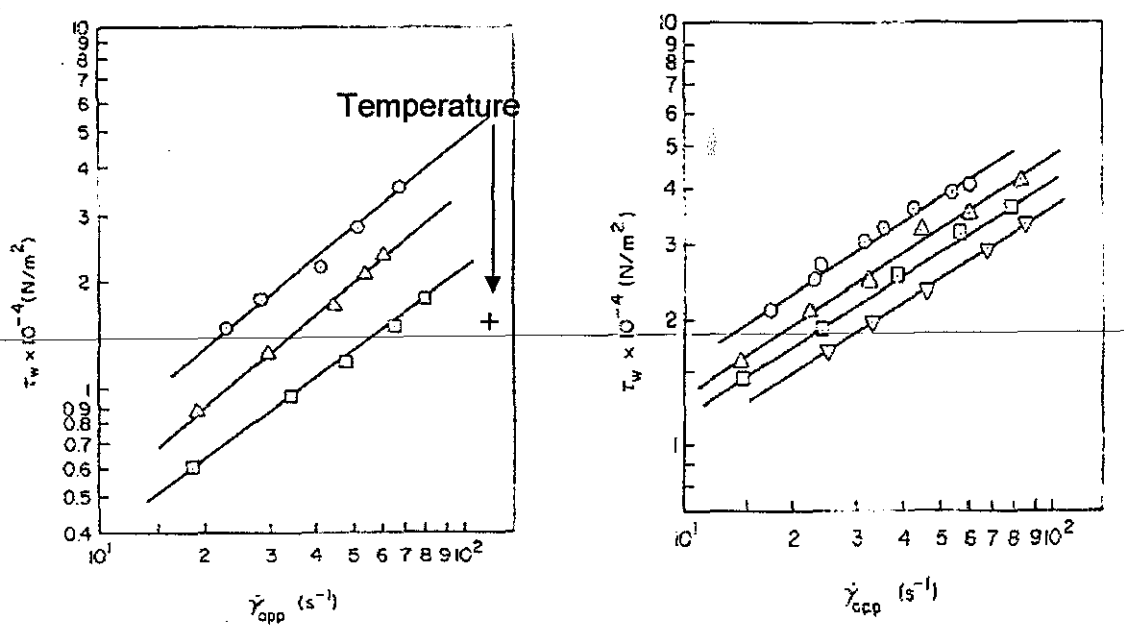

Figure 2-20 - Shear stress versus apparent shear rate for HDPE containing 0.8 wt% chemical blowing agent, at various temperature, 180, 220, 260°C (left). Shear stress vs. apparent shear rate for PS (200°C) without blowing agent (top line), and containing 0.2%, 0.4% and 0.8% (downwards).[78]

In a subsequent studied Han and MA studied the viscosities of LDPE with fluorocarbon blowing agent obtaining the same behaviour of the previous systems.[78]

During foaming, as bubbles grow, extensional flow plays an important role, biaxial stretching being the main mode of deformation. The gas comes out of solution very quickly so that we can assume that its concentration has rapidly dropped to zero, thus the extensional deformation is applied to the neat polymer. Even though biaxial stretching is the main mode of deformation most studies report on uniaxial extension due to technical difficulties associated with measuring biaxial deformations.

Strain-hardening is a characteristic associated with the foamability of a resin that is not present in linear polyolefins but is exhibited by polystyrene and LDPE, being defined as an increased extensional viscosity at higher extensional strains, well above the linear viscoelastic curve, as is exemplified in the next figure.

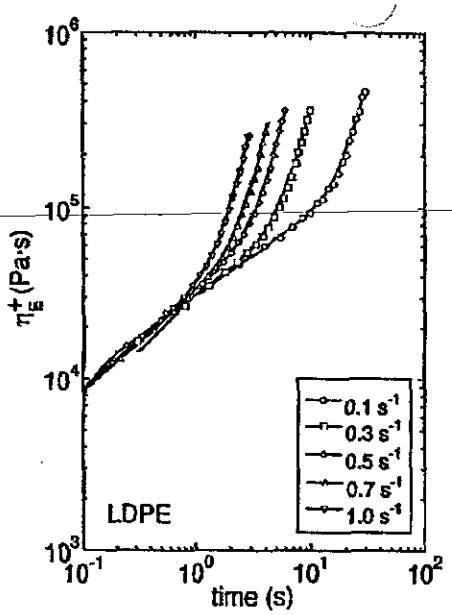

Figure 2-21– Typical stress growth functions at 200°C for a branched polyethylene, LDPE.[8]

This behaviour is generally associated to the inability of macromolecules to disentangle quickly enough after a sudden deformation. Causes to this phenomenon have been linked to long-chain branching, polydispersity and bimodality of MWD. In the case of polystyrene SH is thought to be related to the π-π interactions between aromatic rings.

The initial growth of the bubbles requires an initial low viscosity, but subsequently it is advantageous to have a high extensional viscosity to prevent cell collapse, which is a frequent event with linear polyolefins. To overcome these difficulties research has been attempted to increase the melt strength of the resins.

Polypropylene was until quite recently a very difficult polymer to foam due to its narrow processing window and low melt strength, but when the technology to insert chain-branching in PP was developed it became possible to have high melt strength (HMS) resin with strain-hardening behaviour suitable for foaming. Common strategies to increase melt strength can be blending of polymers and compatibilisation of blends, crosslinking or control of molecular weight and molecular weight distribution.[79]

Recently, Naguib et al.[80] studied the effect of blending branched and linear polypropylene on foamability. Increasing the content of branched high melt strength raised the blends melt strength and extensibility which consequently gave rise to a higher expansion ratio. However, it was pointed out that proper dispersion may not be achieved in a foaming extruder and that severe mixing may cause disentanglement of branched molecules. Yamaguchi and Suzuki[81] studied the effect of blending crosslinked LLDPE on the foam processability of LLDPE, and verified that the addition of a small quantity of LLDPE with a low density of crosslinked points enhanced the strain-hardening behaviour in the elongational viscosity to a great degree which can be seen in Figure 2-212 though having little effect on the shear viscosity, which in the foaming trials produced then a better foam.

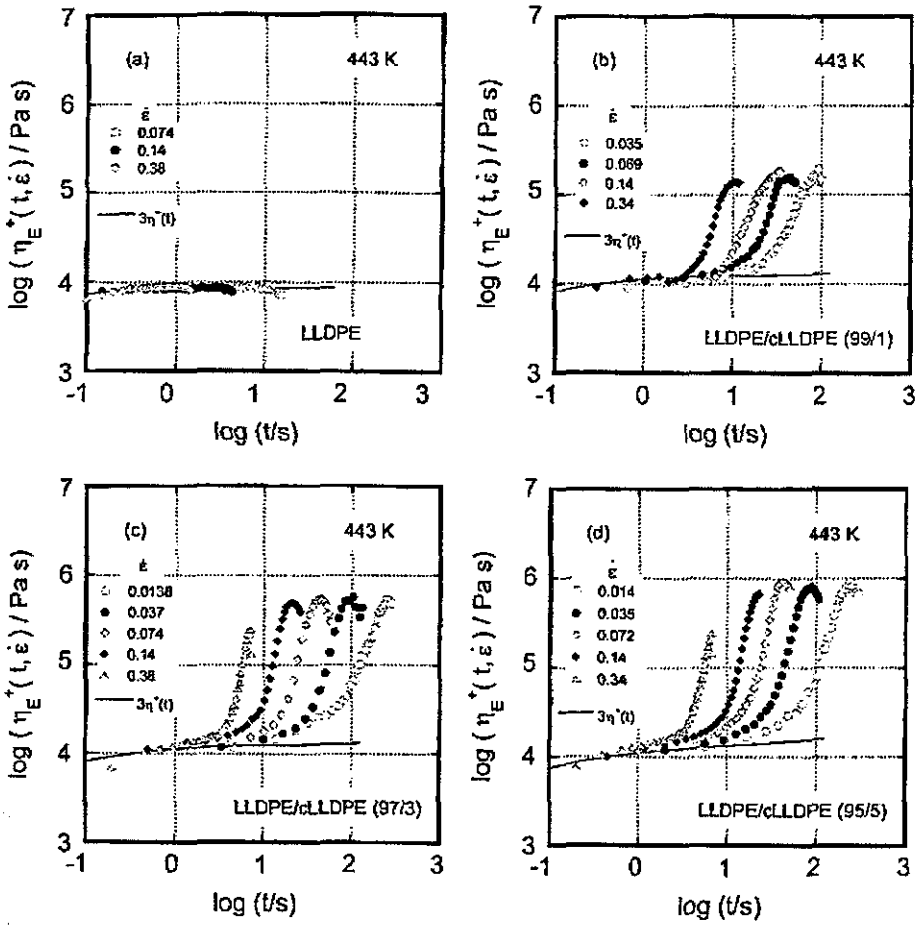

Figure 2-212 - Growth curves of $\eta_E^+(t,\varepsilon)$ at various values of $\dot{\varepsilon}$ at 443K for (a) LLDPE, (b) 99/1 LLDPE-crosslinked LLDPE (cLLDPE), (c) 97/3 LLDPE/cLLDPE and (d) 95/5 LLDPE/cLLDPE.[81]

Other blends that proved successful were blends of ionomers as suggested by Yang and Lee,[82] where an optimum quantity of ionomer that can be incorporated in the blend was identified. In contrast with branched/linear PE blends, blends of either linear/linear or branched/branched PE do not show strain-hardening effects. For melt strength synergism, a mixture of linear and branched species of similar molecular weights may therefore be required.[81] Typically, for resins having the same MI, the melt strength will follow that order: linear HDPE or LLDPE< tubular LDPE, vessel LDPE.

2.3.4 Chemical Blowing Agents

Chemical blowing agents are substances which are sufficiently stable to be incorporated into a polymer under normal process mixing conditions, but which subsequently, at higher temperatures decompose to produce a gas, which emerges from the solution and expands the polymer. The blowing agent choice is determined by the process temperature, the required amount of gas evolution, the decomposition rate and the influence on the process of the exotherm/endotherm of decomposition. A few examples of commercially available chemical blowing agents and their characteristics are shown in Table 2-3.

Name of blowing agent	Endo or Exo	Decomposition Temperature,°C	Gas evolution cm^3/g	Main gas evolved
Citric acid/ sodium bicarbonate	Endo	160-210	120	CO_2
Azodicarbonate	Exo	205-212	220	N_2
Azodicarbonamide	Exo	205-215	220	N_2

Table 2-3 – Commercially used chemical blowing agents.

The blend of citric acid and sodium bicarbonate is also a commonly used formulation whose ratio can be changed to alter the decomposition temperature range.

$$C_6H_8O_7 + 3NaHCO_3 \rightarrow C_6H_5Na_3O_7 \cdot 2(H_2O) + 3CO_2 + H_2O$$

The reaction takes place in two temperature ranges, one at about 160°C and the second at about 210°C, and the gas yield 120 cm^3/g.[5] Carbon dioxide producing CBAs give generally finer cells, lower densities, better surface appearance and easier to control than the one's liberating nitrogen. Additionally, is more soluble and has a lower vapour pressure than nitrogen.

2.3.5 Foam Morphology Development

A foam final cellular structure and density, the two main properties, are dependent on several parameters (not all independent) which make its optimisation a difficult task. The morphology of a polymeric foam is intimately related to the process conditions, blowing agent and the resin, whose combination dictates the foam's final cellular structure and density. The basic approach to foam production is to form a polymer/gas solution, to nucleate a large number of bubbles using thermodynamic instability via pressure drop, to suppress cell coalescence by increasing the melt strength, and to induce a volume expansion to a desired expansion ratio. The quantity of gas used in a certain polymer melt depends on its solubility as the use of an excess amount of gas would result in undesirable voids. The existence of voids suppresses homogeneous nucleation because the gas molecules preferentially diffuse to larger cells, resulting in formation of hollow cavities in the final product.

A crucial step is then bubble nucleation which is promoted by thermodynamic instability induced by varying the pressure or temperature, or both, being the most common way to nucleate a polymer/gas solution with a pressure drop that almost instantly reduces the gas solubility. Subsequently, it is necessary control the growth of the bubbles and to avoid cell collapse or coalescence. These steps are now going to be reviewed.

2.3.5.1 Polymer-Gas Solutions

The first step in foaming is the formation of single-phase gas-polymer solution, where we need to consider the solubility and diffusion of the gas in the polymer melt, therefore an estimate of those parameters are crucial. Diffusion of gases in the polymer melts is a slow process, thus it is necessary to enhance the diffusion to form rapidly that solution. Park[83] has analysed this problem in an extrusion barrel and suggested the use of laminar mixing in the molten polymer shear field, and assuming that in typical extrusion

processes striation thickness happens, he estimated the diffusion time by deriving an expression relating it to the striation thickness, which can be estimated by the dispersive mixing theory.

$$t_D \approx \frac{s^2}{D} \qquad 2.55$$

where s is the striation thickness and D the diffusivity.

Striation Thicknesses	Diffusivity (D)			
	10^{-5} cm^2/s	10^{-6} cm^2/s	10^{-7} cm^2/s	10^{-8} cm^2/s
1μm	0.001 s	0.01 s	0.1 s	1 s
10μm	0.1 s	1 s	10 sec	100 s
50μm	2.5 s	25 s	4 min	42 min
100μm	10 s	100 s	17 min	3 hrs
250μm	63 s	10 min	2 hrs	17 hrs
500μm	4 min	42 min	7 hrs	3 days
750μm	9 min	94 min	16 hrs	7 days
1000μm	17 min	3 hrs	28 hrs	12 days

Table 2-4 – Estimated diffusion times at various striation thicknesses and diffusivities.[8]

The gas solubility is also very important as an excess of gas will result in the formation of undesirable voids in the melt, lowering the performance of the foam. A factor that influences the gas solubility is the polymers crystallinity as it doesn't dissolve in the crystallites, leading then to a non-uniform polymer/gas solution. This effect has been investigated by Doroudiani et al.[84] that found a strong influence of the crystallinity on the foam processing and structure, where increased crystallinity reduced not only solubility but diffusivity as well which had consequences in the following processing stages.

	Solubility (mg/g)	CO_2 Diffusivity (cm^2/s) 10^8	Crystallinity (%)
HDPE1	17.5	44.2	55.9
HDPE2	16.3	16.6	62.8
HDPE3	11.9	8.7	70.4

Table 2-5 - Solubility and diffusivity of CO_2 in HDPE with different crystallinities. (adapted from Doroudiani et al).[84]

2.3.5.2 Nucleation Control

The next critical step is to promote a high bubble nucleation rate by the use thermodynamic instability of the gas and polymer system, which is commonly a pressure drop, the nucleation is influenced by several parameters that are going to be explained.

2.3.5.2.1 Effect of pressure drop rate on nucleation

As the homogeneous nucleation theory[85] predicts that the cell nucleation rate increases with the pressure drop one would think that designing a die for a larger pressure drop would yield the best nucleation rate. If we assume that the pressure drop is instantaneous this is true, however, in reality pressure drop is not instantaneous but varies with distance and position within the die. Therefore it is expected that the nucleation depends on the time period over which the polymer-gas solution suffers from the thermodynamic instability, in other words, the pressure drop rate will affect the nucleation time. This can be understood in terms of a competition between cell growth and nucleation.[79]

The influence of the pressure drop rate has been studied by Park[86] and more recently by Xu et al.[87] They used a set of dies which were designed to have either different pressure drop rates while having identical die pressures and flow rates, or different die pressures while having identical pressure drop rates. It was proved that regardless of the amounts of nucleating agent and blowing agent, the cell-density was significantly improved by applying a die with a high-pressure-drop-rate geometry, which clearly indicates that a large thermodynamic instability induced by a large-pressure-drop-rate is a critical factor affecting cell nucleation. Some of those results can be seen in Figure 2-22. This result is in agreement with Park's previous work,[86] however, the experiments were slightly different because they are conducted only with a constant amount of blowing agent. Thus, the effect of blowing agent on nucleation at various pressures and pressure drop-rates wasn't determined.

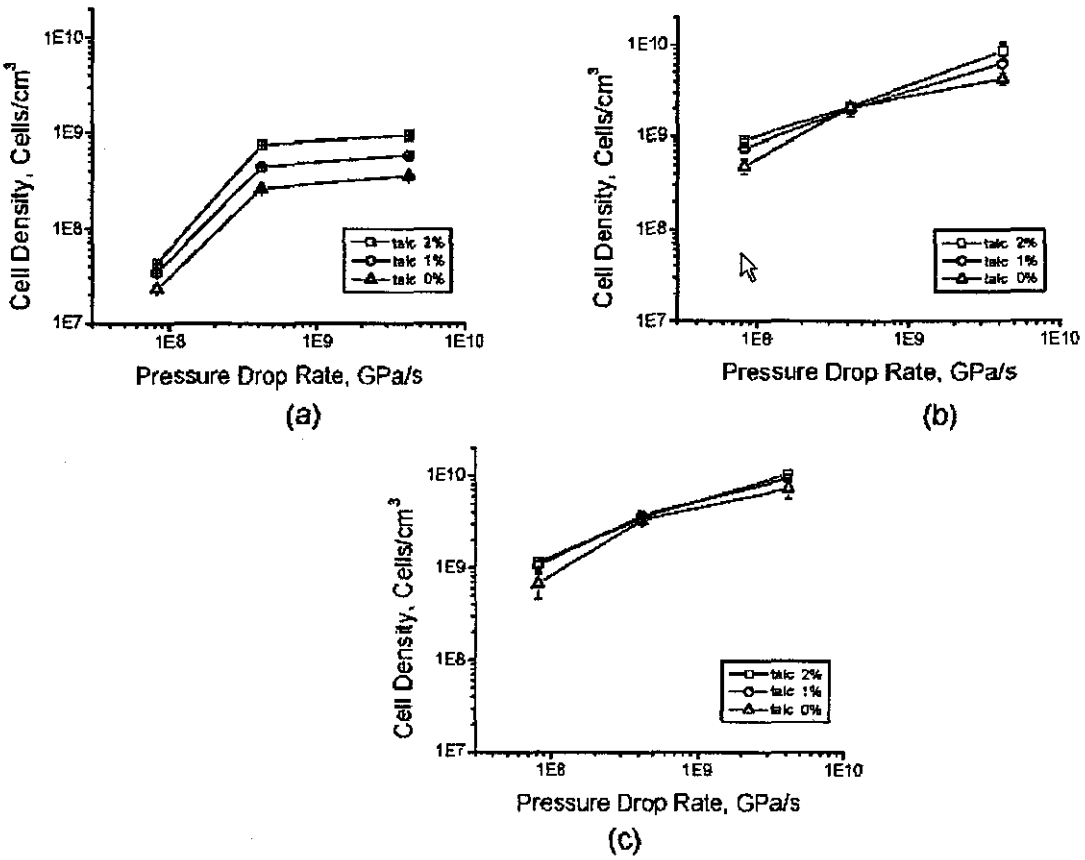

Figure 2-22 - Comparison of cell densities obtained at different die pressure drop rates while varying the fixed CO_2 content, (a) 2% CO_2, (b) 5% CO_2, and (c) 10% CO_2.[87]

2.3.5.2.2 Effect of gases on cell nucleation

This effect has been studied by Park and Suh[83] by injecting the maximum estimated soluble amount of CO_2 and N_2 in PP and HIPS, being injected approximately 10 wt% of CO_2 and 2 wt% of N_2 in each melt. The higher cell densities obtained with CO_2 in each polymer seems to be related to a higher solubility and, therefore induce a greater thermodynamic instability and, thereby, a higher cell density as can be seen in Table 2-6.

Polymer	Cell Density	
	CO_2	N_2
PP	6×10^8 cell/cm^3	3×10^7 cell/cm^3
HIPS	8×10^9 cell/cm^3	9×10^7 cell/cm^3

Table 2-6 – Variation of cell density with blowing agent.[83]

Gendron et al.[88] have also reported a similar result PS with HCF-134a and CO_2 higher cell density as it has a higher solubility. The effect of the amount of gas was also studied by Park.[86] In these experiments, the processing pressure was maintained at 27.6 MPa, while the injected gas amount was varied. When 1 wt%, 5 wt% and 10 wt% CO_2 were used to foam HIPS the cell densities were 10^7 cell/cm^3, 4×10^8 cell/cm^3, and 6×10^9 cell/cm^3, respectively. For this processing pressure, 10 wt% is the maximum soluble quantity of CO_2.

2.3.5.2.3 Effect of processing pressure on cell nucleation

Park and Suh[89] proved the relationship between the processing pressure and cell nucleation. In their experiments, the maximum soluble amount of gas was injected into the HIPS melt at each processing pressure, ranging from 5.4-28.3 MPa, having obtained respectively greater cell densities as can be seen in Figure 2-23.

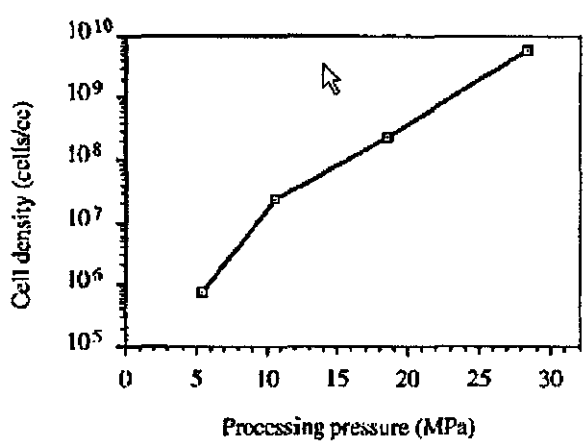

Figure 2-23 - Effect of the processing pressure on the cell density of extruded HIPS.[89]

This result is predictable, since the solubility of gas is approximately proportional to the processing pressure, more gas could dissolve at higher pressures and thus induce a greater thermodynamic instability and higher cell density.

2.3.5.2.4 Effect of Nucleating Agents

In polymer foam processing nucleating agents are usually added to control the foam quality and morphology: small cell sizes and narrower cell size distributions. Good nucleating agents are associated with their ability to increase nucleation rates by inducing heterogeneous nucleation over homogeneous nucleation.[90] Common nucleating agents are talc or calcium carbonate. Several authors have studied the influence of nucleating agents on foaming and cell nucleation[85, 87, 90, 91] and it was found that their effectiveness depends on concentration and particle size.

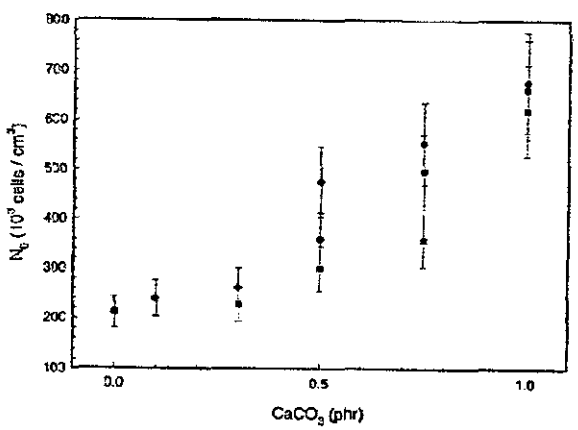

Figure 2-24 - Nucleation density as function of the nucleating agent ($CaCO_3$) concentration and particle diameter for 0.5 phr ACA. ♦:3μm, •:10μm, ■:17μm.[90]

Recently, Rodrigue and Gosselin[92] proposed a new descriptor for comparing nucleating agents, the total available surface area per unit volume that takes into account not only the size and concentration, but also the surface characteristics of the nucleating agent via its specific surface area. With this new parameter it is expected to develop a correlation with cell density so that in the future we could use it in foam design to choose a particle concentration or size to achieve a certain nucleation density. Chemical blowing agents are commonly used as "nucleating agents" when foaming with physical blowing agents to promote heterogeneous nucleation. Nucleating agents are usually used in small quantities, most of the time under 2 wt%, as an excess quantity can in fact produce cell collapse through over-nucleation.[91]

2.3.5.2.5 Shear Stress Nucleation

Shear stress has also been proved to exert some influence in cell nucleation, especially at low gas levels where this effect is believed to be dominant over the pressure drop or pressure drop rate as reported by Chen et al.,[93] Lee[8] and Han[94] have also attributed some of their results from bubble nucleation works to shear stress. Lee and Biesenberger[95] developed the concept of shear nucleation when they discovered that during foam-enhanced devolatilization when the solvent level is slow it is necessary to introduce deformation to achieve foaming. A concept that can easily be linked to bubble formation through the cavitation model,[96] proposing that the presence of shear stress can help to pull the gas phase out of the solid cavities provided by the nucleating agent. The shear force should act as a "catalyst" to lower the energy barrier between the stable gas cavity and unstable bubble phase, helping to explain why in practice that supersaturation is not a sufficient condition for observing bubble nucleation, this phenomenon occurs more readily when exposed to a shear field. Lee[97] in a different study concluded again that shear stress induces nucleation but the corresponding shear thinning reduces the skin melt strength limiting skin expansion in foam extrusion. Han[78] had suggested that bubble nucleation may be induced by flow, which would be the primary mechanism near the centre of the flow, and by shear stress, for positions near the die wall.

Xu et al.[87] have recently supported Han's view as the experimental results confirm that the fast-flowing core region is nucleated by the high-pressure drop rate whereas the slow-flowing surface region is nucleated by shear action.

2.3.5.3 Suppression of cell coalescence

Just after cell nucleation starts there are a few bubbles that start to grow by diffusion of gas inside the bubbles and some will be stretched, increasing the probability under shear fields of growing bubbles to touch each other and coalesce, deteriorating the initial cell density. Thus it is important to control cell coalescence. In order to prevent cell coalesce it has been proposed to increase the melt strength.[79] The melt strength may be defined as the degree of resistance to the extensional flow of the cell wall during the drainage of polymer when volume expansion takes place. Therefore the cell wall stability increases as the melt strength increases. This can be enhanced by branching, crosslinking, temperature reduction, control of molecular weight and molecular weight distribution, and blending of polymers and compatibilisation of blends.[79] The melt temperature reduction has been successfully used both in conventional and microcellular foaming to increase the melt strength even in polymers like HDPE, with high crystallinity, no strain-hardening and low-solubility blowing agents as CO_2, and considered difficult to foam. To foam PP more effectively a new resin with long-chain branching strain-hardening behaviour had to be developed.[98] However these resins are very expensive, and Naguib et al.[80] blended branched and linear polypropylene and foamed it, being successful in reducing cell coalescence, giving the blend higher melt strength and melt extensibility.

Yamaguchi et al.[81] improved the foamability of LLDPE by incorporating a small quantity of crosslinked LLDPE, which introduced strain-hardening behaviour, and consequently produced foam without cell coalescence and a good cellular structure.

2.3.5.4 Volume Expansion Control

The last critical step in foam production is the control of expansion to achieve the right density. By this time cells are growing with gas diffusion into the cells but at the same time some fully grown cells are experiencing diffusion of

gas from the cell through the thin cell walls out to the atmosphere, because complete separation of the two phases is thermodynamically more favourable,[8] and ultimately leaving less gas available for cell growth.

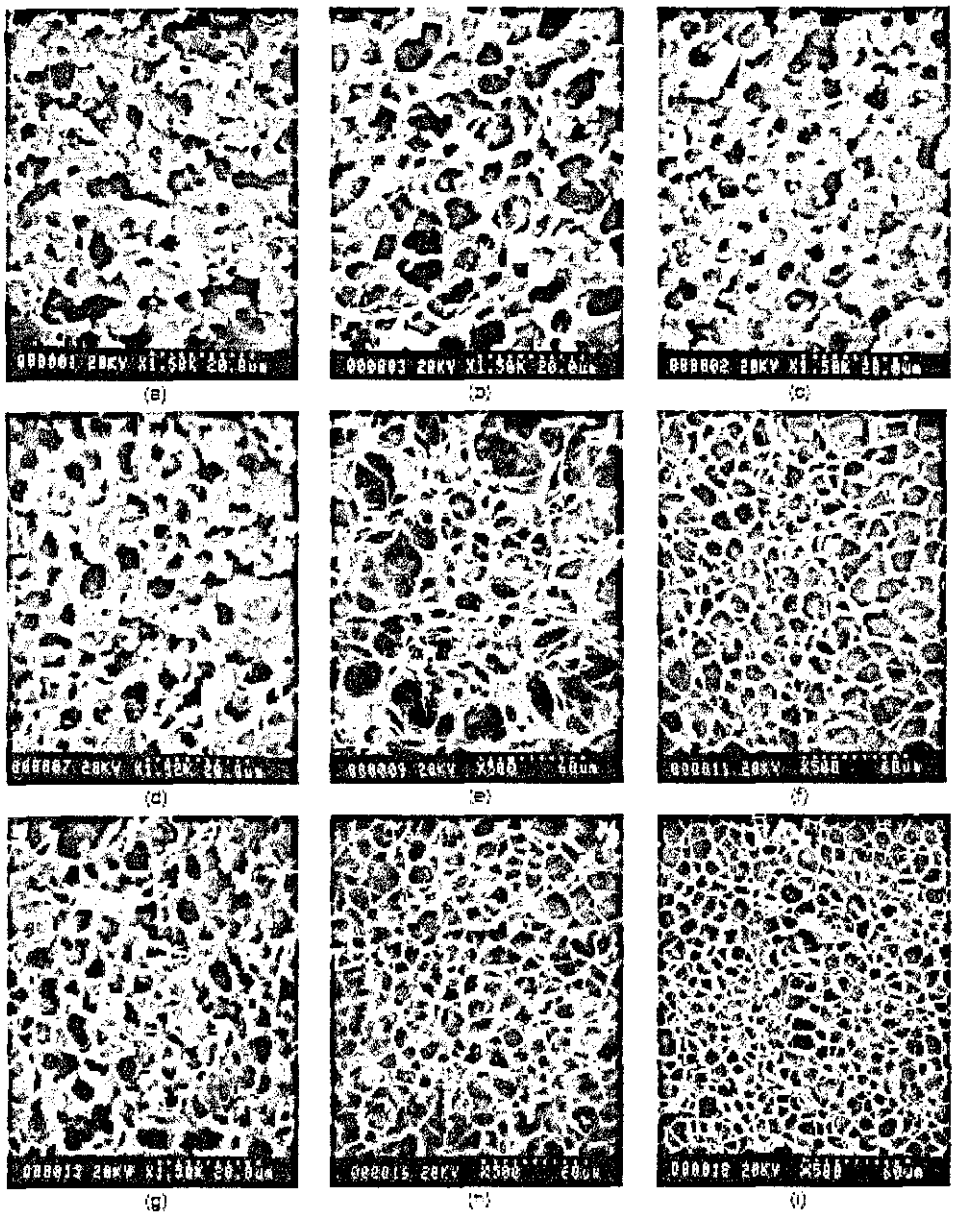

Figure 2-25 – Microstructure of HIPS foams at various melt temperatures (Tm) and die temperatures (Td). a) Tm=170°C, Td=175°C b) Tm=170°C, Td=135°C c) Tm=170°C, Td=110°C d) Tm=150°C, Td=175°C e) Tm=150°C, Td=135°C f) Tm=150°C, Td=110°C g) Tm=120°C, Td=175°C h) Tm=120°C, Td=135°C i) Tm=120°C, Td=110°C.[79]

Therefore if cells are not stabilised, they tend to collapse causing foam contraction, and the final product has a higher density, thus this gas loss should be prevented. Again, with an adequate temperature we freeze the skin preventing further gas loss to the atmosphere s the diffusivity decreases,

which can be achieved by controlling the die temperature closely. In Figure 2-25 the effect of die temperature and melt temperature in preventing cell coalescence can be seen. When the die temperature is too high there is cell coalescence which is reduced as soon as the die temperature is lowered, however, to achieve a nice cellular structure the temperature difference between the melt and the die has to be reduced so that the desired volume expansion is obtained.

2.3.5.5 Foaming Mechanisms in Volume Expansion

Two mechanisms have been proposed for volume expansion of polymer melts which are dependant on melt and die temperature to explain the observations by Behravesh et al.[79] and Naguib et al.[99] This is depicted by Figure 2-26

While studying HIPs and PP they found that the extrudate shape varied according to the processing temperature. While at a low temperature the expansion ratio was not very large but the cellular structure was uniform with small cell, later as the temperature was raised a point was reached where just outside the die there was a very large expansion that then was contracted with cell coalescence leading to a high density foam. This was explained based on a gas loss mechanism that is predominant at high temperatures and a freezing mechanism at lower temperatures.

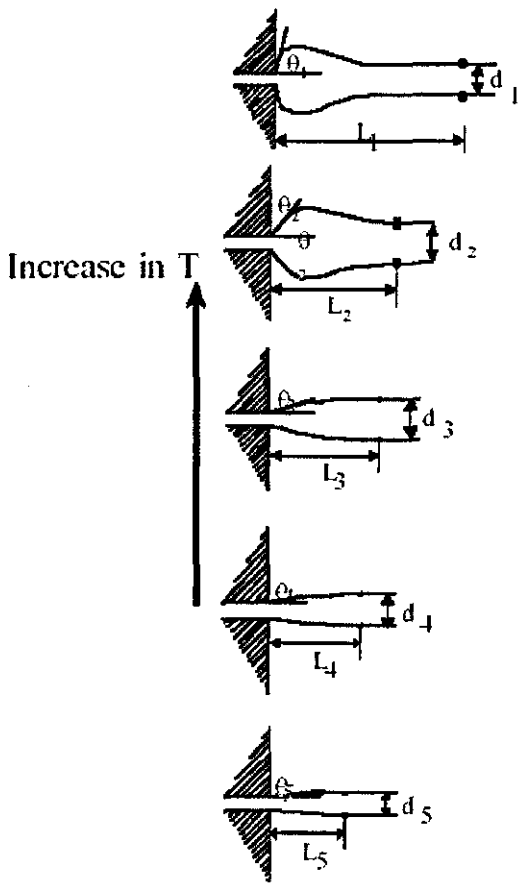

Figure 2-26 - Effect of processing temperature on extrudate shape.[99]

The freezing mechanism can be understood on the basis that when the temperature is low the skin freezes preventing any gas loss, and in case this freezing is premature, i.e. the temperature is too low, it does not allow bubbles to grow and a fine cellular structure is obtained.

If the gas loss mechanism is dominant, then the melt temperature is higher then the optimum expansion temperature and with an increased temperature the diffusivity of the gas is high enough to escape to the atmosphere, lowering the gas available for bubble growth, even before the foam solidifies leading to a contraction.

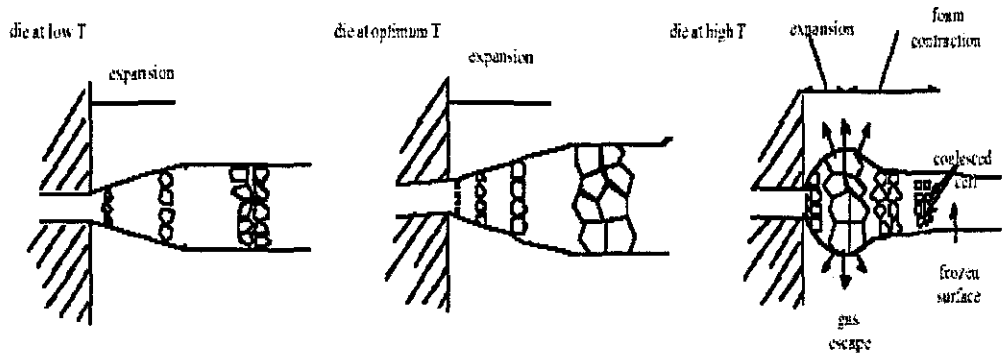

Figure 2-27 – Effect of gas loss and freezing on volume expansion.[99]

However a different foaming mechanism can be found if moisture, that is insoluble, is found in the resin instead of only the blowing agent. When a foam structure is developed at the die exit, the volume expansion attributed to moisture occurs promptly because moisture evaporates immediately at a lowered pressure. These vapours permeate easily through the cell walls or simply rupture them and are lost.

2.3.6 Foaming Polyolefin Blends and Nanocomposites

Foaming blends can be another way of incorporating new properties in foams as it has been made with the resins. Though this is recognized, and it is expected that blends should produce good foams not only because of the resin's properties since it is most of the times a multiphase system of immiscible polymers with heterogeneous interface that should favour a lower activation energy for bubble nucleation and lower crystallinity, not much work has been published despite some good results. In one of those studies Doroudiani et al.[12] foamed a blend of HDPE and isotactic polypropylene (iPP) with improved properties relative to the non-foamed blend. Non-uniformity was observed in the foamed blend when the iPP content was raised to 50 wt%, but below that quantity much finer and more uniform foams that the neat HDPE and iPP were obtained.

Park[100] has produced a high service temperature blend of low-density polyethylene and a syndiotactic polypropylene (sPP) resin, which can replace

equivalent crosslinked foams that are most costly and non recyclable, but used a different approach from Doroudian et al.[12] that had a more difficult blend to foam, since their foam stabilization relied on the freezing transition of the high meting point component that had poor foamability, when using the sPP. Here, as the sPP could stay amorphous in the foam extrusion line at the foaming temperature of the LDPE thereby not interfering with foaming, and undergo crystallization after that allowing the blend foam to withstand a relatively high temperature.

As with foaming polyolefin blends very little work is known on nanocomposite foams, two exceptions are the recent works from Nam et al.[17] and Zeng et al.[18] As mentioned in earlier sections, cell nucleation and growth are two important factor controlling foam morphology, which can be influenced by particles such as nucleation agents to improve heterogeneous nucleation. Fine particles such as nanoclays, intercalated or exfoliated in the polymer melt could also affect the morphology development. Most interesting, Nam et al.[17] showed that a strain-hardening effect had been found in PP/clay intercalated nanocomposites making them possibly suitable for foaming. In a subsequent study, polypropylene-clay nanocomposites were actually produced in a batch process with a very uniform cellular structure and densities ranging 50-300 kg/m^3. Zeng et al.[18] prepared exfoliated and intercalated PS/clay nanocomposites that were batch foamed with CO_2, and the effect of clay dispersion and concentration was investigated. It was found that the cell size is greatly reduced, and the cell density is increased, by adding a small amount of clay. The exfoliated nanocomposite foam provides the highest density and the lowest cell size. For exfoliated nanocomposite foams, a higher clay concentration seems only to improve cell density.

3 Experimental

This chapter describes the raw materials and experimental techniques used throughout the presented work. It will focus on the description and characterization of the raw materials and preparation of the new blends and compounds, followed by rheological characterisation techniques. It explains how flow simulation software was used to model and study the flow behaviour of polymer in a capillary rheometer. An account of the foaming experiments using a capillary rheometer is also included.

3.1 Raw Materials

Three classes of materials were included in this study, namely polymers, both recycled and virgin, a montmorillonite modified organoclay and a chemical blowing agent. A full description follows.

3.1.1 Recycled Polymers

The three different types of recycled polymer used in this work, specifically, HDPE, LDPE and PP, were supplied by Plastics Reclamation Ltd. (PRL) and Centriforce as described in Table 3-1. Originated from municipal post-consumer waste, they are typical low MFI grades suitable for extrusion and foaming processes and were fully characterised as described in chapter 4. The materials were supplied in a granular form in a range of colours, shapes, sizes and bulk densities. The pellet shapes varied between cylindrical, round or flattened, and the colours were typically, white, grey or black. Polypropylene was however transparent. HDPE batches had a characteristic odour that could be associated to detergent products. The other polymers didn't seem to have any distinctive smell.

Code	Supplier	Type	Form
PR-HD1	PRL	HDPE	pellet
PR-HD2	PRL	HDPE	pellet
PR-HD3	PRL	HDPE	pellet
PR-HD4	Centriforce	HDPE	pellet
PR-LD1	PRL	LDPE	pellet
PR-LD2	PRL	LDPE	Pellet
PR-LD3	PRL	LDPE	Pellet
PR-PP1	PRL	PP	Pellet

Table 3-1 – Supplier recycled polymers.

3.1.2 Commercial Virgin Polymers

Commercially available polymers were used in this work for two different purposes. Some of them were used as control samples for the recycled polymers for which it was decided to opt for polymers with melt flow indexes as close as possible to those of the recycled ones. Others were used as compatibilisers in blend or nanocomposite systems.

Eltex 6007XA, a HDPE grade particularly suitable for bottle blow moulding was selected because detergent and milk bottles are the main constituents of the HDPE waste stream. The LDPE's in the waste stream were sought to come from film applications therefore Exxon Mobil LD150BW was selected. HMS Daploy, a high melt strength polypropylene, is a branched polypropylene specifically designed for foaming applications, and was used in this work as a control sample in terms of extensional flow behaviour and as a blend component to improve foamability.

To compatibilise the blend systems studied, Adflex Q 100F and Buna EP T2600, that possess both polyethylene and polypropylene functions, were chosen due to their different natures and specificities. Adflex Q 100F is a thermoplastic polyolefin, which has been developed for the extrusion of blown film. Buna EP T2600 is an ethylene-propylene rubber also suitable for

extrusion applications. For the preparation of polyolefin montmorillonite nanocomposites a suitable maleic anhydride grafted resin needs to be present to improve the miscibility of the mineral and polymeric phase. Polybond resins are adequate for this purpose, carrying usually 1% of the maleic anhydride function grafted to polyethylene or polypropylene.

Code	Commercial name	Supplier	Polymer	Type	Form
PE-HD1	Eltex-Rigidex 6007XA	BP Solvay	HDPE	homopolymer	Pellet
PE-LD1	LD150BW	Exxon Mobil	LDPE	homopolymer	Pellet
PO-PP1	HMS Daploy	Borealis	PP	homopolymer	Pellet
EP1	Adflex Q100F	Basel	PP/PE	copolymer	Pellet
EPR1	Buna T	Bayer	EPR		Bale
PB1	Polybond 3009	Crompton	HDPE-g-MAH	homopolymer	Pellet

Table 3-2 – Commercially available polymers.

3.1.3 Nanoclay

Several kinds of organically modified nanoclays of which montmorillonite is one of the most common, are currently commercially available. The clay used in this work is a modified organoclay trade named Cloisite 15A (Southern Clay, USA) consisting of montmorillonite intercalated by a quaternary ammonium salt, whose dual hidrogenotallow chains render the clay gallery more hydrophobic and more likely to be penetrated by polyethylene and polypropylene chains, thus facilitating intercalation. The hydrogenated tallow typically consists of ~65% C18; ~30% C16; ~5% C14 and the anion present in the salt is chloride. The silicate platelets in Cloisite are 1 nanometre (nm) thick and 70-150 nanometres across.

	Clay Empirical Formula	Organic Modifier	Modifier Concentration
Cloisite 15A	$Na_{0.2}Ca_{0.1}Al_2Si_4O_{10}(OH)_2(H_2O)_{10}$	$CH_3-\underset{\displaystyle HT}{\overset{\displaystyle CH_3}{\overset{\displaystyle \vert}{\underset{\displaystyle \vert}{N^+}}}}-HT$	125 meq/100g clay

Table 3-3 – Typical properties of Cloisite 15A.

3.1.4 Chemical blowing agents

The chemical blowing agent (CBA) used in this study was an endothermic formulation commercially available under the name of Hydrocerol BM70 (Clariant) and supplied as a masterbatch with LDPE as a carrier. Specifically designed for HDPE it can also be used for LDPE and PP. This kind of CBA has an onset decomposition temperature of 150°C.

3.2 Characterisation techniques

The identification and characterisation procedures used for the supplied and prepared materials involved a large number of techniques that are described in this section. They include spectroscopic, thermal and microscopic methods, and were intended to identify the polymers, fillers and morphological aspects. Flow behaviour and processing will be dealt with in separate sections.

3.2.1 Thermal Analysis

3.2.1.1 Differential scanning Calorimetry

Thermal analysis was performed in a TA Instruments 2010 Differential Scanning Calorimeter (DSC) under a nitrogen atmosphere to determine the melting and crystallisation temperature and respective enthalpies; to estimate the degree of crystallinity in the samples and to assess possible cross-

contamination in the recycled polymers. The phase transitions are determined by comparison of the heat flows between an empty reference aluminium capsule and the capsule containing a pre-weighed sample. The heat flow is usually recorded as J/g and the integrated area of a certain phase transition in the thermogram allows the determination its required energy, e.g. enthalpy of fusion.

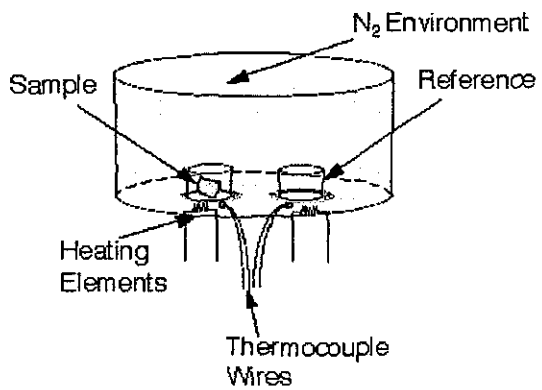

Figure 3-1 – Schematic of a DSC measurement cell.

In a semi-crystalline polymer this allows the determination of the degree of crystallinity, provided we know its inorganic content and estimated enthalpy when fully crystallized, by using the following expression:

$$\textbf{\% crystallinity} = \left(\frac{\Delta H_f}{\Delta H_f^0}\right)\left(\frac{1}{1-W_f}\right) \qquad \textbf{3.1}$$

ΔH_f - Enthalpy of fusion (J/g)

ΔH_f^0 - Enthalpy of fusion of fully crystallized material (J/g)

W_f - Weight fraction of filler

In our procedure, approximately 10 mg of samples were weighed and subjected to a heat-cool-reheat cycle under a nitrogen atmosphere at a rate of 10°C/min, from 40°C to 200°C.

An oxidation induction time (OIT) standard test method (ASTM D3895) was also performed to establish the onset of degradation at certain temperatures on some of PE-HD1 and PR-HD4.

3.2.1.2 Thermogravimetric Analysis

Chemical blowing agents don't usually decompose to release the foaming gases in one single step or temperature; therefore, thermogravimetric analysis (TGA) was carried out to determine the decomposition and gas evolution temperatures. In this technique, the mass of a sample standing on an analytical balance is constantly monitored while subjected to a heating programme.

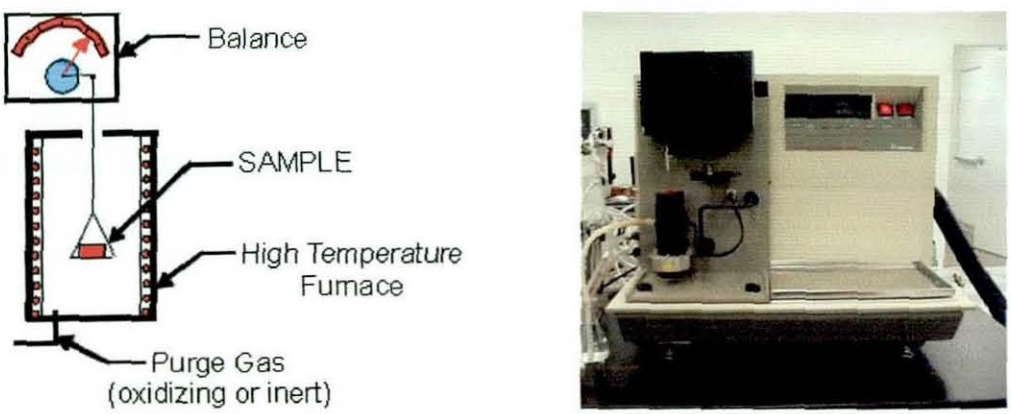

Figure 3-2 – Schematic of a TGA measurement apparatus (left) and picture of TA Instruments 2950 TGA.

The tests were run on TA Instruments 2950 TGA under a nitrogen atmosphere at temperatures between 40 and 600°C with a heating rate of 10°C. The endothermic preparation containing sodium bicarbonate, Hydrocerol BM70 was tested. Knowing the decomposition reaction it is possible to estimate the volume of gas generated per mass unit of chemical blowing agent.

3.2.2 Fourier Transformed Infrared Spectroscopy (FTIR)

Although the infrared spectrum is characteristic of an entire molecule, it is true that certain groups of atoms give rise to bands at or near the same frequency, regardless of the structure of the rest of the molecule. It is the persistence of these characteristic bands that allows useful structural information to be obtained by simple inspection and reference to generalized charts of characteristic group frequency. Infrared radiation in the range from about 10000-100cm^{-1} is absorbed and converted by a molecule into vibrational energy. This absorption is quantified, but vibrational spectra appear as bands rather than lines, because a single vibrational energy change is accompanied by several rotational energy changes. It is with these vibrational-rotational bands, particularly those occurring between 4000-400 that are of interest to identify specific polymers and chemical groups.

Fourier Transformed Infrared Spectroscopy (FTIR) was used for a qualitative assessment of the composition based on group frequency attribution. This allows distinguishing, for example, between types of linear and branched polyethylenes and polypropylene, but also to investigate presence of fillers and to investigate severe degradative processes in the polymeric matrix. The tests were run in a Mattson 3000 FTIR on diffraction mode between 600-4000 cm^{-1}, with 400 scans per sample and background. Samples were prepared by melt pressing pellets on a hot plate into films to produce samples with 70%-80% light transmittance.

3.2.3 Gel Permeation Chromatography

Information about molecular weight distribution, polydispersity or branching of polymers can be obtained by gel permeation chromatography (GPC). In this separative technique, a diluted polymeric sample flows through the chromatographic column packed with porous material but doesn't chemically interact with the stationary phase. The elution relies on the relative size of the pores which makes bigger molecules to have an increased migration speed

as the either don't penetrate the pores or if they do, they can't approach the pore walls and remain in the central zone where flow speed is highest. Calibration with narrow molecular weight distribution samples allows then to convert the concentration and retention times, typically using a refractive index detector, into a full molecular weight distribution curve.

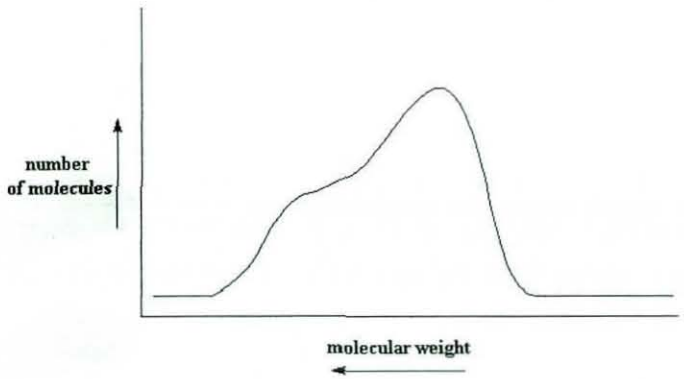

Figure 3-3 – Example of a molecular weight distribution curve.

The polymers used in this work were analysed at the Rapra Technologies Laboratories. Both a refractive index and an online differential pressure viscometer were used to determine the molecular weight distribution curve and to obtain information about branching. Due to low solubility of our polyolefins in the most common solvents for this method, it was necessary to use a high-temperature GPC under the experimental conditions described below. Instrument: Polymer Laboratories GPC220; Columns: Lgel guard plus 2 x mixed bed-B, 30 cm, 10 microns, Solvent: 1,2,4-trichlorobenzene with anti-oxidant, Flow-rate: 1.0 ml/min (nominal), Temperature: 160°C (nominal), Detector: refractive index & Viscotek differential pressure.

3.2.4 Ashing Analysis

The determination of mineral filler content of the supplied materials for subsequent microscopic and X-ray evaluation was carried out following ASTM D5630. For each sample three porcelain crucibles were previously heated while empty in a muffle furnace at 800°C for one hour and

subsequently transferred to a desiccator and allowed to cool before weighing. A sample of every polymeric material was dried in a fan oven at 80°C for one hour and then five grams of each were weighed into a crucible that was then inserted in the muffle furnace at 800°C for one hour. Once the ashing operation was complete the crucibles were carefully removed to the desiccator (for at least one hour) before finally being re-weighed. The percentage of ash (or residue) can be calculated as:

$$\%Ash = \frac{(W_{after} - W_{before})}{W_{before}} \times 100 \qquad 3.2$$

W_{before} - Weight of sample before ashing (g)

W_{after} - Weight of sample after ashing (g)

The average of three ashing determinations for each compound was taken to improve accuracy of the method.

3.2.5 Microscopy

3.2.5.1 Optical Microscopy

Several optical microscopy techniques were used to identify contaminants, mineral fillers and to characterise blend morphologies. These included brightfield, polarized light and phase contrast microscopy. In each of them Köhler illumination was used to optimise the optical path.

Small pellet portions of supplied recycled plastics were melt pressed at 170°C and 20 tonnes in a press to produce thin films under 20μm thick that were subsequently mounted between a clean microscopic slide and a cover slip. These samples were then observed under brightfield and polarized light to identify contaminants and to characterise the crystalline microstructure.

To observe polyethylene or polyethylene-polypropylene blends, phase contrast microscopy is very useful as it enhances the contrast between polymeric phases with very similar refractive indexes. An annular substage condenser is added to the typical brightfield microscope configuration, as well as a phase plate in the objective so that the difference in wavelength between direct and deviated light for a phase specimen is ½ wavelength. The direct and diffracted light arriving at the image level of the eyepiece then produces a destructive interference. As a result, phase specimens yield contrast images as if they were amplitude objects. Since the morphological features in the blends can be very small it was necessary to cryogenically cut with a glass knife samples with thicknesses below 5μm. The samples were then mounted on a microscope slide and covered with a glass slide. The microscope used was a Leica DM RXP equipped with a phase contrast condenser and phase contrast objectives,

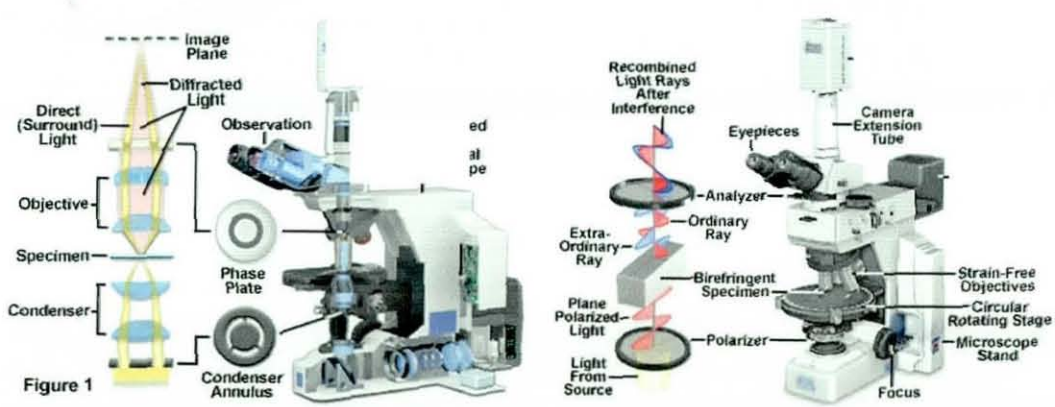

Figure 3-4 – Phase contrast (left) and polarized light (right) microscope configuration.[101]

3.2.5.2 Scanning Electron Microscopy

This technique has several advantages over traditional optical microscopy, such as a greater depth of field and higher magnification, which makes it quite useful to observe morphological features in polymers or particulate fillers. In our case, since the equipment, a Leo S360 Scanning Electron Microscope (SEM), used had an Energy Diffraction Systems for X-ray

detection; it was possible to carry out simultaneous qualitative elemental analysis up to Chlorine atomic number and a morphological inspection of the samples. The sample preparation involved sputtering with gold in an Edwards vacuum unit to increase their conductivity under the electron beam.

3.2.5.3 Transmission electron microscopy

Upon production of electron transparent samples TEM can be used to detect morphological features in the nanometre range, such as features corresponding to dispersed nanoclay particles in polymeric matrices. This kind of microscopy can then be used to assess the degree of delamination obtained from the preparation of polymer clay-nanocomposites. As polyethylene nanocomposites were too ductile to produce good quality electron transparent specimens, i.e. less than 200 nm thick, at room temperature, they had to be cryomicrotomed in Birmingham University. Subsequently they were analysed by a JEOL 100 CX.

3.2.6 X-Ray Diffraction

Interactomic spacing in crystals are of the order of 1Å, therefore electromagnetic radiation such as X-rays that have an equivalent wavelength will be diffracted from crystals with a diffraction angle that depends on the incidence angle. This is formally stated by the Bragg equation:[102]

$$2d_{hkl}\sin\theta = n\lambda \quad \text{n = 1,2,3,...} \quad \textbf{3.3}$$

d – Basal spacing (Å)

θ – Diffraction angle

λ – Incidence angle

Thus, X-ray diffraction can be used to calculate the interlayer spacing in the clay structures. Intercalation and exfoliation can be detected by the increase of the interlayer spacing of the modified organoclays intercalated by the

quaternary ammonium salts as in Cloisite 15A. The nanocomposite samples were analysed by a Bruker D8 X-ray diffractometer (40kV, 40mA) with a Cu X-ray tube, between Bragg angles 1-10° with a scanning step of 0.02°.

3.3 Shear Rheometry

3.3.1 Melt Flow Rate

The melt flow rate (MFR) test is a simple standard test to assess flowability or viscosity performed in an apparatus where a sample is loaded into a vertical heated barrel and extruded through a capillary die with the aid of a piston under a specific load. It yields data of arbitrary units, specifically gram of extruded material in ten minutes (g/10 min). Due to the nature of the test it is usually used for quality control purposes, but in case of polyethylene and polypropylene can be related indirectly to molecular weight of the resin.

The standard procedure that was followed is described by BS 2782-7 method 720 A: 1997 and the equipment was a Tinnius Olsen MP600 melt flow indexer using a 5kg weight. The test temperatures were 190°C for polyethylene and polypropylene.

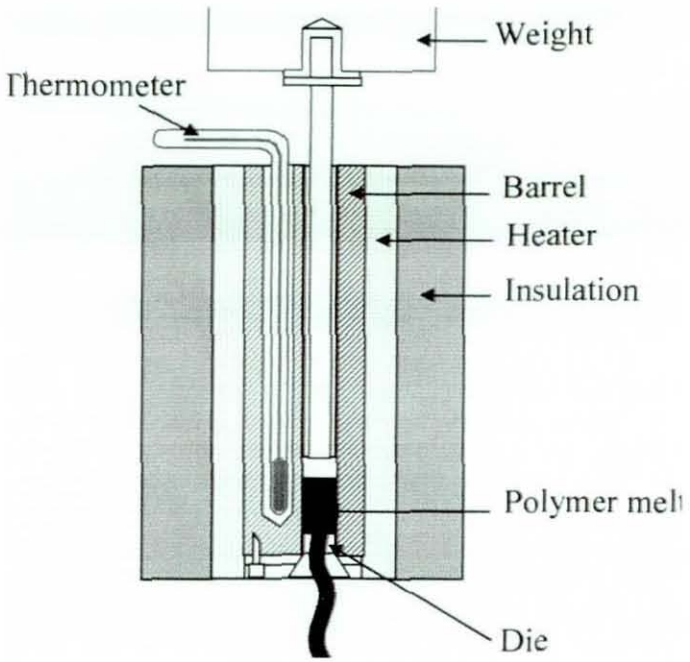

Figure 3-5 – Diagram of melt flow indexer.

3.3.2 Capillary Rheometry

The operating principle of a capillary rheometer is similar to that of a melt flow indexer; however, unlike this one the rate of deformation of the fluid can be controlled by means of a motor that controls the piston speed. It also possesses a pressure transducer at the entrance of the capillary die, thus allowing a relationship between rate of deformation and stress. Hence, rheological properties can be determined. Important information that can be extracted from these experiments are the onset of melt fracture, shear and extensional viscosity, temperature dependence of viscosity, flow activation energies, elasticity and wall slip effects. This information can then be inserted into flow simulation software such as Flow 2000, to predicted flow behaviour under arbitrary conditions.

Tests were performed in a Rosand RH-7 dual bore capillary rheometer using long and zero length mild steel, flat entry, L/D=16 capillary dies to measure shear and extensional viscosities and wall slip.

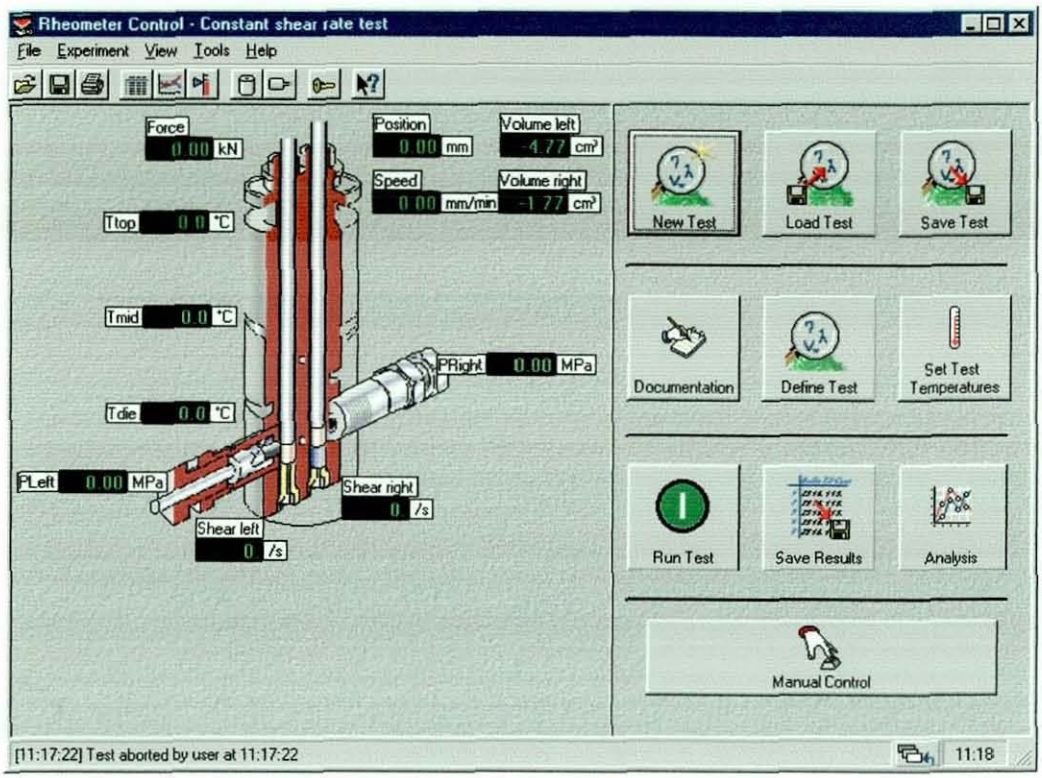

Figure 3-6 – Rosand rheometer control menu with cross view of barrel.

Before performing any experiment the dies were fitted into the barrel and a preheating period of 30 minutes to reach thermal equilibrium for each test temperature was required. Then the materials were charged into the barrels in approximately one minute and compressed manually, after which the pistons were lowered at constant velocity until a pressure of 0.5 MPa was obtained in both barrels and a new period of thermal equilibrium with duration of 9 minutes is used, including another compression to 0.5 MPa at minute 3.

Prior to the determination of the shear flow curves, the melt fracture behaviour was examined at several temperatures for the supplied polymers to determine the rate of deformation range where the flow is stable with a 24x1.5 mm die.

Due to the fact that to fit a curve into a non-linear flow model, such as a Carreau model, a few low shear rate measurements are necessary, a 24x1.5mm die was designed and used from shear rates of $1s^{-1}$ till the onset of melt fracture. Details on the choice of the design of the die can be found in

Appendix II. Also, care was taken to ensure that around 16 points were included in each measurement, so that the confidence bands of the non-linear regression were small. The temperatures ranged between 150°C-230°C depending on the melting temperature of the polymer. Simultaneously to the use of the long die, a zero length die was also used to estimate the extensional flow behaviour according to the Cogswell method,[57] and to determine the true shear rates with the Rabinowitsch procedure. Additionally, the viscosity temperature dependence and flow activation energy were determined.

Wall slip measurements were done on high-density polyethylenes PR-HD4 and PE-HD1. For this procedure a set of five long flat entry dies described in Table 3-4 were used, following the Mooney technique. After this, a combined set of 24x1.5 mm and 0x1.5 mm dies were used to obtain the shear flow curves, using the relationships expressed in equations 2.12 and 2.13.

Die	Dimensions (length x diameter) mm
1	24 x 1.5
2	19 x 1.2
3	16 x 1
4	12 x 0.75
5	8 x 0.5

Table 3-4 – Die dimensions used for wall slip determinations.

3.4 Extensional Rheometry – Free Surface Method

3.4.1 The Rutherford rheometer – general description

The Rutherford extensional rheometer (RER) is an instrument that was developed in Loughborough University and has been extensively described over the years.[53, 103, 104] It consists of a horizontal temperature controlled oil bath and computer controlled displacement system connected to a load cell that measures the force of an oval shaped, uniaxially deformed sample. The specimen is mounted and clamped on two specimen holders immersed in a

high-temperature silicone-based oil. These are connected to carriage arms which are attached to two guide rails parallel to the axis of elongation. One end of the sample is held fixed while the other is pulled by moving the specimen holder, whose carriage arm is connected to a variable speed motor-driven pulley by a rubber band. Designed to cope with different materials, it uses the mechanical advantage principle with a lever arm whose fulcrum can be adjusted allowing for different force ranges to be determined with a single transducer. This instrument allows us to investigate melt state deformation and rupture of polymers at constant velocity.

Figure 3-7 – Top view of the Rutherford elongational rheometer.

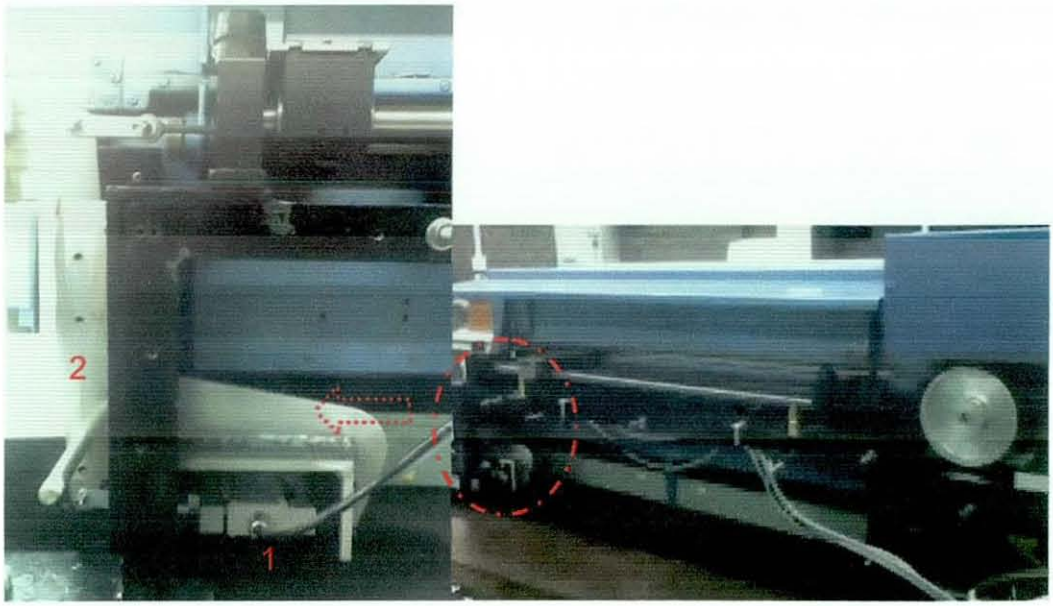

Figure 3-8 – Detail of the load cell (1), mechanical amplifier beam (2) and back view of the Rutherford elongational rheometer.

3.4.2 Force measurement system

The variable fulcrum (pivot) position means that the beam acts as a mechanical amplifier using the following principle:

$$F_1L_1 = F_2L_2 \qquad 3.4$$

Where,

F_1 = the maximum force the transducer can indicate (constant at 10kg or 98.1N, using 1kg ≡ 9.81N)

F_2 = the maximum force for each pivot position

L_1 = the distance from A in figure to the selected pivot position (cm)

L_2 = the distance from B in figure to the selected pivot position (cm)

The distance between A and B is 20 cm (Figure 3-8). The force range for each pivot is shown in Table 3-5.

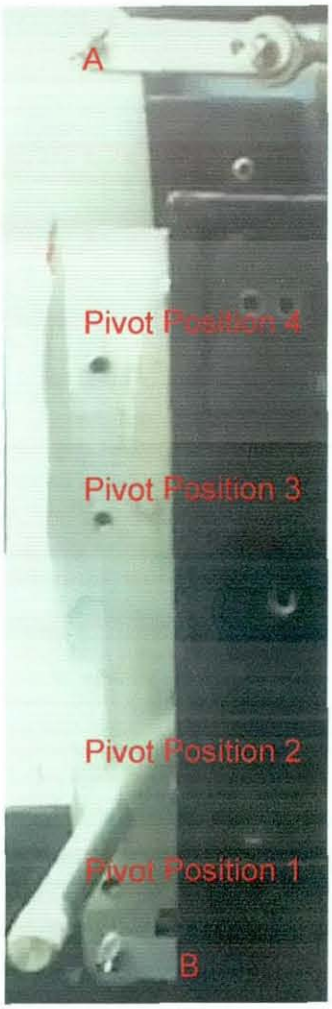

Figure 3-9 – Pivot positions in the mechanical amplifier

Pivot Position	L_1/L_2 (cm/cm)	F_2 (N)	Force range (N)
1	1.88/18.1	10.2	0-10
2	3.40/16.6	20.1	0-20
3	10.1/9.9	100	0-100
4	13.4/6.6	201	0-200

Table 3-5 – Force ranges for each pivot position.

3.4.3 New Rutherford Modifications

After being developed by Smoker[103] this instrument and the measurement method has been developed on several occasions, for example, by Axtel[104] and by Jumpa.[53] These focused in the development of the sample holder system and preparation methods according to requirements of different materials. More recently, during the course of this research, new computerised data acquisition, load cell and drive systems, as well as new guide rails and crosshead arms were installed. After this recent upgrade several adjustments had to be made to the rheometer, specifically to improve the signal to noise ratio in the low force detection range and test data acquisition due to premature sample failure in recycled plastics, related to internal inhomogeneties.

Subsequent to the rheometer upgrade commissioning, the signal to noise ratio in the low force detection range was too small to study the elongational melt deformation of the polyethylene samples. An investigation to its cause revealed a manufacturing fault in the crosshead arm connected to the load cell, leading to a catch and pressure from the lid that ultimately masked and reduced the signal detected by the transducer. Further to this, the stiffness of the mechanical amplifier system proved too low at pivot positions 1 and 2. This allowed the static carriage to move forward prior to the sample elongation, subsequently leading to a spring like forward and backwards motion that resulted in a sinusoidal damping signal. Ultimately, this offset could lead to inaccuracies in the mechanical amplification coefficients and force readings. This situation was corrected by redesigning the connection between the mechanical amplifier and the static carriage, and the sample holder. Final fine adjustments are then executed with the screw and nuts of the static carriage (see Figure 3-10).

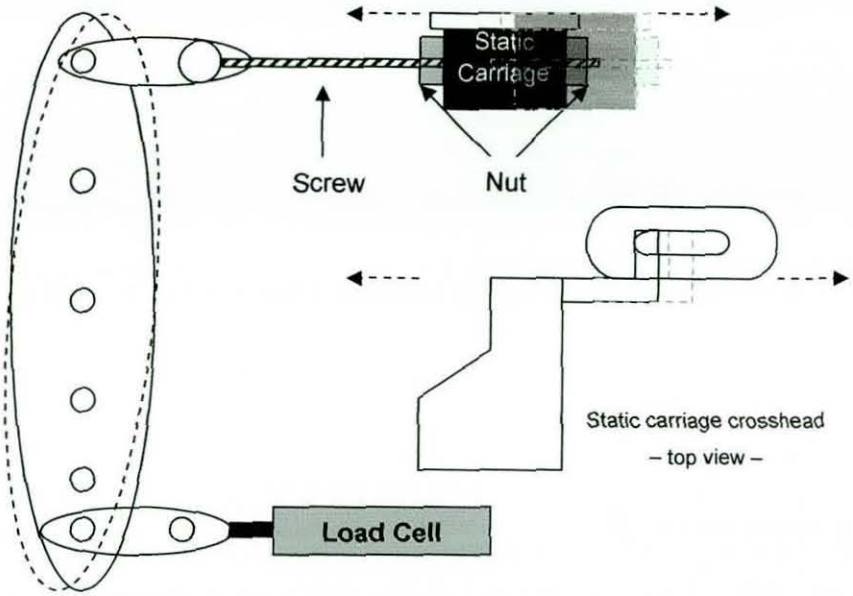

Figure 3-10 – Schematic depicting static carriage backwards and forward movement *with low stiffness adjustment, lateral and top views.*

After the adjustment of the stiffness of the system it was necessary to enlarge the cross-sectional area, to amplify the signal to noise ratio. It was decided to continue using the oval-shaped samples with (rectangular cross-section) and to increase the cross-section area by increasing the thickness of the sample. At a thickness of 1.5 mm the signal detected with polyethylene samples in pivot position 1 was at about 20% of the transducer's full scale. With recycled samples it was very common to have premature failure in the samples with half (i.e. one side) of the testing area intact for a longer period during the test. Therefore it was decided to clamp the samples to the sample holder to ensure the continuation of the test and obtain a more representative failure at break.

The new design as depicted in Figure 3-11 and Figure 3-12 prevented the sample from slipping from the clamping system, allowing force reading to be obtained though with just one sample arm. The butterfly design leaves the testing area stress free and only clamps onto the sample by the raised profile in the back rim of the grip plate.

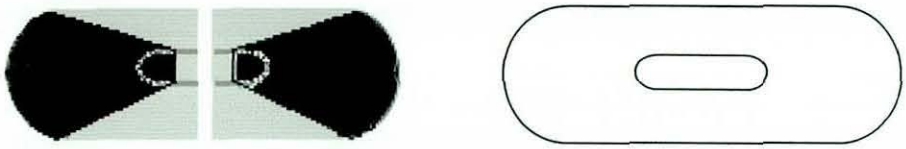

Figure 3-11 – Top view of the sample holder and oval ring sample. In black, the butterfly shaped screwable grip plates attached to the sample holder block. In white, the oval ring sample.

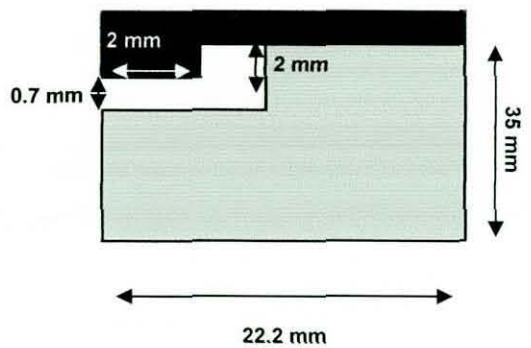

Figure 3-12 – Side view detail of one sample holder block and grip plate.

3.4.4 Sample preparation

Careful sample preparation is necessary to provide homogeneous and completely relaxed samples of the correct size. Samples were prepared by direct compression moulding of pellets by means of appropriate metal moulds into a plate of 2x20x20 mm^3 (thickness x length x width) and cut by means of an oval die cutter into the desired sample dimensions. The metal moulds were loaded with pellets and placed between two metal plates separated by thin sheets of pure PTFE. The pressing tool was placed into a hot press at moulding temperature for at least 10 min to preheat the polymer. Then the pressure was loaded in steps in order to obtain a relaxed polymer sample. Subsequently, the whole pressing tool was removed from the press and cooled down to at least the heat distortion temperature of the polymer under pressure before the polymer plate was removed from the metal mould.

3.4.5 Testing

The samples were placed in the silicone oil bath for 10 minutes to reach thermal equilibrium before being elongated at a constant speed of 50 mm s-1 to obtain a maximum Hencky strain rate of 3. The test temperature for the polyethylene and polyethylene nanocomposites was 150°C, and was 170°C for polypropylene, their blends and nanocomposites. The raw load data and displacement signals were then translated into extensional stress (σ_E) and Hencky strain rate ($\dot{\varepsilon}$) curves according to the following equations:

$$\dot{\varepsilon} = \frac{Lt}{L - L_0} \qquad 3.5$$

$$\sigma_E = \frac{F_t L}{A_0 L_0} \qquad 3.6$$

L – sample length

L_0 – initial sample length

A_0 – initial cross-sectional area

F_t – measured force

By plotting the extensional stress versus the Hencky strain rate it is possible to obtain from the curve the melt state elasticity, the elongation at break and the strain energy density (area under the curve). Data treatment example can be found in appendix III. Each measurement was performed five times and the results are the average of those measurements. The %RSD is typically 15%

3.5 Blends and Clay Nanocomposites

For a long time melt blending of polymers has been used to produce new alloys and compounds with different characteristics without production of new resins, but research on polyethylene-propylene blends suitable for foaming

has been scarce. In this context, we focused our research on understanding how the rheological properties of the resins and processing conditions of an internal batch mixer influence the development of the blend morphology in compatibilised and uncompatibilised recycled systems of LDPE:PP and HDPE:PP. Subsequently, we tried to understand the relationship between the blend morphology, the melt extensional flow and free foaming behaviour. More recently, melt intercalated layered-silicate nanocomposites have been used to improve the foaming behaviour of some polymers,[17] but the foaming behaviour of nanocompound blends has not yet been reported. This work also explores the effect of the processing conditions in an internal mixer in the development of compound morphology.

Essentially four blend and clay nanocomposite systems were studied in this work. They included two polyethylene-polypropylene blends and two layered-silicate high-density polyethylene and HDPE-PP nanoclay compounds. The influence of processing conditions and blend composition on the melt extensional flow behaviour and morphology present a complex analytical problem.

For some experiments commercial statistical software, *Statistica*, was used to design experiments and analyse the results. A response surface methodology[105] was used for the evaluation of the relationships between the controlled experimental factors and the observed results. In this case a second order design was employed. The design used leads to a fit of a second degree equation, for example, in case of two variables, x_1 and x_2, with interactions:

$$Y = a_0 + a_1x_1 + a_2x_2 + a_{11}x_1^2 + a_{22}x_2^2 + a_{12}x_1x_2 \qquad \textbf{3.7}$$

The design defines the minimum number of experimental combinations and their compositions in the explored domain to obtain the maximum amount of information to fit the proposed model. Replicate experiments were carried out in the centre of the design to find out the experimental error. The advantage

of this type of design is that besides the individual effect of each variable, their combined effect can also be analysed.

The response variables measured include melt flow indices and elongational flow properties such as elongation at break, melt state tensile strength and strain energy density.

3.5.1 Polyethylene-Propylene Blends

To investigate the influence of the rheological properties of the blend constituents on its morphology two different polyethylenes, one linear and one branched, were chosen to be alloyed with a polypropylene at selected compositions. They were melt mixed in a Haake Rheomix 600 fitted with roller rotors, the mixing chamber had a volume of 70 cm^3, but the fill factor was kept at 70%, which meant the use of 40g of materials.

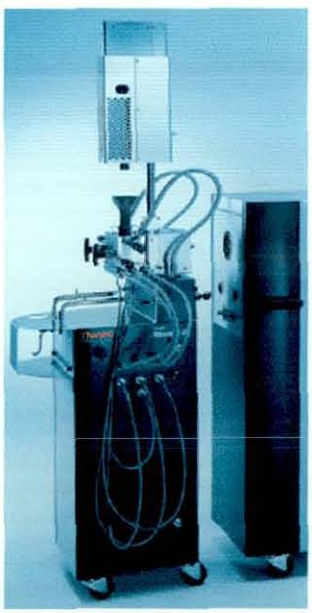

Figure 3-13 – Haake Rheomix 600 batch mixer.

3.5.1.1 Blend system I: LDPE:PP

Blends of recycled LDPE and PP were melt mixed at 190°C with a screw speed of 31.8 rpm. The variables of the process were the mixing time and the

composition. The influence of the compatibilisers was studied in the blend system PR-PP1/PR-LD1 40:60. The compatibiliser levels were varied between 0-5 %(w/w). The summary of the prepared samples can be found in Table 3-6. The rotor speed was chosen so that the viscosity ratio was maximised between the blend components at the corresponding temperature. This was determined analytically by dividing the shear flow curves of each polymer and determining its maximum at 190°C. Then, the approximate shear rate at the wall was determined according to the equation:[106]

$$\dot{\gamma} = \Omega / \delta \qquad \textbf{(3.8)}$$

Ω – Angular speed of the rotor tip.

δ – Gap opening between the rotor tip and the mixing chamber (0.45mm).

PP:LDPE ratio	Compatibiliser		Mixing time (min.)			
	Type	%(w/w)	2.5	5.0	7.5	10
80:20	-	-	x	x	x	x
60:40	-	-	x	x	-	-
40:60	-	-	x	x	-	-
40:60	EP1	2.5	x	x	-	-
40:60	EP1	5	x	x	-	-
40:60	EPR1	2.5	X	x	-	-
40:60	EPR1	5	x	x	-	-
20:80	-	-	x	x	x	x

Table 3-6 – Alloy compositions and mixing times of melt mixed recycled PP:LDPE.

3.5.1.2 Blend system II: HDPE:PP

A blend system containing recycled HDPE and PP, PR-HD4 and PR-PP1, respectively was also subject to our attention. We introduced a linear polyethylene and continued to study the influence of composition and processing variables in a similar way to that of the previous blend system. However, unlike the previous blend system, the shear rate and temperature

were not kept constant, and to accommodate these extra parameters, a central composite experimental design was chosen that included composition

HDPE:PP ratio	Rotor (rpm)	Time (min.)	Temperature (°C)
50:50	50	1.5	170
80:20	50	2.5	170
20:80	150	1.5	190
80:20	150	2.5	170
20:80	125	2.5	190
80:20	150	3.5	190
80:20	50	3.5	190
80:20	150	1.5	190
80:20	150	2.5	190
50:50	100	1.5	170
20:80	50	2.5	190
80:20	50	1.5	170
20:80	100	1.5	190
20:80	150	3.5	170
80:20	150	1.5	170
20:80	150	3.5	190
20:80	50	3.5	190
50:50	50	2.5	190
80:20	150	3.5	190
80:20	100	1.5	170
50:50	100	3.5	190
50:50	50	3.5	170
20:80	50	1.5	190
80:20	100	2.5	190
80:20	50	3.5	190
20:80	150	3.5	170
20:80	150	1.5	170
80:20	100	3.5	170

Table 3-7 – Compositions and processing conditions used in the preparation of HDPE:PP blends.

ratio, rotor speed, time and temperature as independent variables. The response variables used to analyse the results were melt state extensibility and strain energy density. The experimental details can be found in Table

3-7. Subsequently, and based on elongational flow results, namely strain energy density and extensibility, it was decided to use the samples prepared with a HDPE:PP ratio of 80:20 and a short mixing time to study the influence of compatibilisers as this blend had the maximum values for these response variables. The experimental details follow in Table 3-8.

HDPE:PP ratio	Compatibiliser (w/w)	Speed (RPM)	Time (min.)	Temperature. (°C)
80:20	2.5% EPR1	150	1.5	170
80:20	5% EPR1	150	1.5	170
80:20	2.5% EPR1	150	2.5	170
80:20	2.5% EPR1	150	1.5	190
80:20	5% EPR1	150	1.5	190

Table 3-8 – Formulation and processing conditions of compatibilised HDPE:PP blends.

3.5.2 Layered-silicate Nanocomposites

3.5.2.1 HDPE Layered-silicate nanocomposites

The preparation of polyethylene layered silicates by melt intercalation is still the subject of debate, with several authors quoting very different experimental procedures.[33,39,107] To better understand the influence of the processing conditions such as temperature, shear rate and clay content a $3^{(k-p)}$ full factorial design was chosen to identify the preferential parameters and to test for linear and quadratic effects.

A virgin and a recycled high-density polyethylene, PE-HD1 and PR-HD4 respectively, were each melt mixed for 5 minutes with variable amounts of modified organoclay, Cloisite® 15A, and a constant amount of compatibiliser, 5% (w/w) of PB1, in a Haake Rheomix 600. This internal mixer was equipped with roller rotors and a 70 cm^3 mixing chamber, but the fill factor was kept at 70%, which meant the use of 40g of materials. The full processing conditions can be found in Table 3-9.

After analysis of the relationship between the melt flow index results and the processing variables it was decided to investigate the influence shear rates, clay and compatibiliser ratio, with temperature and time in recycled HDPE nanoclay composites. Low shear experiments were made to determine the lower threshold for exfoliation and intercalation, by varying the rotor speed, mixing time and clay-compatibiliser ratio. The experimental conditions used can be found in Table 3-10 and Table 3-11.

Mixing temperature (°C)	Rotor Speed (rpm)	Organoclay content (% w/w)		
		5	1	0
150	50	X	X	X
	100	X	X	X
	150	X	X	X
170	50	X	X	X
	100	X	X	X
	150	X	X	X
190	50	X	X	X
	100	X	X	X
	150	X	X	X

Table 3-9 – Processing conditions used in the preparation of HDPE nanoclay composites.

Time (min.)	Speed (RPM)	% Clay (w/w)	Clay-PB1 ratio
1.50	50	5	5/5
3.63	50	2	2/5
1.50	50	3	3/5
1.50	30	2	2/5
1.50	50	1	1/5
5.75	30	5	5/5
10.0	50	1	1/5
10.0	30	3	3/5
5.75	50	1	1/5
10.0	50	3	3/5
1.5	30	1	1/5
5.75	30	1	1/5

Table 3-10 – Experimental conditions for the preparation of HDPE clay nanocomposites at 150°C.

The influence of mixing time and clay-compatibiliser ratio was later also extended to samples with virgin and recycled HDPE prepared at 170°C. Details can be found in Table 3-12.

Mixing Time (min.)	Rotor Speed (RPM)	% Clay (w/w)	Clay-PB1 ratio
10.0	30	3	3/5
5.75	50	5	5/5
10.0	50	5	5/5
10.0	30	1	1/5
3.63	30	2	2/5
5.75	30	3	3/5
10.0	30	5	5/5
1.5	30	3	3/5
10.0	30	5	5/5
10.0	50	5	5/5
5.75	50	3	3/5
10.0	50	1	1/5
10.0	30	1	1/5

Table 3-11 – Experimental conditions for the preparation of HDPE clay nanocomposites at 150°C.

Mixing Time (min.)	Rotor Speed (RPM)	% Clay (w/w)	Clay-PB1 ratio
6	100	0	0/5
6	100	1	1/5
6	100	2	2/5
6	100	3	3/5
6	100	4	4/5
6	100	5	5/5
6	100	5	5/0
6	100	5	5/1
6	100	5	5/2
6	100	5	5/3
6	100	5	5/4
6	100	5	5/5
1.5	150	5	5/5
1.5	150	5	5/5
2	150	5	5/5
2	150	5	5/5
2.5	150	5	5/5
3.5	150	5	5/5

3.5	150	5	5/5

Table 3-12 – Experimental conditions for the preparation of HDPE clay nanocomposites at 170°C.

The compilation of all these experiments led to a sufficient extension of the experimental domain allowing the construction of a central composite design. The results were analysed with the help of *Statistica* and used to optimise the processing conditions in order to minimise the melt flow index.

3.5.2.2 HDPE-PP nanocomposites

The influence of the blend composition and processing conditions, namely temperature and mixing time, on the preparation of HDPE-PP nanocomposites was studied. For this, 40 g samples were prepared by melt mixing in a Haake Rheomix 600 at a rotor speed of 150 rpm under conditions described in Table 3-13.

HDPE:PP ratio	PB1 % (w/w)	Clay % (w/w)	Mix. Time (min.)	Temperature (°C)
80:20	5	1	1.5	170
60:40	5	1	1.5	170
60:40	5	1	2.0	170
80:20	5	1	2.0	190
60:40	5	1	2.0	190
80:20	5	1	2.0	170
80:20	5	1	1.5	190
60:40	5	1	1.5	190
80:20	0	1	1.5	170
80:20	5	0	1.5	170

Table 3-13 – Formulations and processing conditions of prepared polyethylene-polypropylene compounds at a constant rotor speed of 150 rpm.

3.6 Extrusion Foaming

After having studied the rheological properties of the raw materials, blends and compounds, foaming experiments were carried out to understand the relationship between rheology and foaming behaviour as well as processing parameters. For this a new technique was developed using a capillary rheometer.

3.6.1 Extrusion Foaming in a Capillary Rheometer

In extrusion foaming of polyolefins after having produced the polymer-gas solution the material is cooled down in the die and expanded when the gas comes out of solution after a sudden pressure drop. A similar process can be adapted to capillary rheometer with long barrels if independent heating zones are created and controlled. The Rosand RH-7 rheometer has three heating zones, one for the capillary die and another two along the barrel in the middle and top sections, respectively. Setting different heating temperatures for each zone leads to a temperature profile similar to that of an extruder. Material should then be loaded to the barrel so that after a compression stage the polymer containing a chemical blowing agent melts and remains below the gas evolution temperature. The ram speed and capillary die should then be chosen so that the material has an appropriate residence time and experiences a certain shear rate at the die wall, as shear induced nucleation may affect the foaming process.

In our experiments we have set zone temperatures at 145°C -170°C -145°C (top-middle-die) and loaded the barrel with approximately 40g of material. Die temperature was set higher for compounds containing PP. The material was previously melt mixed with the chemical blowing agent below its decomposition temperature in a Haake Rheomix 600 internal mixer at 30 rpm for 3 minutes, to ensure a good polymer-gas solution on foaming. The compound was not compressed until 6 minutes had passed, and the ram was

then lowered from its resting position to 182 mm above the die, and left to pre-heat for another 3 minutes. The ram was after this lowered at 33 mm/min to a distance of 100mm of the die where the velocity was changed to 11.3 mm/min to extrude the material through an L/D 16, 24 mm long die at a shear rate of 50/s. The influences of blowing agent content and die temperature were also investigated for some raw polymers and those conditions are included in Table 3-14.

	Blowing Agent % (w/w)	Die Temperature (°C)		
		147	160	170
PE-HD1	1	x	x	x
PR-HD4	2	x	x	x
PR-LD1	3	x	x	x
PR-PP1		-	x	x

Table 3-14 – Die temperatures and blowing agent content used in extrusion foaming raw polymers.

3.6.2 Foaming blends

To investigate the influence of linear and branched recycled polyethylene in polypropylene blends, some blend compositions were selected based on previous extensional flow behaviour determinations. The effect of increased compatibility in recycled polypropylene and long-chain branched polyethylene, with a rubbery and co-polymeric material was also considered. The following table summarizes the compositions and conditions used in extrusion. We incorporated 3% of blowing agent, *Hydrocerol BM70*, in each of the blends. The foam extrusion followed a similar procedure used for the raw polymer blowing agent compounds. The die temperature was kept at 170°C.

Polymer Blend		Ratio	Compatibiliser % (w/w)	Temperature (°C)	Rotor Speed (rpm)	Mix. Time (min.)
PR-PP1	PR-HD4	80:20	-	170	150	1.5
PR-PP1	PR-HD4	20:80	-	170	150	1.5
PR-PP1	PR-HD4	20:80	-	170	150	3.5
PR-PP1	PR-HD4	20:80	-	190	150	1.5
PR-PP1	PR-LD1	80:20	-	190	31.8	5
PR-PP1	PR-LD1	40:60	-	190	31.8	5
PR-PP1	PR-LD1	40:60	5 EP1	190	31.8	5
PR-PP1	PR-LD1	40:60	2.5 EP1	190	31.8	5
PR-PP1	PR-LD1	40:60	5 EPR1	190	31.8	2.5
PR-PP1	PR-LD1	40:60	2.5 EPR1	190	31.8	2.5
PR-PP1	PR-LD1	20:80	-	190	31.8	5

Table 3-15 – Formulations and processing conditions of selected recycled polypropylene-recycled polyethylene foams.

3.6.3 Foaming of Nanocomposites

The influence of processing conditions and clay content on nanocomposite foams were studied on selected single polymer and polymer blend nanocomposites. For high-density polyethylene nanocomposites, using a die temperature of 145°C, the effects of mixing time, rotor speed, mixing temperature and clay content were investigated in both recycled and virgin systems. The details of those samples can be found in Table 3-16. By having introduced recycled PP as a lower viscosity phase in the composition of the nanocomposite blend at an optimum level we aimed to study the influence of such a phase, and observe the reinforcement obtained at different clay levels.

3.6.4 Foam Density Determination

The density of the foams was determined gravimetrically. As an approximation it was assumed that the foamed strands were cylindrical and the length and diameter was measured in three different points to determine the volume. The mass of the sample was weighed using an analytical balance. The results are the average of the measurement of three foamed strands. The relative standard deviation is typically around 3.5%.

Polymer	PB1 %(w/w)	Clay %(w/w)	Temperature (°C)	Rotor Speed (rpm)	Mix. Time (min.)
PE-HD1	5	5	190	50	6
PE-HD1	5	5	170	50	6
PE-HD1	5	5	170	150	6
PE-HD1	5	5	150	150	6
PE-HD1	5	5	150	150	1.5
PR-HD4	5	5	190	150	1
PR-HD4	5	5	170	150	1.5
PR-HD4	5	3	170	150	1.5
PR-HD4	5	1	170	150	1.5
PR-HD4	5	5	170	150	2
PR-HD4	5	5	170	150	6
PR-HD4	5	5	170	100	6
PR-HD4	5	5	170	50	6
PR-HD4	5	5	150	150	2
PR-HD4	5	5	150	100	6
PR-HD4	5	5	150	50	6
PR-HD4	5	5	150	30	10
PR-HD4	0	5	170	50	6

Table 3-16 – Formulations and processing conditions of selected high-density polyethylene nanocomposite foams.

3.7 Extrusion simulation

To assist in the interpretation of some experimental results a commercial polymer flow simulation software package, *Flow 2000*, was used. This software solves equations of motion that describe the flow of polymer melts under non-isothermal and arbitrary boundary conditions by the Galerkin finite element method of weighed residuals.[108] Those solutions allow us to analyse flow situation by discriminating flow lines, recirculation flows, stress distribution, fluid velocity, shear and elongation rate, pressure and temperature profiles, for example.

The finite element method is a method for solving partial differential equations involving a function u(x) defined for all x in the domain with respect to some given boundary condition. The purpose is to determine and approximation to the function u(x). The method requires the discretisation of the domain into sub-regions or cells. For example a two-dimensional domain can be divided and approximated by a set of triangles (the cells). On each cell the function is approximated by a characteristic form. For example u(x) can be approximated by a linear function on each triangle.[108] Thus, one has to specify geometry and the subdivisions, the boundary conditions and a mesh must be generated.

With Flow 2000, after defining the flow geometry by creating notes that are then linked in groups of four to create smaller elements (Figure 3-14), six-node triangular elements (Figure 3-15) are then used with quadratic interpolation for velocity and temperature and linear interpolation for pressure. The scientific basis of this package is described in a series of papers that have appeared in the literature since 1983.[109-112]

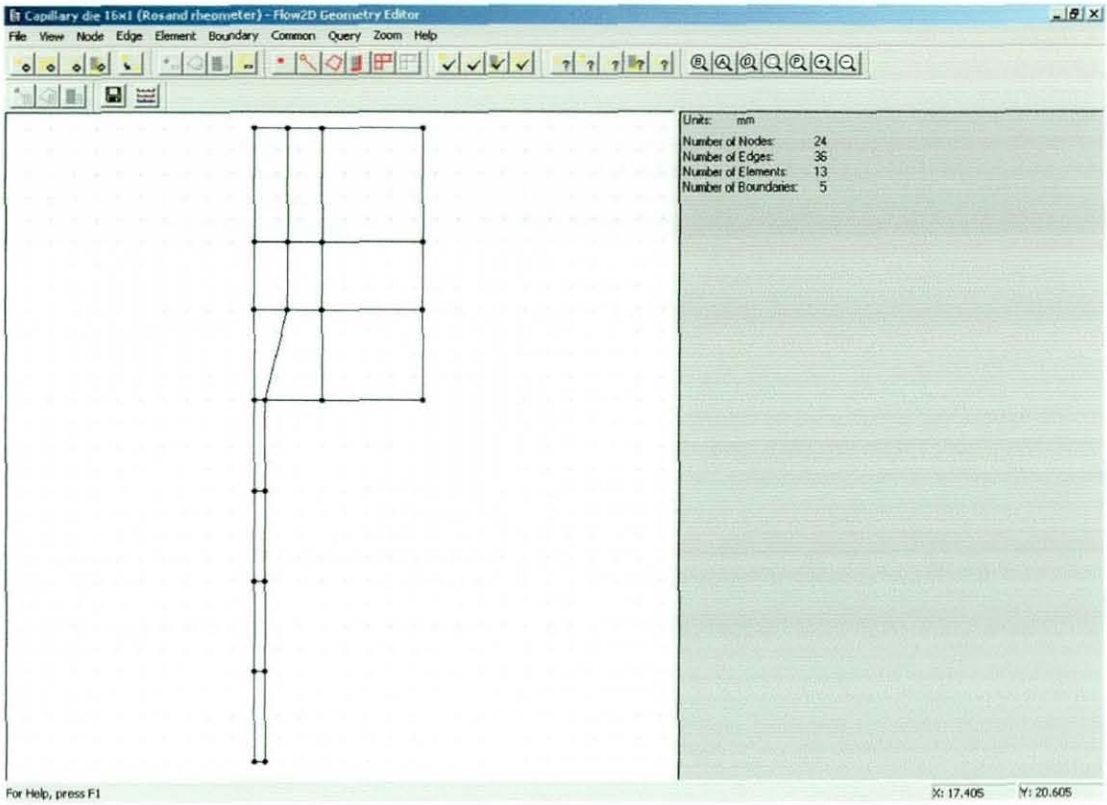

Figure 3-14 – Screenshot of a flow domain of half a capillary die with discrete nodes and elements.

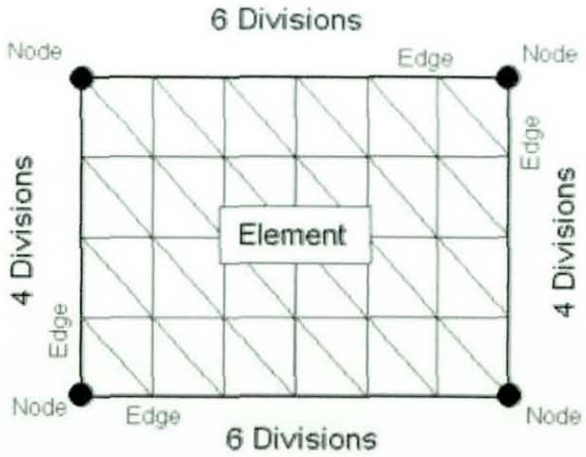

Figure 3-15 – Example of division of a flow element into cells.

Boundary conditions, such as wall temperatures, material velocity and temperature and subsequently added. Material functions for instance flow

and thermal properties need then to be linked to this flow domain and solved by an integrated post-processor.

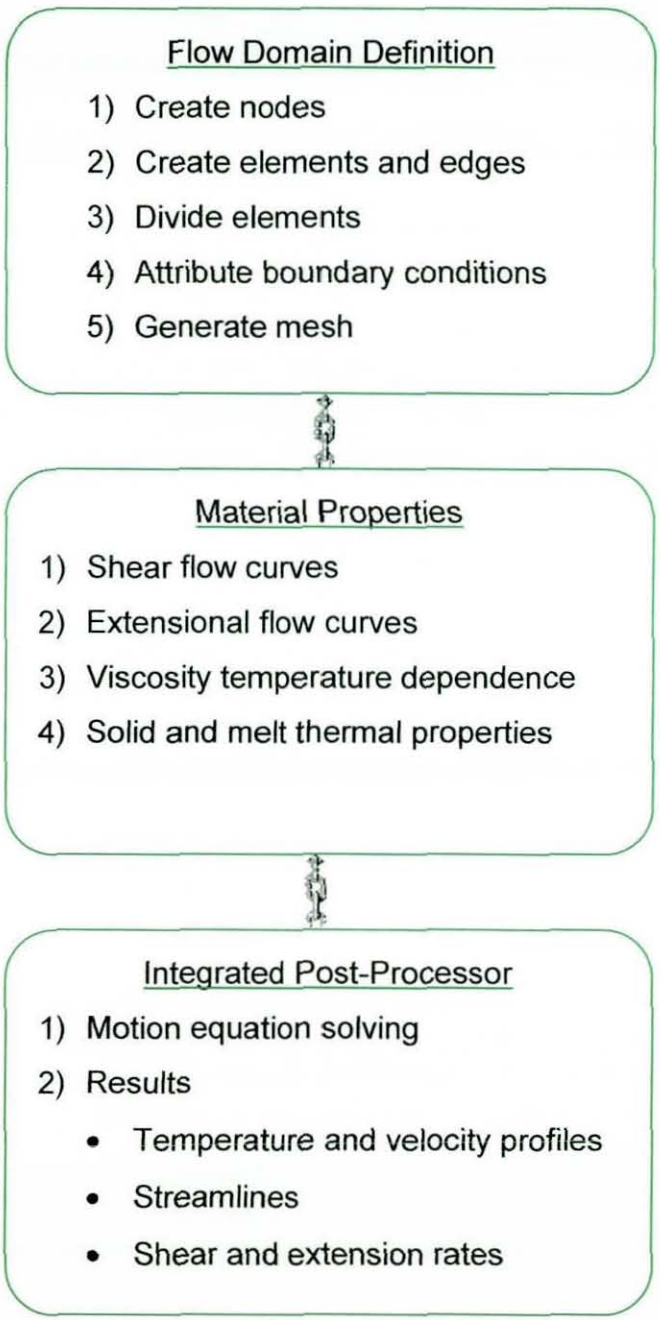

Figure 3-16 – Flowchart of the main operations for simulation of polymer flow state with *Flow 2000*.

3.7.1 Capillary Die Flow Domain

In this study, the author used Flow 2000 to define a two-dimensional flow domain for a flat entry 24x1.5mm Rosand RH-7 capillary die to simulate several flow states. Due to symmetry, only half of the full flow domain was needed to be represented as is depicted in Figure 3-17.

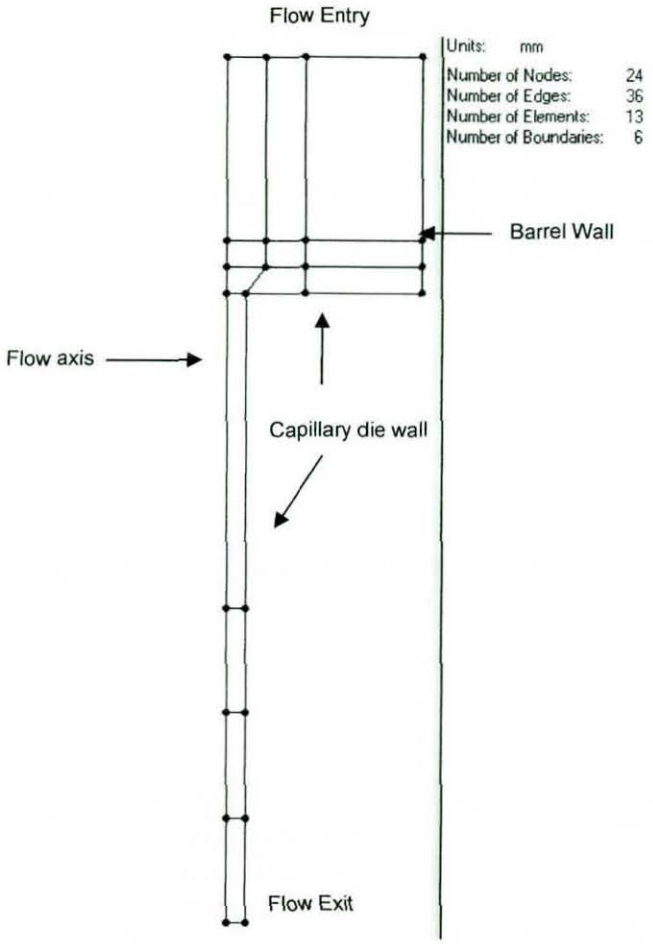

Figure 3-17 – Flow domain of a 24x1.5mm capillary die for constant shear rate measurement simulation.

The flow domain was defined with 24 nodes, creating 13 elements and 36 edges each with 6 regular divisions. Six boundaries were added, including two capillary die walls, a barrel wall, a flow axis and a flow entry and exit. The material flow properties were determined by fitting shear and extensional flow models from capillary rheometry measurements as described in the capillary rheometry section 3.3.2. Thermal properties such as enthalpy of fusion and crystallisation, crystallisation and melting points were determined by DSC.

Density of the melt was determined within MFI measurements. Details of the material properties can be found in Appendix V.

3.7.1.1 Capillary Rheometry Simulation Validation

To validate the bi-dimensional flow model of the 24x1.5mm capillary die, shear flow experimental curves from PR-HD4 at different temperatures were plotted against the shear flow curves obtained from simulated data points. To obtain simulated data points one must specify matching boundary conditions, such as piston speed and wall temperatures, then define a cut close to the position of the pressure transducer and take the value by the wall for each pre-defined piston speed.

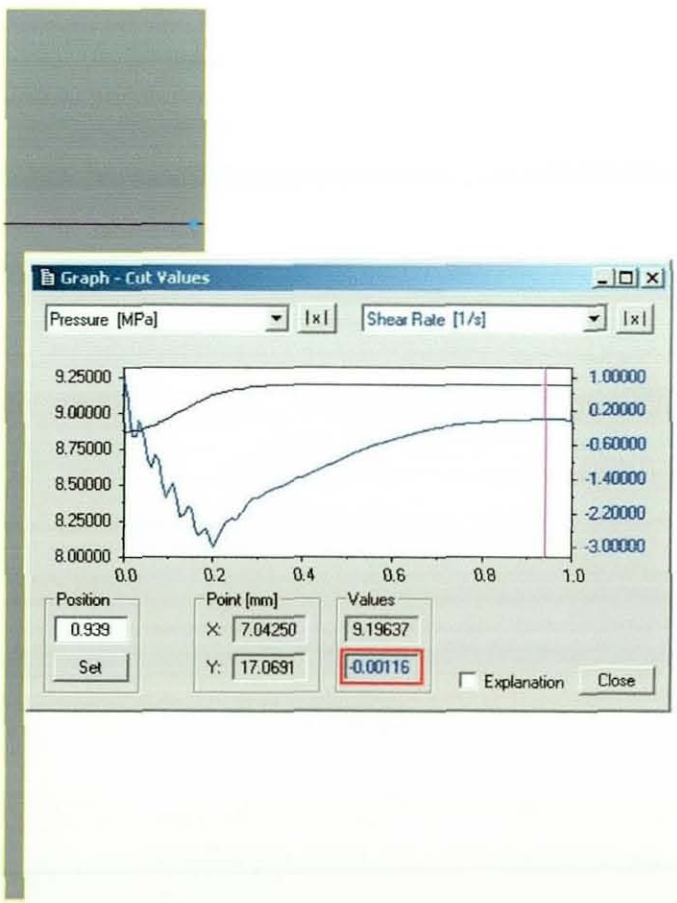

Figure 3-18 – Example of a capillary die cut with an adjacent graph showing the pressure and shear rate by the pressure transducer.

3.7.1.2 Capillary Foam Extrusion simulation

To understand the foaming behaviour of some samples, a two-dimensional flow domain representing the Rosand RH-7 24x1.5mm die under foaming conditions was created with *Flow 2000*. Contrary to the constant shear rate, a larger portion of the barrel was included in the domain to obtain a broader picture regarding the temperature profile of the material. Also, the temperature of the barrel zones and die had to be set independently. This meant an increase in the number of nodes, elements and boundaries as depicted in Figure 3-19.

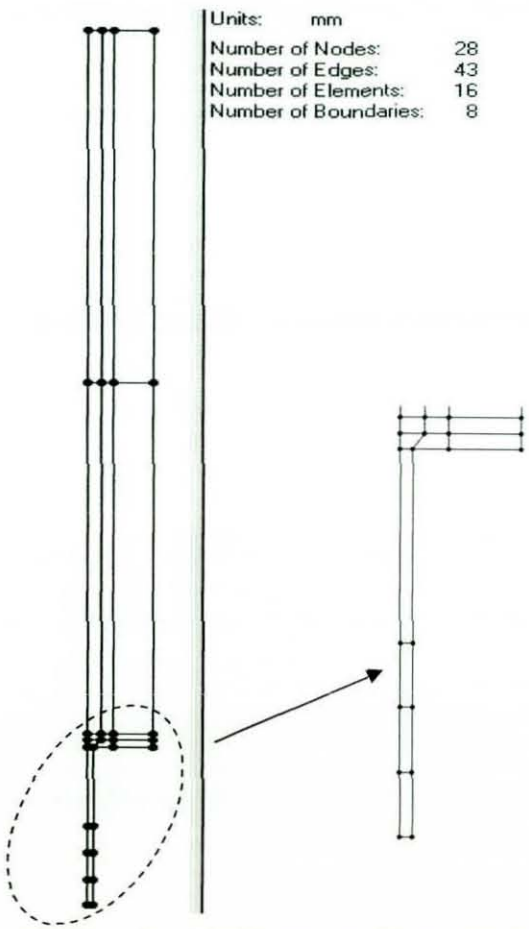

Figure 3-19 – Flow domain of a 24x1.5mm capillary die for foaming experiment simulation.

4 Raw Materials Characterisation

In this chapter the materials characterisation experimental results will be presented and discussed for the supplied raw materials. The main interest was to compare the purity and rheological properties of recycled polyolefins with virgin equivalents.

The characterisation sequence started with the identification of polymer contaminants and mineral particulates in the recycled polymers. For this, the vibrational spectra were scanned by FTIR; contaminants observed and identified by optical, electron microscopy and energy dispersive X-rays; mineral particulate filler content determined by ashing tests and thermal properties determined by DSC. The molecular weight distribution curves were determined by gel permeation chromatography. Thermogravimetric analysis of the chemical blowing agent was also performed.

A rheological characterisation of all polymers then followed and near equivalent virgin polymer grades were chosen as control samples.

4.1 Raw Polymer Characterisation

The recycled raw materials were supplied in pellets of various shapes, colours, and HDPE in particular still had an odour resembling detergent. The bulk density of the recycled polymers ranged from 318-591 kg/m^3.

4.1.1 Ash Analysis

Several types of mineral fillers are used for different purposes in packaging plastics. A suspected source for the recycled HDPE is milk bottles were the presence of both calcium carbonate and titanium dioxide (white pigment) is likely. In the case of LDPE's that originate mainly from film applications such

as plastic bags, a certain amount of titanium dioxide is also expected. To quantify the total amount of mineral fillers present in the polymer samples, they were ashed according to the procedure described in section 3.2.4 and results showed the presence of mineral fillers in almost all recycled polymers, except for PR-PP1, PR-HD4 and the virgin polymers. These amounts varied between 7% and 0.3% as specified in Table 4-1.

Polymer	Form	Bulk density (kg/m^3)	Inorganic content % (w/w)
PR-HD1	pellet	0.380	7.0
PR-HD2	pellet	0.569	0.3
PR-HD3	pellet	0.550	1.8
PR-HD4	pellet	0.591	0.0
PR-LD1	pellet	0.530	3.5
PR-LD2	pellet	0.318	1.0
PR-LD3	pellet	0.469	1.0
PR-PP1	pellet	0.540	0.0

Table 4-1 - Physical characteristics of the recycled polymers and inorganic content.

4.1.2 Microscopical Identification of Contaminants

The recovered inorganic content from the ashing tests was observed using a SEM equipped with an XRD Energy Dispersive System (EDS) for a qualitative elemental identification. Calcium and titanium were the main elements detected in the recycled HDPE's and LDPE's with X-ray energy dispersive scans as exemplified in Figure 4-1.

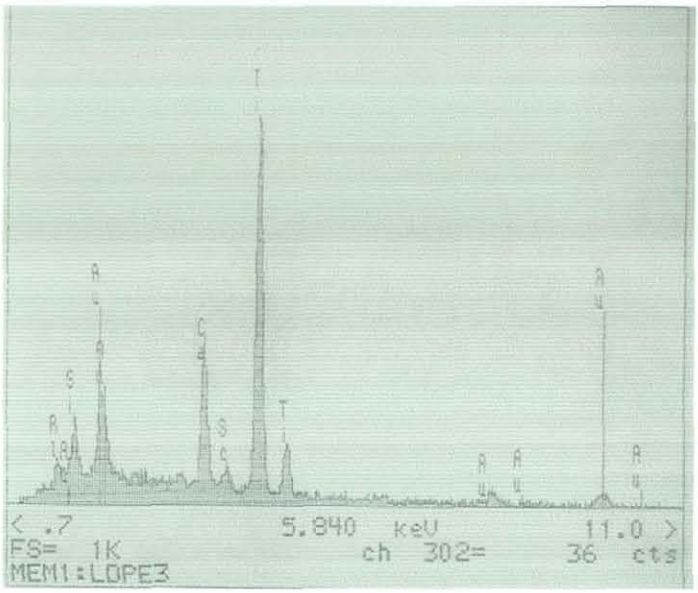

Figure 4-1 – Elemental Energy Dispersive X-ray scan of PR-LD3.

The mineral fillers of the recycled HDPE's were larger than the one's found in LDPE's, ranging from 1-10 μm and with some larger agglomerates present.

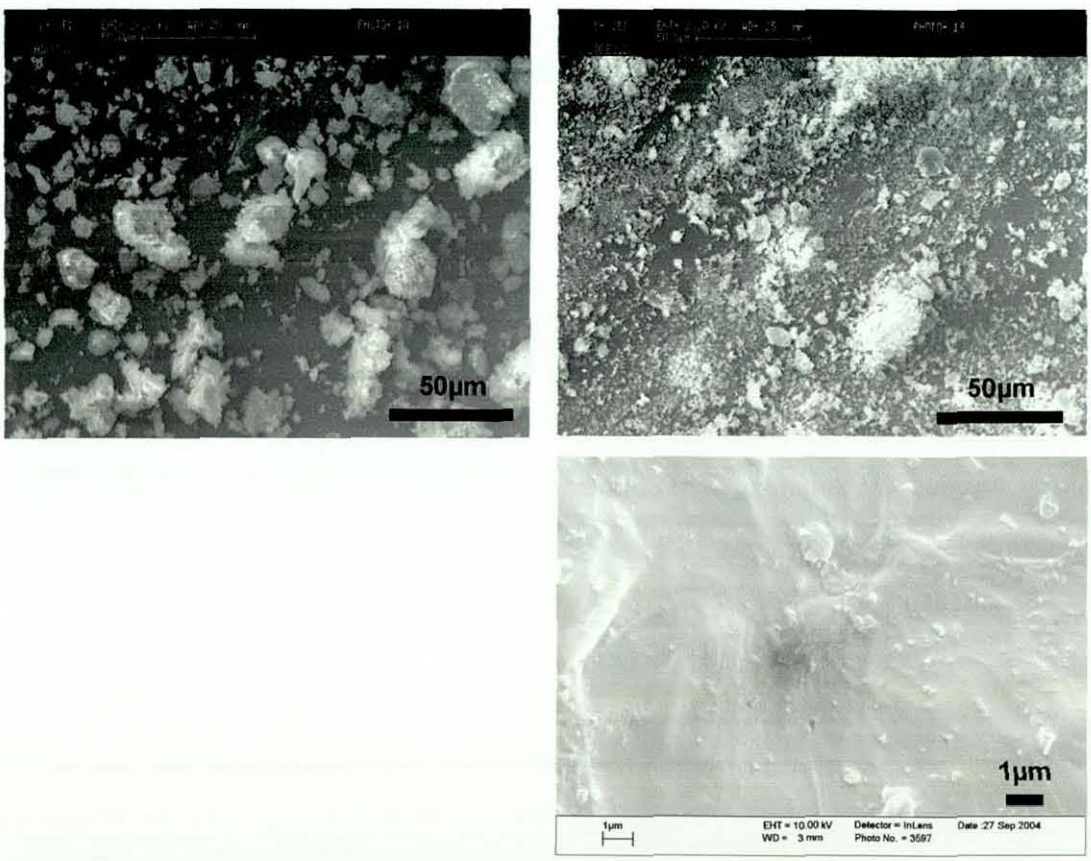

Figure 4-2 – SEM micrographs of recycled HDPE (left) and LDPE (right).

This information then allowed us to use optical microscopic techniques to identify those minerals. The inorganic content of the ashing analysis was then observed by brightfield and polarizing optical microscopy. Under brightfield optical microscopy it was possible to distinguish between calcium carbonate and titanium dioxide based on their refractive indexes (ω) which are, respectively, 1.656 (calcite) or 2.5-2.7 (depending on crystalline form).

Melt pressed films of the recycled polymers with an approximate thickness of 25μm were observed by both brightfield and polarising optical microscopy and revealed the presence of several particulates. Apart from the confirmed presence of calcium carbonate and titanium dioxide, paper fibres and metal wire was also detected. The bright spots in Figure 4-3 are the mineral particulates whereas the elongated bright particles are paper fibres.

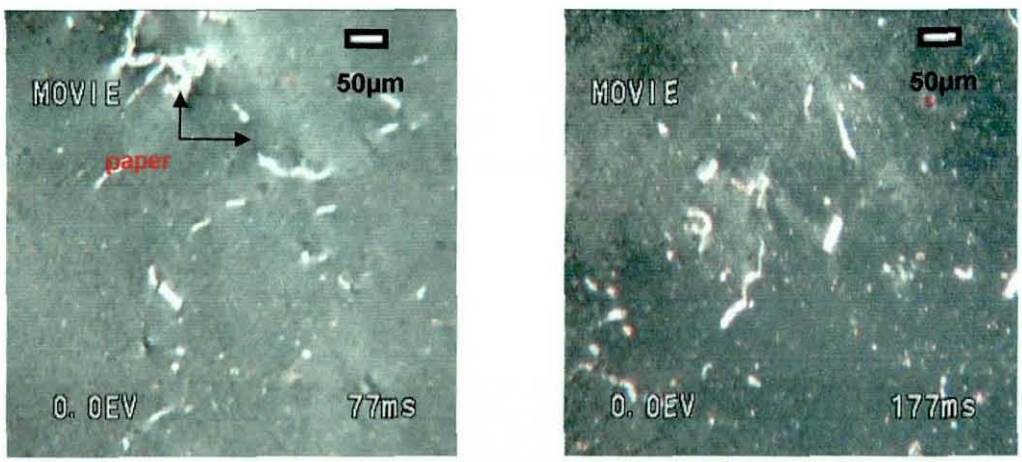

Figure 4-3 – Contaminants in recycled polymer (PR-LD3) under polarized light (x 160)

4.1.3 Differential Scanning Calorimetry

The thermal analysis of the polymers by DSC allowed the detection of polymeric phase transitions, polymer cross-contamination and determination of the degree of crystallinity.

4.1.3.1 High-density polyethylene

The thermograms of the recycled HDPE's showed only one single phase transition assignable to their melting endotherm and the corresponding crystallization curve. The melting points varied between 131-135°C, a value that is similar to that of the virgin HDPE,[19] with the crystallization temperatures varying between 110-113°C. The degree of crystallinity varied between 37-74%, with the lowest degree of crystallinity being found in the batch with the highest filler content. The heat of fusion of the virgin and recycled high-density polyethylenes is in agreement with typical values found in the literature,[113] except for PR-HD1 that is lower than usual. This suggests that that the post-consumer waste stream for HDPE is virtually free from relevant quantities of other polymers.

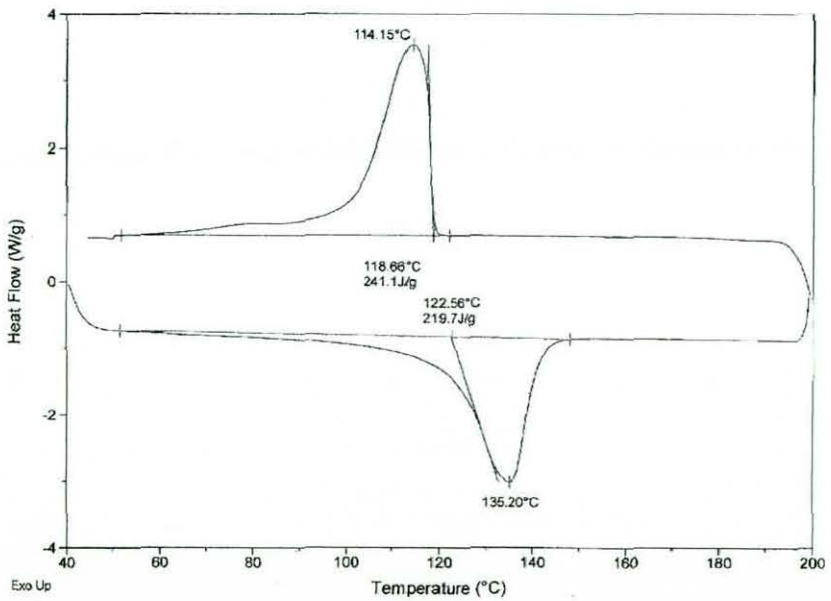

Figure 4-4 – Typical DSC thermogram of PE-HD4.

4.1.3.2 Low-density polyethylene

The DSC curves of the recycled LDPE's were more complex, by exhibiting up to three melting endotherms. LDPE's are generally difficult to separate from LLDPE. These blends are very common, thus endotherms are likely to show

two melting peaks at 110°C and 125°C.[114] LLDPE has two phase transitions that are assigned to the each of the comonomer, whereas LDPE only has a single melting transition.[115] Based on the relative intensities of each phase transition it is clear that the LDPE is not the dominant phase. A weaker third peak was found at circa 160°C that is not assignable to these materials but rather polypropylene homopolymer, suggesting a small contamination. The heat of fusion of the first endotherms is more consistent with a rich blend LLDPE.

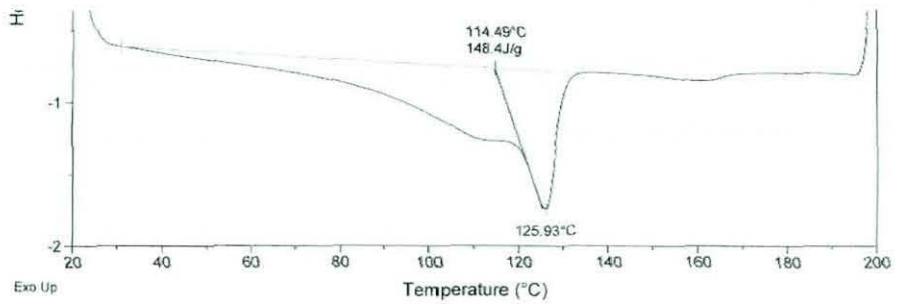

Figure 4-5 – DSC thermogram of recycled LDPE.

4.1.3.3 Polypropylene

The recycled polypropylene thermogram shows a melting endotherm at 151°C with a shoulder at 137°C. This is indicative of a polypropylene-ethylene copolymer. The ethylene comonomer affects the crystallization of the isotactic polypropylene homopolymers by lowering the melting point of the PP crystals. This is due to the interruption of the isotactic polypropylene homopolymer chain by the ethylene monomer.

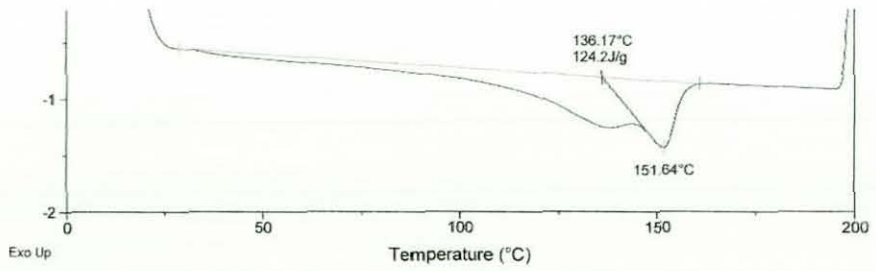

Figure 4-6 – DSC thermogram of recycled PP.

A summary of the results can be found in Table 4-2.

Polymer	Tm (°C)	Onset Tm (°C)	Tc (°C)	Onset Tc (°C)	ΔH_f (J/g)	ΔH_c (J/g)	% Inorganic	% X_f
PE-HD1	135.7	126.4	116.9	117.8	224.2	112.4	0.0	76
PR-HD1	129.2	125.4	115.1	116.2	101.5	97.6	7.0	37
PR-HD3	135.1	125.3	117.9	120.9	190.1	197.3	1.8	64
PR-HD4	135.2	122.6	114.1	118.7	219.7	241.1	0.0	74
PE-LD1	129.2	112.1	115.2	95.1	120.8		3.5	43
PR-LD2	127.2	119.1	112.1	115.1	129.1	120.0	1.0	44
	162.5	151.4						
PR-LD3	125.9	114.5	112.5	115.1	148.4	138.4	1.0	41
PR-PP1	151.6	136	117.8	122.1	124.2	104.7	0.0	-
PB1	130.3	121.0	113.1	116.2	168.0	162.7	0.0	-

Table 4-2 – Thermal properties, filler content and degree of crystallinity of raw polymers.

4.1.4 Vibrational Spectroscopy

Three types of polyethylenes, HDPE, LDPE and LLDPE can be distinguished based on two frequencies. High-density polyethylene does not possess a vibrational frequency at 1377 cm^{-1} that is associated with chain branching, whereas LLDPE and LDPE do.[116] Also, when the absorbance at 1377 cm^{-1} is higher than the absorbance at 1366 cm^{-1} then the polymer is LLDPE. Conversely, when the contrary is true the spectrum belongs to LDPE. Polypropylene can be distinguished from polyethylenes by considering other frequencies. For pure PP the peak at 1168 cm^{-1} is relevant being absent in polyethylenes. Other two frequencies exclusive to PP are 972 cm^{-1} and 997 cm^{-1}.[116] Based on this information it is possible to identify polyolefinic cross-contaminants by the interpretation of the infrared spectrum. Table 4-3 summarises the main group absorption frequencies assignable to polyethylene and polypropylene.

Band (cm^{-1})	Assignment	Intensity
2919	CH_2 asymmetric stretching	Strong
2851	CH_2 symmetric stretching	Strong
1473 and 1463	Bending deformation	Strong
1377	CH_3 symmetric deformation	Weak
1366 and 1351	Wagging deformation	Medium
1306	Twisting deformation	Weak
1176	Wagging deformation	Very weak
990, 910, 908	Terminal vinyl groups	-
888	Vinylidene type unsaturations	-
731-720	Rocking deformation	medium
1219	Helicoidal conformation of PP	-
1167	Same as 1219 cm^{-1}	-
997	Helicoidal conformation of PP, Isotactic sequence of 11-12 units	-
972	Two or more head to tail units of Following PP	-
720	Sequence of five or more contiguous Methylene groups	-

Table 4-3 - Main absorptions of polyethylene and polypropylene in the IR region and their assignment.[115, 116]

Both PE-HD1 and PR-HD4 exhibited very similar FTIR spectra with the typical absorption bands assignable to polyethylenes, 1472, 1462, 730 and 720 cm^{-1} and specifically to high-density polyethylene such as the 1351-1366 cm^{-1} doublet. No group frequency associated to ethylene chain branching or polypropylene was present. PE-HD1 showed the characteristic 908 and 990 cm^{-1} absorption frequencies of high-density polymers produced by the Phillips process.[19] These frequencies are much weaker in PR-HD4 but were more easily detected in the other recycled HDPE batches. We can assume that based on FTIR analysis and previous thermal analysis that the degree of polymer cross-contamination is not significant for the reclaimed high-density polyethylenes.

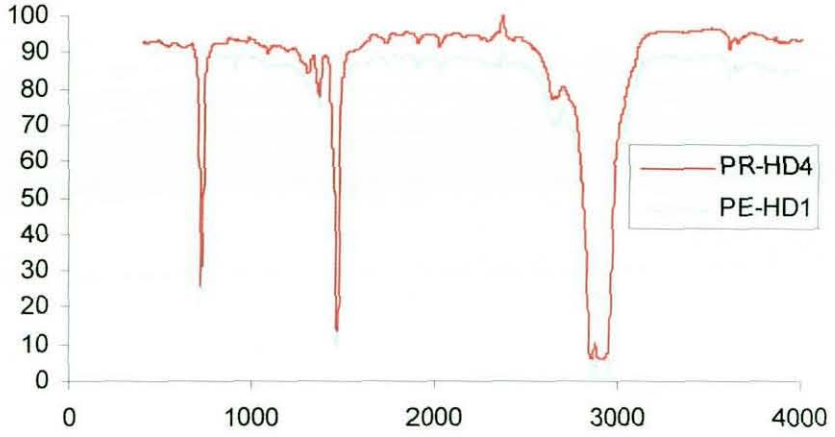

Figure 4-7 – Infrared spectrum of PR-HD4 and PE-HD1.

The infrared spectra of the recycled LDPE polymers, PR-LD1 and PR-LD2, also show the main polyethylene peaks. According Gulmine et al.[116] we should be able to resolve between 1376 cm^{-1} and 1366 cm^{-1} to distinguish between pure LLDPE and LDPE, however in our case we only see an unresolved peak at 1375 cm^{-1}. This does not allow us to determine the relative polymer quantities in such blends. This could be related to technical limitations or interference from pigments and fillers.[117] The position of the methyl deformation band usually centred at 1378 cm^{-1} varies with the type of LDPE and can be used to identify branches in pure LDPE. However, the absence of a band at 888 cm^{-1} characteristic from high pressure polyethylenes and the presence of a vinyl characteristic band at 908 cm^{-1} suggest that these materials may be LLDPE rich. One can also see specific absorption frequencies to isotactic PP at 972 and 997 cm^{-1} which confirms the previous results from the DSC analysis that these samples are contaminated with polypropylene.

The spectrum of recycled PP, Figure 4-9, shows characteristic peaks from isotactic PP at 972 and 997 cm^{-1}. The bands in 997 and 840 cm^{-1} particularly, show that the length of the isotactic segments are long, from 11 to 15 units, and their intensity ratio can be used for measuring the degree of isotacticity.[115] By exhibiting a peak at 732 cm^{-1}, this is consistent with the

DSC results that show a typical thermogram from a random polypropylene copolymer.

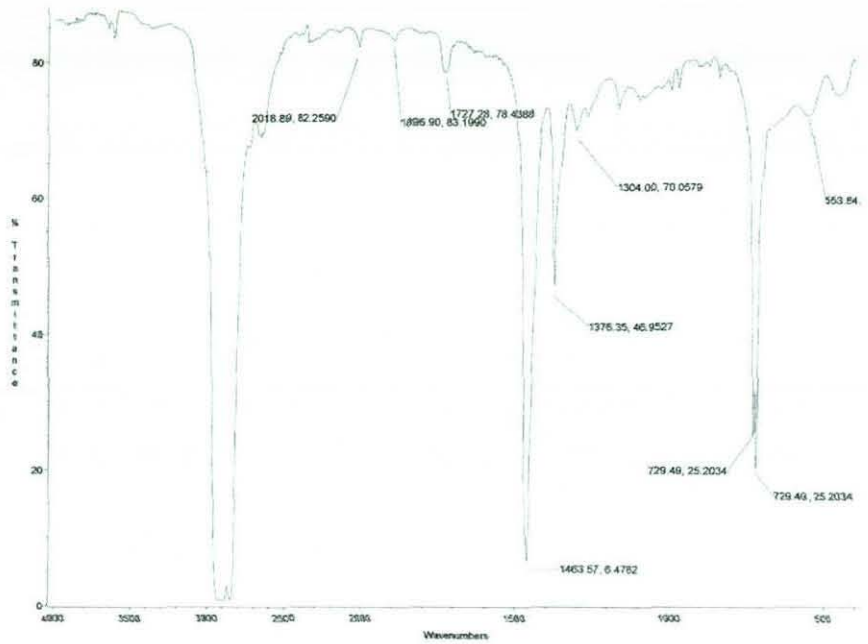

Figure 4-8 – FTIR spectrum of PR-LD3.

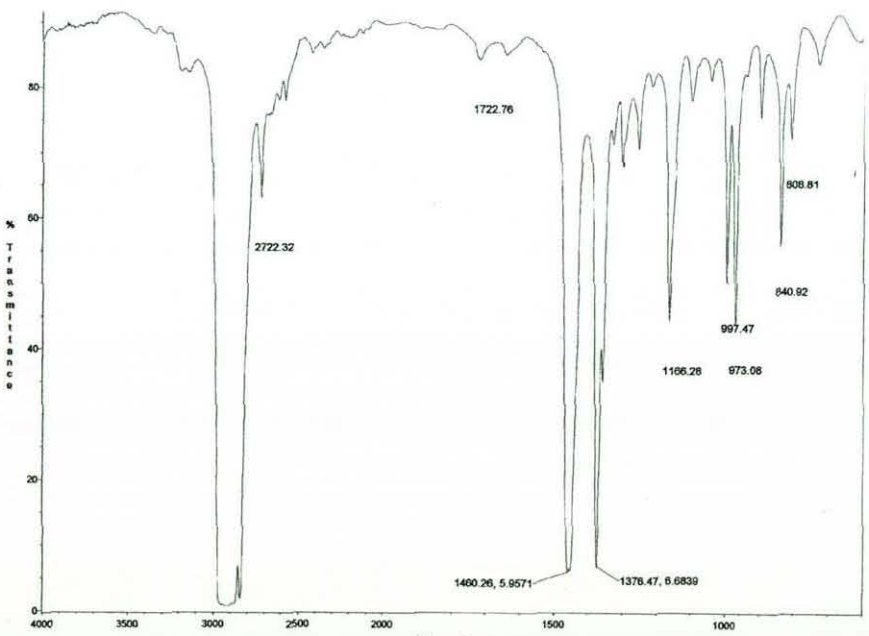

Figure 4-9 – FTIR spectrum of PR-PP1.

In contrast the FTIR spectrum of HMS Daploy (Appendix VI) is more consistent with a PP homopolymer, as can be confirmed by its DSC thermogram, with one single phase transition assignable to the melting band. In summary, both virgin and recycled HDPE didn't show any significant contamination from branched polyethylenes or propylene and appear to be constituted solely by HDPE. The recycled LDPE's seem to be contaminated by LLDPE and isotactic propylene. Recycled polypropylene is not isotactic, being more likely a random copolymer.

4.1.5 Gel Permeation Chromatography

Two different techniques were used to determine the resins molecular characteristics. Conventional GPC was used for the HDPE's and GPC-viscosity for LDPE's and PP's. In conventional GPC the retention volume is followed over time by detecting differences in the refractive index of the solvent and the analytes. But this technique is not well suited for branched polymers. With GPC the polymer is fractionated as a function of its solvated size, branching tends to restrict the solvation and the polymer appears to be of lower molecular weight than actually the case. The GPC-viscosity approaches allow for this difference in solvation and give the 'true' molecular weight.

4.1.5.1 Conventional GPC

4.1.5.1.1 High-Density Polyethylene

Both PR-HD4 and PE-HD1 were analysed by conventional GPC. In the chromatograms - Figure 4-10, Figure 4-11 - PR-HD4 appears to be of higher molecular weight and marginally narrower molecular weight distribution than the PE-HD1. One must note that the chromatograms are reversed with respect to the molecular weight distributions. High molecular weight material is observed at low retention volume so appears on the left but on the right

hand side of molecular weight distributions. Figure 4-11, which plots the on-line differential pressure detector signal shows that despite the calculated averages - Table 4-4 - PE-HD1 does include material of lower retention volume (higher molecular weight) than the PR-HD4. It is surprising to see that the recycled polymer PR-HD4 has a narrower molecular weight distribution which clearly suggests that this particular batch originated from a very consistent waste stream. The fact that the virgin HDPE includes a higher molecular weight fraction will help explain some of its flow properties in comparison with the recycled HDPE in the coming sections. These fractions contribute significantly to the polymers relaxation time and extensional viscosity.

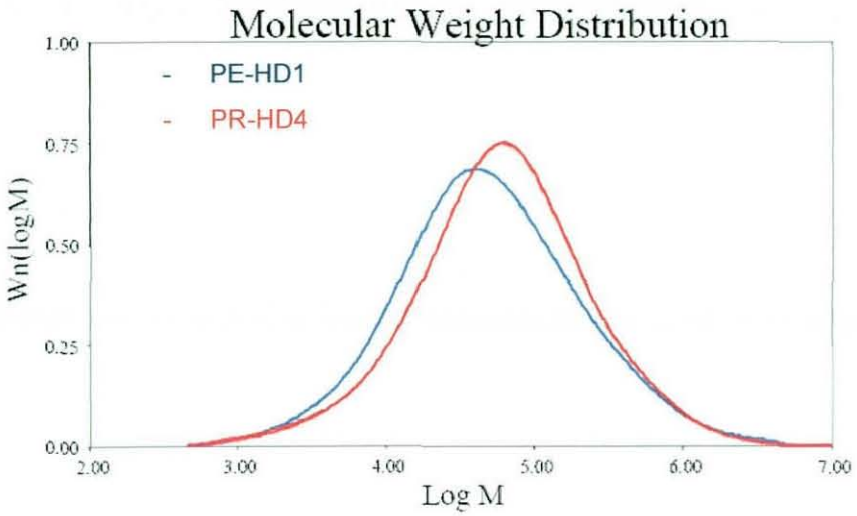

Figure 4-10 - Molecular weight distribution for virgin and recycled HDPE.

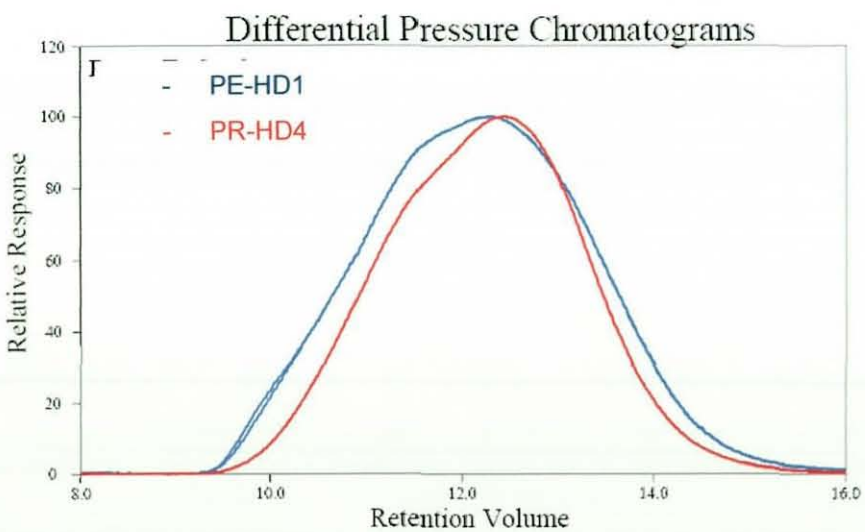

Figure 4-11 – Differential pressure chromatogram for virgin and recycled HDPE.

Polymer	Type	Mw	Mn	Polydispersity
HDPE	Virgin	138000	18600	7.4
	Recyclate	146000	21300	6.8

Table 4-4 - Molecular weight, and polydispersity from conventional GPC test.

4.1.5.2 Universal GPC-viscosity

4.1.5.2.1 Low-Density Polyethylene

The molecular weight distribution curves for the virgin LDPE (PE-LD1) and a recycled LDPE (PR-LD3) can be found in Figure 4-12. The superposition of the two curves shows that the near-equivalent virgin LDPE resin chosen was an adequate choice for a control. The parameters derived from this curve are in Table 4-5

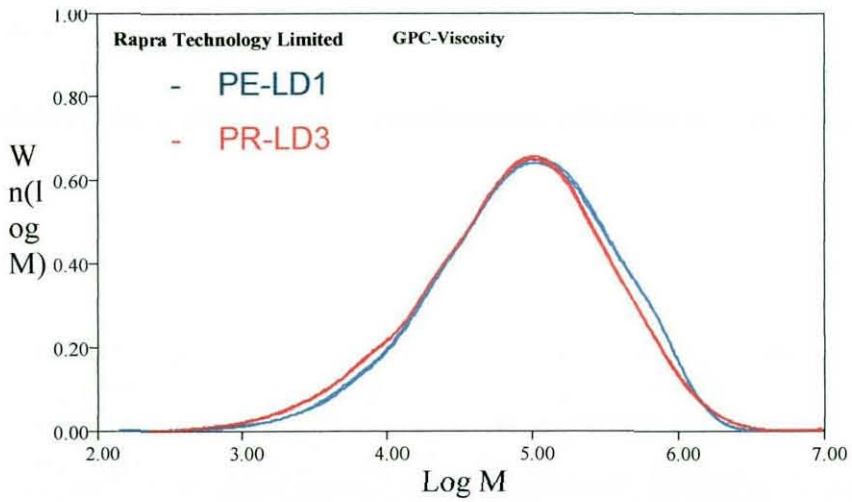

Figure 4-12 – Molecular weight distribution of LDPE virgin and recyclate – universal GPC.

The virgin sample appears to be of a slightly higher molecular weight. The polydispersity of the recycled sample is higher but this is not obvious from the universal approach.

Polymer	Type	Mw	Mn	Polydispersity	Log K	alpha	$[\eta]_L$
LDPE	Virgin	195000	26,100	7.5	-2.62	0.53	1.53
	Recyclate	187000	20,800	9.0	-3.35	0.70	2.19

Table 4-5 - Molecular weight, and polydispersity from universal GPC test.

The intrinsic viscosity plot - Figure 4-13 – compares intrinsic viscosity of polyethylene standards with the virgin and recycled LDPE. This gives an indication of the level of chain branching present. Generally, the higher the level of chain branching the lower the gradient of the intrinsic viscosity plot. By comparing the supplied LDPE's with the NBS 1475 (linear polyethylene) and NBS 1476 (branched polyethylene) it can be seen that the virgin LDPE has a shallower slope than the standard branched polyethylene. This is indicative of a higher branching content. By using the same argument it can be said that PR-LD3 has lower level of branching than both the branched standard and PE-LD1. These results support the idea that the recycled LDPE sample may indeed be a blend of LDPE with some other linear polyethylenes and the already identified polypropylene contaminant.

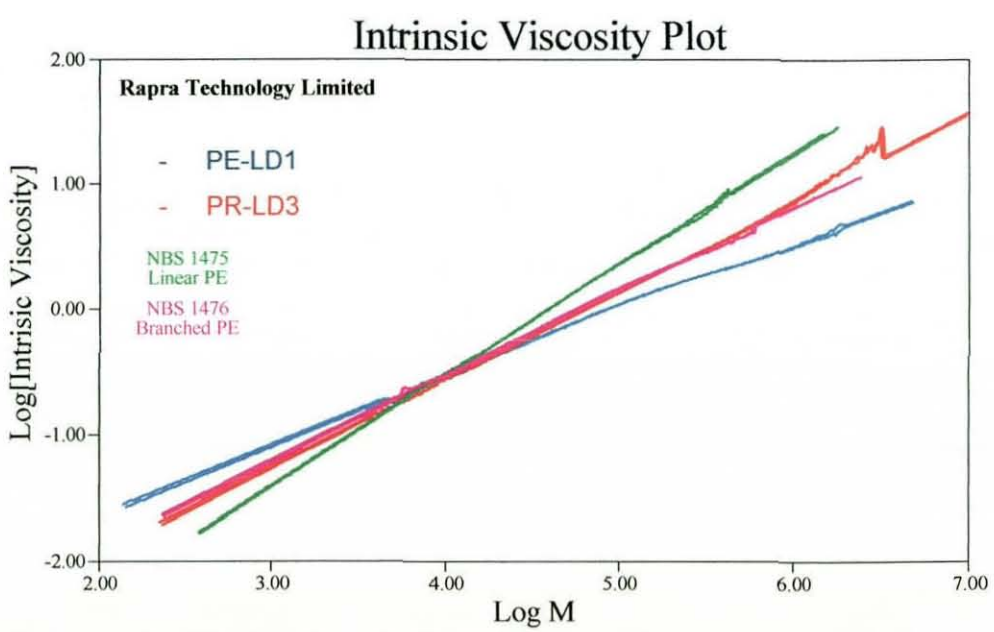

Figure 4-13 – Intrinsic viscosity vs. molecular weight for virgin and recycled LDPE.

4.1.5.2.2 Polypropylene

The molecular weight distribution curves and molecular parameters for the virgin PP (PO-PP1) and a recycled PP (PR-PP1) can be found in Figure 4-14 and Table 4-6, respectively. The branched PP sample appears to be overall higher molecular weight and broader molecular weight distribution than the recycled one. The molecular weight distribution of the branched virgin PP does not appear to be symmetric and it is possible that it consists of lower molecular weight polymer blended with high molecular weight branched polymer.

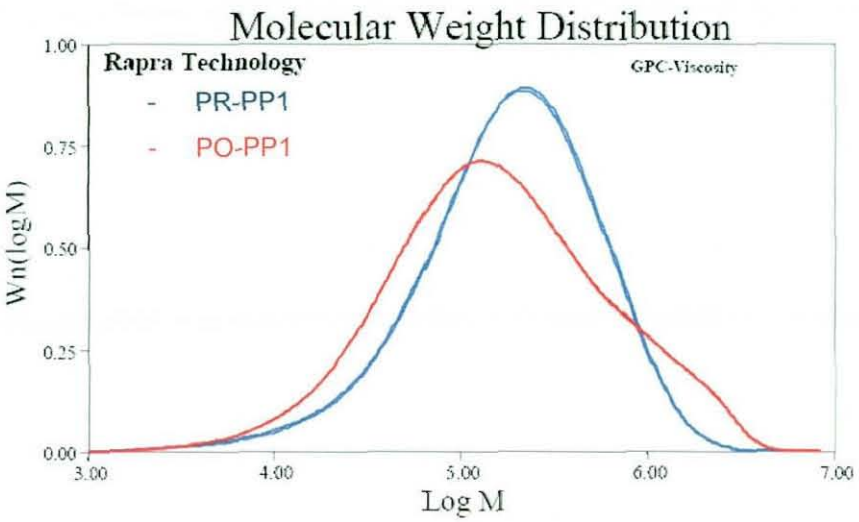

Figure 4-14 – Molecular weight distribution of virgin and recyclate PP – universal GPC.

Polymer	Type	Mw	Mn	Polydispersity	Log K	alpha	$[\eta]_L$
PP	Virgin	357000	60100	5.9	-3.12	0.59	1.41
	Recyclate	309000	95100	3.3	-3.93	0.76	1.74

Table 4-6- Molecular weight, and polydispersity from universal GPC test.

The intrinsic viscosity plot of the polypropylene samples is depicted in Figure 4-15. A linear stock PP was compared to the other polypropylenes. The superposition of the recycled PP curve with the linear PP indicates that this is a linear molecule and the departure of this curve with a lower slope by the virgin PP proves that it has a higher branching content. This is also reflected in the calculated Mark-Houwkin parameters.

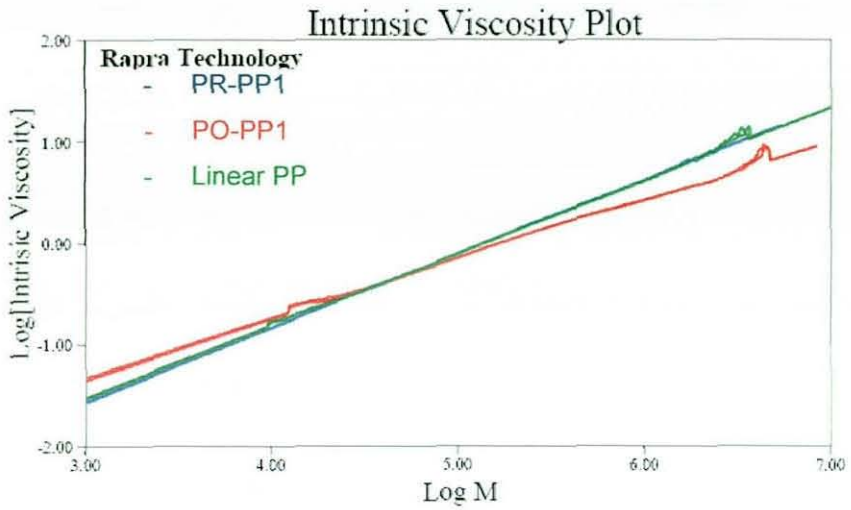

Figure 4-15 – Intrinsic viscosity vs. molecular weight for virgin and recycled PP.

Branching calculations were provided by Rapra Technology. These calculations involved various assumptions and the values are best considered as comparative, rather than being absolute. The average values for the number of branches per thousand repeat units and the radius of gyration (g') has been computed.

Sample	Nr. Branches (per 1000 C)	g'
PR-PP1	0.22	0.98
PO-PP1	2.87	0.87
PP standard	0.20	0.98

Table 4-7 – Branching content and gyration radius of recycled and virgin PP.

4.1.5.3 Summary

For all three polymer types there are distinct differences in the molecular weight distributions of the 'Recyclate' as compared to the 'Virgin' material. The degree of difference is possibly surprising, particularly when in all three cases the 'Recyclate' includes material of higher molecular weight than the 'Virgin' material. With the exception of the 'HDPE' there also appear to be differences in branching.

4.1.6 Thermogravimetry

From a blowing agent thermogram it is possible to determine not only the decomposition onset for gas evolution, but also, the approximate amount of gas evolved assuming the according stoichiometry, whether we are using pure bicarbonate or an acid/carbonate blend. From the thermogram it can be seen that Hydrocerol BM70 is a blend of citric acid/sodium bicarbonate. The stoichiometry for this blowing agent was described previously, in section 2.3.4. It was found that the decomposition temperature of the CBA started around 150°C and that the amount of gas evolved varied was approximately 83cm^3/g. In the thermogram, apart from the weight vs. temperature plot (green curve), the weight loss derivative (blue curve) is also plotted, making it easy to identify the onset of CBA agent decomposition, subsequent decompositions of blowing agent and degradation of the polymer carrier if present. For Hydrocerol BM70, a first decomposition due to gas evolution starts at about 150°C, followed by an unidentified small decomposition but not assignable to more gas evolution, and finally the polymer carrier degradation.

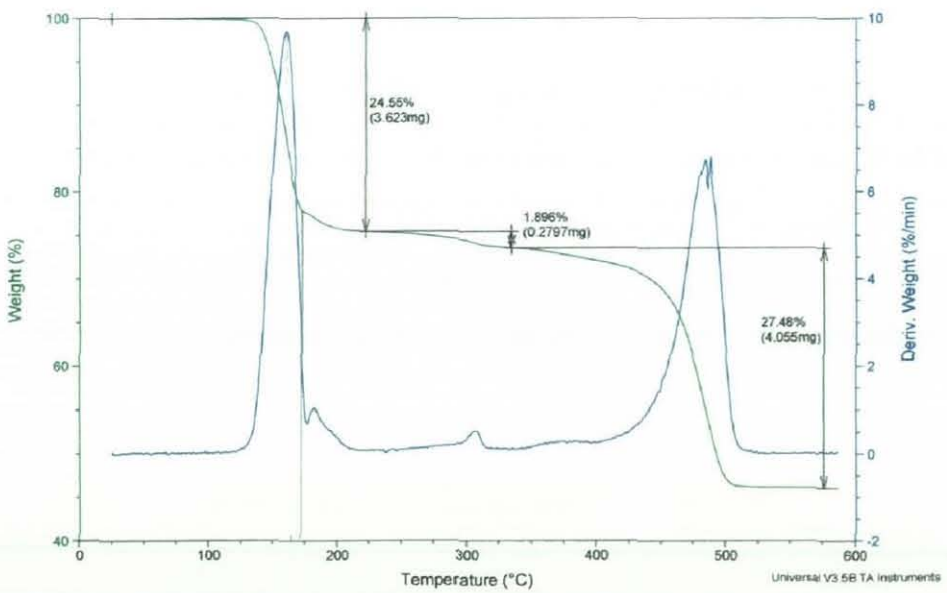

Figure 4-16 - Thermogram from Hydrocerol BM 70.

4.2 Rheological Characterization

4.2.1 Melt Flow Index

The melt flow index of the supplied polymers was determined in order to assess the molecular weight and choose a suitable virgin control sample. For linear polyethylenes the MFI can be directly related to the molecular weight.[41] These results can be found in Table 4-8.

Polymer	MFI (dg min^{-1})
PE-HD1	1.18 (±0.03)
PR-HD1	1.19 (±0.04)
PR-HD2	1.20 (±0.03)
PR-HD3	1.26 (±0.06)
PR-HD4	1.73 (±0.04)
PR-LD1	1.10 (±0.07)
PR-LD2	1.04 (±0.04)
PR-LD3	1.14 (±0.05)
PO-PP1	2.1 (±0.08)*
PR-PP1	4.33 (±0.08)
PB1	13.9 (±0.06)

Table 4-8 – Melt flow rate of the supplied polymers tested at 190°C with a 5 kg load. * - tested at 230°C.

All recycled polyethylenes show high viscosity exemplified by very low MFI values, typical of extrusion grades. Considering the melt flow index of the recycled high-density polyethylenes, and knowing that the majority of the waste stream is constituted by blow moulded milk bottles, it was decided to choose Eltex HD6007XA from Solvay (PE-HD1) which is recommended for rigid plastic bottles and has a similar MFI. Of all the batches of recycled high-density polyethylene tested PR-HD4 showed the highest MFI. The recycled polypropylene, due to its low melting point was also tested at 190°C with a 5kg load. The clear recycled polypropylene which is thought to be a random copolymer used for food containers or cups, due to its high clarity has a melt flow index that suggests it is a grade suitable for extrusion, thermoforming and injection blow moulding. Because polypropylene is not suitable for

foaming it was decided to compare this grade with a special branched polypropylene grade Borealis, HMS Daploy (PO-PP1). All the recycled LDPE's exhibited similar melt flow indexes consistent with extrusion grades.

4.2.2 Melt Fracture Behaviour

Melt fracture behaviour for each polymer was assessed at several temperatures before the final capillary rheometry measurements to determine the range of shear rates where fully developed flow assumptions that this technique is based on are valid. Only the measurements in this interval should be used to produce a flow curve at different temperatures. For these determinations, a 24x1.5 mm and a 0x1.5 mm flat entry dies were used. Table 4-9 summarizes the flow behaviour the polymers tested at 190°C.

Polymer	Shear range (s^{-1})	Sharkskin	Slip-stick	Gross melt fracture
PE-HD1	1-400	-	-	-
PR-HD1	1-1000	-	> 400 s^{-1}	-
PR-HD2 ; PR-HD3 ; PR-HD4	1-400	-	-	-
PE-LD1	1-400		90-300 s^{-1}	> 300 s^{-1}
PR-LD1 ; PR-LD2 ; PR-LD3	1-400	-	90-200 s^{-1}	> 200 s^{-1}
PO-PP1	50-400	-	-	50-400 s^{-1}
PR-PP1	1-400	-	-	-
EP1	1-400	-	> 150 s^{-1}	-

Table 4-9 – Melt fracture behaviour of virgin and recycled polymers at 190°C.

Apart from PR-HD1, no other high-density polyethylene showed evident flow instability behaviour over the deformation rates tested, when tested between 150°C-210°C. PR-HD1 showed slip-stick instability at all temperatures that worsened when the temperature was lowered. This material also showed melt fracture due to cardboard fibber contamination. The recycled low-density polyethylenes show wall slip onset from around $90s^{-1}$ when tested between 150°C-210°C that then turns into gross melt fracture from $200s^{-1}$. The virgin low-density polyethylene had a similar behaviour with gross melt fracture starting at around 300 s^{-1}.

The recycled polypropylene didn't show any kind of noticeable flow instability, contrary to the branched high-melt strength polypropylene that showed slip-stick and gross melt fracture between 50-400 s^{-1} when tested between 190°C-230°C. EP1, the ethylene-propylene copolymer was also tested in the same range of temperatures of polypropylene exhibiting a clear transition from a smooth extrudate to waving sharkskin extrudate between $100s^{-1}$ and $200s^{-1}$.

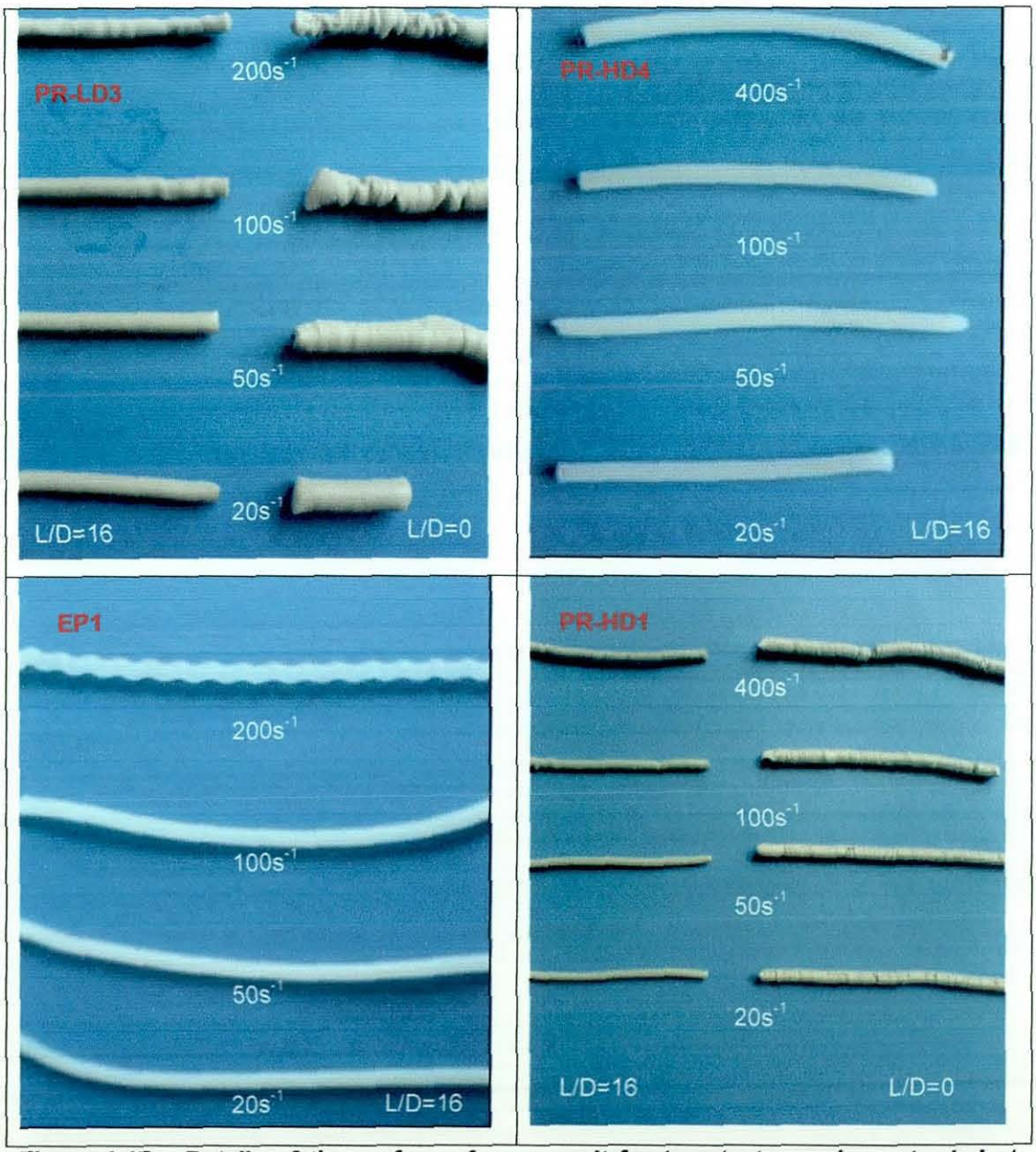

Figure 4-17 – Details of the surface of some melt fracture test samples extruded at 190°C.

4.2.3 Capillary rheometry

A more complete rheological evaluation of each material was performed by studying the flow behaviour of the resins with a capillary rheometer equipped with a L/D 16 (24x1.5 mm) flat entry steel die and also a 0x1.5 mm die. The determinations were done at several temperatures and over a range of rate imposed deformations where the fully developed flow assumptions were valid.[45] Thus it was possible to establish the temperature dependence of the viscosity. Shear rates as low as 1 s^{-1} were used to improve the fit of flow data to the Carreau-Yasuda model.[43] This model allows the estimation not only of the pseudoplasticity index but also the zero shear rate viscosity, and the characteristic relaxation time. Compiling this information is important to predict flow behaviour at arbitrary conditions with fluid dynamics software.

4.2.3.1 Recycled Polymers

The typical shear flow behaviour of the different types of recycled polymers is illustrated in Figure 4-18.

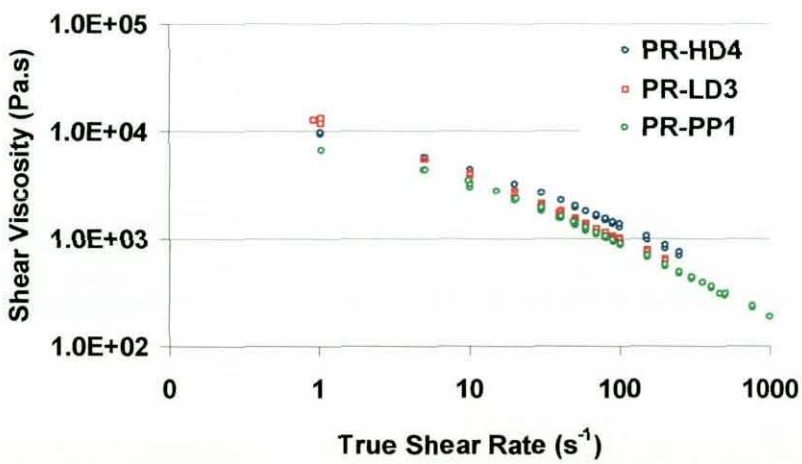

Figure 4-18 – Comparison of shear flow behaviour of recycled polymers at 190°C.

Despite have the highest M_w, PR-PP1 is the least viscous material over the entire shear deformation range tested which is expectable based on the melt

flow index results. The shear viscosity of pure polymers is affected by several parameters such as molecular architecture, molecular weight or polydispersity.[39,42,43]

Short and long-chain branching can increase the free volume, reduce the radius of gyration compared to a linear chain of the same molecular weight; increase the entanglement density for LCB.[121,128] The length of the side chain is critical. Small side chains like in polypropylene can increase the free-volume, making little contribution to flexibility and enlarging the inter chain distance, thus reducing viscosity. When the side chain is longer, but shorter than the critical molecular weight of the linear chain the radius of gyration is reduced, and consequently the number of entanglements and viscosity is decreased. These arguments can help to explain the differences in shear flow. The lower viscosity of LDPE at higher shear rates, despite the higher M_w compared to HDPE is possibly related to the influence of the LCB that can reduce the gyration ratio, however one cannot rule out the viscosity negative deviating behaviour when PP is present. Long-chain branching has a big effect in the shear flow behaviour in branched polyethylenes but also in linear polyethylenes that possess some LCB. These affect mainly the linear viscoelastic part of the shear flow curves.[47]

4.2.3.2 High-density Polyethylene

The behaviour from the recycled HDPE's doesn't differ much from the chosen virgin resin (Figure 4-19). The recycled HDPE is less non-Newtonian compared to virgin HDPE having the highest pseudoplasticity index. Lower molecular polymers exhibit the Newtonian plateau over a greater shear rate range.[121] Based on this information and on the GPC results one could expect that PE-HD1 would exhibit this plateau earlier than PR-HD4, but the opposite was observed. This can be tentatively explained by the influence of the higher molecular fractions or even the presence of a small amount of LCB. Comparatively, PE-HD1 seems a more suitable resin for extrusion blow

moulding due to its lower shear viscosity over most of the shear range and a higher zero shear rate viscosity (see Table 4-10).

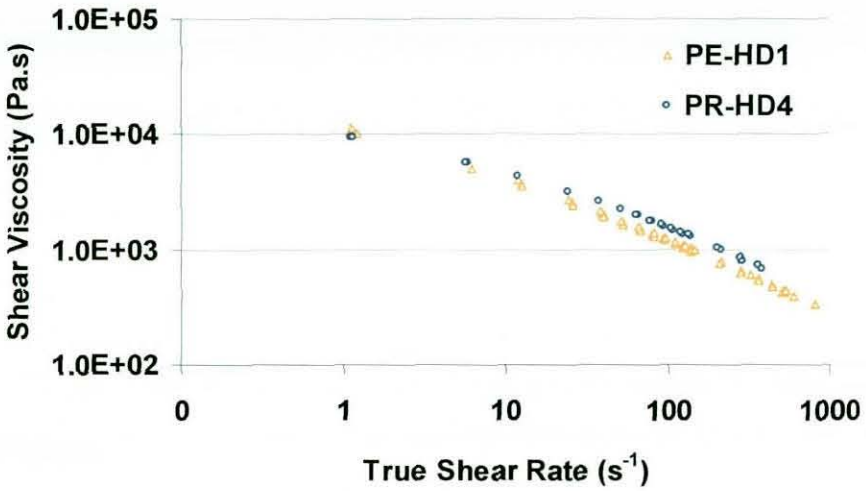

Figure 4-19 – Shear flow curves of PE-HD1 and PR-HD4 at 190°C.

4.2.3.3 Polypropylene

In Figure 4-20 it is compared the flow behaviour of the polypropylene based materials. It is quite clear that the virgin long-chain branched PP is much less viscous than the recycled PP, which is undoubtedly related to its high LCB content, which is a parallel behaviour to LDPE resins.

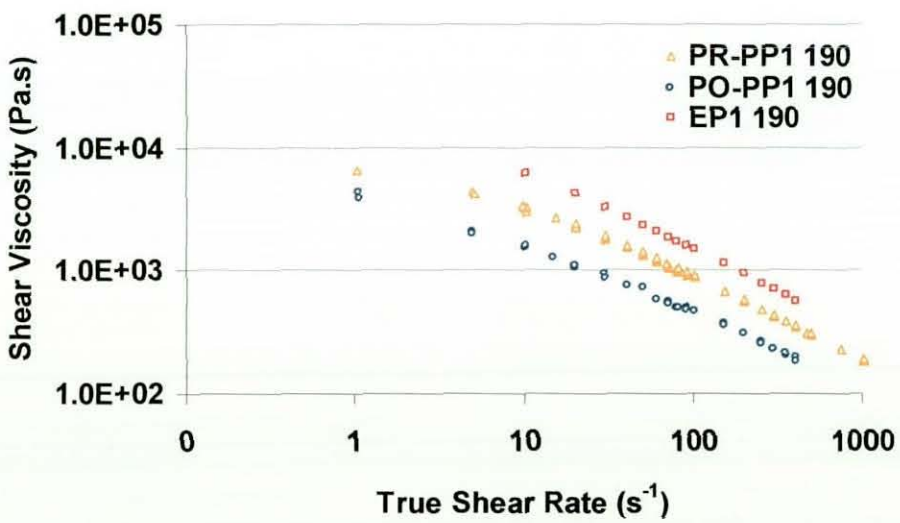

Figure 4-20 – Shear flow behaviour of polypropylene based resins at 190°C.

The polypropylene-ethylene copolymer exhibits a much higher viscosity than the recycled polypropylene which may indicate higher ethylene content or molecular weight.

4.2.3.4 Low-density Polyethylene

The flow behaviour of the recycled LDPE's is similar to that of the virgin resin, which is expected based on the melt flow index results. The lower shear viscosity of the virgin LDPE is possibly related to its higher long-chain branching content, despite having a higher M_w. It is not possible to conclude more on PR-LD3 because of its PP content which, as mentioned is likely to lower the shear viscosity of the blend.

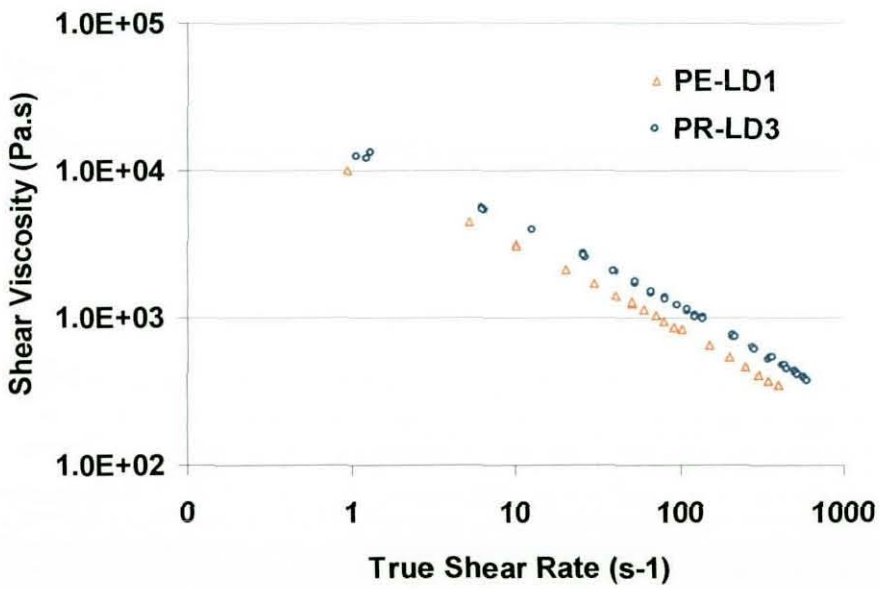

Figure 4-21 – Shear flow behaviour of low-density polyethylenes at 190°C.

4.2.3.5 Influence of melt temperature

The effect of temperature on the flow curves didn't show any difference from relative viscosities of the polymers, though some were more temperature

sensitive than others. This can be evaluated in the sequence of graphs that follows.

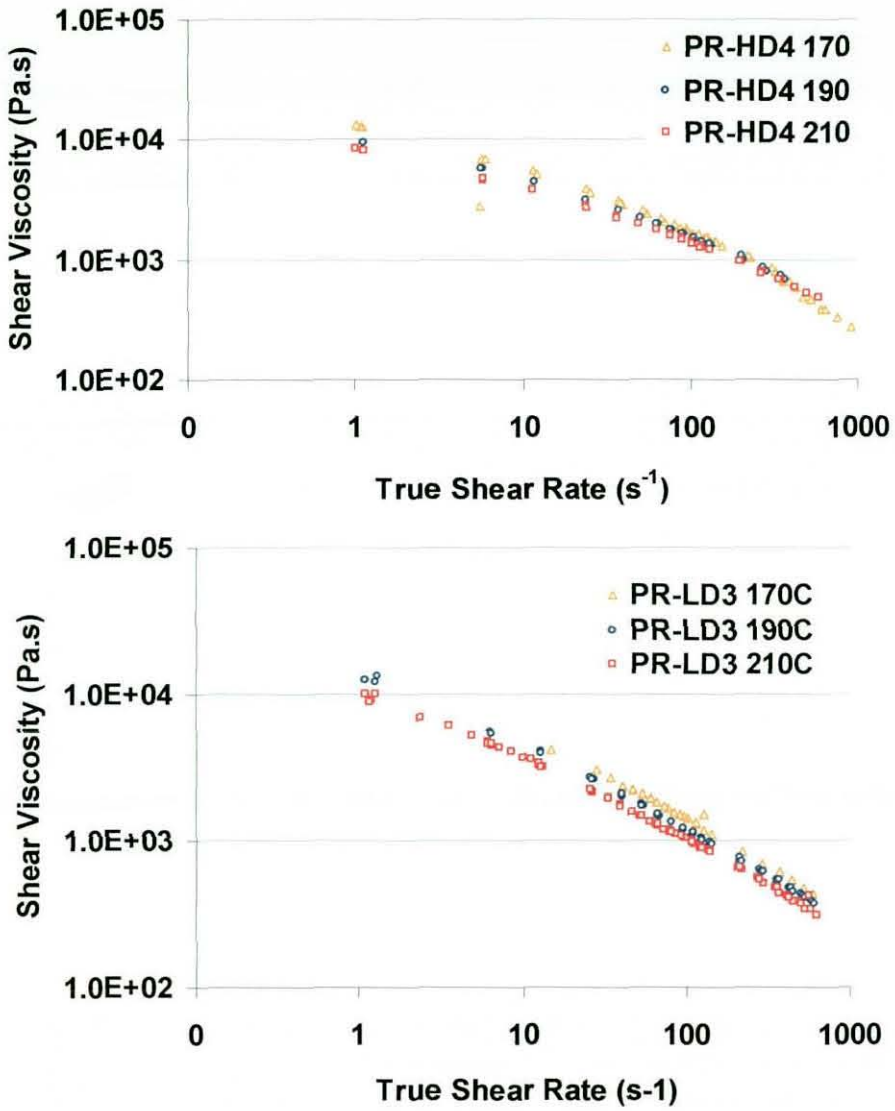

Figure 4-22 – Shear flow curves of recycled HDPE (top) and LDPE (bottom) at several temperatures.

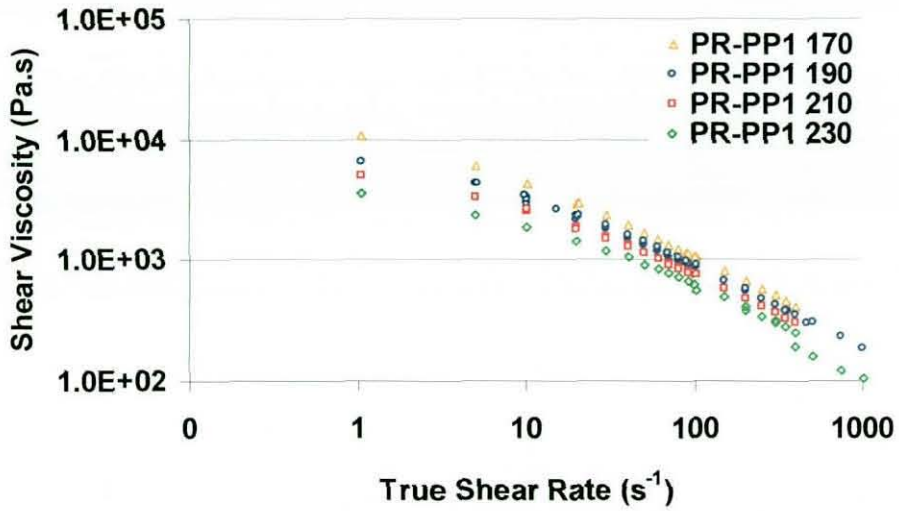

Figure 4-23 – Influence of temperature on shear flow behaviour of recycled PP.

By fitting the experimental flow data to the generalized Newtonian flow model mentioned previously the relevant parameters were determined and summarized in Table 4-10. The fit improved significantly with the use of low shear rate data points and described correctly the transition between the power law and linear viscoelastic region (Appendix VII). Additionally, assuming an Ahrrenian behaviour, the flow activation energy was estimated by plotting the logarithm of the estimated zero shear rate viscosity against the respective reciprocal absolute temperature.

Polymer	parameters	Temperature (°C)			
		170	190	210	230
PE-HD1	η_0 (Pa s)	15414	13226	6245	-
	t_1 (s)	0.17	0.95	0.23	-
	n	0.44	0.47	0.46	-
PR-HD4	η_0 (Pa s)	14029	10065	8076	-
	t_1 (s)	0.59	0.55	0.69	-
	n	0.48	0.53	0.56	-
PR-LD3	η_0 (Pa s)	17928	15940	11289	-
	t_1 (s)	0.24	0.97	0.88	-
	n	0.39	0.43	0.46	-
PR-LD2	η_0 (Pa s)	-	16325	14941	-
	t_1 (s)	-	0.97	1.28	-
	n	-	0.43	0.45	-
PR-PP1	η_0 (Pa s)	-	6445	4961	3421
	t_1 (s)	-	0.373	0.38	0.41
	n	-	0.42	0.46	0.52

Table 4-10 – Fitted parameters of the Carreau model at several temperatures.

As can be seen, decreasing the temperature increases the viscosity of the materials, and accentuates their non-Newtonian behaviour. The effect of temperature on the viscosity of high-density polyethylene illustrates this fact. The magnitude of temperature dependence of the viscosity is related to the flow activation energy being higher for higher activation energy.[45] The levels of polymer cross-contamination and filler content didn't seem to lead to any departure of this behaviour. The length of the side chains bears a significant influence on the values of the flow activation energy. It increases with the length of the side branch going through a maximum then decreases with simultaneous increase in flexibility. This justifies higher flow activation energies for polypropylenes and low-density polyethylenes. Conversely, explains also the lower flow activation energy for HDPE. Literature values are between 30-40 kJ/mol for PP and LDPE; and 20 kJ/mol for HDPE.[127] The flow activation energy of the analysed virgin and recycled polymers can be determined from the slopes of the curves of Figure 4-24. The calculated flow activation energies can be found in Table 4-11. The values for PE-HD1 and PR-LD3 are lower than expected, whereas the ones from the other polymers are close to results reported by other authors.[38]

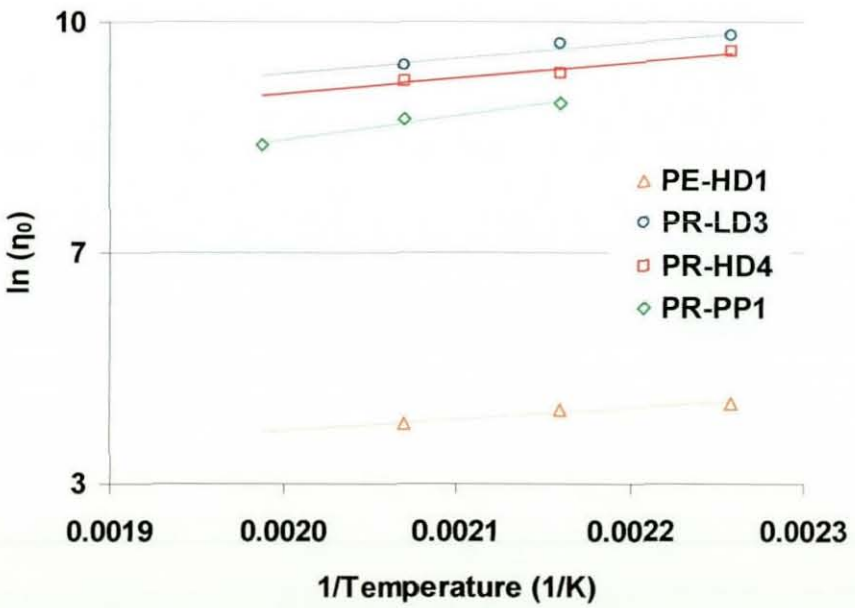

Figure 4-24 – Flow activation energy plot of supplied polymers.

	Flow Activation Energy (KJ/mol)
PE-HD1	13.8
PR-HD4	20.0
PR-LD3	20.4
PR-PP1	30.6

Table 4-11 – Flow activation energy of raw polymers.

4.2.3.6 Wall Slip

During polymer processing flow instabilities such as melt fracture and wall slip occur at extrusion throughput rates exceeding a certain critical stress. Numerous publications have been devoted to understanding these phenomena.[118, 119] Current understanding relates wall slip to the lack of adhesion of the polymer to the wall, though whether this happens at the die entrance or exit is debatable. A recent review from Denn[118] and the work from Robert et al.[120] provide a good overview of the subject.

Particularly in linear long-chain polyethylenes, the typical flow curve exhibits two stable branches separated by the so-called spurt or stick-slip instability area. In this area, the pressure in the reservoir oscillates between two extreme values, although the imposed flow rate is kept constant. The oscillating flow involves both compressibility of the melt in the reservoir and a periodic slip at the wall of the capillary.[120] Wall slip can lead to unacceptable extrudates, therefore it is necessary to characterise it. This is usually performed by the Mooney technique.[44]

As specified in section 3.3.2 five steel dies of different diameters with L/D 16 were used to investigate the possible wall slip behaviour of virgin and recycled HDPE. From those flow curves plots of apparent shear rate vs. the reciprocal radius at arbitrary shear stress levels were produced.

4.2.3.6.1 High-density Polyethylene

The flow curves of recycled high-density polyethylene featuring shear stress as a function of shear rate at 170°C show typical shear flow behaviour

assignable to wall slip. A change of slope in the flow curve (Figure 4-25) and monotony correspond to the onset of the flow instability and oscillating spurt flow as mentioned above.

It can be seen from Figure 4-25 and Figure 4-26 that the onset of flow instability is lower for the virgin HDPE, which corresponds to a higher slip velocity at an equivalent level of stress at the capillary wall.

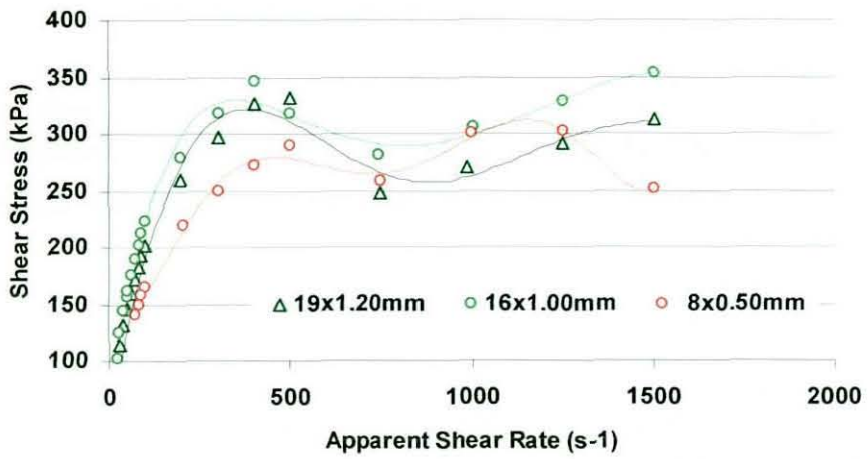

Figure 4-25 – Flow data of PR-HD4 at 170°C obtained with capillary dies of different diameters with constant L/D=16.

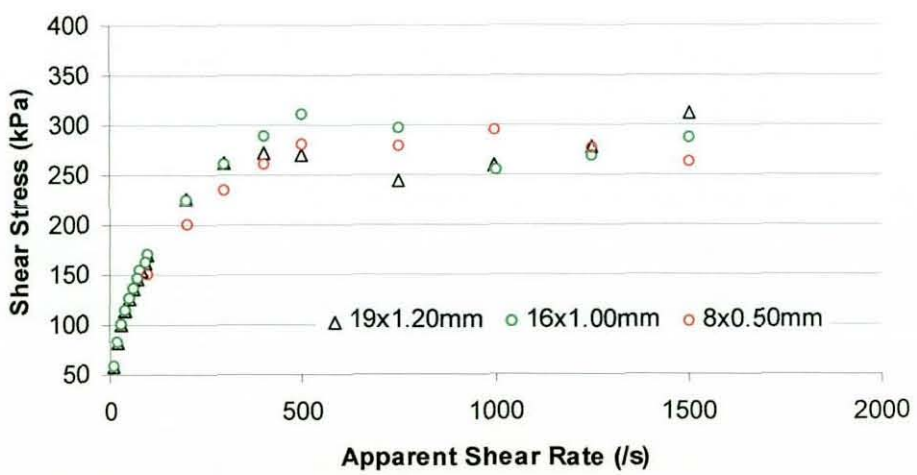

Figure 4-26 – Flow curves of PE-HD1 at 170°C obtained with capillary dies of different diameters with constant L/D=16.

Figure 4-27 shows a clear trend with respect to the die geometry sensitivity of the shear flow data generated from these experiments. In cases where a finite gradient can be detected, the presence of melt instability at the die wall can be confirmed; the gradient is measured and converted to calculated wall slip velocity data. From Figure 4-27, it is observed that there is a clear trend between the wall slip velocity and the shear stress at which measurements were taken.

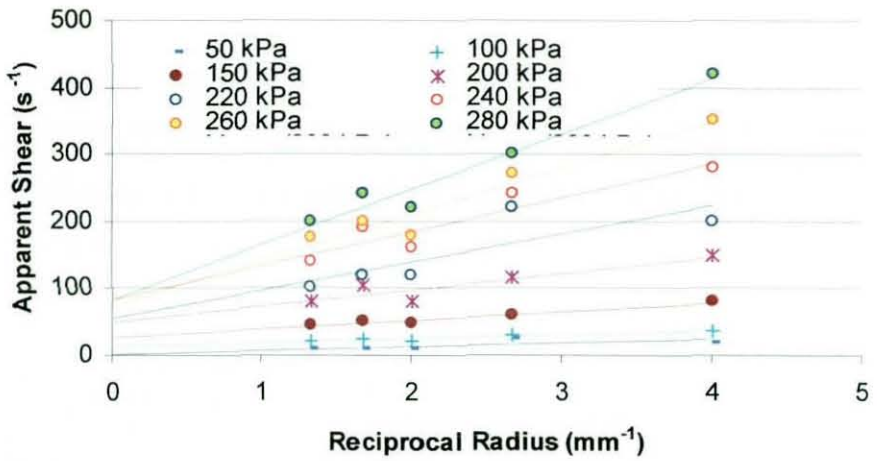

Figure 4-27 – Determination of slip velocity in PR-HD4 using capillary steel dies with L/D=16.

It has been established that the wall slip velocity (v_s) can be related to the wall shear stress (τ_w) by a power law:

$$V_s = A.\tau_w^{\ m} \quad (4.1)$$

This analysis has been used to plot the relationship between these variables in Figure 4-28. The linearity of this plot verifies the use of the power law approach to wall slippage effects in PR-HD4 and PE-HD1; the evaluated constants are:

	A $(MPa)^{-m}$	m
PE-HD1	1.9	1.8
PR-HD4	2.1	2.6

Table 4-12 – Wall slip power law parameters

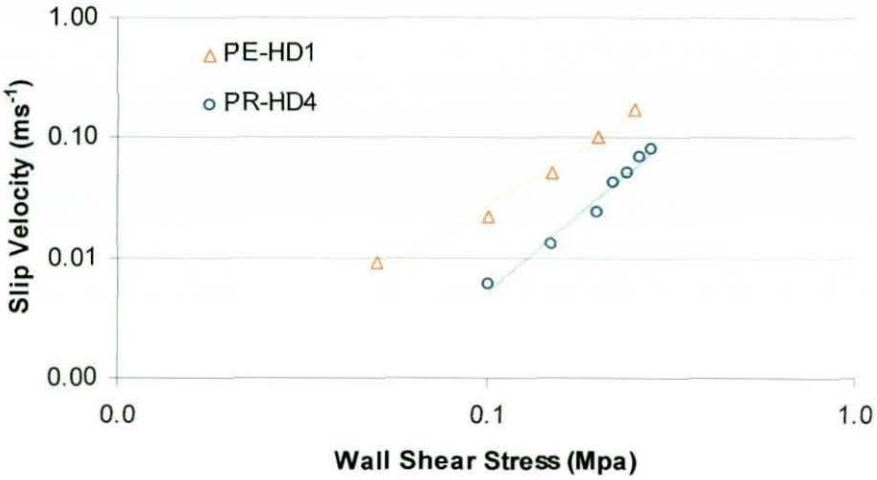

Figure 4-28 – Slip Velocities of PR-HD4 at 170°C.

4.2.4 Elongational flow

The melt state elongational flow behaviour was studied by two distinct techniques, constrained elongational flow method and free-surface constant velocity uniaxial elongation. For the first technique, the Cogswell method[57] was used, although this doesn't allow the measurement of a true extensional flow but rather a mix of shear and extensional flows experienced by the melt in the capillary die. Therefore, it was also decided to use a free surface technique using the Rutherford Elongational Rheometer, described previously (section 3.4).

4.2.4.1 Constrained elongational flow

Due to the difficulties associated with direct measurement of elongational viscosity, the flow in a tube with an abrupt contraction has often been used as an indirect measurement of elongational viscosity.[41] When polymeric liquids flow into an abrupt contraction, the fluid usually channels towards the centreline and forms regions of recirculation in the corners of the contraction. The recirculating regions or vortices dissipate energy, and these vortices, as well as elongational effects and the rearrangement of the velocity profile, are

reflected in the measurement of large entrance pressure-losses. Measurements of entrance pressure combined with a model for the entry flow can lead to an estimate of elongational viscosity.

The simplest analysis of entrance is due to Cogswell[57] who assumed that the entrance pressure drop can be written as the direct summation of the two pressure drops, one due to shear viscosity and the other due to elongational viscosity. Cogswell then solved for each of these two pressure drops individually, applying a force balance on a differential section of the funnel-shaped entry flow region.

4.2.4.1.1 Recycled Polymers

The elongational flow behaviour of the supplied resins was studied at different temperatures using simultaneously the capillary and zero length dies with the same capillary diameter. It can be seen from Figure 4-29 that the elongational flow behaviour is very different between branched and linear polyethylenes. Whereas for the linear polyethylenes the flow behaviour is extension thinning that can be linear by a logarithmic function, the branched polyethylenes show several slope changes.

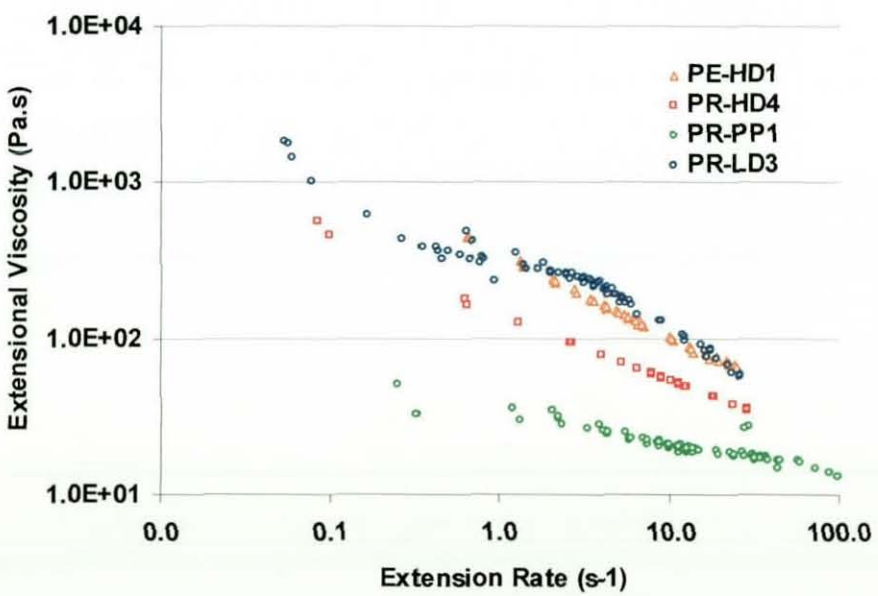

Figure 4-29 – Extensional flow behaviour of polyolefins at 210°C.

In linear polyethylenes the extensional viscosity is a function of the resin's average number molecular weight, with the higher molecular weight fractions contributing more significantly to a higher viscosity.[41] This can be explained based on the larger number of entanglements that restrict the stretching of the backbone between the entanglements. The previous figure illustrates the effect of higher molecular fractions on the extensional flow behaviour of linear polyethylenes. In branched polymers, the viscosity depends also on branch architecture.[47] The main effect of a branched structure is a strain-hardening behaviour this causes an even a more restrictive stretching of the backbone. The extensional flow behaviour detected with the recycled low-density polyethylenes is different from results of other authors and from PE-LD1. Generally, using the same technique, the viscosity of low-density polyethylenes increases monotonously, reaching a maximum, and decreasing slightly till reaching a plateau corresponding to a zero extension viscosity as predicted for the linear viscoelastic region.

4.2.4.1.2 Virgin Polymers

The virgin LDPE showed a similar behaviour to the one just described, with the difference that the maximum was not obvious. Also it can be seen that the chain branching of the virgin polypropylene doesn't produce a strain hardening effect like LDPE, but its behaviour is very similar to that of HDPE. Comparing the shapes of flow curves from both the virgin and recycled LDPE's one may suggest that there must be some HDPE present in the recycled, as polypropylene is unlikely to contribute to such an increase of the extensional viscosity at low extension rates. The recycled polypropylene is the least viscous material tested.

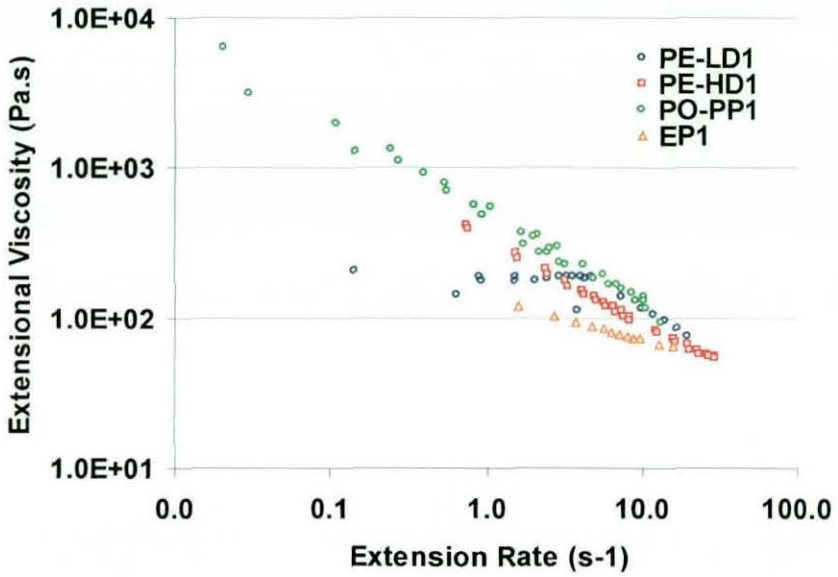

Figure 4-30 – Extensional flow of virgin polyolefins at 190°C.

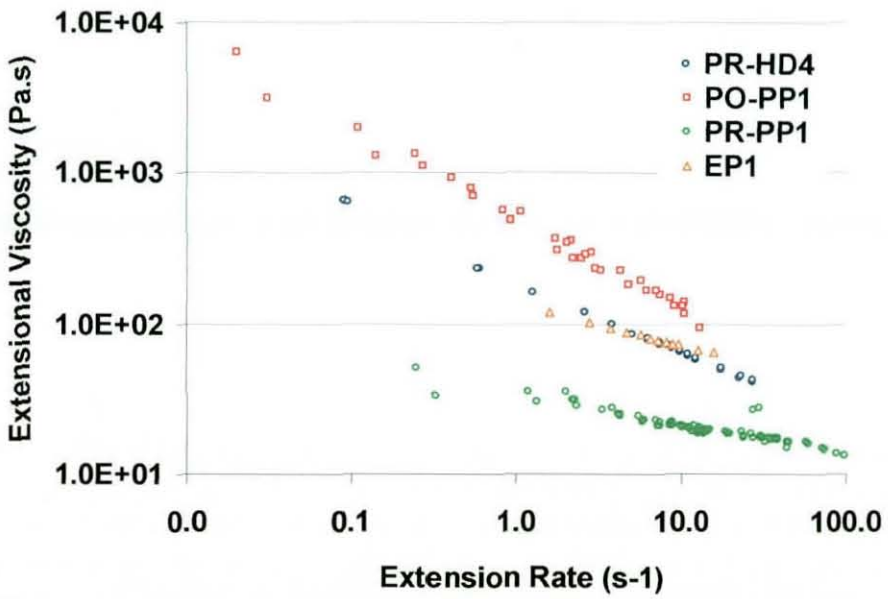

Figure 4-31 – Comparison of extensional flow behaviour of branched and linear polypropylene with polypropylene-ethylene copolymer at 190°C.

4.2.4.1.3 Temperature Dependence of Elongational Flow

The temperature dependence of extensional viscosity was also investigated. The variation of extensional viscosity with temperature was larger for the recycled high-density polyethylenes, that overall exhibited a lower viscosity than the virgin HDPE. The linear polymers show an extension thinning

behaviour that is reflected in their viscosity curves decreasing monotonously with increasing shear rates. The LDPE's still have the same trends reported previously. The recycled LDPE's still present the double inflected curve to the one described previously as can be seen in Figure 4-34.

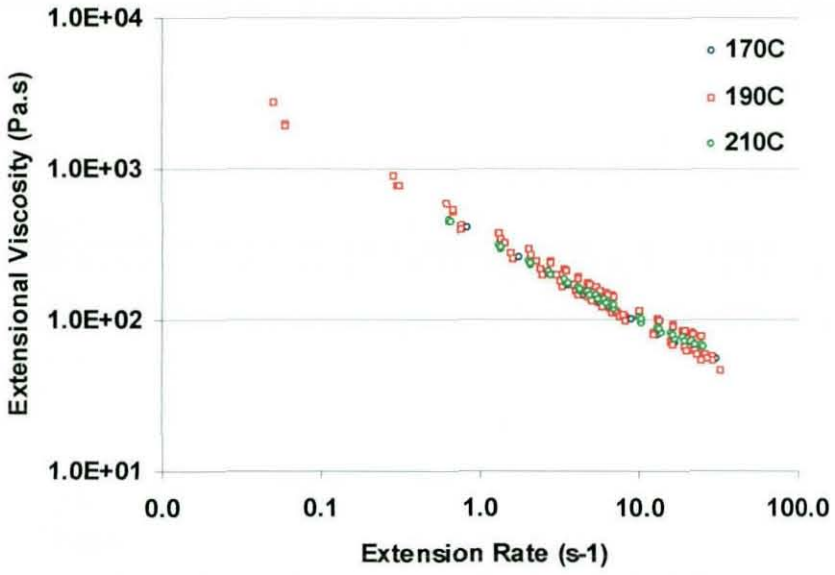

Figure 4-32 – Effect of temperature on the extensional viscosity of PE-HD1.

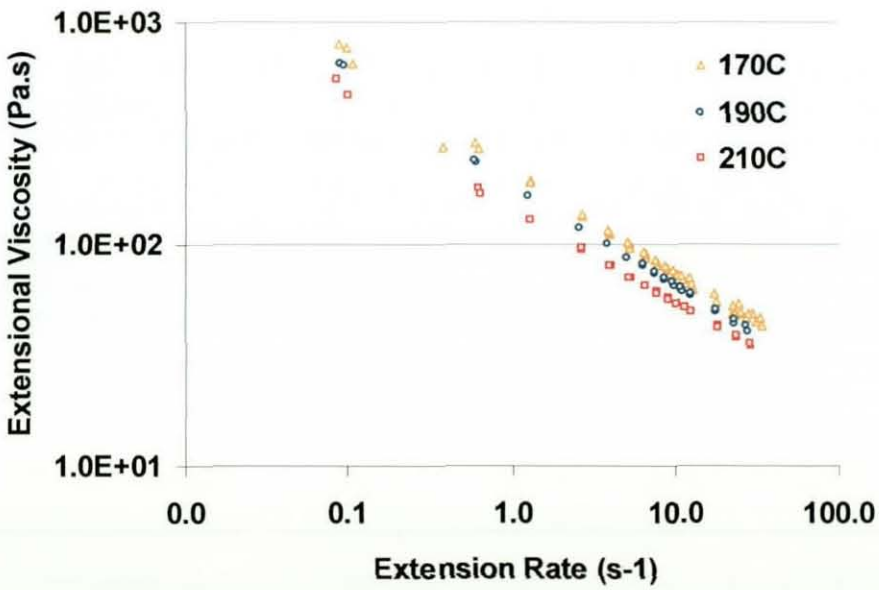

Figure 4-33 – Effect of temperature on the extensional viscosity of PR-PP1.

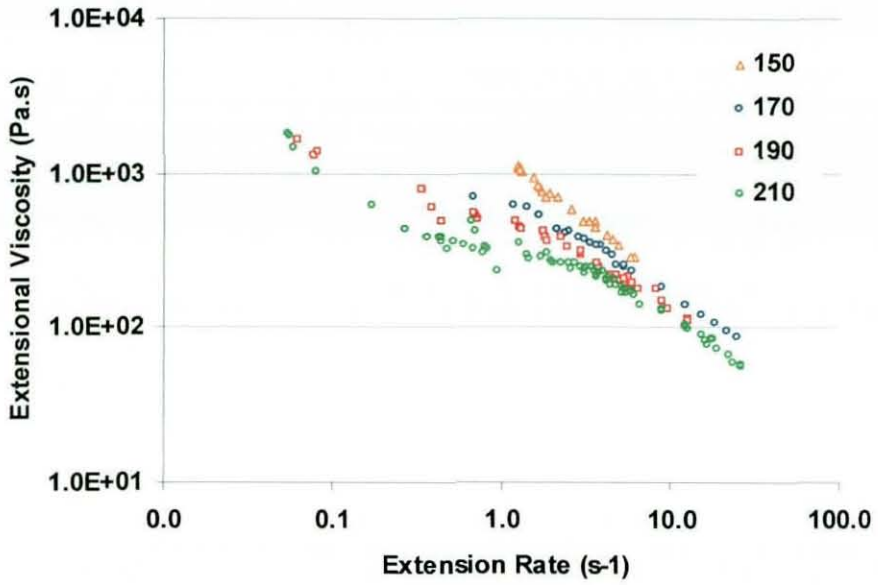

Figure 4-34 – Effect of temperature on the extensional viscosity of PR-LD3.

4.2.4.2 Free Surface Uniaxial Elongational Flow

In a free surface uniaxial elongational flow experiment at constant velocity, deformation rate decreases continuously. An exponential increase in velocity would be required to produce a constant extensional strain rate. Therefore, due to the strain rate sensitive nature of the material the viscosity will increase with time until the sample fails, so that an elongational rupture stress can be obtained.

The raw materials were tested at 150°C or 170°C (PP's) and at a constant velocity of 50 mm s-1 because with the used sample design the strain rates obtained were between 3 and 1 s^{-1} which are typical values for foaming.[8]

A force vs. displacement plot of the raw data can be seen Figure 4-35. The samples had approximately the same cross-sectional size. Even from a plot like this, one can see that the elongational flow is different between linear and branched polyethylenes. The latter ones tend to have higher extensibility, and the virgin one didn't fail within a displacement of 400 mm. All the samples exhibit a typical ductile behaviour with a maximum followed by necking, with a progressive reduction in load as deformation proceeds.

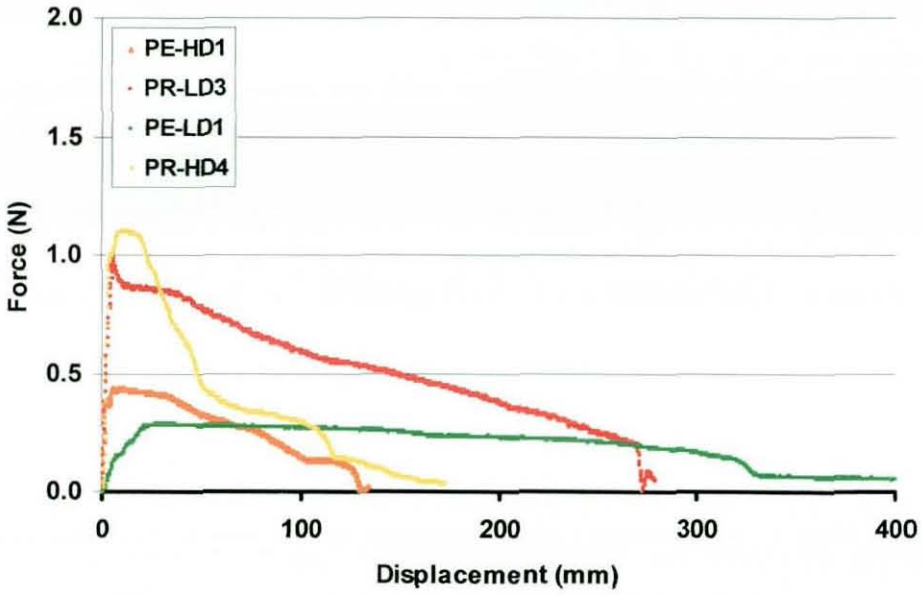

Figure 4-35 – Load-displacement curves of polyethylenes at 150°C and 50 mm s-1.

After treatment of the load-displacement data the stress-strain plot of Figure 4-36 can be obtained (see example in appendix III). Performing the experiments and interpreting these results are complicated because of design issues regarding the choice of the force transducer, thickness of the sample and temperature of the test. In this work it was assumed that 10 minutes were sufficient to ensure complete melting of the samples at the chosen temperatures, but others consider that being 15 °C above the melting point may not be enough for melting the higher molecular weight fractions. The comparison of these results with work from other authors is not straightforward the main of deformation is constant strain rate. In this research the deformation rate started at $3s^{-1}$ and declined with time. While studying the effects of molecular structure of polyethylene on the melt state extensional flow behaviour it has been found that for linear polyethylenes there is no strain-hardening behaviour contrary to low-density polyethylene that exhibits strain-hardening from $0.1s^{-1}$. Being the materials behaviour history dependent, it may pass through a series of flow regimes as defined by Malkin and Petrie[123], with the time-scale of the deformation and of flow being of fundamental importance. In the uniaxial elongation experiments of the polymers, the Deborah number decreased; therefore memory effects and

elastic behaviour become more important. Also, the deformation enters the time-scale of the relaxation time of the material. Several criteria for the rupture of polymeric liquids have been proposed.[123] One of them states that if a polymeric liquid reaches a weissenberg number of 0,5 during a constant strain rate mode, it will eventually fail. Figure 4-36 illustrates the melt-state stress-strain behaviour of uniaxially stretched polyolefins. In the studied mode of deformation it was considered to use an energetic criterion to evaluate the suitability of a resin for foaming. This criterion was the melt strength that was defined as the area under the stress-strain curve, which is equivalent to the total energy required for a sample to fail by rupture. A second criterion is the extensibility or Hencky strain at rupture. This criterion is more qualitative because after the material yields, and according to the Considere criterion, the flow is unsteady and no longer purely extensional.

The curves of the low-density polyethylenes are markedly different. The behaviour of the recycled low-density polyethylene with a much increased extensional stress before failure may be related to the filler and polypropylene content. Fillers can increase the stiffness but so can non-molten droplets of polypropylene. The virgin LDPE has a much lower yield stress but rather higher extensibility. The use of small quantities of polypropylene has been reported in elongation experiments of polyethylene melts to induce a pseudo strain-hardening behaviour below PP melting points.[121] The high-density polyethylenes show comparatively with the LDPE's a much lower extensibility and lower level of stress before yielding. This translates in a smaller area under each curve that can be ultimately related to the energy absorption of the melt or melt strength. The virgin LDPE sample does not seem have a very well defined yield stress. The melt strength is a function of the temperature and so is the deformation/curve behaviour with a tendency for a decrease in yield stress and increase in extensibility. If melt strength was the sole criterion, the HDPE's and the virgin LDPE should have a similar foamability, but this is obviously incorrect, therefore a second parameter such as extensibility should also be considered. It is difficult to explain the differences between the HDPE's. One

would expect that the virgin HDPE should be more extensible due to the presence of the higher molecular weight fractions, but his is not the case. In fact, PR-HD4 is not only capable of absorbing more energy, but also more extensible.

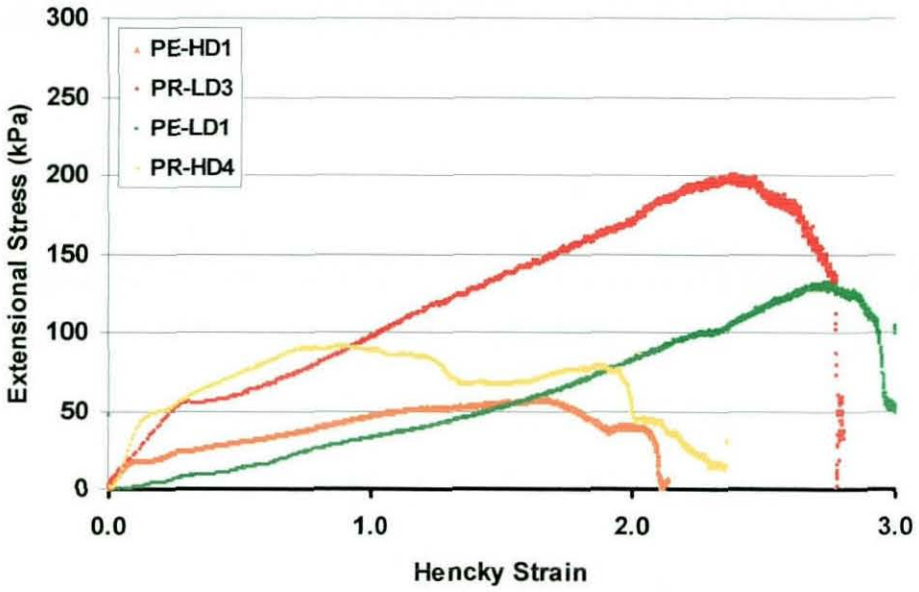

Figure 4-36 – Elongation behaviour of polyethylenes at 150°C and 50 mm s-1.

Polypropylene cannot be tested at 150°C but rather at 170°C. At this temperature the yield stresses of the polyethylenes are decreased but the extensibility increases. Comparatively the extensibility of PP is lower. PP is known not a have good melt strength and being a difficult material to foam. It shows higher toughness within certain deformation rates, but the lack of extensibility doesn't allow the material elongate over a wider range of deformations, leading to failure and cell rupture.

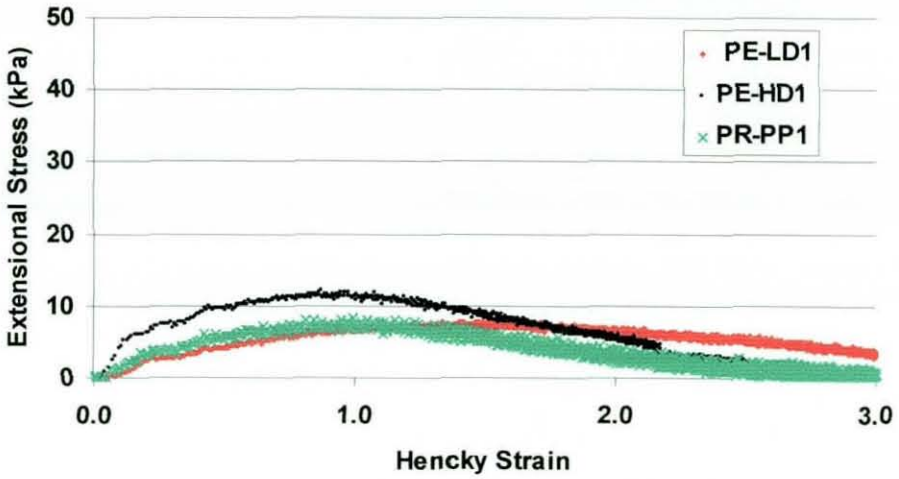

Figure 4-37 - Elongation behaviour of polyolefins at 170°C and 50 mm s-1.

4.3 Chapter Review

The supplied materials were characterised in terms of their chemical compositions, thermal and flow properties. It was found that the recycled high-density polyethylenes were virtually free from polymeric contaminants but may have some inorganic content. The low-density polyethylenes were contaminated with PP and some LLDPE may be present. They also had some inorganic content. The recycled PP proved to be a random-copolymer material. The inorganic content proved to be calcium carbonate and titanium dioxide. The flow behaviour of the recycled polymers was consistent with high molecular weight resins suitable for extrusion. Free surface elongational measurements showed that branched materials had the highest strain energy density and extensibility. The melt strength of the linear polymers was related to their molecular weight.

5 Recycled Polyolefins Blends and Nanocomposites

This chapter is divided in three parts. The first two are dedicated to the discussion of the results of binary blend systems of recycled LDPE:PP and recycled HDPE:PP. The influence of the blend composition, with and without compatibilisers, and processing conditions on the shear and extensional flow behaviour are discussed. An optimisation procedure is used to maximise the melt strength and extensibility. The third part is dedicated to the study of the preparation of virgin and recycled HDPE, and a blend of recycled LDPE:PP layered-silicate nanocomposites. Evidence of the prepared structures is shown. Similarly to the first two parts, rheological results are also presented and discussed.

5.1 Blend System I – LDPE:PP

The properties of blends depend on the morphology of the combined polymeric phases and dispersion of other components. These blends are immiscible although some degree of miscibility was found by Kukaleva.[30] This incompatibility leads to a negative deviation blend,[48] i.e., the viscosity of the blend is lower than the logarithmic sum of the individual components – logarithmic additivity rule. To overcome this it is necessary to optimise the composition, processing conditions and to use compatibilisers that reduce the interlayer slip that is usually associated with inferior mechanical properties.

Blends of recycled co-continuous blends may have better properties than their dispersed counterparts at the same composition level. According to Willemse et al.[122] These can be produced at any composition level, provided that the viscosity ratio is higher than one and the mixing time is adequate, so that phase inversion can occur. Further guidelines for the production of co-continuous blends were recently published.[106] Their preparation was

investigated in this study. In this context, and as described in the experimental section 3.5.1.1, a composition range of recycled LDPE:PP blends with increments of 20% (w/w) was produced by batch mixing in the Haake rheometer at 190°C with a rotor speed of 31.8 rpm using different mixing times. The objective is to identify the composition and mixing time that give either the highest extensional viscosities or melt strength. The optimum composition and mixing time will then be used to illustrate the effects of compatibilisers on the flow properties. The results are also compared to a virgin branched polypropylene and a blend.

5.1.1 Influence of composition

The first set of experiments was performed with the RER at 170°C and at a constant cross-head speed of 50 mm s^{-1} with samples of different ratios of recycled polypropylene and recycled low-density polyethylene. Figure 5-1 illustrates the effect of composition on the extensional flow behaviour of these blends.

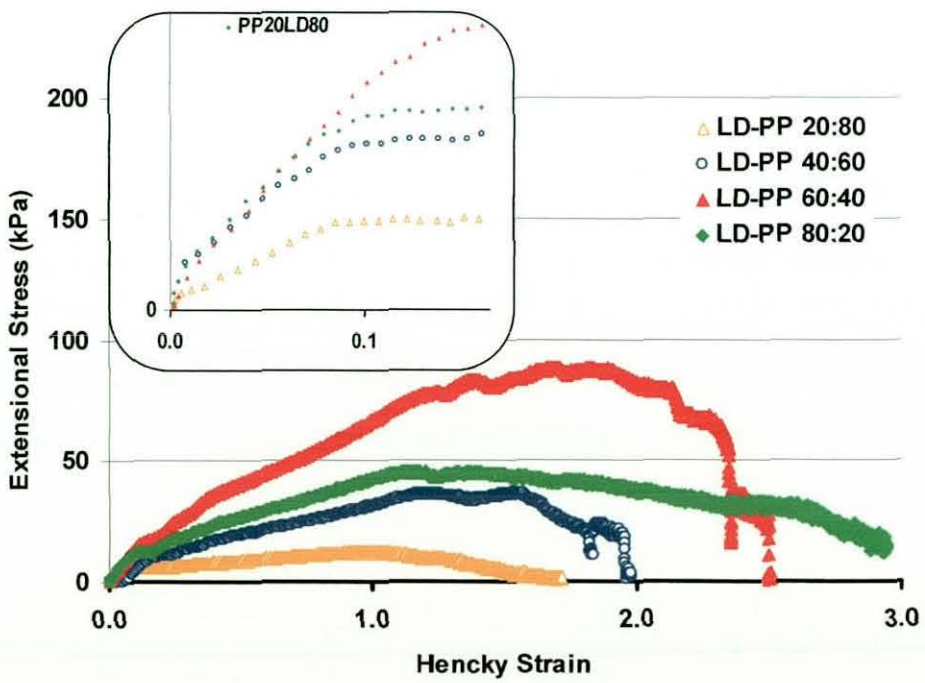

Figure 5-1 – Flow behaviour of different compositions of recycled LPDE:PP blends mixed at 190°C for 2.5 minutes.

When melt blending immiscible and incompatible resins, such as LDPE and random PP copolymer, the degree of incompatibility can be evaluated by the degradation of ultimate properties, such as elongation and stress at break.[121,122] This degradation is evident in the previous figure. The yield point seems to occur at Hencky strains of 0.1, after which work hardening occurs, followed by necking and leading to ultimate failure. This yield point is more readily identifiable from a force vs. extension plot. According to a modified Considere Criterion [123,124], this is the limit where a steady extensional flow can be observed. After this flow regime, and due to non-homogeneity that develops only approximate values of properties at rupture can be determined. For some samples there is necking instability that leads to localized yielding. The type of rupture changed with composition. It varies with increasing LDPE content from a ductile to cohesive failure, if we use Ide and White's terminology.[123] This is in agreement with their work where LDPE's were found to be more strain rate sensitive and exhibited cohesive failure. They also concluded than linear HDPE and PP suffered ductile failure. For all samples the stress grows with time, but it grows more rapidly for LDPE-rich samples. LDPE-PP 80:20 and 40:60 curves show a discontinuity that represents the failure of the first waist of the oval samples. As Table 5-1 shows, by enriching the blend with PP, the maximum stress, strain at maximum stress, strain at rupture and strain energy density are reduced. It is known that PP does not exhibit strain hardening behaviour, and can be seen that by adding 20% of LDPE no significant increase in extensional stress is observed. It is interesting to note that the yield stress occurs in a very narrow region for all blends.

LDPE:PP (w/w)	80:20	60:40	40:60	20:80
Stress at yield (kPa)	14	17	10	5
Maximum stress (kPa)	84	93	37	13
Strain at maximum stress	1.18	1.86	1.53	1.00
Strain at rupture	2.9	2.5	2.0	1.6
Strain energy density (kPa)	170	162	51	10

Table 5-1 – Uniaxial elongational deformation properties of LDPE:PP blends.

5.1.2 Effect of mixing time

In batch mixers a stable morphology is expected after a certain period of time.[125] Depending on composition, interfacial tension and viscosity ratio this morphology will change between, co-continuous, fibrillar and dispersed.[28]
The mixing time had a substantial effect on the elongational flow behaviour of the blends, particularly the ones with more than 20% PP (w/w). It can be seen in the following graph that using a mixing time of 2.5 minutes the maximum stress increased but the extensibility decreased. The melt strength increased as well. In these blends, there was an inverse relationship between extensibility and melt strength. In them one can consider LDPE as the dispersed phase, being the viscosity ratio lower than 1. The extensional flow behaviour of these blends has not been much reported. LDPE will melt first forming a continuous phase. Since PP is less elastic and viscous than LDPE under the shear and elongational flow generated by the batch mixer it will take more time for the droplets to be reduced in size and thus increasing the interfacial area between the LDPE and PP, and obviously, enhancing interlayer slip.

The behaviour was slightly different for blends containing only 20% (w/w) of PP, where the melt strength was not so affected - Table 5-2. Increased mixing time seems to have a positive effect in terms of extensibility as can be seen in Table 5-3, but can lead to lower strain energy density. This has to be related to the blend morphology. When mixing PP-rich blends, there is a transition between an LDPE continuous phase with possibly large PP dispersed droplets because LPDE melts first. This morphology is inverted with increasing mixing time leading to a change from a cohesive failure of the blend to a more ductile failure.

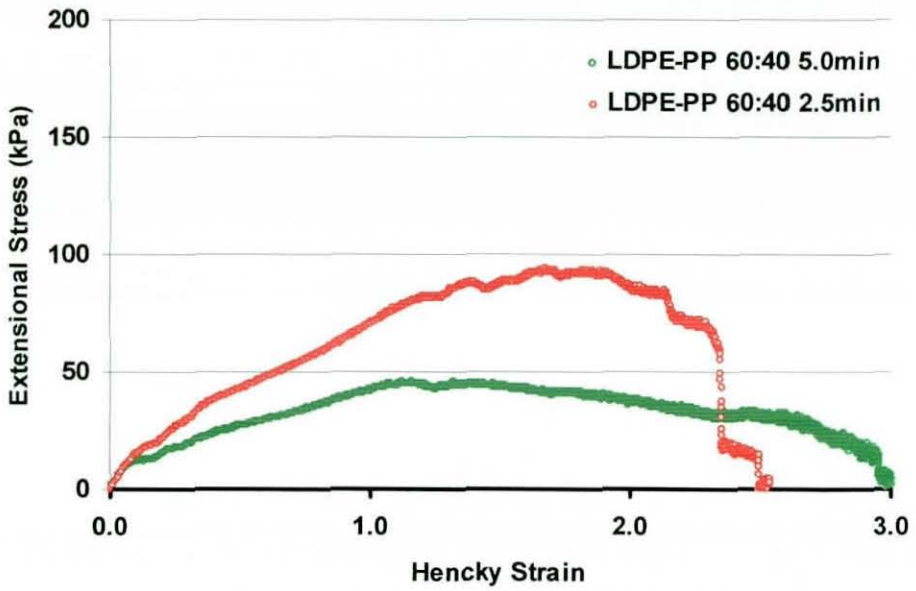

Figure 5-2 – Influence of mixing time on LDPE:PP 60:40 blends.

Mixing Time (min.)	Composition of LDPE:PP Blends			
	80:20	60:40	40:60	20:80
10	200	-	-	2
7.5	209	-	-	3
5	190	89	31	13
2.5	172	162	51	10

Table 5-2 – Strain energy density of recycled LDPE:PP blends.

At smaller mixing times we have a continuous phase of LDPE until we obtain a transitory co-continuous structure. After that, we should obtain a dispersed morphology of PP droplets. Since the viscosity and elasticity of the PP phase is lower than LDPE, the deformation and reduction of the droplet size of PP is not difficult in the strong flows generated by the internal batch mixer.

Mixing Time (min.)	Composition of LDPE:PP Blends			
	80:20	60:40	40:60	20:80
10	3.0	-	-	1.7
7.5	3.0	-	-	1.7
5	2.9	2.8	2.7	1.7
2.5	2.9	2.5	2.0	1.6

Table 5-3 – Extensibility of recycled LDPE:PP blends

5.1.3 Capillary rheometry

The prepared blends were then analysed by capillary rheometry at 190°C. As with free surface elongational measurements it is possible to discriminate the effects of the different processing conditions and composition in shear (Figure 5-3). Samples with higher PP content and mixed for shorter periods of time exhibit higher zero shear viscosity. The results also show that these are negative deviating blends (Figure 5-5). This is a typical result for these blends that is usually explained in terms of interlayer slip.[48] In terms of extensional flow behaviour, there is a significant increase in viscosity with LDPE content.

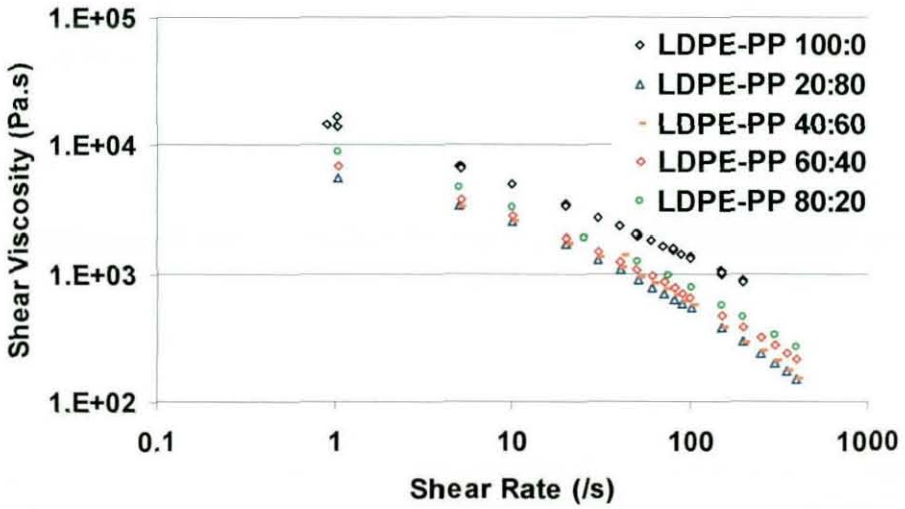

Figure 5-3 – Influence of blend composition at 190°C on shear viscosity. Blends mixed for 2.5 minutes.

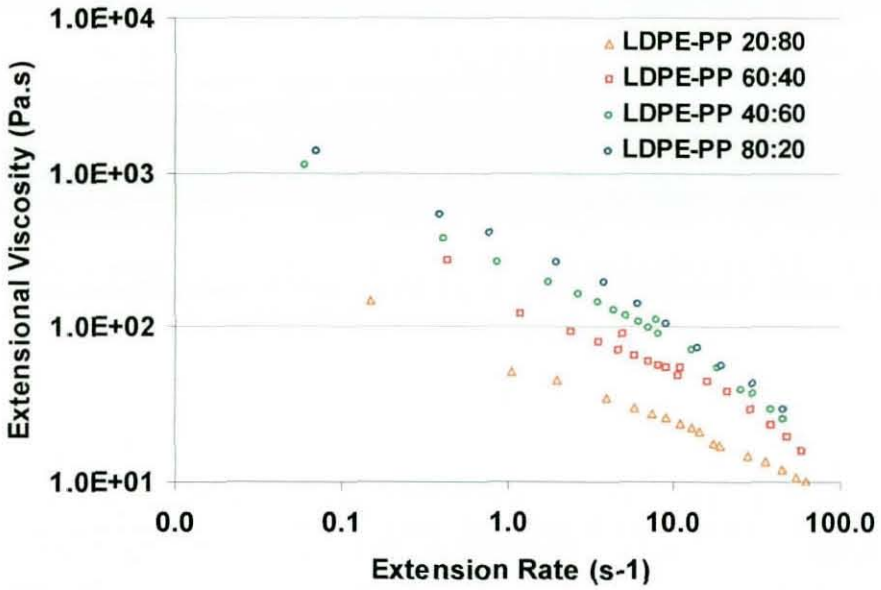

Figure 5-4 – Influence of blend composition at 190°C on extensional viscosity. Blends mixed for 2.5minutes.

The following graph compares the expected additive behaviour using a linear mixing rule with the obtained results. The zero shear viscosity is not very much affected by blend composition up to LDPE content of 0.6.

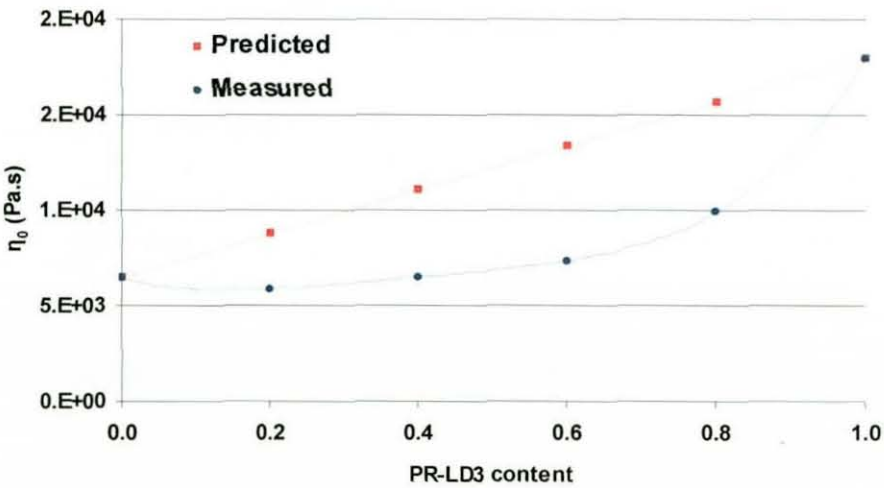

Figure 5-5 – Compositional dependence of the zero-shear viscosity for blends of PR-LD3 with PR-PP1 mixed for 2.5 minutes.

5.1.4 Optimum Composition: LDPE-PP 60:40

Based on the previous results it was decided to use a PP-LDPE 40:60 blend to study the effect of compatibilisers on the flow behaviour of the blends. This was because at this ratio the extensional flow behaviour was similar to that of a LDPE-PP 80:20 (Figure 5-4). Two compatibilisers, EPR1 and EP1 (see Table 3-2), were used at different addition levels. The mixing time was proved previously to be important therefore it was decided to continue to be studied. The effect of using a branched PP was also investigated. Free surface elongational and capillary rheometry data of these blends are presented.

5.1.4.1 Effect of EPR1 addition

The effect of adding EPR1 at two addition levels to a LDPE-PP 60:40 blend was investigated. As a compatibiliser EPR1 should lower the interfacial tension between the phases and reduce coalescence. Also, the morphology obtained after a certain period of time in the batch mixer is expected to remain stable. The effect of the mixing time, 2.5 and 5 minutes, was also taken into consideration. The addition of EPR1 to this blend seems to have a positive impact by increasing the strain energy density, however at a 5% level and when mixed for 5 minutes this value is lower than the uncompatibilised blend. EPR1 is very elastic and may be difficult to elongate and disperse even under strong extensional flows. It may happen that under those conditions the EPR1 phase coalesced resulting in a ternary blend. Apart from this result the extension at break improved which indicates that a certain degree of compatibilisation was achieved.

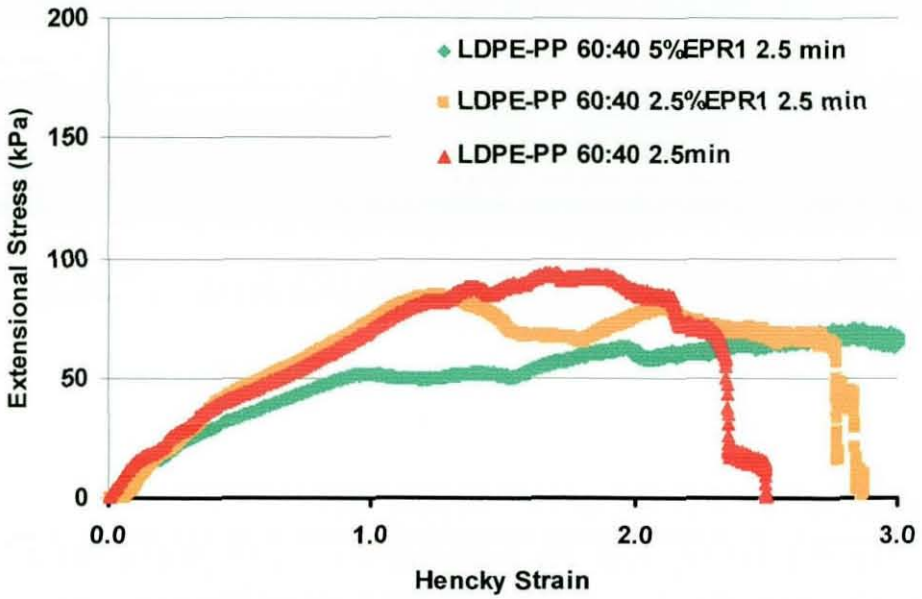

Figure 5-6 – Influence of EPR1 content on the extensional flow properties at 170°C of LDPE-PP 60:40 blends mixed for 2.5 minutes.

The mixing of 5% EPR1 for 2.5 minutes produces the highest extensibility and no failure has been observed. At this addition level the rubbery phase dispersion seems to be able to store more elastic energy in the thermoplastic melt matrix and dissipate the stresses more effectively than any of the other compositions, leading to a higher extensibility.

LDPE-PP 60:40	2.5 minutes			5.0 minutes		
EPR1 content	0%	2.5%	5%	0%	2.5%	5%
Stress at yield (kPa)	17	18	15	12	17	24
Maximum stress (kPa)	93	85	71	48	102	46
Strain at maximum stress	1.9	1.2	2.8	2.8	2.8	2.8
Strain at rupture	2.5	2.9	3.2	3.0	3.2	2.2
Strain energy density	162	184	180	89	205	50

Table 5-4 – Uniaxial elongational deformation properties of compatibilised LDPE:PP blends.

Increasing the mixing time to 5 minutes does not yield further improvements; quite the contrary. This was not expected, as it was thought that increasing the mixing time would lead to more dispersion of the EPR1 and a lower interfacial tension between the LDPE and PP phases.

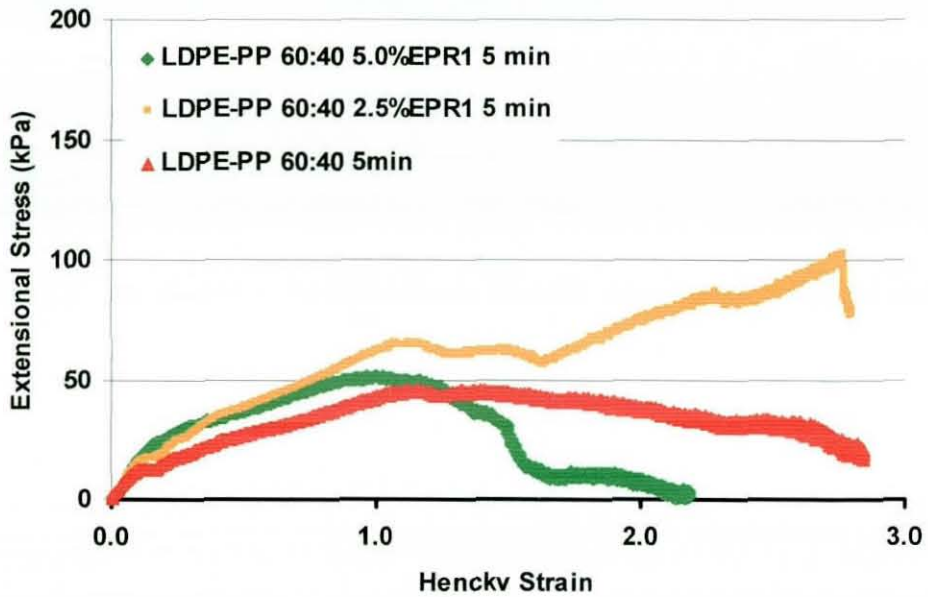

Figure 5-7 – Influence of EPR1 content on the extensional flow properties of LDPE-PP 60:40 Blends mixed for 5 minutes.

On the other hand, at a 2.5% addition level, by increasing the mixing time the level of extensional stress generated by the deformation is lower and the extensibility increases leading to no rupture. This suggests that the optimum quantity of EPR1 is possibly around 2.5% or lower for the chose composition and processing conditions.

5.1.4.2 Effect of EP1 addition

The effect of adding EP1 was studied in a similar set of experiments as described in the previous section. The same addition levels and mixing times were used. By adding 5% of EP1 to this system and mixing for 2.5 minutes, the extensional stress decreased and the extensibility increased (Figure 5-8). A similar result to that obtained when using EPR1 as a compatibiliser.

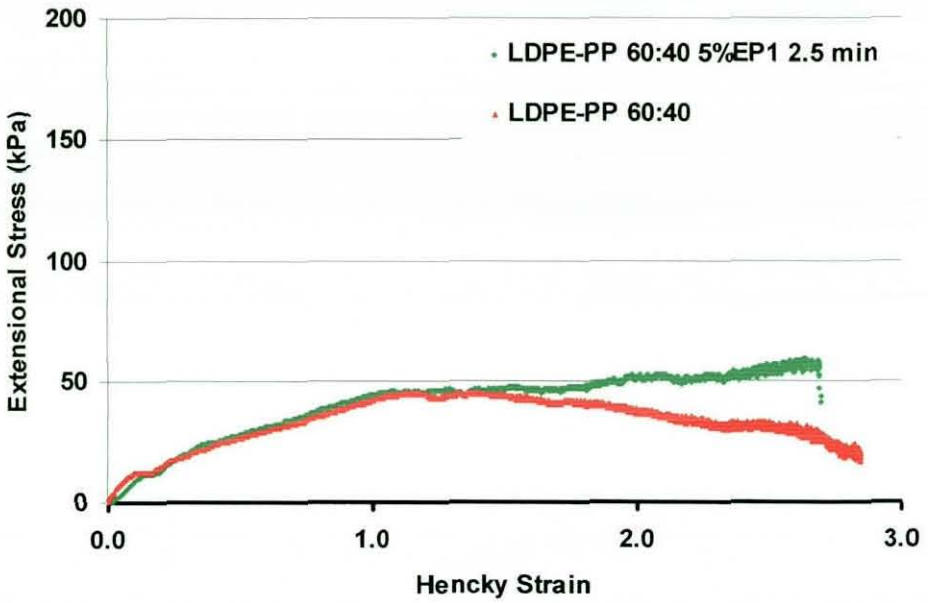

Figure 5-8 – Influence of EP1 content on the extensional flow properties of LDPE-PP 60:40 blends mixed for 2.5 minutes.

Unlike with EPR1 however when increasing the mixing time there was no decline in terms of extensibility or strain energy density. A full description of elongational deformation properties can be found in Table 5-4 and Table 5-5. This may be related to the fact that EP1 is less elastic than EPR1 and possibly does not coalesce and remains between the interface of LDPE and PP.

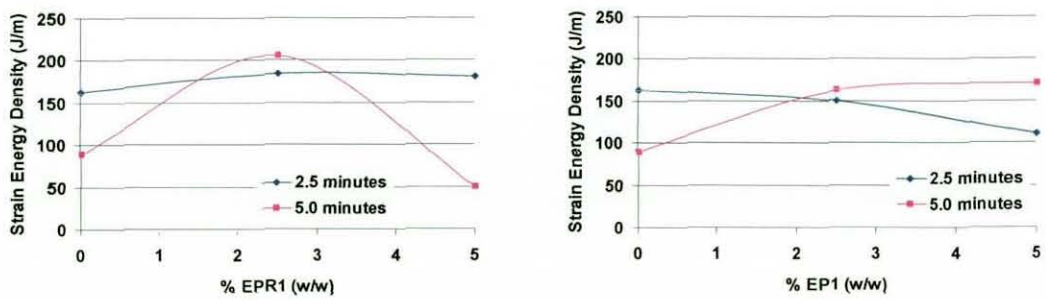

Figure 5-9 – Influence of compatibiliser and mixing time on strain energy density.

LDPE-PP 60:40	2.5 minutes			5 minutes		
EP1 content	0%	2.5%	5%	0%	2.5%	5%
Stress at yield (kPa)	17	14	12	12	13	29
Maximum stress (kPa)	93	50	57	48	83	75
Strain at maximum stress	1.9	2.7	2.7	2.8	1.8	1.6
Strain at rupture	2.5	2.7	3.0	3.0	2.8	2.9
Strain energy density	162	100	111	89	162	170

Table 5-5 - Uniaxial extensional properties of EP1 compatibilised LDPE:PP blends.

5.1.4.3 Capillary Rheometry

The shear and extensional flow behaviour of the compatibilised materials was characterised at 190°C by capillary rheometry. The measurements were carried out simultaneously with a long die and a zero length die. Despite the differences in the free surface uniaxial elongational measurements their shear flow behaviour is very similar - Figure 5-10. When compared to uncompatibilised blends they show less non-Newtonian behaviour and a higher viscosity overall, in shear. This increase in shear viscosity is not translated to a higher extensional viscosity when determined by the constrained flow method - Figure 5-11.

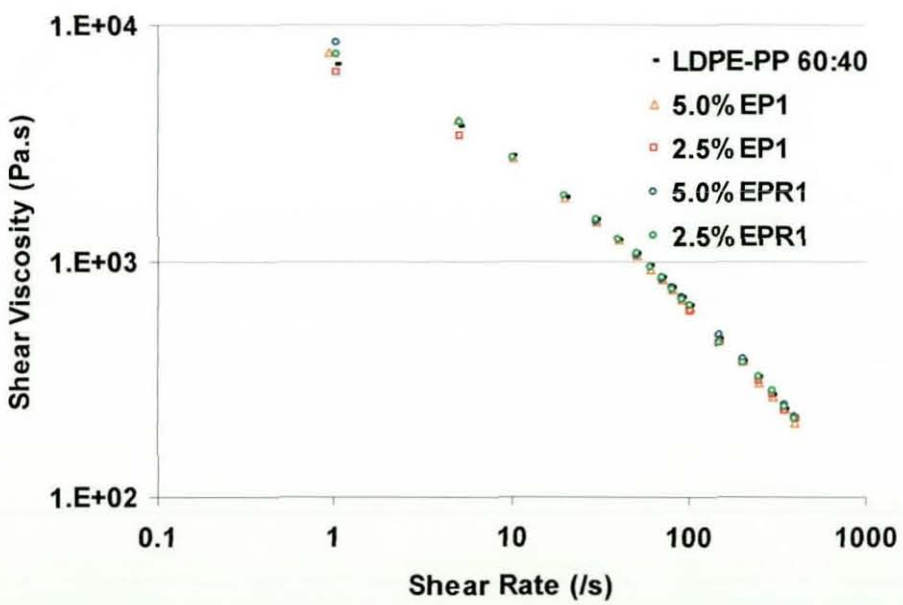

Figure 5-10 – Shear flow behaviour of compatibilised recycled LDPE-PP blends at 190°C; mixed for 5 minutes.

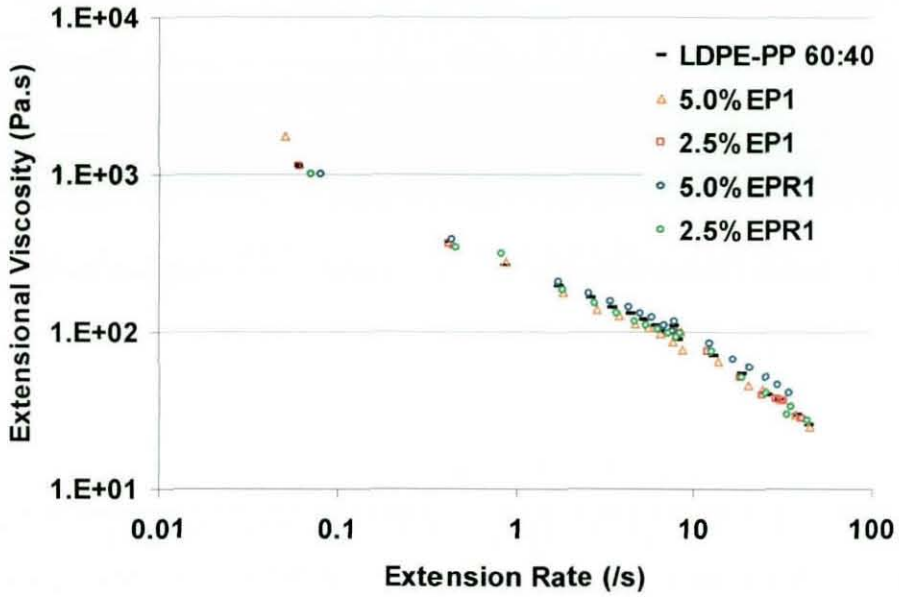

Figure 5-11 – Extensional flow behaviour of compatibilised blends at 190°C; mixed for 5 minutes.

5.1.4.4 Effect of Branched PP

The effect of branch content was studied by replacing the linear random polypropylene copolymer by a branched polypropylene - Figure 5-12. The addition of a small amount of branched PP to PR-LDP3 doesn't show any deterioration in the elongational uniaxial flow behaviour of the blend unlike when we use PR-PP1. After a pseudo-yield point at Hencky strain of 1.4, further work-hardening leads to a maximum stress at 200 kPa and an elongation at break of 2.8. The failure mode is by cohesive failure. There are some similarities between this blend and a compatibilised blend with EPR1. After a pseudo-yield point the stress reaches and maximum and the samples fail. Also, the strain energy density has increased when compared to the uncompatibilised blends. The branching content of PO-PP1 has a great influence on the strain energy density of the blend.

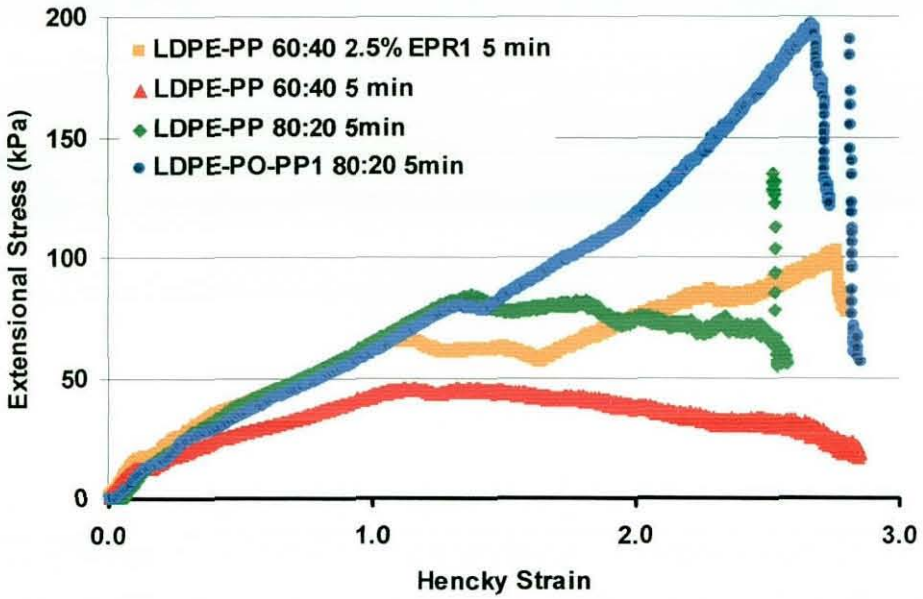

Figure 5-12 – Comparison of uncompatibilised blends with an EPR1 modified blend and a LDPE-PO-PP1 blend.

5.1.5 Summary

In free surface elongational measurements, both EPR1 and EP1 can improve the strain energy density and extensibility when added to the blends. This is dependent on the mixing time and quantities used. EPR1 seems more sensitive to these parameters. When used at 5% (w/w) EPR1 for 5 minutes shows a reduction in extensional flow properties. With EP1 there is a benefit by increasing the mixing time and EP1 content. By using a branched PP the strain energy of the blend increased unlike when using a recycled linear PP copolymer.

Shear viscosity measurements showed and increased in viscosity and Newtonian behaviour by adding EPR1 and EP1, with no apparent differences in the flow curves. The extensional measurements by the constrained elongational flow didn't show any significant differences as well.

5.2 Blend System II: HDPE-PP

An additional blend system composing only recycled linear polymers was studied. These were a recycled HDPE, PR-HD4 and a recycled PP, PR-PP1. To study the influence of the processing conditions on the flow properties it was chosen to use a central composite experimental design to investigate possible second order relationships between the processing variables, blend composition and response variables. The processing variables were the mixing time, temperature and rotor speed. The response variables of interest were the extensional maximum stress, strain energy density and Hencky strain at break.

5.2.1 Blend Optimization

The blends were prepared in a Haake batch mixer by a procedure described in 3.5.1.2. The composition of the blends, processing conditions and response variable results are described in Table 5-6. The analysis of the central composite design results for melt strength shows that the main effects are linear and that the temperature effect was redundant. The effect estimates calculated with Statistica software package showed a poor fit with the R-square coefficient being 0.75 - Figure 5-13. The main effects are the HDPE:PP ratio and the combined effects of (HDPE:PPxTime) and (HDPE:PPxSpeed). Their values, standard error and confidence intervals are highlighted in red in Figure 5-13.

Effect Estimates; Var.:STRESS; R-sqr=.75312; Adj:.59883

EXPERIM. DESIGN: 4 factors, 1 Blocks, 27 Runs; MS Pure Error=141.6043
DV: STRESS

Factor	Effect	Std.Err. Pure Err	t(5)	p	-95.% Cnf.Limt	+95.% Cnf.Limt	Coeff.	Std.Err. Coeff.	-95.% Cnf.Limt	+95 Cnf.
Mean/Interc.	43.92521	2.413347	18.20095	.000009	37.7215	50.12892	43.92521	2.413347	37.7215	50.1
(1)RATIO (L)	36.53680	7.270332	5.01994	.004035	17.8273	55.24635	18.26840	3.635166	8.9136	27.6
(2)TIME (L)	8.62435	5.924226	1.45578	.205223	-6.6044	23.85306	4.31218	2.962113	-3.3022	11.9
(3)SPEED (L)	-5.32636	5.712153	-.93246	.393900	-20.0099	9.35719	-2.66318	2.856076	-10.0050	4.6
(4)TEMP (L)	-.59914	4.836315	-.12388	.906234	-13.0313	11.83301	-.29957	2.418158	-6.5156	5.9
1L by 2L	21.80557	7.835439	2.78294	.038767	1.6639	41.94720	10.90278	3.917720	.8320	20.9
1L by 3L	26.79749	8.563419	3.12930	.025978	4.7845	48.81046	13.39874	4.281710	2.3923	24.4
1L by 4L	.64540	7.022783	.09190	.930346	-17.4072	18.69804	.32270	3.511392	-8.7036	9.3
2L by 3L	7.15436	6.562115	1.09025	.325334	-9.7141	24.02281	3.57718	3.281058	-4.8570	12.0
2L by 4L	-9.49312	5.759953	-1.64812	.160243	-24.2996	5.31331	-4.74656	2.879977	-12.1498	2.6
3L by 4L	.62481	5.732943	.10899	.917453	-14.1122	15.36180	.31240	2.866471	-7.0561	7.6

Figure 5-13 – Effect estimates for the melt strength (MS).

These results translate into the highest melt strength being directly related to a higher HDPE content.

	HDPE:PP Ratio	Rotor (rpm)	Time (min.)	Temperature (°C)	MFI (g/10min)	Max Stress (kPa)	Hencky Strain	MS (kPa)
1	50:50	50	1.5	170	3.89	37	0.84	35
2	80:20	50	2.5	170	2.30	46	0.80	13.6
3	20:80	150	1.5	190	-	14	0.87	11.9
4	80:20	150	2.5	170	2.21	29	0.96	82
5	20:80	125	2.5	190	-	15	0.91	6.2
6	80:20	150	3.5	190	-	70	1.04	115
7	80:20	50	3.5	190	-	42	0.76	31.4
8	80:20	150	1.5	190	-	53	0.97	105
9	80:20	150	2.5	190	2.30	55	0.93	48.0
10	50:50	100	1.5	190	-	52	1.05	31.7
11	20:80	50	2.5	190	3.90	40	0.84	49.7
12	80:20	50	1.5	170	-	50	0.94	51.5
13	20:80	100	1.5	190	-	45	0.81	32.0
14	20:80	150	3.5	170	-	28	0.79	21
15	80:20	150	1.5	170	-	49	0.93	53.6
16	20:80	150	3.5	190	-	11	0.71	12.7
17	20:80	50	3.5	190	-	34	1.06	33.1
18	50:50	50	2.5	190	-	45	0.88	70.7
19	80:20	150	3.5	190	-	47	1.84	66.9
20	80:20	100	1.5	170	-	47	0.80	64.0
21	50:50	100	3.5	190	-	37	0.67	34.8
22	50:50	50	3.5	170	3.29	52	0.89	45.4
23	20:80	50	1.5	190	-	38	0.78	48.9
24	80:20	100	2.5	190	-	52	0.82	54.4
25	80:20	50	3.5	190	-	56	0.97	68.3
26	20:80	150	3.5	170	4.13	8	0.71	7.41
27	20:80	150	1.5	170	-	19	0.73	25.7
28	80:20	100	3.5	170	-	35	0.73	51.7

Table 5-6 – Compositions and processing conditions used in the preparation of HDPE:PP blends.

The M_w of PR-HD4 is lower than PR-PP1, but despite this fact the melt strength is directly proportional to its content. This can be explained by the

5.2 Blend System II: HDPE-PP

An additional blend system composing only recycled linear polymers was studied. These were a recycled HDPE, PR-HD4 and a recycled PP, PR-PP1. To study the influence of the processing conditions on the flow properties it was chosen to use a central composite experimental design to investigate possible second order relationships between the processing variables, blend composition and response variables. The processing variables were the mixing time, temperature and rotor speed. The response variables of interest were the extensional maximum stress, strain energy density and Hencky strain at break.

5.2.1 Blend Optimization

The blends were prepared in a Haake batch mixer by a procedure described in 3.5.1.2. The composition of the blends, processing conditions and response variable results are described in Table 5-6. The analysis of the central composite design results for melt strength shows that the main effects are linear and that the temperature effect was redundant. The effect estimates calculated with Statistica software package showed a poor fit with the R-square coefficient being 0.75 - Figure 5-13. The main effects are the HDPE:PP ratio and the combined effects of (HDPE:PPxTime) and (HDPE:PPxSpeed). Their values, standard error and confidence intervals are highlighted in red in Figure 5-13.

Effect Estimates; Var.:STRESS; R-sqr=.75312; Adj:.59883

EXPERIM. DESIGN

4 factors, 1 Blocks, 27 Runs; MS Pure Error=141.6043
DV: STRESS

Factor	Effect	Std.Err. Pure Err	t(5)	p	-95.% Cnf.Limt	+95.% Cnf.Limt	Coeff.	Std.Err. Coeff.	-95.% Cnf.Limt	+95 Cnf.
Mean/Interc	43.92521	2.413347	18.20095	.000009	37.7215	50.12892	43.92521	2.413347	37.7215	50.1
(1)RATIO (L)	36.53680	7.270332	5.01994	.004035	17.8273	55.24635	18.26840	3.635166	8.9136	27.6
(2)TIME (L)	8.62435	5.924226	1.45578	.205223	-6.6044	23.85306	4.31218	2.962113	-3.3022	11.9
(3)SPEED (L)	-5.32636	5.712153	-.93246	.393900	-20.0099	9.35719	-2.66318	2.856076	-10.0050	4.6
(4)TEMP (L)	-.59914	4.836315	-.12388	.906234	-13.0313	11.83301	-.29957	2.418158	-6.5156	5.9
1L by 2L	21.80557	7.835439	2.78294	.038767	1.6639	41.94720	10.90278	3.917720	.8320	20.9
1L by 3L	26.79749	8.563419	3.12930	.025978	4.7845	48.81046	13.39874	4.281710	2.3923	24.4
1L by 4L	.64540	7.022783	.09190	.930346	-17.4072	18.69804	.32270	3.511392	-8.7036	9.3
2L by 3L	7.15436	6.562115	1.09025	.325334	-9.7141	24.02281	3.57718	3.281058	-4.8570	12.0
2L by 4L	-9.49312	5.759953	-1.64812	.160243	-24.2996	5.31331	-4.74656	2.879977	-12.1498	2.6
3L by 4L	.62481	5.732943	.10899	.917453	-14.1122	15.36180	.31240	2.866471	-7.0561	7.6

Figure 5-13 – Effect estimates for the melt strength (MS).

These results translate into the highest melt strength being directly related to a higher HDPE content.

	HDPE:PP Ratio	Rotor (rpm)	Time (min.)	Temperature (°C)	MFI (g/10min)	Max Stress (kPa)	Hencky Strain	MS (kPa)
1	50:50	50	1.5	170	3.89	37	0.84	35
2	80:20	50	2.5	170	2.30	46	0.80	13.6
3	20:80	150	1.5	190	-	14	0.87	11.9
4	80:20	150	2.5	170	2.21	29	0.96	82
5	20:80	125	2.5	190	-	15	0.91	6.2
6	80:20	150	3.5	190	-	70	1.04	115
7	80:20	50	3.5	190	-	42	0.76	31.4
8	80:20	150	1.5	190	-	53	0.97	105
9	80:20	150	2.5	190	2.30	55	0.93	48.0
10	50:50	100	1.5	190	-	52	1.05	31.7
11	20:80	50	2.5	190	3.90	40	0.84	49.7
12	80:20	50	1.5	170	-	50	0.94	51.5
13	20:80	100	1.5	190	-	45	0.81	32.0
14	20:80	150	3.5	170	-	28	0.79	21
15	80:20	150	1.5	170	-	49	0.93	53.6
16	20:80	150	3.5	190	-	11	0.71	12.7
17	20:80	50	3.5	190	-	34	1.06	33.1
18	50:50	50	2.5	190	-	45	0.88	70.7
19	80:20	150	3.5	190	-	47	1.84	66.9
20	80:20	100	1.5	170	-	47	0.80	64.0
21	50:50	100	3.5	190	-	37	0.67	34.8
22	50:50	50	3.5	170	3.29	52	0.89	45.4
23	20:80	50	1.5	190	-	38	0.78	48.9
24	80:20	100	2.5	190	-	52	0.82	54.4
25	80:20	50	3.5	190	-	56	0.97	68.3
26	20:80	150	3.5	170	4.13	8	0.71	7.41
27	20:80	150	1.5	170	-	19	0.73	25.7
28	80:20	100	3.5	170	-	35	0.73	51.7

Table 5-6 – Compositions and processing conditions used in the preparation of HDPE:PP blends.

The M_w of PR-HD4 is lower than PR-PP1, but despite this fact the melt strength is directly proportional to its content. This can be explained by the

fact that the radius of gyration is smaller for PP, leading to a lower number of entanglements, and also the regeneration of those entanglements is possibly more difficult because of conformation dynamics. However, HDPE content alone cannot totally explain the melt strength results, and we need to consider the melt multiphase structure of these immiscible polymer blends developed during the mixing process.

With the results being independent of temperature, the discussion of the results will be exemplified by the results at 170°C. As can be seen from the sequence of graphs (Figure 5.14-5.17), relating melt strength with processing conditions at each composition, there is a change on the effect of mixing time and speed depending whether the blend is rich in HDPE or PP. The highest melt strength is in red. For HDPE rich blends, the increase of melt strength is obtained with a higher mixing time and mixing speed. On the other hand, to obtain maximum melt strength from a HDPE-PP 20:80 blend it is more important to use lower mixing speeds and time.

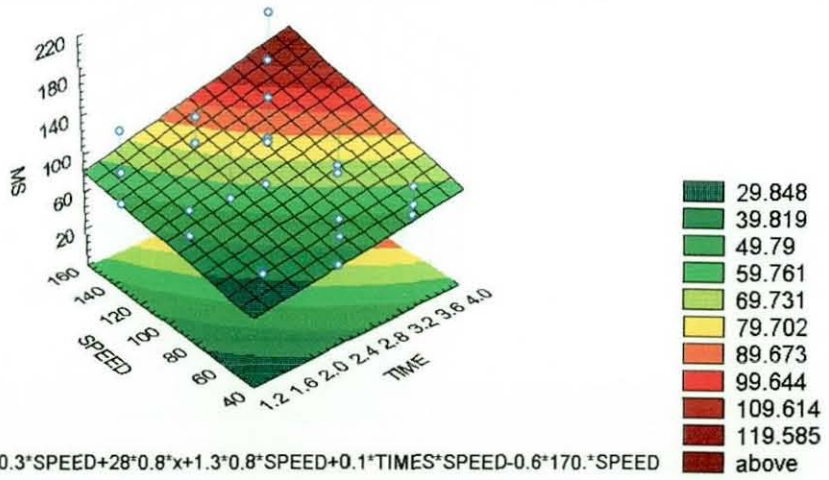

Figure 5-14 – Predicted melt strength for a HDPE-PP 80:20 blend mixed at 170°C.

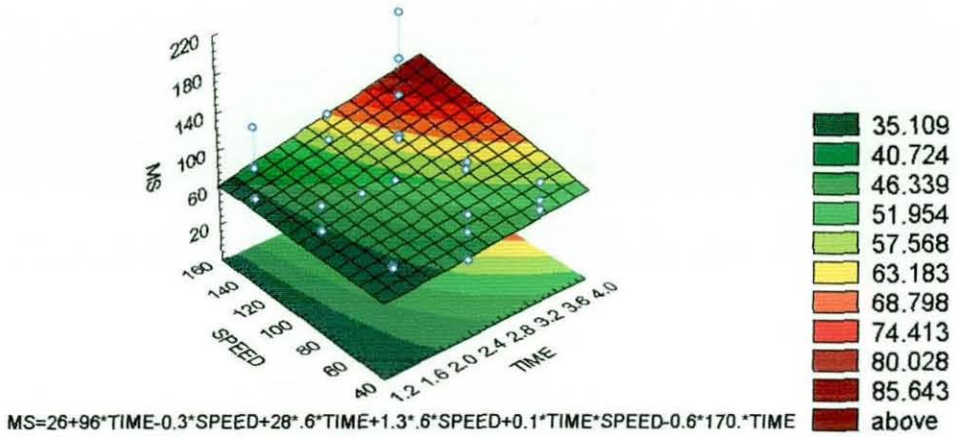

Figure 5-15 - Predicted melt strength for a HDPE-PP 60:40 blend mixed at 170°C.

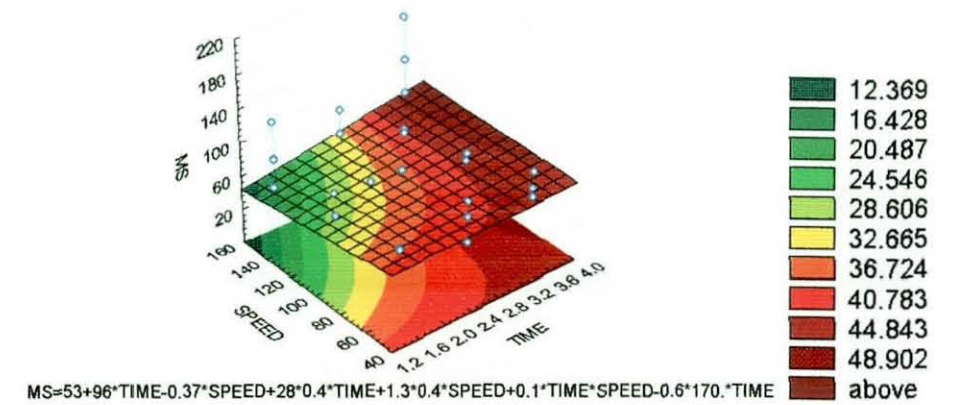

Figure 5-16 - Predicted melt strength for a HDPE-PP 40:60 blend mixed at 170°C.

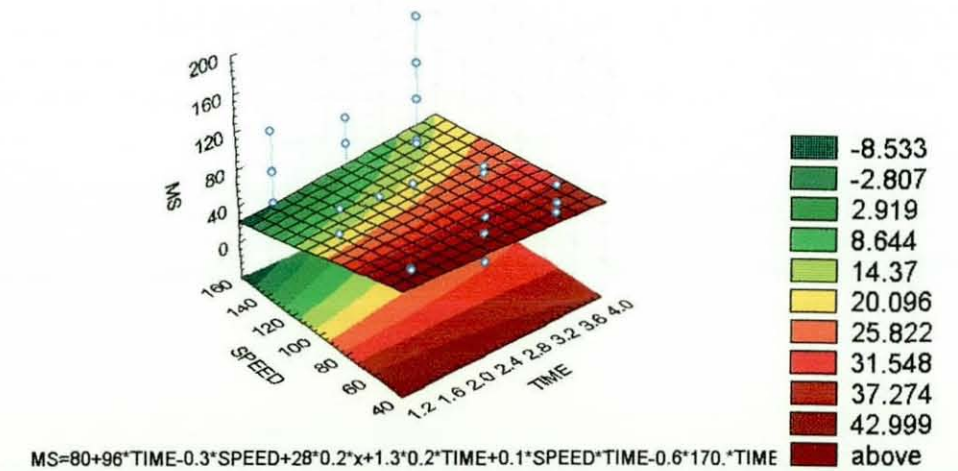

Figure 5-17 - Predicted melt strength for a HDPE-PP 20:80 blend mixed at 170°C.

These melt strength results can be explained on the basis of morphology development within the mixing process of two immiscible polymers with

different viscosity and prepared at a viscosity ratio higher than one. At these viscosity ratios the predicted morphology is a dispersed morphology.[28] However, as published recently,[106] when a lower viscosity polymer is melt mixed with a higher viscosity polymer that also has a lower melting point to prepare a blend rich in the lower viscosity component, an unstable co-continuous structure can be created. In our case, when preparing a PP-rich blend with low % HDPE, firstly the HDPE would melt and form a continuous phase - Figure 5-18. In this micrograph the darker background is PR-PP1 and the lighter phase is PR-HD4. Later, when PP melts a phase inversion occurs, it leads to a transition co-continuous structure that is transformed to a droplet dispersion of HDPE in a PP continuous phase.

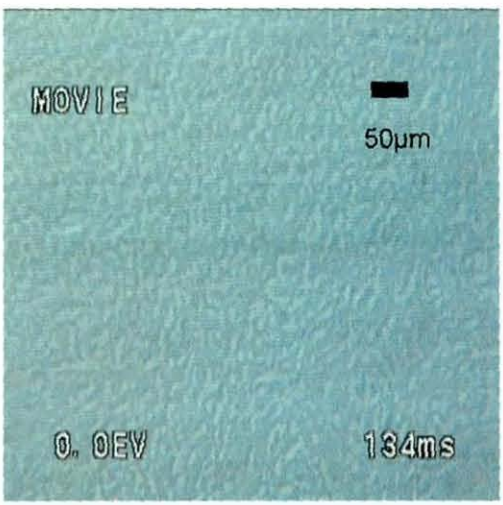

Figure 5-18 – Co-continuous morphology in a recycled HDPE-PP 20:80 blend – phase contrast microscopy.

With increased dispersion of HDPE droplets the extensional flow behaviour of the blend becomes dominated by the PP matrix. This reduces the extensional viscosity and consequently the melt strength. When the blend is richer in HDPE only a dispersed morphology of PP droplets can be obtained, with the highest melt strength being obtained at higher mixing times and speeds. This is because by forming droplets the surface area for a given amount of PP is minimal, thus reducing interfacial slip.

The extensional flow behaviour curve for the highest melt strength HDPE-PP blends are shown in Figure 5-19. It can be seen that the HDPE rich blends

have the highest melt strength, followed by the 50:50 blend and HDPE:PP 80:20. The extensibility is smaller when compared with the equivalent LDPE:PP blends, although the extensional stress can be higher. The yield points are similar those of the LDPE:PP blends. Generally, and even under optimum processing conditions, the strain energy density of the HDPE:PP blends is smaller than LDPE:PP blends. The deformation behaviour of the HDPE:PP blends can be considered ductile. The fact that PR-HD4 and PR-LD3 have similar M_w but the LDPE-PP blends in uniaxial extensional flow shows greater melt strength proves the influence of branching. Although the yield point of LDPE-PP and HDPE-PP blends occurs at a similar Hencky strain, the yield stress is higher for HDPE-PP blends.

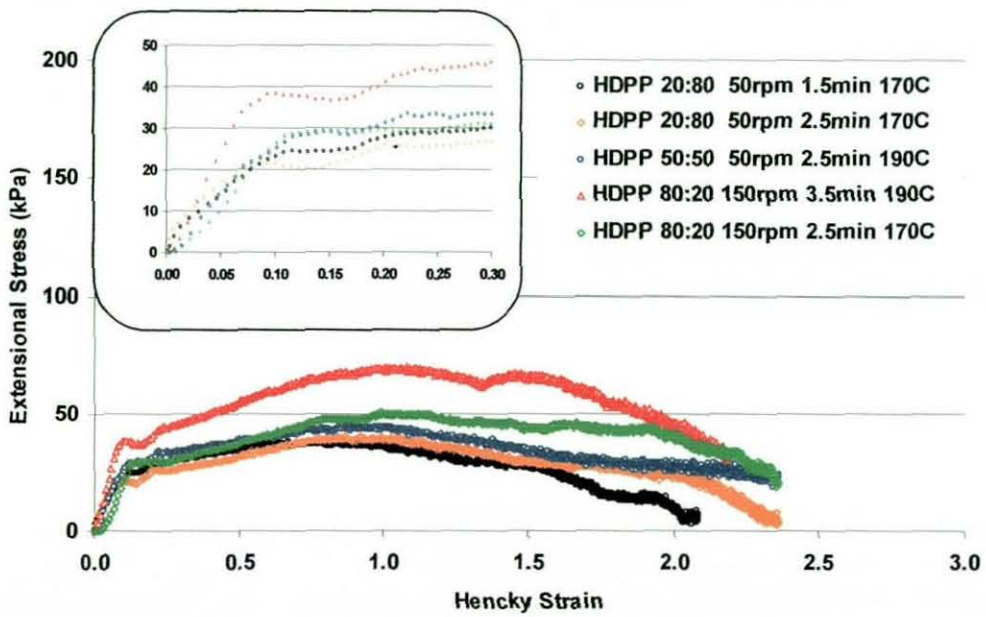

Figure 5-19 – Highest melt strength uncompatibilised recycled HDPE:PP blends.

The melt flow index measurements (Table 5-6) show a reduction in shear viscosity with increased HDPE content.

In summary, the results give evidence that the extensional flow properties are sensitive to the melt phase structure of the immiscible blend and composition of the blend. The higher the HDPE content, the higher viscosity and melt strength.

5.2.2 Effect of EPR1 Content

The effect of using EPR1 as a compatibiliser was investigated at two addition levels, 2.5% and 5.0%, on a recycled HDPE:PP 80:20 blend. These blends were prepared at 170°C, mixed at 150 rpm and using a mixing time of 1.5 and 2.5 minutes. As can be seen from Figure 5-20, this compatibiliser under these processing conditions shows an increase in the yield stress but lower strain at break. The strain energy density is smaller but the maximum stress is higher. The rupture mode has not changed by the incorporation of EPR1. One would expect that the incorporation of EPR1 would improve the extensibility of the blend as it has with some recycled LDPE-PP blends hat were described previously - section 5.1.4.1. In that previous study there was an optimum mixing time and EPR quantity to increase the extensibility of the blend system. The degradation of the extensibility suggest that under a strong shear and extensional flow field such as the one generated by the batch mixer at 150 rpm the EPR phase becomes so elastic that cannot be dispersed into droplets and flow to the interface between the HDPE and PP. It is also possible that some degree of coalescence may occur and both these phenomena ultimately degrade the extensibility of the blend. The influence of mixing conditions of EPDM in a PP matrix has been reported. In this study is suggested that at lower temperatures, higher speeds and viscosity ratios lower than one, the interfacial tension overcome the shear forces producing an elongated morphology instead of droplet dispersion.
With a higher yield stress but reduced extensibility the impact modified recycled HDPE-PP blend shows lower melt strength than uncompatibilised systems. There seems to be no extensional flow benefit for foaming when processing the studied blend under these conditions, although the mechanical properties of the foam could be enhanced.

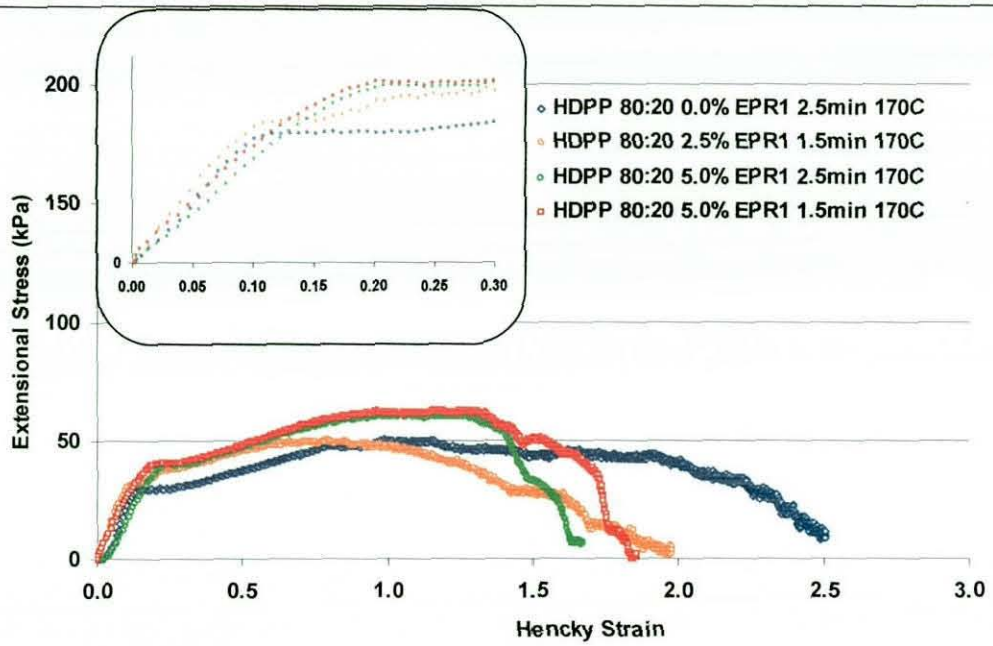

Figure 5-20 – Effect of EPR1 on HDPE:PP 80:20 blend.

5.2.3 Summary:

The most suitable recycled HDPE-PP blends for foaming are blends with high HDPE content, that are melt blended at high speeds and longer periods of time. The inclusion of EPR1 has a detrimental effect on the overall extensional flow properties. The melt strength and extensibility of HDPE-PP blends is generally lower than LDPE-PP blends at most compositions, which makes the latter more suitable for most foaming applications.

5.3 Polyolefin Layered-silicate Nanocomposites

Several routes have been reported to prepare polyolefin layered-silicate nanocomposites, but the one that is technologically easier is by melt compounding. This technique is particularly interesting with a view of upgrading the properties of recycled polymers. It is understood that to produce these compounds it is necessary the use a compatibiliser such as a polyethylene grafted maleic anhydride to facilitate the intercalation and exfoliation of the mineral. Also, it is necessary to optimise the processing conditions according to each resin, though some guidelines have been proposed by Vaia.[35] Compounding procedures diverge from low temperature and low shear stresses to higher temperatures and higher stresses. The batch mixing time is usually in the order of 10 to 15 minutes. Debate remains whether it is more important to allow diffusion into the clay gallery with a low mixing speed and high temperature or using low temperature to achieve higher stresses. In this context the research objectives for this section were:

- To prepare virgin and recycled polymer layered-silicate nanocomposites under different processing conditions (time, temperature, mixing time, mixing speed and clay ratio).
- To study the shear and elongational flow behaviour of the compounds.

5.3.1 HDPE Layered-silicate Nanocomposites Preparation

Several compounds based on PE-HD1 and PR-HD4 were prepared according to conditions described in section 3.5.2.1. Some of these compounds were subjected to X-ray analysis and observed under TEM to establish if clay nanometric structures were present. The melt flow index of the compounds was determined to assess the influence of the processing conditions on shear flow before performing a more in-depth rheological analysis by capillary and free surface elongational rheometry.

5.3.1.1 Preparation of Nanocomposites: Effect of Processing Conditions

The following two tables (Table 5-7, Table 5-8) illustrate the effect of processing parameters on the melt flow index of HDPE layered-silicate nanocomposites. These parameters were investigated on PE-HD1 and PR-HD4 for a fixed amount of compatibiliser (5% PB1) and by varying the rotor speed, temperature and organoclay content. The mixing time was set at 6 minutes. As seen in Table 5-7, the addition of clay to the HDPE:PB1 matrix increased the viscosity of the melt in all cases. This cannot be explained solely on the basis of the addition of PB1 or Cloisite 15A, it has to be a synergistic effect. The lowest melt flow indexes were achieved with lower mixing temperatures.

Mixing temperature (°C)	Rotor Speed (rpm)	Organoclay content (% w/w)		
		5	1	0
150	50	0.94	1.16	1.28
	100	0.92	1.19	1.39
	150	1.31	1.50	1.98
170	50	0.94	1.22	1.44
	100	1.09	1.24	1.41
	150	1.49	1.25	2.58
190	50	1.10	1.59	-
	100	1.39	1.95	-
	150	1.57	1.48	-

Table 5-7 – Melt flow index of PE-HD1 + 5% PB1 compounds.

There is a trend that shows an increase in melt flow index with increasing temperature and screw speed even in the absence of any organoclay. This suggests a possible thermomechanical degradation of the polymer under these processing conditions. It was confirmed by the resin's manufacturer that the resin contains a small amount of antioxidant incorporated in the formulation. Before discussing the possible degradation of the polymers during compounding, results from X-ray and TEM will be examined.

Mixing temperature (°C)	Rotor Speed (rpm)	Organoclay content (% w/w)		
		5	1	0
150	50	1.05	1.27	1.38
	100	1.13	1.09	1.48
	150	1.30	1.85	2.22
170	50	1.17	1.32	1.57
	100	1.24	1.24	1.78
	150	1.77	1.61	2.98

Table 5-8 – Melt flow index of PR-HD4 + 5% PB1 compounds.

Figure 5-21 is an X-ray diffractogram that illustrates the effect of temperature and polyethylene grafted maleic compatibiliser in the preparation of polyethylene layered-silicate nanocomposites. As a control, a curve of a compound containing simply 1% of 15A organoclay exhibited the typical peak basal spacing of a non-intercalated structure.[32]

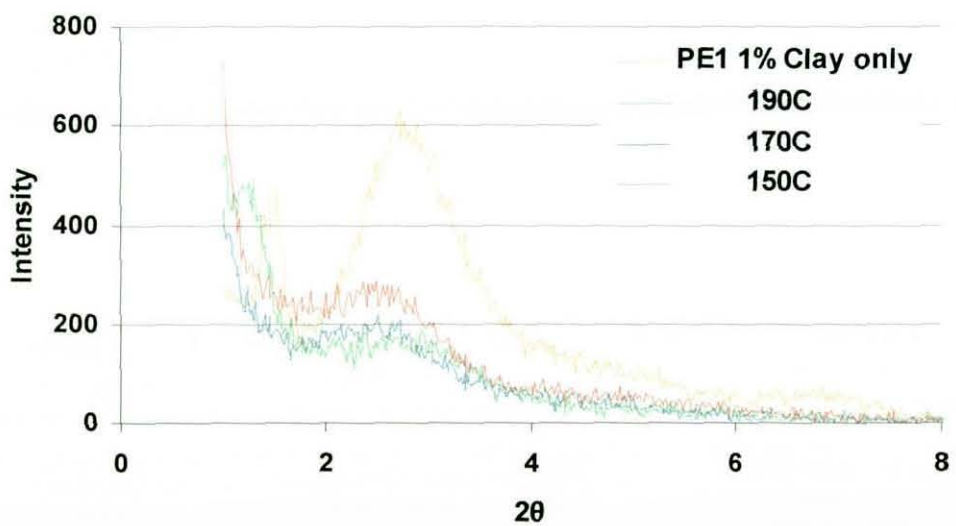

Figure 5-21 – X-ray Diffractogram of PE-HD1 + 5%PB1 + 1% 15A nanocomposites prepared at 100 rpm.

Because of its chemical affinity, the compatibiliser chains can diffuse into the clay galleries.[34] This modifies the chemical nature of the gallery and facilitates the diffusion of the polyethylene into it. Thus the interlaminar distance of the clay platelets increases. Also, when an intercalated structure is obtained the peak shifts to lower Bragg angles. By continued shearing of intercalated structures, delamination occurs, leading to a decrease of the

peak height, and correspondingly of their intensity. When the clay is completely delaminated no peak should be observed. For all the compatibiliser containing compounds, the X-ray curves of Figure 5-21 show a noticeable shift of the Bragg angle to angles corresponding to higher gallery spacing. Simultaneously a decrease in the peak intensity is observed when compared to the compound containing only 1% organoclay. This suggests that the two types of structure may be present in the polymeric matrix, one of them being the intercalated polymer clay structure, whilst the other would be the exfoliated structure. One can also infer that mixing for 6 minutes at any of the temperatures, polyethylene layered-silicate nanocomposites were produced.

Sample	Mixing temperature	Bragg Angle (2θ)	Basal spacing (Å)
PE1 + 1% 15A	170°C	2.92	30.6
PE1 + 5% PB1 + 1% 15A	150°C	2.50	35.9
PE1 + 5% PB1 + 1% 15A	170°C	2.62	34.2
PE1 + 5% PB1 + 1% 15A	190°C	2.78	32.2

Table 5-9 – Basal spacing of different virgin HDPE compounds.

The observation of these samples by TEM (Figure 5-22) at two different magnifications reveals a good dispersion of the organoclay with no agglome-

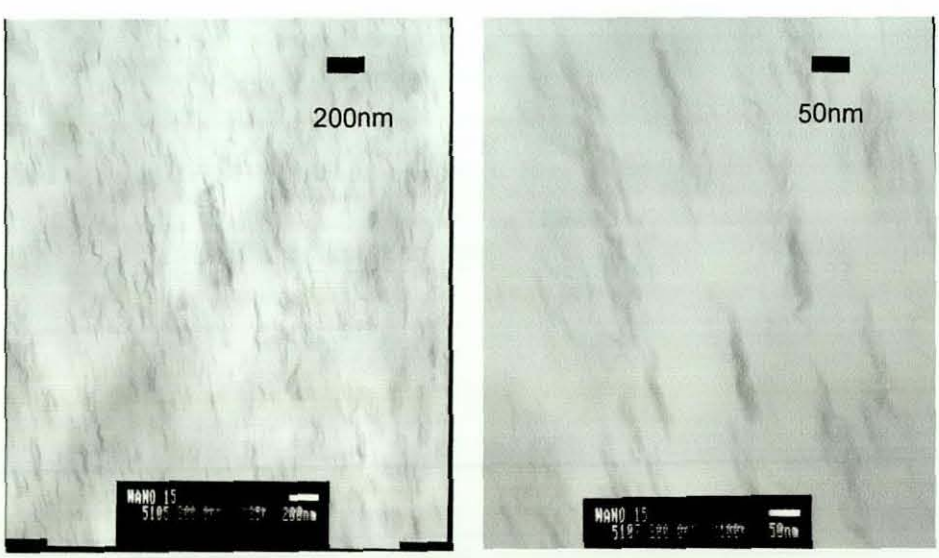

Figure 5-22 – TEM micrographs of PE-HD1 + 5%PB1 +5%15A (scale bar left 200nm, right 50 nm).

rates, but not a complete exfoliation as suspected from the X-ray diffractogram.

Thermal analysis by DSC was carried out to investigate variations in melting point and crystallisation temperatures in the compounds of higher melt flow indexes, but no changes were detected compared to the virgin resins. Cannevarollo[124] has suggested that thermomechanical degradation of polyethylene cannot be detected by such methods but rather by GPC, because DSC is not sensitive enough. Unfortunately, high-temperature GPC was not available to evaluate molecular weight changes. Alternatively, Fourier-transform infrared measurements were made on thin films of multiple compounds that had been prepared under different processing conditions. These revealed the presence of peaks assignable to hydroperoxides[126] in some of the samples - Figure 5-23.

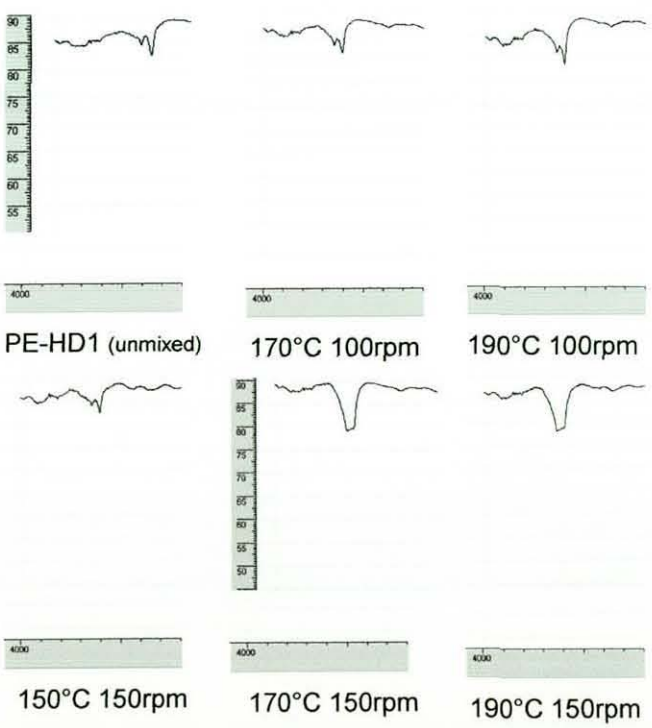

Figure 5-23 – Influence of processing conditions on the degradation of PE nanocomposites mixed for 6 minutes.

One could think that this could be related either to the degradation of the polymer or the degradation of the maleic-anhydride, or even the effect from the degradation of the organoclay, but the control samples without organoclay exhibited a similar behaviour. Therefore it must be related to the decomposition of either the compatibiliser or the HDPE. The virgin HPDE was confirmed by the supplier as a grade that had a certain amount of antioxidant to withstand normal processing. It may be the case that under these processing conditions, with a fill factor of 70% in an oxygen-rich environment, the amount of antioxidant required is insufficient to stabilise the system against a degree of thermomechanical-oxidation.

Melt flow index results therefore show that the mixing time, temperature and rotor speed have a great influence in the low shear rate behaviour of the nanocomposites. Thus it was decided to use a central composite experimental design to study the effect of those variables. Additionally it was decided to include the polymer clay ratio as another process variable.

5.3.1.2 Optimization of processing conditions

In order to determine the optimum processing conditions and the lowest threshold of conditions that lead to reinforcement of the polymeric matrix an experiment was designed using a central composite design. In this design lower mixing speeds (30 – 50 rpm) and times (1.5 - 3.5 minutes) were used. The temperature was set at 150°C. Previous experimental results – Table 5-8 - at higher mixing speeds (100-150 rpm) and times (6 minutes) were included to extended the range of conditions and improve the accuracy of the model. The chosen response variable was the melt flow index at 190°C and 5 kg load. This variable can be linked to molecular weight to infer extensional viscosity. Due to the similarity of results between PE-HD1 and PR-HD4 only the latter material was used. These results can be found in Appendix VIII. Figure 5-24 shows a surface representation of those results without discriminating the clay:compatibiliser ratio.

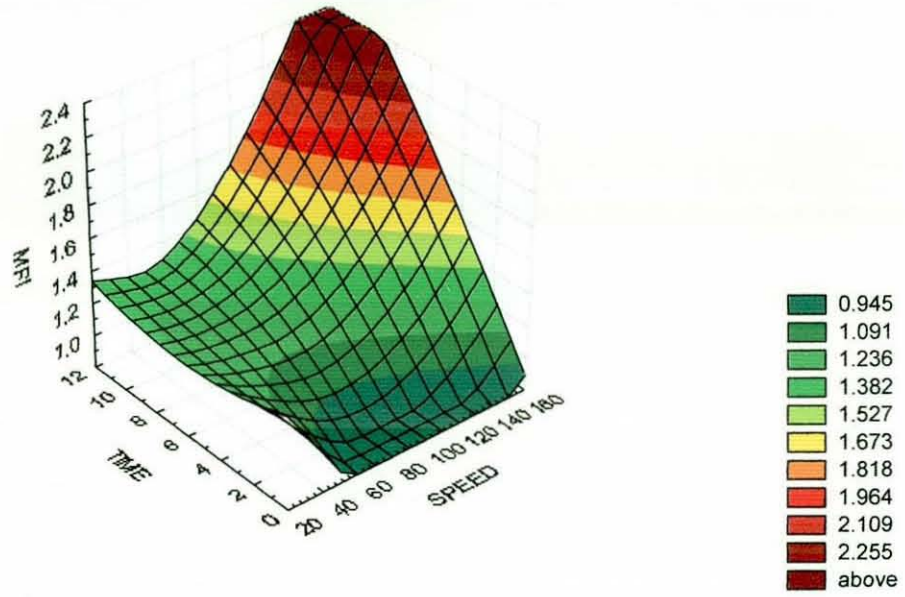

Figure 5-24 – Surface representation of the MFI results for PR-HD4 nanocomposites.

A model with linear (L), quadratic (Q) and linear interaction ("effect" L x "effect" L) effects was fitted to the experimental MFI results. The analysis of variance of those results can be found in Table 5-10. It shows in red that all main effects should be included in the model plus interactions of (time x speed) and (speed x clay:compatibiliser ratio), as their p values are minima.

	SS	df	MS	F	P
(1)TIME (L)	.088754	1	.088754	11.93923	.004264
TIME (Q)	.000121	1	.000121	.01631	.900319
(2)SPEED (L)	.009594	1	.009594	1.29061	.276446
SPEED (Q)	.373016	1	.373016	50.17831	.000008
(3)CLAY (L)	.223889	1	.223889	30.11764	.000104
CLAY (Q)	.057653	1	.057653	7.75552	.015471
1L by 2L	.074298	1	.074298	9.99455	.007505
1L by 3L	.023100	1	.023100	3.10738	.101415
2L by 3L	.143097	1	.143097	19.24952	.000734
Error	.096640	13	.007434		
Total SS	1.855877	22			

Table 5-10 – Analysis of variance of a second order model with linear interactions.

The response surface function of MFI was minimized in order to obtain the desirability plot over the range of processing conditions. With these plots

(Figure 5-26, Figure 5-25) it was possible to determine the processing conditions that minimize the MFI, and hence maximise extensional viscosity .

The desirability contour plots show that in order to minimize the MFI in PR-HD4 *nanocompounds clay:compatibiliser ratios of 0.3 – 1.2 should be used* with low mixing times and mixing speeds ranging 60 – 150 rpm.
The optimum desirability plot (Figure 5-26) shows that the optimum processing conditions are: a mixing speed of 150 rpm, mixing time of 1.5 minutes and a clay compatibiliser ratio of 0.8 or 1.0.

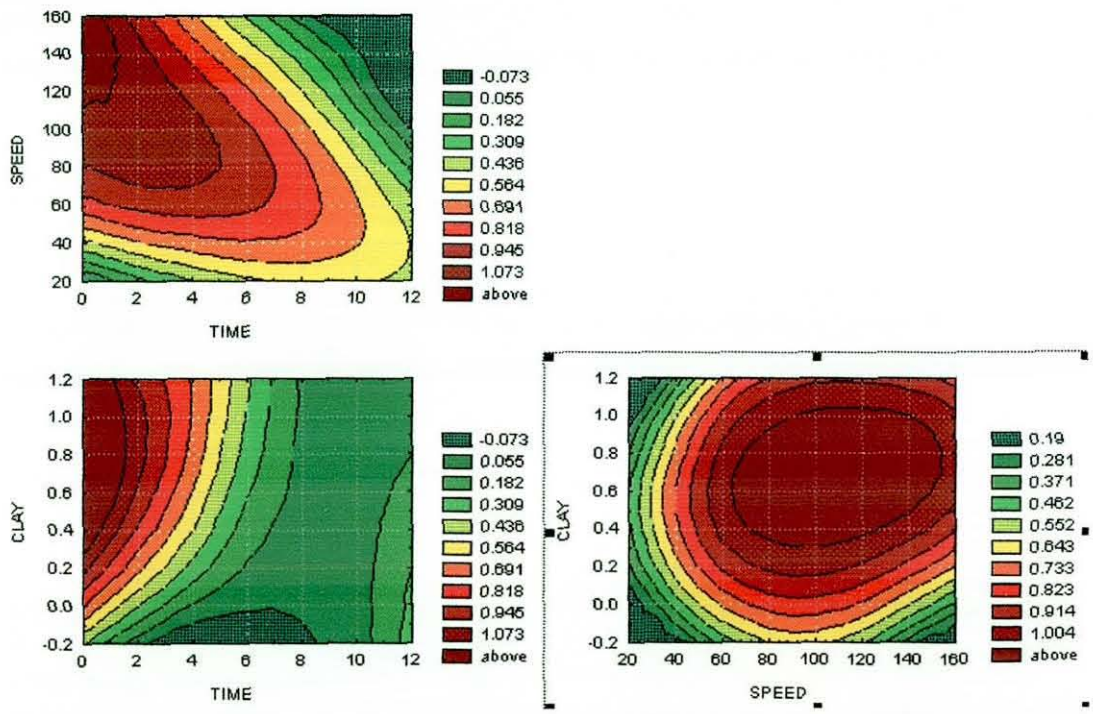

Figure 5-25 – Desirability function contour plot as function of rotor speed, mixing time and clay-compatibiliser ratio at prepared at 150°C

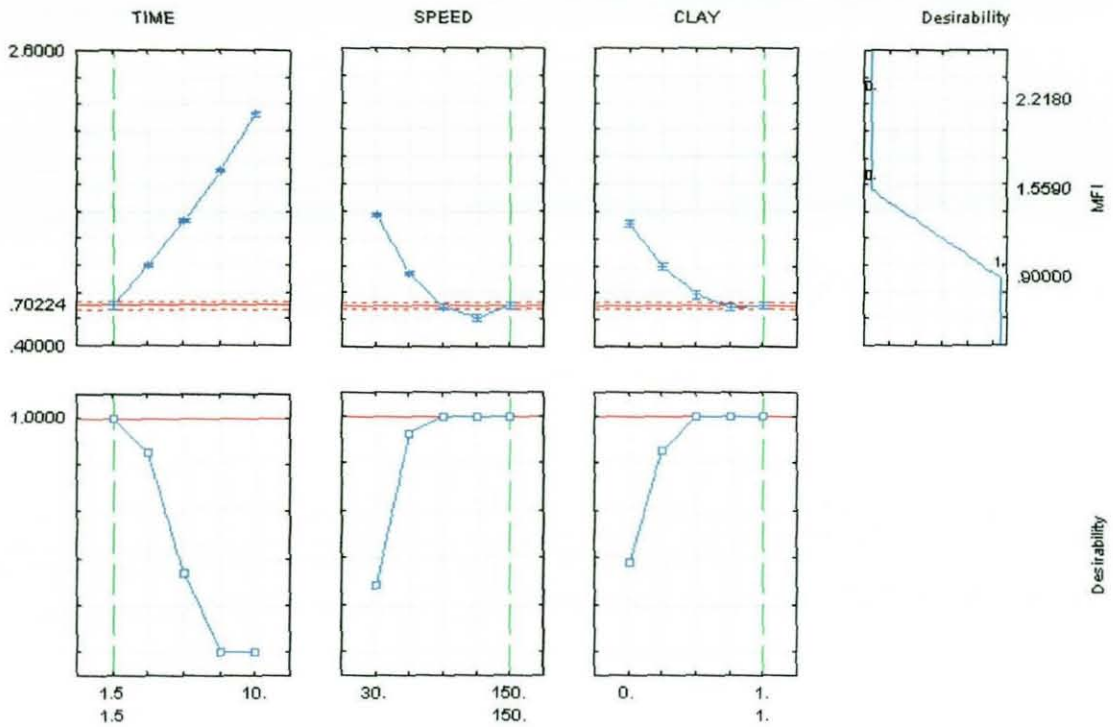

Figure 5-26 – Optimum process conditions desirability plot.

Based on these results it was decided to run experiments at higher mixing speeds and different mixing times, at 150°C and 170°C. These results can be found in Table 5-11 and confirm the predictions of the surface response model with the lowest melt flow indexes being obtained at the lowest mixing times.

	Time (minutes)			
	1.5	2	2.5	3.5
150°C	0.62	0.77	0.76	0.76
170°C	0.71	0.81	0.81	0.83

Table 5-11 – Influence of mixing time on melt flow index of PR-HD4 + 5% PB1 + 5% 15A at 150°C.

5.3.1.3 Summary

Virgin HDPE and recycled HDPE montmorillonite nanocomposites have been prepared under different processing conditions. Some of those conditions induced thermomechanical and oxidative degradation of the compounds. The

morphology of the nanocomposites is a mixture of intercalated and exfoliated structures. In order to obtain low melt flow index HDPE montmorillonite nanocomposites it is best to use low temperatures, short mixing times, high rotor speeds and a clay-compatibiliser between 0.6-1.

5.3.1.4 Capillary Rheometry

The melt flow index results presented previously (5.3.1.1) showed differences of shear flow behaviour at low deformation rates, but no information can be inferred about the higher shear rates. Thus, it was decided to investigate the influence of clay content, mixing time, rotor speed and temperature with capillary measurements in the range of 1 - 400 s^{-1} at 170°C. The results discussed are relative to 'control' PR-HD4 samples.

5.3.1.4.1 Effect of Organoclay Content

The influence of organoclay content was studied in samples prepared at 150°C and 170°C and rotor speed of 150 rpm for 1.5 minutes. As seen in Figure 5-27 a discontinuity arises between the curves at around 100s^{-1} which could be linked to the onset of wall slip. With increasing shear this effect is accentuated and the sample with the highest organoclay content. This could be due to the fact that the clay at higher deformation rates induces slippage with the polymer, reducing the viscosity. Figure 5-28 illustrates a plot of shear stress vs. apparent shear rate where a degree of wall slip can be inferred. However, full wall slip studies should be performed; also not many studies on slip behaviour of nanocompounds have been reported. Increased wall slip may be beneficial in blow molding resins[125] [31] as it reduces the amount of shear heating and help control the melt temperature. In other processes screw design may need to be review, possibly by reducing the metering zone or extending the compression zone and increasing the channel depth.

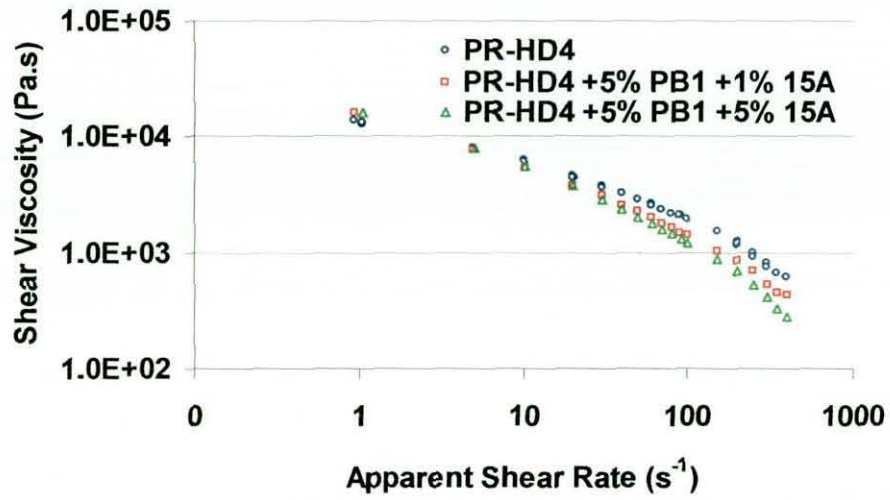

Figure 5-27 – Effect of organoclay content on PR-HD4 nanocomposites prepared at 170°C.

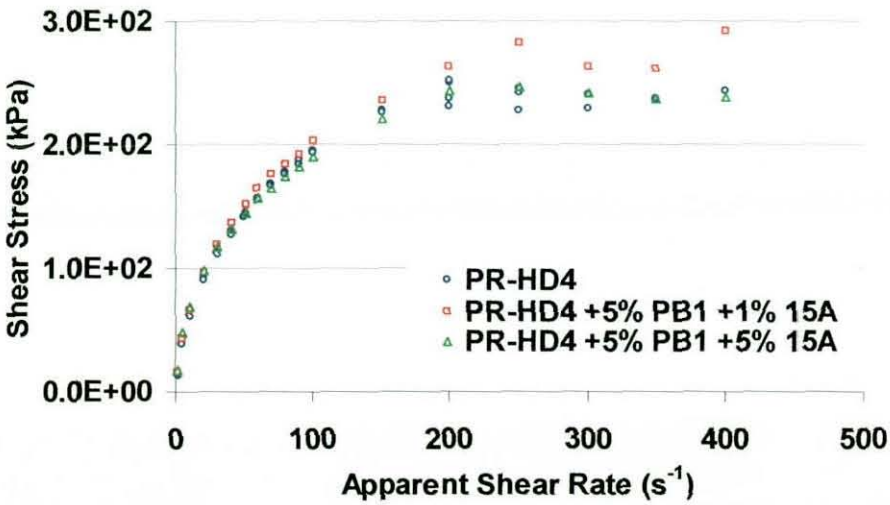

Figure 5-28 - Effect of organoclay content on PR-HD4 nanocomposites prepared at 170°C.

The extensional flow behaviour studied by the Cogswell method shows a much higher viscosity for matrices containing organoclay, which has been attributed to the existence of intercalated or exfoliated structures.[16] This shows that high-density polymer waste can be upgraded by using melt intercalation to increase its processability when melt strength is required. Within the typical experimental uncertainty it is not possible to distinguish between the clay loading for an optimum clay-compatibiliser ratio or loading.

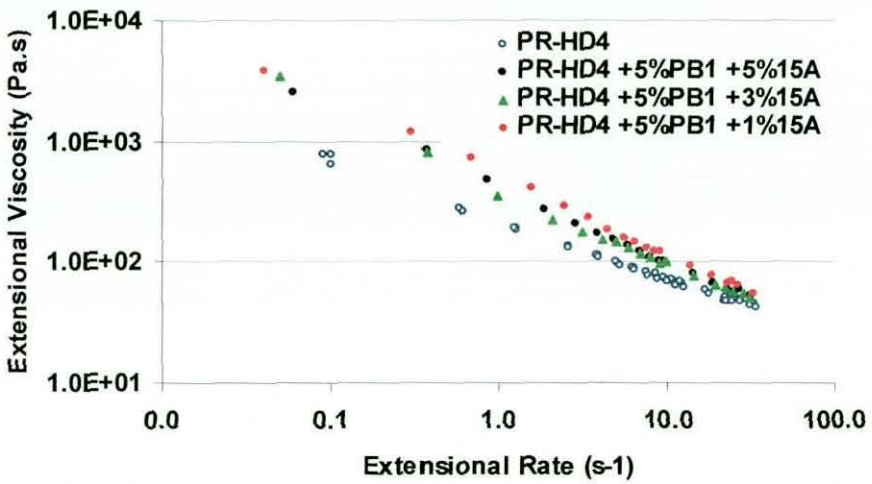

Figure 5-29 – Effect of organoclay content on the extensional flow behaviour of PR-HD4 nanocomposites prepared at 170°C.

5.3.1.4.2 Effect of mixing time

The influence of mixing time was studied in samples prepared at 150°C and 170°C and rotor speed of 150 rpm for 1.5 minutes and 6 minutes. The previous melt flow index results (Table 5-8) have shown that the low shear rate viscosity decreases with mixing time. The same is visible in Figure 5-30, but apart from the differences in zero shear rate viscosity the pseudoplasticity behaviour is still very similar. This is somewhat unexpected as it is known with 6 minutes of mixing the sample has suffered some oxidative degradation and a lower viscosity was expected. Curiously, also the sample that was mixed for a short time exhibited lower viscosity. The effect is similar when a small portion of high molecular weight material is added to HDPE or LCB has been introduced.

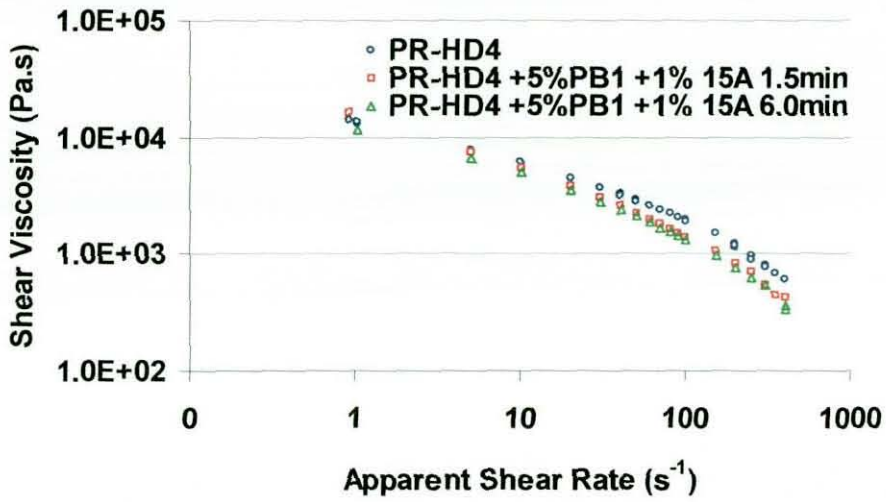

Figure 5-30 – Effect of mixing time on shear flow behaviour of PR-HD4 nanocomposites.

There is however a significant difference in the extensional flow behaviour between samples prepared for 1.5 minutes and samples prepared for 6 minutes, with the former being more viscous - Figure 5-31.

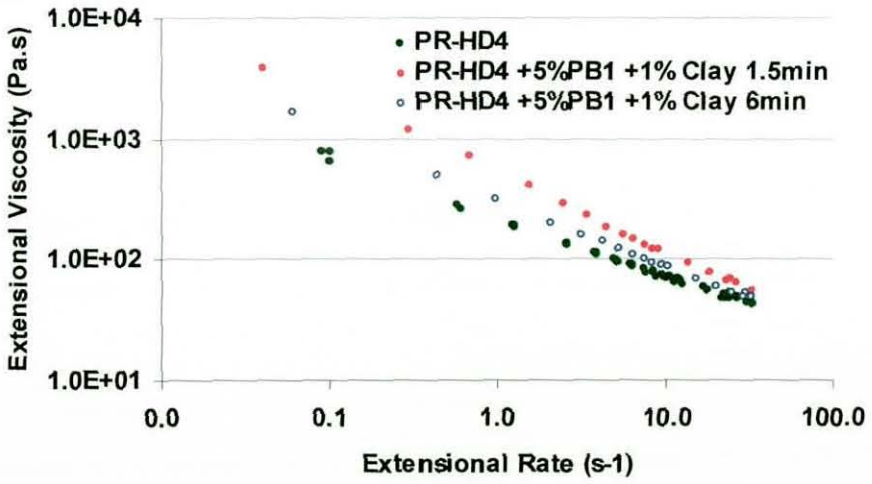

Figure 5-31 – Effect of mixing time on extensional flow behaviour.

5.3.1.4.3 Effect of mixing speed

Samples prepared with different mixing speeds but same mixing times show the same degree of pseudoplasticity but samples prepared at lower mixing speeds tend to have a lower zero shear rate viscosity.

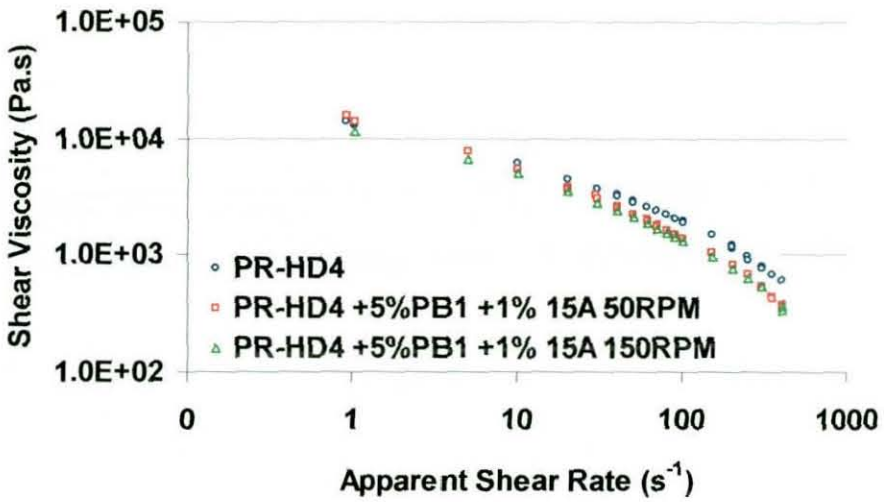

Figure 5-32 – Effect of mixing speed.

5.3.1.4.4 Summary

High-density polyethylene nanocomposites have distinct shear flow behaviour when compared to their unfilled compounds. They exhibit a pseudoplastic behaviour that is influenced by the nanoclay loading, with decreasing 'n' index with increased clay content. The zero shear rate and extensional viscosity is also larger.

5.3.1.5 Free Surface Elongational Measurements

The elongational flow behaviour has been studied for all the prepared samples, however only a summary representative of these results will be presented to illustrate the effects of processing and composition. Examples shown are only from PR-HD4 compounds.

5.3.1.5.1 Effect of Composition

The influence of several components in the HDPE matrix were considered and investigated in two component systems. This is illustrated in Figure 5-33. Adding 5% PB1 to PR-HD4 yields a blend that has a different behaviour from PR-HD4 alone. The melt elasticity as seen by the slope until the first yield point and yield stress is clearly larger. The addition of clay alone shows no significant departure from the behaviour of plain PR-HD4. The combined effect of 5% PB1 and 1% 15A however show an increase in the yield stresses but decrease in extensibility when compared to plain HDPE. The high-density polyethylene nanocompound failure behaviour shifts from a ductile to cohesive failure which is more similar LDPE materials.[123] A secondary yield point seems to appear in some samples. This is not related to the ultimate failure or rupture of any of the test areas of the oval sample.

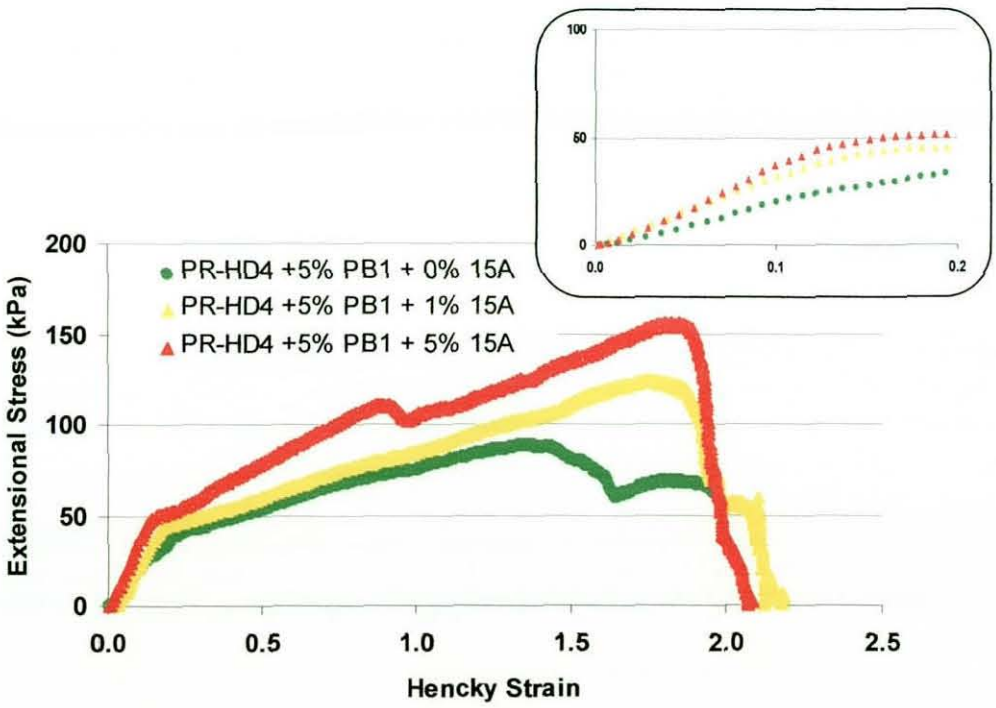

Figure 5-33 – Influence of organoclay content on HDPE-PB1 compounds mixed at 170°C, 100rpm for 6 minutes.

5.3.1.5.2 Effect of mixing time

It was already seen that very small mixing times lead to higher viscosities. In linear polyethylenes the lower the MFI the higher the extensional viscosity. The yield stress point doesn't seem to change much but the work hardening before rupture is completely different. Samples mixed for less time have a higher maximum stress, but all seem to fail at the same Hencky strain. There seems to be a transition that occurs in merely 0.5 minutes. After 1.5 minutes a plateau seem to develop in samples mixed for 2.0 minutes. Still after mixing for 6 minutes the melt strength of the compound is still higher than that of the HDPE:PB1 blend.

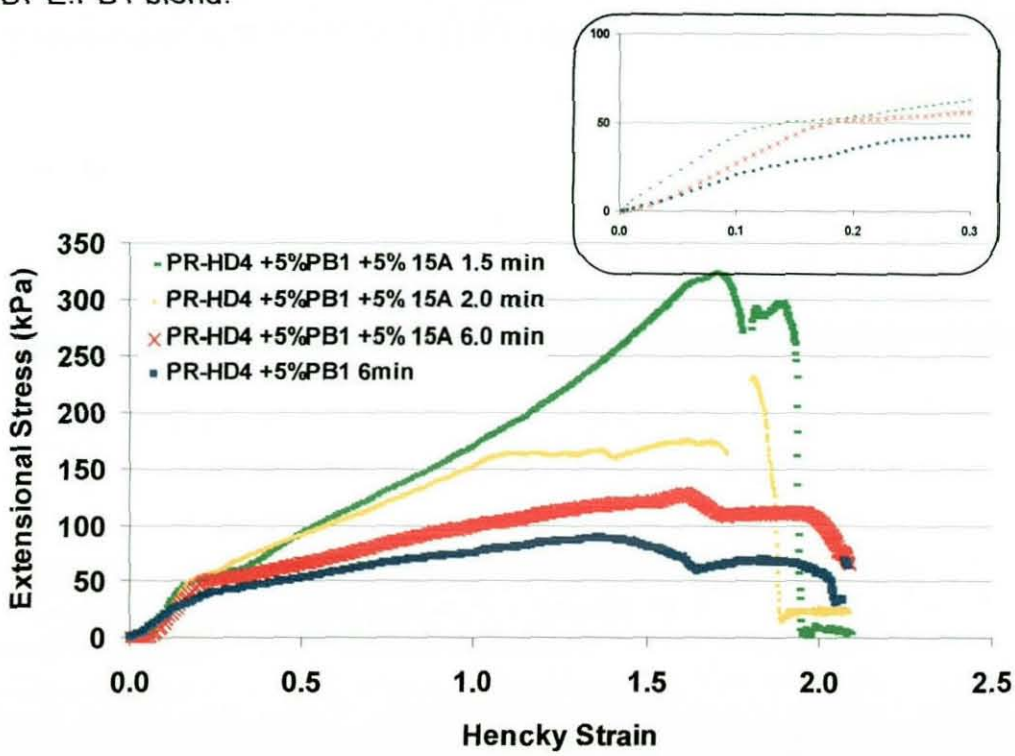

Figure 5-34 – Influence of mixing time on PR-HD4 + 5% PB + 15% 15A compounds mixed at 170°C and 150 rpm.

The extensional flow behaviour of the sample mixed for 1.5 minutes shows work hardening behaviour similar to that of branched materials (5.1.4.4). It is therefore possible to think that the structure produces a strain hardening behaviour.

5.3.1.5.3 Effect of Clay Content

The influence of organoclay loading on the HDPE:PB1 matrix was studied on samples prepared at 170°C, 150 rpm and mixed for 1.5 min (Figure 5-35).

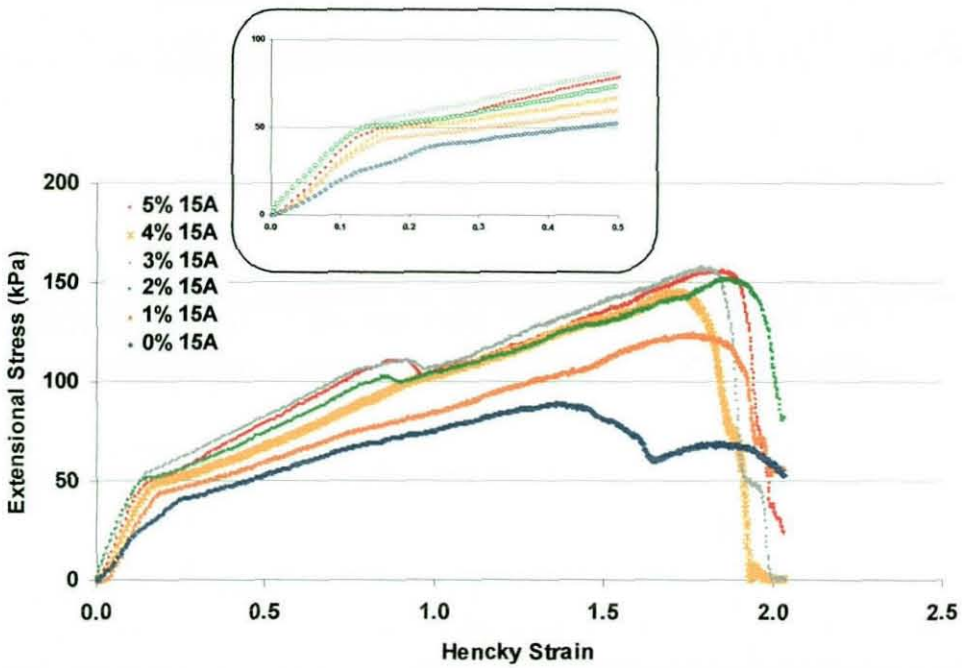

Figure 5-35 – Effect of clay content on PR-HD4 + 5%PB1 compounds mixed at 170°C, 100 rpm for 6 minutes.

Adding clay to this matrix results in an obvious change of the melt elasticity and work hardening past the yield stress, which suggests different degrees of reinforcement or intercalation/exfoliation. The HDPE nanocomposite with the least clay loading sample is less viscous which suggests that this may not be an optimum clay-compatibiliser ratio. This is in agreement with the response surface results.

5.3.1.5.4 Effect of compatibiliser content

The influence of the compatibiliser was evaluated on samples containing 5% 15A. For this type of loading it was observed that using as much as 2% PB1 can produce a significant improvement.

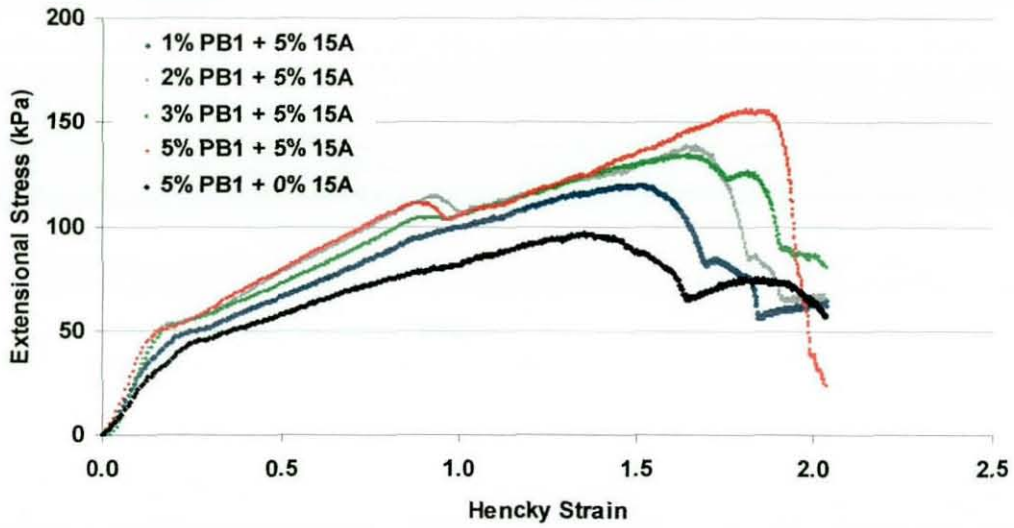

Figure 5-36 – Effect of compatibiliser content on PR-HD4 compounds with variable PB1 content mixed at 170°C and 100 rpm for 6 minutes.

5.3.1.5.5 Summary

HDPE clay nanocomposites show improved extensional flow behaviour with increased melt elasticity, yield stress and strain energy density, which is a result of a higher extensional viscosity. Samples produced at 170°C, 150 rpm for 1.5 min showed the highest melt strength.

5.3.2 HDPE-PP Layered-silicate Nanocomposites

After having studied the preparation and rheological properties of HDPE: PP blends and HDPE layered-silicate nanocomposites, it was decided to investigate properties and preparation of HDPE:PP layered-silicate nanocomposite blends. Two HDPE:PP ratios, 80:20 and 60:40, were used. They were melt mixed in a batch mixer with 5% PB1 and 1%15A at 150 rpm. The effect of mixing time and temperature was investigated. The melt flow index of the compounds was then determined to examine the low shear rate behaviour and to assess the degree of reinforcement. Then for some of the

compounds free surface elongational and capillary rheometry measurements were performed.

5.3.2.1 Melt Flow Index Measurements

The preparation conditions of the blends and MFI results can be found in Table 5-12. It can be seen from these results that there is clear relationship between HDPE content, mixing time and temperature. For each of the tested compositions the melt flow index is reduced by increasing the HDPE content, the mixing temperature and mixing time.

HDPE:PP ratio	PB1 % (w/w)	Clay % (w/w)	Mix. Time (min.)	Temperature (°C)	MFI (g/10min)	MS (kPa)
80:20	0	1	1.5	170	2.33	80
80:20	5	0	1.5	170	1.55	115
80:20	5	1	1.5	170	1.06	216
80:20	5	1	2.0	170	1.16	205
80:20	5	1	1.5	190	1.21	118
80:20	5	1	2.0	190	1.35	151
60:40	5	1	1.5	170	1.38	122
60:40	5	1	2.0	170	1.48	144
60:40	5	1	1.5	190	1.48	150
60:40	5	1	2.0	190	1.72	125

Table 5-12 - MFI of HDPE:PP compounds determined at 190°C with a 5kg load.

The effects of adding clay to a HD-PP 80:20 blend at a 1% level is not significant, whereas adding 5% PB1 significantly reduces the melt flow index. This shows that adding the PB1 makes the ternary blend deviate positively from a mixture rule, as the melt flow index is lower than the sum of the individual contributions. The addition of 1% of 15A also shows a beneficial effect which can possibly be attributed to an intercalated or exfoliated morphology.

Composition	MFI (g/10 min)
HD-PP 80:20	2.30
HD-PP 80:20 + 1% 15A	2.33
HD-PP 80:20 + 5% PB1	1.55
HD-PP 80:20 + 5% PB1 + 1% 15A	1.06

Table 5-13 – Effect of composition on the MFI of HD:PP compounds.

5.3.2.2 Free Surface Elongational Flow

The first results to be discussed are the effects of the blend composition as illustrated by Figure 5-37 for a HDPE:PP 80:20 blend. The orange curve is related to a blend without any additives or fillers. The graph shows that a simple addition of 5% of PB1 increases the yield stress after which work hardening follows before the sample ruptures at a Hencky strain of 1.8. The addition of EPR shows a similar behaviour, however, unlike in the case of LDPE:PP blend with the same condition a higher content seems to be more beneficial in terms of extensibility and strain energy density. When 1% 15A is added to a sample containing 5% PB1 the yield stress decreases significantly but in contrast the work hardening prolongs itself to higher Hencky strain resulting in higher melt strength.

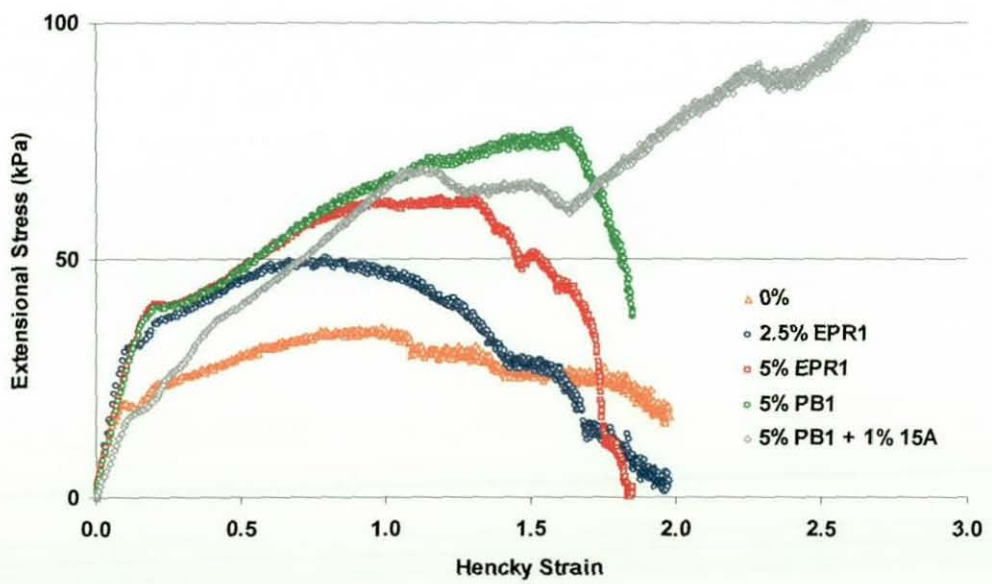

Figure 5-37- Effect of composition on PP-HD 20:80 mixed at 170C, 150 rpm, 1.5m.

A comparison between the blend ratios follows in Figure 5-38. A fundamental difference in the behaviour can be found in HDPE:PP 60:40 nanocomposite blends was found. Unlike the HDPE richest blend no increased extensibility was found, but instead an increase in yield stress and maximum stress.

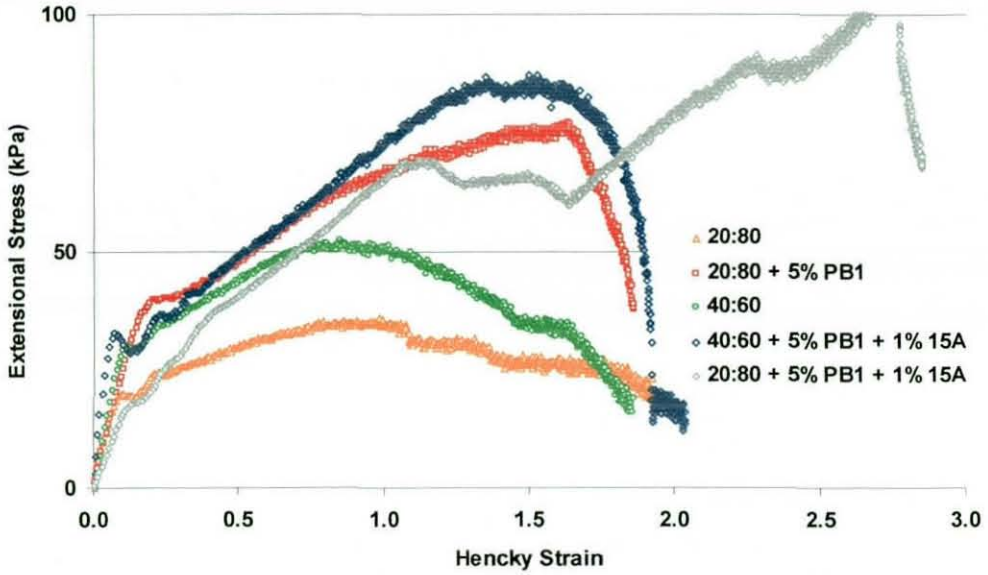

Figure 5-38 – Effect of composition on PP-HD blends mixed at 170°C, 150 rpm, 1.5 min.

The effect of mixing time and temperature on HDPE:PP 80:20 blends show that the temperature can play a significant effect of the flow behaviour of these compounds. A result that is not entirely repeated for a HDPE:PP 60:40 blend (Figure 5-40).

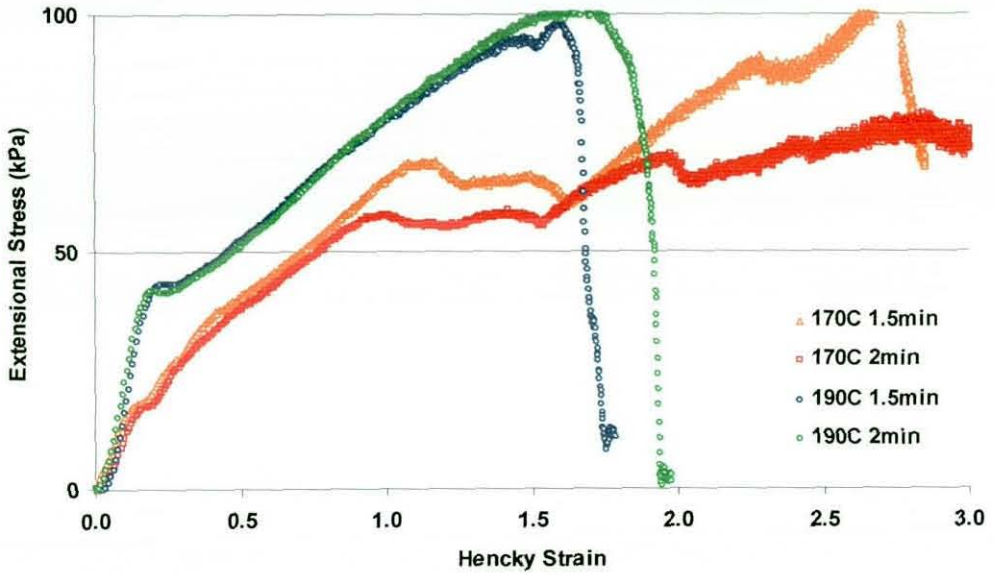

Figure 5-39 – Effect of mixing time and temperature on PP-HD 20:80 + 5% PB1 + 1%15A mixed at 150 rpm.

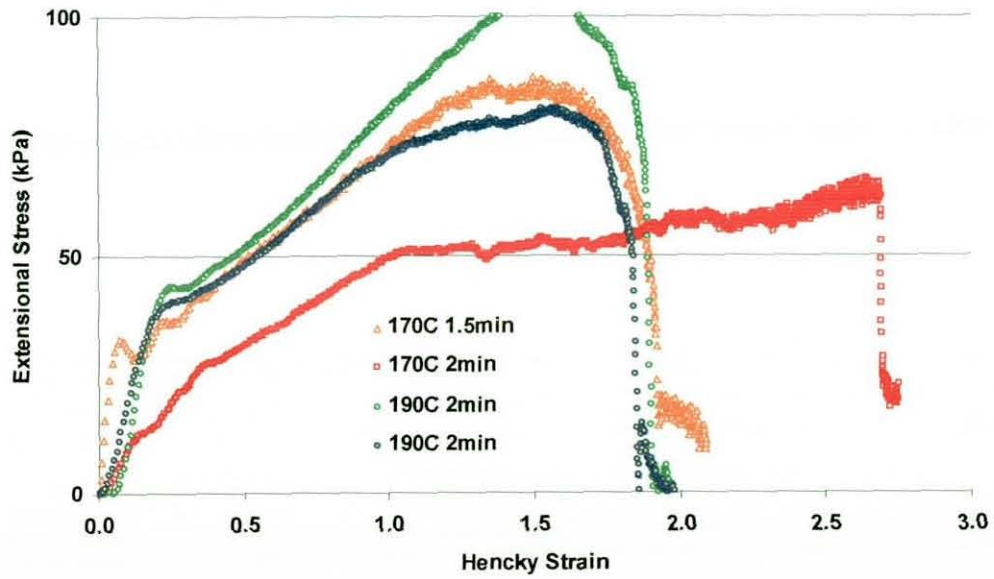

Figure 5-40 – Effect of mixing time and temperature on PP-HD 40:60 + 5% PB1 +1% 15A mixed at 150 rpm.

5.3.2.3 Summary

Uncompatibilised blends of PP:HDPE show low strain energy density, extensibility and yield stress at any composition, when compared to plain

HDPE or LDPE, or even PP:LDPE blends. The blends richer in HDPE show the highest viscosity. Adding either EPR1 or PB1 significantly improve the extensional viscosity of the blends. The combined use of 5% PB1 and 1% 15A leads to an increase in elasticity, yield stress and maximum stress. Under certain processing conditions, it is possible to significantly improve the extensibility of the nanocomposite system instead of an increase viscosity.

5.3.3 Influence of processing variables on flow behaviour of polyolefin nanocomposites - summary

As it has been shown over the last few sections there is an important interplay between the processing conditions that lead to different morphologies and the flow behaviour of the nanocomposites. The individual effects are summarised in Table 5-14, but their combination require further explanation. It is understood that to produce a layered-silicate nanocomposite the polymer needs to diffuse into the clay gallery and then, under shear stress delamination occurs. Therefore, provided that the viscosity of the melt is sufficiently low and compatibilisation enough, the polymer will diffuse into the clay gallery. At this stage by using a high mixing speed for sufficient time, so that delamination is possible, one also has to guarantee that the melt temperature doesn't too quickly above the decomposition temperature of the organic modifier of the clay. Otherwise, intercalation and exfoliation is not possible. If a nanocomposite is produced, the zero shear rate viscosity will increase due to an increase in extensional viscosity, but wall slip will increase. The pseudoplastic index did not seem to change between 1-5% clay. The amount of clay directly increases the zero shear rate and extensional viscosity. Under uniaxial flow the nanocomposite exhibits reduced extensibility and increased melt strength. This type of flow is more discriminating towards the clay and compatibiliser content. They influence melt state elasticity, melt strength but show no effect on extensibility, with the exception of HDPE-PP nanocomposites where it was

possible under certain processing conditions to increase melt strength and extensibility simultaneously.

Processing Variable	Shear flow	Extensional flow
Mixing Temperature	Temperatures closer to melting point ↑ low shear viscosity. Too high temperature ↓ η.	Low mixing temperatures ↑ η, ↓ elongation@break, ↑ MS. High temperature ↓ MS, ↓ η,
Mixing Speed	Higher mixing speed ↑ low shear rate viscosity. No difference in η at higher shear rates	↑ η. ↓ elongation@break. ↑ melt state elasticity. ↑ MS.
Mixing Time	Shorter mixing times ↑ low shear rate viscosity. No difference in η at higher shear rates.	Differences according to mixing time. Shorter mixing time ↑ η. Longer mixing time ↓ η.
Clay	↑ η_0. ↑ wall slip.	↑ η. ↓ elongation@break. ↑ melt state elasticity. ↑ MS. ↑ clay content leads to double yielding in free surface measurements
Compatibiliser		↑ η. ↓ elongation@break. ↑ melt state elasticity. ↑ MS. ↑ compatibiliser leads to double yielding in free surface measurements

Table 5-14 - Influence of processing conditions on the flow behaviour of polyethylene layered-silicate nanocomposites.

6 Extrusion Simulation and Foaming

After having determined thermal and rheological properties of the raw polymers, blends and compounds, it was possible to create a new materials database for the flow simulation software package: Flow 2000. The flow domains representing the 24x1.5 mm capillary were completed as described in section 3.7.1. The shear flow behaviour of the raw polymers in a capillary die was simulated at several piston speeds and temperatures to obtain shear flow curves. These were compared with the measurements made previously to determine the validity of the model. Foam extrusion experiments were also modelled and rheological data was generated to optimise the foaming of different materials through this die. A foam extrusion technique was developed for a Rosand RH-7 rheometer. In addition, practical foam extrusion experiments were carried out with a Rosand RH-7 using chemical blowing agents. Recycled and virgin polymers, as well as blends and nanocompounds were foamed. The foam density was evaluated. The objectives were:

- To develop a correlation between the foam extrusion experiments and the simulations to optimise the foam processing conditions.
- To develop a new simulative tool for the modelling of foam extrusion processes.

6.1 Extrusion simulation

Two general flow situations were modelled with Flow 2000 during this research. The first was half of the flow domain of the 24x1.5 mm capillary die (detailed in section 3.7.1.1) to replicate rheological measurements and validate the simulation results against the capillary determinations discussed in Chapters 4 and 5. The second was the flow domain of the 24x1.5mm

capillary die for foam extrusion technique (detailed in section 3.7.1.2). This section describes the results of such simulations obtained doing this phase of the research.

6.1.1 Material Properties

Thermal properties and flow properties of the virgin and recycled polymers as well as from some blends and nanocompounds for which simulated flow was to be studied were determined and included in the Flow 2000 database. Thermal properties determined experimentally by DSC were enthalpy of fusion and crystallisation, melting and crystallisation points. For other properties such as heat capacity at constant pressure (C_p), thermal conductivity (k) and density, literature values used.[113] The 3-parameter Carreau model was fitted to shear flow data obtained in a similar procedure described previously in section 3.3.2. The White-Metzner model[43] was used to calculate the relaxation time and determine elongational properties. These properties are summarised in Appendix V.

6.1.2 Flow in a Capillary Die

6.1.2.1 Flow Analysis

The software is able to describe flow details as illustrated by the sequence of figures. It can detect the effects of shear heating, shear rate at the capillary wall, entrance contraction flow, pressure drop across a capillary die and recirculating flow in capillary measurements. These pictures refer to a measurement of PR-HD4 at 190°C at an apparent shear rate in the capillary die of $250s^{-1}$.

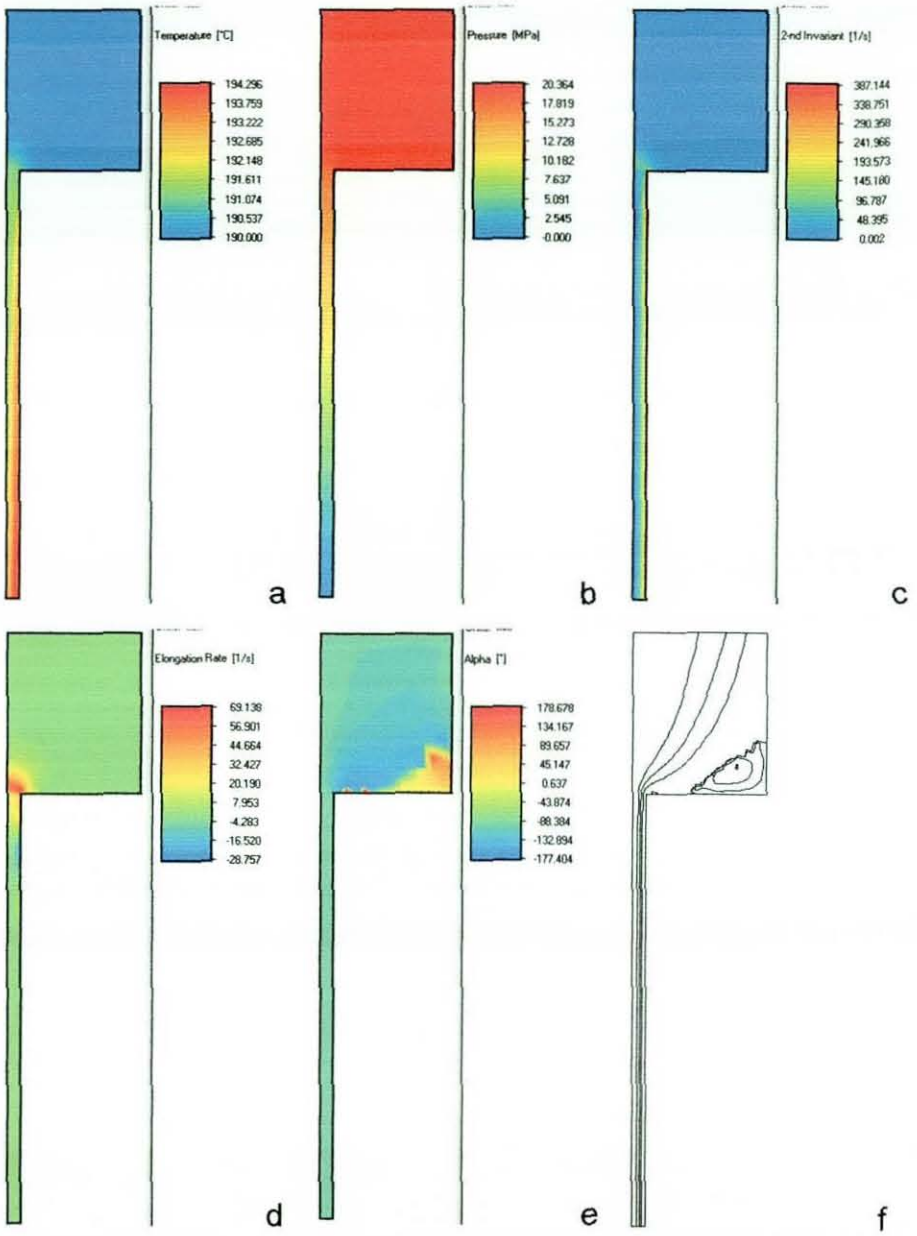

Figure 6-1- Simulated flow of PR-HD4 in a capillary die at 190°C and 250/s.

The most important flow features are represented by the model. At a certain piston speed with an abrupt contraction of the flow at the die entrance, the velocity of the fluid increases. The fluid elongates due to this contraction and in some cases this may lead to rupture. In Figure 6-1, it can also be seen negatives values of elongation rate (d), which may indicate that the fluid contracts to some extent after this sudden elongation.

The shear rate at the wall or true shear rate is going to be higher than the apparent shear rate quoted (c). With HDPE there is also an increase in temperature of the melt due to viscous dissipation (a).[45]

Recirculating flow may appear when there are dead spots (f), which is the case when a flat entry die (180° angle) is used. This is characterised by the alpha value that describes the direction of the flow. It has negative values when the flow changes direction (e). The size and shape of that recirculating flow is an important rheological consequence of molecular architecture or in the case of blends, of composition. Under similar circumstances, a branched polyethylene is likely to have a bigger vortex that can be correlated to strain hardening in extensional flow.[48]

6.1.2.2 Effect of temperature

The effect of temperature was simulated at two temperatures for PR-HD4, PR-LD3 and PR-PP1. Simulated pressure readings in the RH-7 24x1.5mm capillary die model were determined at the barrel wall from a cross-sectional cut at 17 mm above the die, which is were the pressure transducer is located in the real RH-7. The comparison of those results for PR-HD4 can be found in Figure 6-2. As can be seen from the simulated flow data the viscosity is generally under predicted. The situation is inverted at higher shear rates and is not totally unexpected as it has been seen that the fit of the 3-parameter Carreau model over predicted the viscosity in that region, a fact that was propagated to these simulations. These observations are repeated with the other materials.

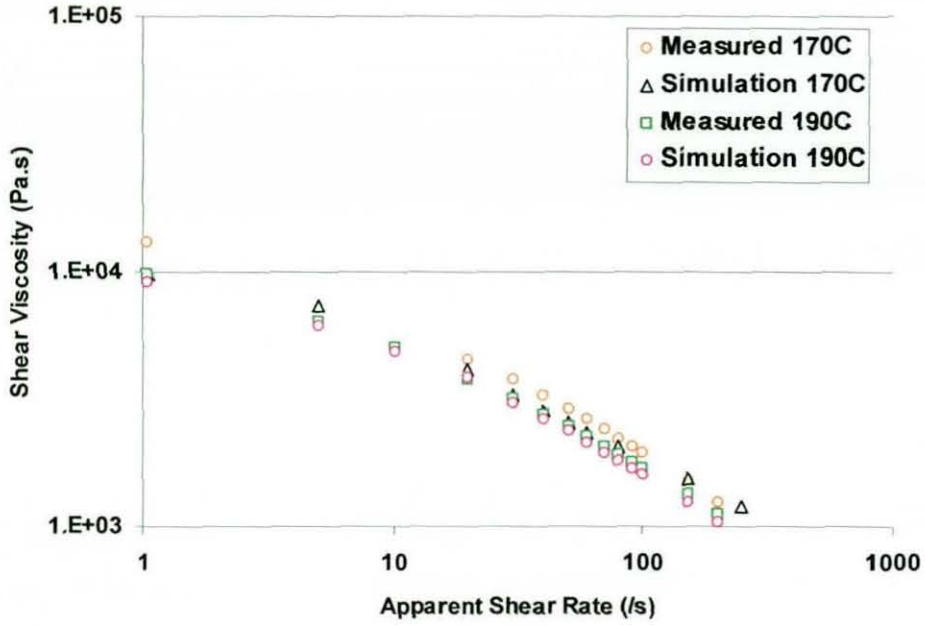

Figure 6-2 – Comparison of simulated and determined PR-HD4 shear flow data.

Despite being able to describe the flow curve behaviour reasonably well viscosity temperature dependence seems to be less obvious.

6.1.2.3 Polymer Comparison

The simulation model predicts well the trends determined by capillary rheometry, with the exception of PR-HD4 that should have a higher viscosity when compared with PR-LD3 from shear rates of $15s^{-1}$. Therefore, the polymer whose viscosity is less accurately predicted is PR-HD4.

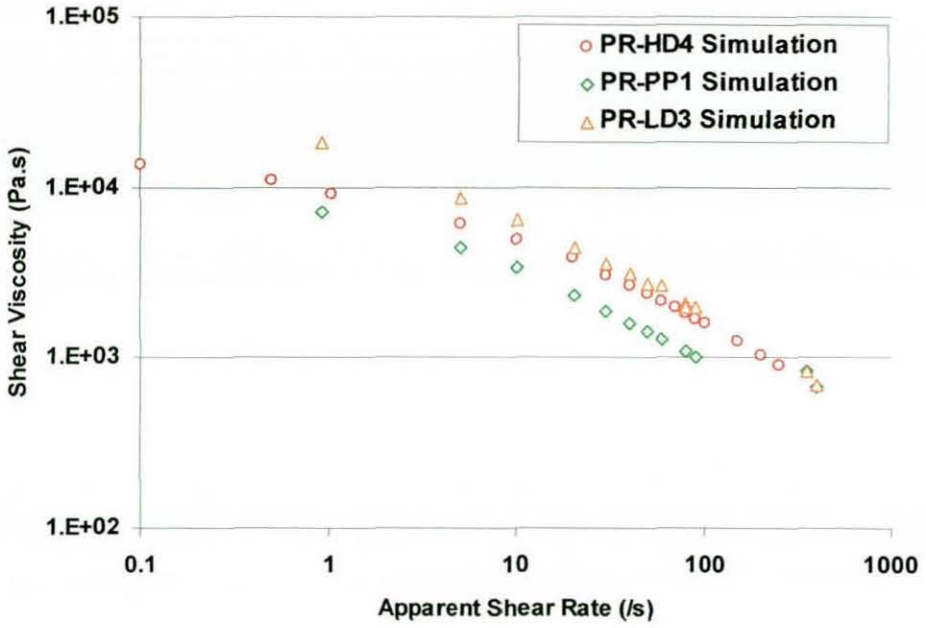

Figure 6-3 – Comparison of simulated capillary data at 190°C, comparing HDPE, LDPE and PP.

6.2 Capillary Extrusion foaming

This section discusses the development of an extrusion foaming technique with a Rosand RH-7 capillary rheometer and foaming experiments with chemical blowing agents. It presents results for those foaming experiments that aimed to study the influence of blowing agent content and foaming temperature when foaming the raw materials. Foams of some of the blends and compounds discussed in Chapter 5 were produced and an attempt is made to link their material properties to their foaming behaviour by modelling the flow domain of the rheometer in the foaming experiment.

6.2.1 Capillary Foaming Technique Development

The Rosand RH-7 has a barrel that is 315 mm long with three independent heating zones. If set correctly this allows us to load the material in the barrel knowing that after compaction some of it will be heated below the

decomposition temperature of the blowing agent but above its melting point. It was determined that 40 g of material could be loaded into the barrel whose heating zones had been set at 145°C (top) and 170°C (middle), then compacted down to 182 mm. Then it was necessary to adjust the piston speed so that the residence time inside the rheometer barrel was enough to decompose the blowing agent and foam the extrudate at a shear rate that no melt fracture is found. With these restrictions it was decided to start by loading 40 g of material and leave it non-compacted for 6 minutes for the material to soften before compacting it down to 182 mm and leave it to heat up for a further 3 minutes. At this stage all the material at reached at least 140°C. Then the piston was lowered to 100 mm displacement at 33 mm/min which takes 2.5 minutes. Since the used die was 24 mm long this means that there was a volume corresponding to 76 mm of material inside the rheometer. It was considered that 35 mm of material would produce a relevant sample. The piston speed was then set at 11.3 mm/min which is equivalent to an apparent shear rate of $50s^{-1}$ in a die with a diameter of 1.5 mm.

6.2.2 Foaming simulation studies

After having modelled the flow domain of the rheometer to include all the three heating zones it was possible to visualise the heating profile of the raw materials during the foaming experiment. This is illustrated by Figure 6-4, which represents the predicted temperature distribution when the three heating zones have been set independently to 140°C-170°C-160°C. The material starts to reach the decomposition temperature of the chemical blowing agent (150°C) at the wall first, and later at the centre of the flow. According to this, all the material reaches a temperature of 160°C before the die entrance. A close inspection reveals that the temperature inside the die is also 160°C.

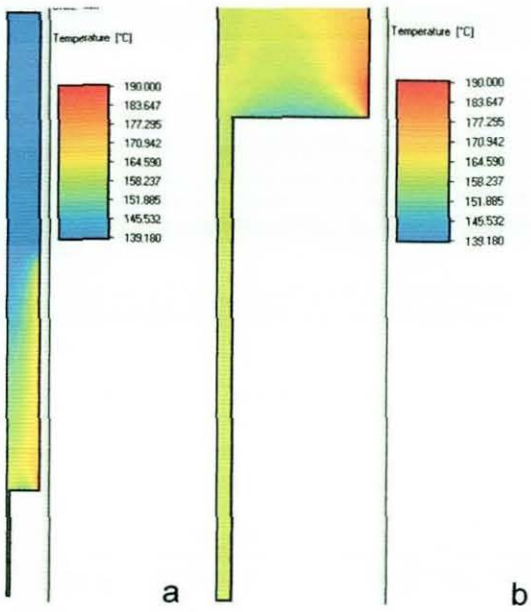

Figure 6-4 – Temperature profile of the rheometer barrel during foaming. Piston speed 33.1 mm/minute.

The effect of die temperature and piston speed was evaluated. The response variables of interest to be determined were the melt temperature, pressure, extension rate at the die entrance, and residence time in the die. This procedure was evaluated for three recycled materials: PR-HD4, PR-LD3 and PR-PP1.

Table 6.1 summarises the findings. This tells us that for all materials the predicted melt temperature was the same or almost the same as the die temperature, irrespective of piston speed. The piston speed of 33 mm/min leads to a residence time inside the die of 1 second, which is increased to 2 seconds when the piston speed is 11.3 mm/min. PR-LD3 is the material that has the highest pressure reading, therefore, the highest pressure drop rate along the die. The extension rates at the die entrance are higher for the linear polymers. We know from the characterisation of constrained elongational flow that at equivalent elongation rates the elongation viscosity is highest for PR-LD3>PR-HD4>PR-PP1 (Figure 4-29). These results do not account for any plasticisation of the melt from the gas generated by the blowing agent. The vortex size was compared for all these materials during a simulation of a foaming experiment with a die temperature at 160°C – see

Figure 6-5. It is clearly shown that the PR-LD3 has the largest vortex which indicates a higher strain-hardening behaviour.

	Die Temperature (°C)	Melt Temperature (°C)	Pressure (MPa)	Rt	Extension rate (s^{-1})
PR-HD4	147	149	10.6	2.0	11.3
	147	147	15.8	1.0	16.4
	160	161	10.0	2.0	7.1
	160	160	14.4	1.0	13.7
PR-LD3	147	149	13.4	2.0	10
	147	156	17.9	1.0	7.1
	160	161	12.0	2.0	3.5
	160	160	16.3	1.0	9.7
PR-PP3	160	161	6.1	2.0	7.0
	160	164	8.2	1.0	15

Table 6-1 – Summary of predicted material properties results.

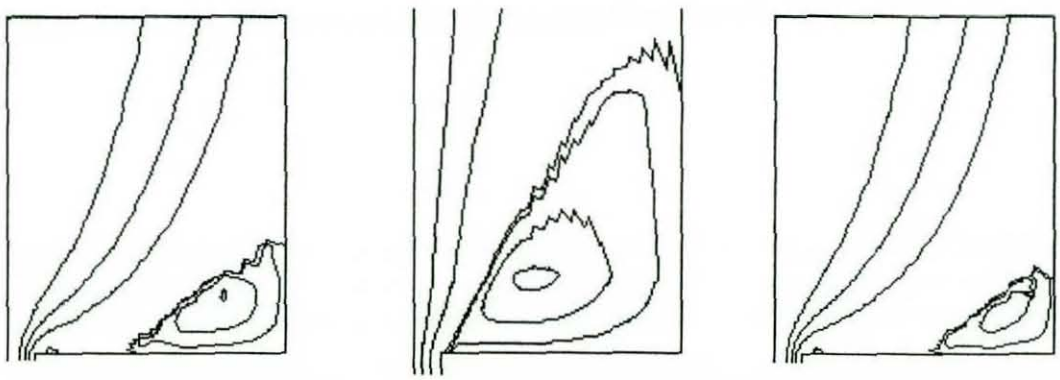

Figure 6-5 – Comparison of vortex size of PR-HD4, PR-LD3 and PR-PP1, respectively.

After the flow analysis with the Flow 2000 software, practical foaming experiments were conducted with the Rosand RH-7 to confirm the simulation results and evaluate the best foaming conditions experimentally.

6.2.3 Foaming Raw Materials

Usually the quantity of blowing agent used in extrusion foaming vary between 1-3% (w/w), it was therefore decided to investigate the influence of blowing agent content when foaming the raw materials. The temperature profile used was 145°C -170°C -147°C (die), expect for PP where the die temperature was set at 160°C. Since a capillary rheometer was used it was possible to record the pressure drop against the blowing agent content and estimate the degree of plasticisation of the melt.

6.2.3.1 Effect of Blowing Agent Content

An increased blowing agent content not only provides a higher gas content that may lead to a higher expansion, but also has the effect of plasticisation of the melt resulting in a lower melt viscosity. Results in Table 6-2 show that using 1% of blowing agent is insufficient to obtain a significant density reduction. When this is increased to 2-3% blowing agent a typical reduction of density for this type of foaming agent was observed. For some of the polymers it was possible to observe reduction in shear flow viscosity consequence of an increased plasticisation with blowing agent content.

	% Blowing Agent (w/w)		
	1	2	3
PE-HD1	600	550	520
PR-HD4	570	560	550
PR-LD3	800	470	430
PR-PP1	750	680	660

Table 6-2 – Effect of blowing agent on density (kg/m^3) of virgin and recycled polyolefins.

6.2.3.2 Effect of Extrusion Rate

The extrusion rate effect was studied for samples containing 3% of CBA. Piston speed has an influence on the extrusion rate as well as on the residence time and pressure drop rate across the die. The lowest densities were obtained by higher piston speeds for all the materials. This shows that the pressure or the pressure drop rate used influence the final density.

	Shear Rate (/s)		
	50	100	300
PE-HD1	550	500	520
PR-HD4	660	560	550
PR-LD3	800	500	430
PR-PP1	730	680	660

Table 6-3 – Effect of extrusion rate on density (kg/m^3) of virgin and recycled polyolefins.

6.2.3.3 Effect of Die Temperature

The die temperature showed a direct relationship with foam density. Lower density foams were achieved by using lower die temperatures. This is not surprising as the foaming processing window semi-crystalline polymers is defined by its crystallisation temperature. Ideally, one should foam as close to this temperature as possible so that the surface freezes, allowing the cell to grow instead of the gas diffusing out to the atmosphere.

	Die Temperature (°C)		
	147	160	170
PE-HD1	500	550	650
PR-HD4	520	560	550
PR-LD3	430	660	800
PR-PP1	-	660	700

Table 6-4 – Effect of die temperature on foam density (kg/m^3) of virgin and recycled polyolefins.

This helps to explain why there was such a big influence of die temperature on the densities achieved by PR-LD3. This polymer had a lower crystallinity than the others, and a lower crystallization temperature, which altogether amount for a higher period of time where the gas can diffuse out of the growing foam after leaving the die. Thus, the expansion ratio is smaller.

The higher molecular weight HDPE achieved the lowest density. The foaming behaviour of linear polyethylenes is very dependent on the entanglements produced by longer chains as with the degree of crystallinity that are usually associated with higher molecular grades. The higher molecular weight results in higher extensional viscosities that result in samples being able to withstand higher extensional stresses without cell rupture or collapse. If we compare the free-surface extensional measurements the melt flow behaviour of PR-HD4 and PE-HD1 are markedly different in terms of yield stress and strain energy density. The values were higher for PR-HD4, which led to believe that under similar circumstances PR-HD4 would. Therefore, since the thermal properties and crystallinity are very similar, the justification for this behaviour has to be found in the in the molecular weight distribution, elasticity of the resin or extensional stress.

Polypropylene was the polymer with the highest density which can be related to its lower strain energy density.

6.2.4 Foaming of Polymer Blends

The foaming behaviour of several recycled polyolefin blends was investigated using a die temperature of 160°C. The effects of composition with and without compatibilisers were investigated for recycled LDPE-PP and recycled HDPE-PP blends.

6.2.4.1 Blend System I : LDPE:PP

The two main effects investigated with this blend system were influence of composition and compatibilisers at optimum LDPE:PP ratio. Additionally, the effect of adding a branched PP to the system was also investigated. The densities obtained are summarised in Table 6-5.

Blend Composition		Compatibiliser % (w/w)	Mix. Temperature (°C)	Rotor Speed (rpm)	Mix. Time (min)	Density (kg/m^3)
LDPE-PP	20:80	-	190	31.8	5	720
LDPE-PP	40:60	-	190	31.8	5	690
LDPE-PP	60:40	-	190	31.8	5	700
LDPE-PP	80:20	-	190	31.8	5	610
LDPE-PP	60:40	5 EP1	190	31.8	5	680
LDPE-PP	60:40	2.5 EP1	190	31.8	5	660
LDPE-PP	60:40	5 EPR1	190	31.8	2.5	640
LDPE-PP	60:40	2.5 EPR1	190	31.8	2.5	720

Table 6-5 – Influence of blend composition on density of recycled LDPE-PP blends.

It can be seen that LDPE content influences positively the density of the foam obtained. The addition of compatibilisers at the optimum composition level shows an increase in density. In terms of extensional flow behaviour the blends containing EP1, these blends are very similar, which is reflected on their densities. The situation is distinct for blends containing EPR1. Where similar extensional flow behaviours lead to different densities.

6.2.4.2 Blend System II: HDPE:PP

In this blend system the effects of composition, process temperature and mixing time were studied. The results are summarised in Table 6-6.

Blend Composition		Mix. Temperature (°C)	Rotor Speed (rpm)	Mix. Time (min)	Density (kg/m^3)
HDPE-PP	80:20	170	150	1.5	720
HDPE-PP	20:80	170	150	1.5	640
HDPE-PP	20:80	170	150	3.5	700
HDPE-PP	80:20	190	150	1.5	660

Table 6-6 – Influence of composition on density of recycled HDPE-PP blends.

From the density results we can see that the lowest density was obtained with a recycled HDPE-PP blend rich in PP. It is known that blending increases the foamability of HDPE:PP blends when the temperature and time are appropriate. However, HDPE can lower the crystallinity of PP in the blends and this makes the matrix too soft to maintain the cellular structure, resulting in higher density foam. No difference in crystallinity was detected for the blends therefore these differences have to be explained based on the melt phase elongation behaviour of the material inside the rheometer. HDPE has a higher melt strength and extensibility than PP, but still, blend rich in HDPE didn't show a distinct decrease in density.

6.2.5 Foaming of Nanocomposites

Two types of polyolefins layered-silicate systems have been studied. One containing only HDPE and another one containing a HDPE-PP blend. The effects of mixing temperature, speed, time and clay content were investigated for the first one. For the second, only the effect of clay content was investigated. The PP containing blend was foamed at 160°C whereas the other compounds were foamed at 147°C.

6.2.5.1 HDPE Nanocomposites

It has been shown in section 5.3.1.5 that the effect of clay content in the extensional flow behaviour after adding 1% of clay is mainly that of increasing the yield stress and melt state elasticity, with the extensibility being predominantly the same for all the samples, as was the stress at break.

6.2.5.1.1 Effect of Temperature and Speed

The effect of temperature and speed was investigated on a compound system containing 5% 15 A and 5% PB1 and mixed for 6 minutes as

described in Table 6-7. It can be seen that the lowest density was determined for a compound mixed at the lowest temperature and speed. There is an evident relationship with mixing temperature and speed that favours especially lower temperatures. It is possible that during the process of incorporating the blowing agent further exfoliation occurs leading to an additional dispersion of the platelets. This would probably act as a barrier to gas diffusion during expansion. However, the same potential benefit was not observed for the other samples.

% Composition (PR-HD4/PB1/15A)	Mixing temp. (°C)	Rotor speed (RPM)	Density (kg/m^3)
PR-HD4 90/5/5	150	50	360
PR-HD4 90/5/5	150	100	400
PR-HD4 90/5/5	150	150	480
PR-HD4 90/5/5	170	50	400
PR-HD4 90/5/5	170	100	430
PR-HD4 90/5/5	170	150	500
PE-HD1 90/5/5	170	50	500
PE-HD1 90/5/5	170	100	480
PE-HD1 90/5/5	170	150	520
PR-HD4 100/0/0	170	50	520
PE-HD1 100/0/0	170	50	500

Table 6-7 – Effect of mixing temperature and speed.

The same experiment was repeated for PE-HD1 nanocomposites but the previous results were not replicated. This could be related to an unsuitable foaming temperate, probably too low makes the polymer crystallise too quickly.

6.2.5.2 HDPE:PP Nanocomposites

For these nanocomposites the only effect that has been studied was the effect of clay content on a HDPE-PP 60:40 blend containing 5%PB1.The results were then compared to the plain HDPE-PP blends.

Blend Composition		PB1 %(w/w)	Clay %(w/w)	Temperature (°C)	Rotor Speed (rpm)	Mix. Time (min.)	Density (kg/m^3)
HDPE-PP	40:60	5	0	170	150	1.5	720
HDPE-PP	40:60	5	1	170	150	1.5	680
HDPE-PP	40:60	5	2	170	150	1.5	690
HDPE-PP	40:60	5	3	170	150	1.5	710

Table 6-8 – Formulations and processing conditions of selected recycled polypropylene-recycled polyethylene nanocomposite foams.

It can be seen from these results that the results are all very similar despite there being a significant difference in terms of their extensional flow behaviour. Compared to the unfilled blends discussed previously the density is also not very different. This suggests that the foaming conditions allowed for too much gas diffusion and that the temperature of the die or melt should have been lower.

7 Conclusions

The post-consumer polymers were characterised in terms of their chemical composition, inorganic content, molecular weight distribution, thermal and flow behaviour were compared to 'virgin equivalent' materials. It was established that the recycled HDPE's were virtually free from polymeric contaminants, but some batches contained calcium carbonate and titanium dioxide particles with dimensions between 5-25μm, in compositions up to 7% (w/w). Thermal and spectroscopic analysis of the recycled LDPE's showed the presence of PP and possibly LLDPE cross-contamination. Calcium carbonate and titanium dioxide were also detected in recycled LDPE but the particle size was between 1-10μm, with concentration varying between 1-3.5% (w/w). The presence of paper fibres was also detected. The recycled PP was confirmed to be a random copolymer. GPC results confirmed the high molecular weights of all the polymers and allowed the investigation of branching content; molecular weight and weight distribution for all polymers studied. Melt flow index results ranged between 1-2 dg min^{-1} (5kg, 190°C) and were fully characterised for all materials used in the study.

Shear flow measurements revealed a typical pseudoplastic behaviour, with n-values (pseudoplasticity indices) varying between 0.39 to 0.56; with branched materials were more non-Newtonian than linear polymers. Zero shear viscosities were estimated by fitting the three-parameter Carreau model to the experimental data and were highest in the following order LDPE>HDPE>PP. The non-Newtonian behaviour was consistent with the architecture of the polymers, with branched materials being more non-Newtonian than linear polymers. Flow activation energies were also in agreement with the architecture and viscosity temperature dependence factors, being again higher for branched materials, but with PE-HD1 exhibiting energy far lower than reported elsewhere for HDPE, at 13.8 kJ mol^{-1}. Both virgin and recycled HDPE exhibited wall slip effects, with the slip velocity being higher for PR-HD4 for a given shear stress. Typical melt fracture behaviour was also detected in some of polyolefins; starting at about

$200s^{-1}$ for LDPE and $50s^{-1}$ for branched PP (PO-PP1) at 170°C and 190°C, respectively.

Extensional viscosity measurements from constrained flow capillary rheometry demonstrate the influence of molecular architecture on the extensional viscosity of polymers with LDPE being the most viscous, followed by HDPE and then by the PP. PR-LD3 exhibited an unusual yield point that is possibly due to multiphase flow. Free surface extensional measurements performed at a constant velocity of $50mms^{-1}$ at 150°C and 170°C, showed that HDPE and PP had the lowest extensibility and strain energy density and a ductile mode of failure (viscous flow dominated). LDPE exhibited the highest extensibility and strain energy density as well as a cohesive failure mechanism.

LDPE-PP and HDPE-PP recycled blends with several component ratios were prepared in a batch mixer with and without compatibilising agents, ethylene-propylene rubber (EPR) and ethylene-propylene (EP) copolymer. Processing parameters such as mixing time, temperature and rotor speed were controlled to generate different melt state morphologies and study the influence on flow behaviour of the different blend systems.

In blend system LDPE-PP, composition ratio and mixing time had a significant influence on the elongational flow properties. Extensibility and strain energy density increase with LDPE content, increasing from 1.6 and 10 kPa to 2.9 and 170 kPa, respectively, from an LDPE-PP (20:80) to a LDPE-PP (80:20) blend mixed for 5 minutes. In blends with at least 40% (w/w) PP, shorter mixing times yield higher strain energy densities but lower extensibilities. This is probably due to a morphology transition during mixing from co-continuous to a fibril/droplet type dispersion. In shear flow these blends show a lower viscosity than the combined sum of the components. It was found that a LDPE-PP 60:40 blend yielded the most suitable combination in terms of extensibility (2.5) and strain energy density (162 kPa) for further improvement studies with compatibilisers. In small quantities (2.5-5.0%), both EPR1 and EP1 improved the extensibility but the increase of strain energy density depends on mixing time. EP1 modified blends showed

a decrease in strain energy density. The use of these compatibilisers has no significant effect on the shear flow curves of the blend.
HDPE-PP blends show lower strain energy density and extension compared to LDPE-PP at any composition, and unmodified HDPE or LDPE. The analysis of a central composite design experiment used to optimise the melt strength suggests that a morphological transition occurs when mixing HDPE-PP blends rich in PP. Experimental results also show that in such PP-rich blends lower mixing times and rotor speeds produce higher strain energy density, whereas in blends rich in HDPE this can only be achieved by longer mixing times, and probably by a dispersed phase morphology. Dispersing EPR1 led to no visible improvement in extensional flow.

HDPE layered-silicate nanocomposites were prepared using modified montmorillonite organoclay and a maleic anhydride grafted polyethylene under diverse processing conditions (temperature, mixing time, rotor speed) and compositions. The intercalation/exfoliation was confirmed by the increase of the De Bragg angle (therefore and increased interlayer spacing) by XRD and by micrographs obtained by TEM. Melt flow index measurements were used to assess the degree of exfoliation/intercalation by the increase of extensional viscosity; when intercalation was successful the melt flow index was reduced. For nanocomposites preparation, the batch mixing process should be used with a nitrogen blanket or with added heat stabiliser when preparing the nanocomposites at 190°C or with rotor speeds higher than 100 rpm otherwise polyethylene thermomechanical degradation is expected, which can be confirmed by presence of hydroxyperoxide bands in FTIR samples. To prepare intercalated/exfoliated structures with minimum melt flow index it was necessary to use a mixing time of 1.5 minutes, a rotor speed of 150 rpm and temperatures of 150°C or 170°C. The melt flow index for the recycled nanocomposites prepared by using 5% compatibiliser and 1% nanoclay under these conditions is 0.62 dg min^{-1} (5kg, 190°C), reduced from 1.77 dg min^{-1}. Constant velocity free surface elongational measurements at 150°C for the HDPE layered-nanocomposites showed an increase in yield stress and maximum stress when compared to unfilled

HDPE. At higher clay loadings, 3-5% (w/w), samples exhibit a very pronounced secondary yield point. The melt state elasticity is dependent on the clay to compatibiliser ratio, being highest when it is 1:1. The strain energy density of the nanocompound with MFI of 0.62 had a strain energy density of 405 kPa and an extensibility of 2 (Hencky strain at break). Shear flow measurements reveal that the addition of clay increases the viscosity at lower shear rates but there is an increase in wall slip behaviour at higher shear rates. This is thought to be due to lack of adhesion at the die wall and strain-hardening behaviour at the die entrance. Constrained elongational flow measurement show an increase in extensional viscosity with clay loading and also when compared to the unfilled control samples.

HDPE-PP layered-silicate nanocomposites were prepared by using and 80:20 and 60:40 composition ratio, 5% maleic anhydride grafted polyethylene and 1% modified montmorillonite organoclay at 150 rpm using different temperatures and mixing times. Significant reductions in MFI were detected when both clay and compatibiliser were added but not when one was absent from the formulation. The free surface elongational measurements were sensitive to composition changes and morphology/dispersion of the nanocomposites. The processing conditions, especially temperature seem to affect the mechanism under which the nanocomposites are produced; contrary to HDPE nanocomposites (where only reduced extensibility was observed), in the HDPE-PP blends one can see an increase in elongation in some blend compositions. These were detected in both HDPE-PP 60:40 and 80:20 blends.

The simulated flow model was developed to analyse arbitrary flow conditions in a capillary die. It predicted shear flow measurements for the recycled polymer with reasonable accuracy and allowed the estimation of residence times, and visualisation of strain hardening, melting profiles and foaming temperatures.

Extrusion foaming experiments performed with the capillary rheometer showed that the polymers exhibit sensitivity to the die temperature, chemical

blowing agent content and residence time in the capillary die. The use of 3% CBA (w/w) was the composition that yielded the highest density reduction for all the polymers. The densities ranged 430-660 kg m^{-3}, with the lowest being achieved by PR-LD3 and the highest by PR-PP1. This is consistent with expectation, as the polypropylene had the lowest extensional viscosity and extensibility and the recycled LDPE had the highest. It was found that by reducing the residence time inside the die the densities obtained were lower for all the polymers. By matching the temperature of the die as close as possible to the crystallisation temperature of the polymer the lowest densities were achieved. This is due to the fact that by being able to crystallise the surface of the extrudate faster, the gas diffusion rate out during foaming is slowed down and more gas is available for melt expansion, and this can explain why HDPE-PP or LDPE-PP blends with improved extensional flow behaviour obtained similar results in comparison to unmodified recycled PP. HDPE nanocomposites showed a significant density reduction when compared to their unfilled counterparts because of a reduction in gas diffusion during foaming and increase in extensional viscosity. HDPE-PP nanocomposite foams didn't show a reduction in density compared to their unfilled equivalents, again, despite improved extensional flow behaviour.

8 Future Work

The influence of processing conditions on the morphology of the blends studied throughout this research and its effect on flow properties has been evident. Although, the importance of the morphology of polyolefin blends on the mechanical properties has been recognised and studied, parallel work in terms of extensional flow properties is a largely unexplored subject. Not many studies can be found relating extensional melt flow behaviour of immiscible polymer blends, and the biggest drive has been focussed on commercial LDPE/LLDPE blends. The morphology developed in extrusion can probably be fine tuned by extensional deformation of the shaping operations as in foaming of film blowing either for mechanical performance or

processing efficiency. But during foaming, how will the melt-state morphology and cellular structure of the foam correlate? The effects should be more significant in foams with a fine high-cell density and low density with little cell growth. Constant velocity melt-state uniaxial elongational measurements provide some information regarding the deformation mechanisms and some tensile properties, but in order to improve the understating in terms of flow behaviour, one should also measure true rheological properties under either constant stress or constant strain rate. This information is vital for a first approximation and further development of nucleation and foam growth theories in multiphase gas-charged systems.

HDPE nanocomposites showed improved foaming performance but the influence of their morphology on cell size or number of cells was not investigated during this research. Mechanical properties of these types of foams are also limited. Also, it would be quite interesting to investigate how much the heat distortion temperature or the fire performance increased and how do they compare with non-foamed nanocomposites. In order to achieve low density foams with superior mechanical properties in the order of 30kgm^{-3} or less irradiation crosslinking by electron beam or gamma can be used for subsequent expansion in a batch foaming process, it is likely that the fire performance and heat stability may be enhanced by the crosslinking but doubts remain whether the nanocomposite sites would act as catalysts for degradative processes at higher temperatures and outweigh this benefit. The PP-HDPE nanocomposites showed the most interesting behaviour because of their different extensional behaviour when prepared under similar processing conditions. Further work is required to elucidate if there are different mechanisms involved during intercalation/exfoliation. Finally, recycled foam systems could be incorporated as cores in sandwich panels and the properties tested against panel containing cores made from virgin plastic.

Extensional Flow, Rupture and Foaming of Nanocomposites Containing Recycled HDPE

L.M.C. Conceicao (a) and B. Haworth

PPS – 21 - Leipzig, Germany, June 19-23, 2005

Extensional Flow, Rupture and Foaming of Nanocomposites Containing Recycled HDPE

L.M.C. Conceicao (a) and B. Haworth (a)*

(a) Institute of Polymer Technology and Materials Engineering (IPTME), Loughborough University, Loughborough, LE11 3TU, United Kingdom

Abstract

Research has been carried out to measure the shear and extensional flow characteristics of various compounds based upon post-consumer, recycled HDPE, including nanoclay / recycled HDPE composites in order to predict foaming behaviour in extrusion processes. Montmorillonite-based composites were prepared by melt-state mixing and the influence of temperature, compatibiliser and degree of mixing was investigated in terms of intercalation and flow behaviour. Shear flow characteristics show conventional pseudoplastic behaviour and temperature sensitivity; 3-parameter Carreau model constants have been obtained, in order to model extrusion behaviour in predictive mode. There is a tendency to observe wall slip in HDPE recyclate at a critical shear stress level and slip velocity has been related to shear stress, using a power law model. Constrained extensional deformations within fixed flow boundaries do not clearly discriminate the influence of nanoclay addition to HDPE. However, free surface measurement of extensional deformation and rupture are presented, so that the influence of recycled polymer and nanoclay content are fully characterised. To complement the rheological data, practical foam extrusion processing (using chemical blowing agents) of both recycled polymer and HDPE nanocomposites has also been investigated and attempts have been made to correlate the rheological data with practical foaming response.

* To whom correspondence should be addressed: (B.Haworth@lboro.ac.uk)

1. Introduction and objectives

Greater volumes of plastics are being consumed and recycled every year with waste streams continuously changing as improvements are incorporated in their production. Municipal post-consumer waste in the UK includes a large proportion of high-density polyethylene (HDPE) derived from extrusion blow moulded milk and detergent bottles but due to property modification, investigations are ongoing to upgrade those properties and search for new applications. One potential route for exploitation is to prepare polymer-layered silicate nanocomposites for use in recyclate; previous studies have demonstrated improvements in mechanical performance, barrier properties, flame retardancy and thermal stability [1,2,3,4]. Montmorillonite is among the most common types of clay used for the preparation of nanocomposites due to its high specific surface area and aspect ratio, and when properly dispersed in the polymer matrix a more effective reinforcement may be obtained with lower loadings, relative to conventional inorganic modifiers. However, belonging to the layered silicate family it is hydrophilic in nature making it difficult to disperse in apolar polymeric matrices. These modifiers therefore they need to be treated by an appropriate surfactant such as alkyl ammonium cations to lower the surface energy of the clay and to improve wetting characteristics with the polymer matrix.

Nanocomposites can be prepared by several routes which have been reviewed by Alexandre and Dubois [5], but the most convenient method for recycled polymers is melt intercalation which was first proposed by Vaia et al.[6]. Depending on the type of dispersion obtained, two nanocomposite structures have been identified: intercalated and exfoliated. In an intercalated structure polymer chains or other mobile species are able to migrate between the silicate layers, whereas if exfoliated, these layers are completely and uniformly dispersed within the polymer matrix. If suitable thermodynamic and rheological conditions are met the polymer chains diffuse into the clay galleries, increasing inter-layer spacing and provided there is sufficient mechanical energy, delamination occurs in the inorganic phase. The influence of processing conditions on the preparation of polyolefinic clay nanocomposites by melt intercalation has been subject to many studies [7-10]. However there are still contradictory suggestions regarding the optimum mixing process conditions required for their preparation. Many of those reports emphasize the influence of shear flow properties with very few extending the research to extensional flow behaviour and melt rupture [11]. Similarly, relatively few publications have reported details on the foam processing of nanocomposites [12,13], which would be expected to be significantly modified if the extensional deformation characteristics exhibit sensitivity to the amount and degree of dispersion of the nanoclay particles.

In the present study the influence of processing conditions on virgin and recycled high-density polyethylene (HDPE) nanoclay composites is assessed in terms of shear flow, constrained-boundary and free surface extensional flow behaviour, in an attempt to correlate deformation properties to the influence of recycled polymer in extruded foam applications.

2. Experimental

2.1 Materials

The polyethylene materials investigated in this study were a virgin high-density polyethylene (HDPE) denominated PE1 (Eltex 6007X, supplied by BP Amoco) and a recycled HDPE (from Centriforce Ltd., UK) denominated PE2 with melt flow indexes (MFI) of 1.2 and 1.7 dg min^{-1} (5kg, 190°C), respectively. Polybond 3009 (supplied by Crompton Chemicals, PE-MAH) with a MFI of 14 dg min^{-1} (5kg, 190°C) and functionality level of 1% was also included in the study. The organically modified clay was Cloisite 15A (Southern Clay, USA), a montmorillonite clay modified by ditallow-dimethylammonium salts. The chemical blowing agent used was Hydrocerol BM70 (Clariant, UK).

2.2 Preparation of nanocomposites

The various polyethylene-organoclay compositions were prepared in compositions on a mass basis using a Haake Rheomix 600 according to the conditions detailed in Table 1 with the total amount of material being set at 40g and a constant mixing time of 6 minutes was used in all cases.

Sample No	% Composition (PE/PE-MAH/Clay)	Mixing temp. (°C)	Rotor Speed (RPM)
1	PE2 90/5/5	150	50
2	PE2 90/5/5	150	100
3	PE2 90/5/5	150	150
4	PE2 90/5/5	170	50
5	PE2 90/5/5	170	100
6	PE2 90/5/5	170	150
7	PE2 94/5/1	150	50
8	PE2 94/5/1	150	100
9	PE2 94/5/1	150	150
10	PE2 94/5/1	170	50
11	PE2 94/5/1	170	100
12	PE2 94/5/1	170	150
13	PE2 95/5/0	150	50
14	PE2 95/5/0	150	100
15	PE2 95/5/0	150	150
16	PE2 95/5/0	170	50
17	PE2 95/5/0	170	100
18	PE2 95/5/0	170	150
19	PE1 90/5/5	170	50
20	PE1 90/5/5	170	100
21	PE1 90/5/5	170	150

Table 1 – Experimental conditions for preparing PE/clay nanocomposites.

2.3 Materials characterisation

X-ray diffraction was used to assess the intercalation or exfoliation characteristics of the polyethylene nanocomposites. Shear flow behaviour of nanocomposites and supplied materials was investigated by means of a capillary rheometer and a melt flow indexer whereas elongational properties were determined by both free surface and constrained flow measurements by an elongational rheometer developed at Loughborough [14] and a commercial capillary rheometer, using an orifice die [15]. Details of the techniques are described below.

- **X-ray diffraction**

The HDPE nanocomposite samples were analysed by a Bruker D8 X-ray diffractometer (40kV, 40mA) with a Cu X-ray tube, between Bragg angles 1-10° with a scanning step of 0.02°.

- **Capillary Rheometry**

Shear and extensional constrained flow properties were determined at 170°C and 190°C with a twin-bore Rosand RH-7 capillary rheometer using a 24x1.5mm and 0x1.5mm dies with a L/D=16. Wall slip measurements were performed using a set of five capillary dies with L/D=16 and die diameters in the range 1.5-0.5 mm. MFI data were determined using a Tinnius Olsen melt flow indexer at 190°C and a 5kg weight according to BS 2782-7.

- **Free Surface Elongational Deformation**

A Rutherford Elongational Rheometer (RER), derived from an earlier design from Munstedt [16] and which is described in detail elsewhere [14] has been used to develop free-surface deformation data on the HDPE nanocomposites. The equipment uses double waisted O-ring samples (1.5mm thickness and gauge length 16mm) that were die-cut from compression-moulded plaques produced using the following conditions: preheat time, 3 minutes; moulding time, 7 minutes; temperature 170°C; moulding pressure 10 bar ; cooling time, 45 minutes. The instrument was operated in constant velocity mode at 150°C, using a crosshead speed of 0.050 ms^{-1} to simulate strain rates in the order of $1s^{-1}$ (conditions quite common in foaming processes), and to be able to distinguish tensile stress-strain behaviour between the compositions.

2.4 Foam Extrusion

Some selected materials were compounded in a Haake Rheomix 600 at 143°C for 3 minutes at 30RPM with 3% (w/w) of Hydrocerol BM70, granulated and foam extruded through a Rosand RH-7 capillary rheometer. A temperature profile was set along the barrel and die (145°C-170°C-145°C), the sample was loaded into the barrel, preheated for 6 minutes, compressed, heated for another 3 minutes and extruded through a (24 x 1.5) mm capillary die at a shear rate of 100 s^{-1} . Subsequently the morphology of the foams was analysed by optical microscopy and the density determined by measuring the nominal volume and overall weight of the samples.

3. Results and Discussion

3.1 HDPE - raw material and rheological characterisation

Prior to a rheological analysis it was verified by FTIR that the recycled HDPE was not contaminated by chain-branched polyolefins which was later confirmed by DSC. An equivalent grade to that of the recycled HDPE was chosen accordingly to match its MFI, and subsequently both materials were tested by capillary rheometry. The shear flow behaviour of these materials is typically pseudoplastic, with decreasing shear viscosity as the apparent shear rate increases (*Figure 1).* The shear flow curves are similar in shape and magnitude as might be anticipated due to the small differences in melt flow index. Carreau 3-parameter model constants have been obtained from shear flow curves at 190°C, in order to model extrusion behaviour in predictive mode; the predicted model coefficients can be found in *Table 2*, and confirm a lower index of pseudoplasticity from PE1, together with and a higher zero shear viscosity.

	$ç_0$ (Pa.s)	T1 (s)	n
PE1	11967	0.73	0.46
PE2	8602	0.62	0.55

Table 2 – Parameters for the 3-parameter Carreau model at 190°C.

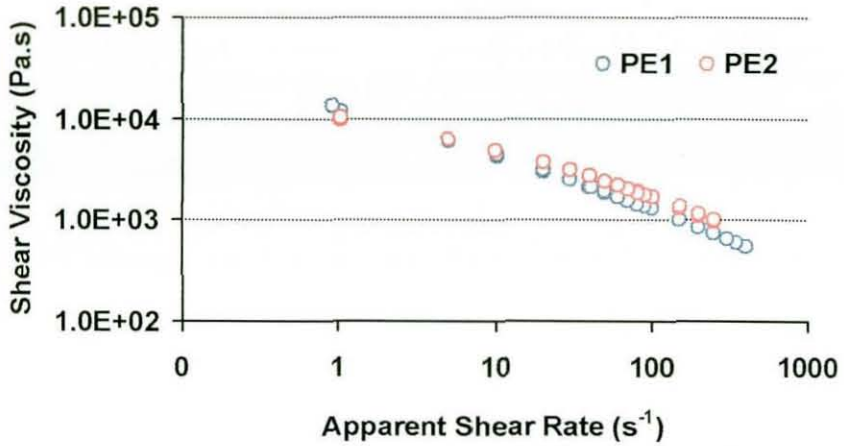

Figure 1 – Shear flow curves of PE1 and PE2 at 190°C.

The extensional flow curve (*Figure 2)* obtained by the Cogswell method reveals an extension thinning behaviour and overall, is more discriminating between the samples. The virgin PE sample has a higher extensional viscosity (in agreement with melt flow index data) across the strain rate range, in contrast to the shear flow comparisons (*Figure 1)* which are more complex and suggest that the virgin PE sample is more shear sensitive.

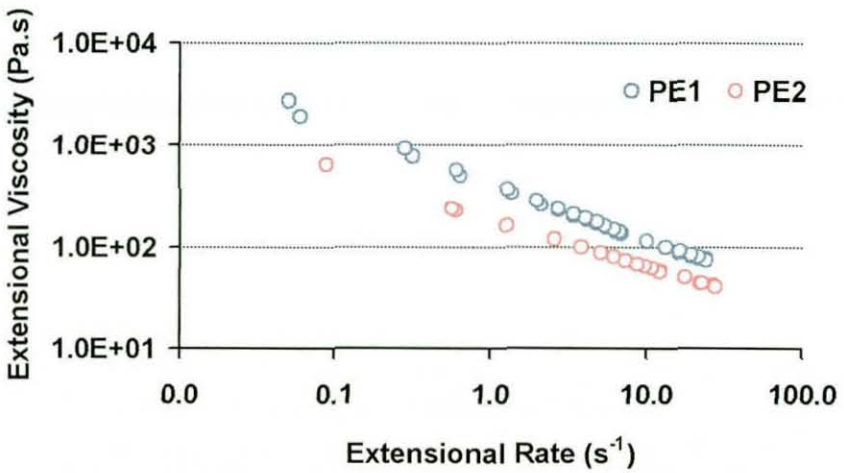

Figure 2 – Extensional flow behaviour of PE1 and PE2 obtained with the Cogswell method.

During the rheological analysis it was observed that above certain shear rates the pressure would oscillate between two extreme values, which is a phenomenon widely reported [17,18] as a flow instability. In the case of linear polyethylenes including HDPE, this flow instability lies between two stable deformation regimes in a shear stress vs. shear rate plot. There is still disagreement on the origin of this behaviour though the majority of authors suggest an alternating stick / slip conditions at the die wall due to the onset of wall slip at the flow boundary. A shear stress vs. apparent shear rate plot for recycled HDPE obtained at 170°C (using different die diameters and a constant L/D ratio of 16, *Figure 3*) shows that the recycled HDPE shows a flow instability around a shear rate of 400 s^{-1} (corresponding to a critical shear stress that may be evaluated using the Mooney technique), so that this procedure [19] was subsequently used to determine the slip velocities beyond this critical condition (*Figure 4*).

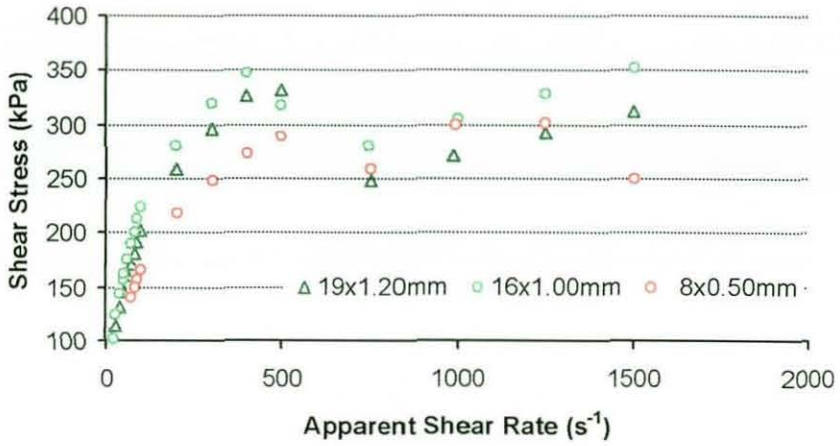

Figure 3 – Flow curves of recycled HDPE at 170°C obtained with capillary dies of different diameters with constant L/D=16.

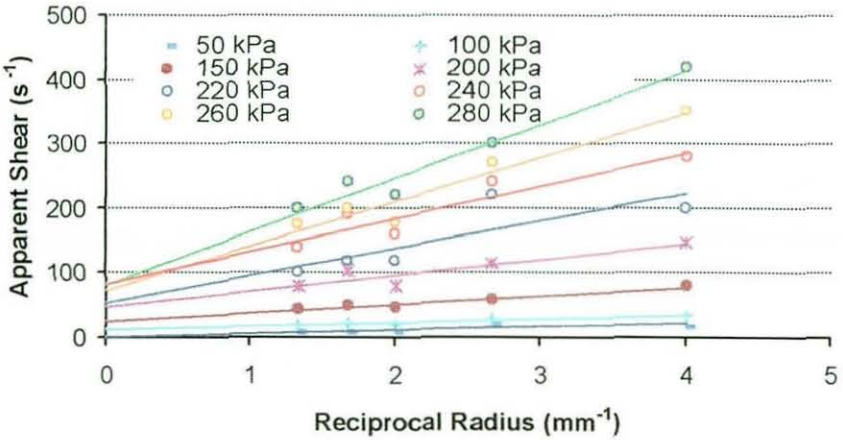

Figure 4 – Determination of slip velocity in recycled HDPE using capillary steel dies with a L/D=16.

Figure 4 shows a clear trend with respect to the die geometry sensitivity of the shear flow data generated from these experiments. In cases where a finite gradient can be detected, the presence of melt instability at the die wall can be confirmed; the gradient is measured and converted to calculated wall slip velocity data. From *Figure 4*, it is observed that there is a clear trend between the wall slip velocity and the shear stress at which measurements were taken. It has been established that the wall slip velocity (v_s) can be related to the wall shear stress (τ_w) by a power law:

$$V_s = A.\tau_w^{\ m}$$

This analysis has been used to plot the relationship between these variables, in *Figure 5* (below). The linearity of this plot verifies the use of the power law approach to wall slippage effects in recycled HDPE; evaluated constants are:

$$A = 2.1\ (MPa)^{-m}.ms^{-1} \text{ and } m = 2.60$$

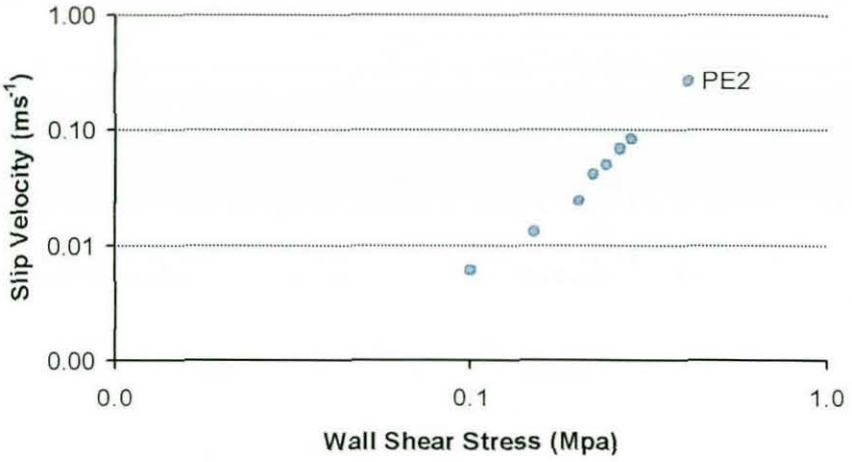

Figure 5 – Slip Velocities of PE2 at 170°C.

To complete the rheological characterisation of the unmodified HDPE materials, free surface elongational deformation was carried out in constant velocity mode. These data can be quite discriminating between small differences in extensional viscosity, or generalised deformation behaviour, when compared to a constrained extensional flow method such as the Cogswell approach. It has the advantage of being directly controllable and free from complexities due to mixed-mode flows when deforming the sample. In HDPE samples, molecular contributions to the extensional viscosity arises mainly from chain length, with longer chains providing more entanglement points than shorter ones, thus higher molecular weight samples exhibit increased deformation resistance and hence increased viscosity in melt-state analysis. A comparison between the extensional flow behaviour of virgin and recycled HDPE obtained by this technique has been plotted in *Figure 6* Under uniaxial extensional the qualitative behaviour is quite similar for both HDPE materials. Differences observed probably relate to sample PE2 having a narrower molecular weight distribution than PE1, a result still subject to confirmation. Extensional melt rupture data can also be determined from this type of analysis and critical conditions at which rupture occurs can be determined. It can be seen that the samples exhibit ductile-mode extensional melt rupture behaviour, with the recycled grade PE2 showing a rupture onset point at a slightly higher Hencky strain, but at a lower stress value, 2.2 and 5kPa, respectively.

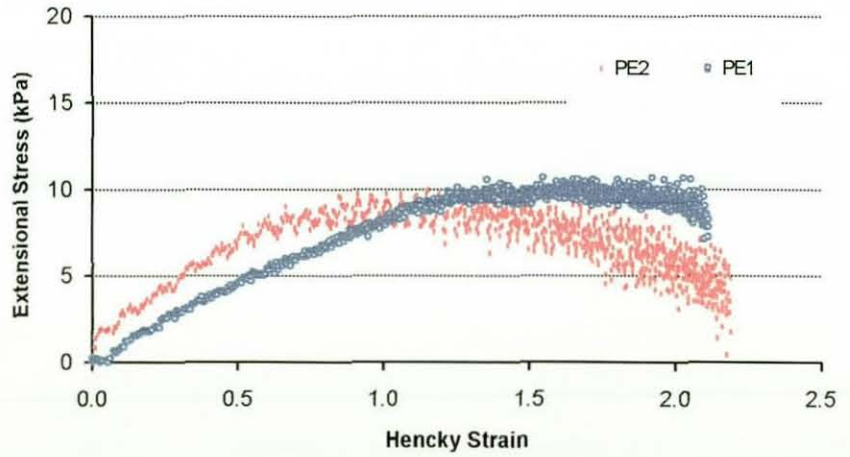

Figure 6 – Extensional flow curve of PE1 and PE2 at 150°C and 50mms^{-1}.

Experimental techniques used have been sufficiently sensitive to determine some differences in both shear and extensional deformation behaviour between virgin and post-consumer recycled grades of HDPE polymer. Since the majority of the recycled feedstock was re-processed from extrusion blow moulded containers (also the application area for the near-equivalent virgin material), it is perhaps not too surprising that the overall deformation and viscous behaviour of each of these polymers is qualitatively similar. More in-depth characterisation of molecular structure is required, before more exact conclusions can be drawn.

3.2 Nanocomposite Characterisation

In the preparation of nanocomposites by melt intercalation using compatibilisers, especially in the case where recycled polymers are involved, it is important firstly to investigate the possible modifying effect of the compatibiliser. In this study, and since the modified organoclay is not compatible with the polyethylene matrix, a maleated high-density polyethylene was used promote the desired intercalation of the clay galleries by the non-polar HDPE polymer chains.

Under equivalent conditions to those used for the production of nanocomposites (as described in *Table 1*), the recycled high-density polyethylene and compatibiliser were initially melt mixed and subsequently analysed for shear and extensional deformation behaviour. As can be seen in *Table 3*, a blend of PE2 and 5% PE-MAH shows both shear and temperature sensitive behaviour. Notably the incorporation of PE-MAH produces an increase in viscosity. As the melt flow indices of the materials involved are 1.8 dg min^{-1} for PE2 and 13 dg min^{-1} for the compatibiliser under the same testing conditions, it can be seen that increasing speed and temperature raise the low-shear flow response of the blends. This behaviour, particularly the melt flow indices obtained following mixing at high rotor speed, suggests the existence of a degradation mechanism in either the recycled polymer or the compatibiliser. Time and shear dependent rheology of maleated polyethylene clay hybrids has been reported by some authors [20,21] which suggest that dipole-dipole and/or hydrogen bonding interactions between the pendant functional groups within maleated high-density polyethylene establish a physical network. This observation is currently under investigation.

	Temperature (°C)	Speed (RPM)	5%15A	1% 15A	0% 15A
PE2 + 5% PE-MAH	150	50	1.05	1.27	1.38
		100	1.13	1.09	1.48
		150	1.30	1.84	2.22
	170	50	1.17	1.32	1.57
		100	1.24	1.51	1.78
		150	1.77	1.61	2.98
PE1 +5% PE-MAH	170	50	0.94	1.22	-
		100	1.09	1.24	1.41
		150	1.49	1.52	-
PE1 +0% PE-MAH	170	50	1.25	1.27	-
		100	1.34	1.32	1.18
		150	1.35	1.36	-

Table 3 – Melt flow indices (in dg min^{-1}) for HDPE nanocomposites and blends. (Clay particles and content are designated "15A")

The effect of addition of clay without compatibiliser was also investigated in a smaller number of samples and is also summarised in *Table 3*; since PE1 has a melt flow index of 1.2 dg min^{-1}, no significant change in flow behaviour under arbitrary, low shear conditions was observed.

The level of intercalation of nanocomposites was confirmed by X-Ray diffraction and results are shown in *Figure 7*, corresponding to PE1 nanocomposites containing 5% PE-MAH and 1% Clay at different processing temperatures, using a rotor speed of 100RPM. A reference sample PE1 containing only 1% clay shows two peaks that are reduced after the addition of PE-MAH accompanied with a distinctive shift to lower angles, confirming that the quantity of non-intercalated organo-clay was significantly reduced and that intercalation of the prepared samples increased when mixing at lower temperatures.

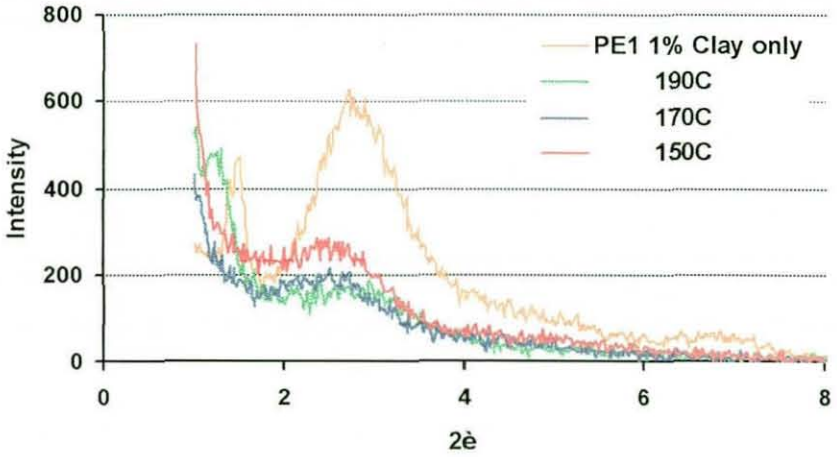

Figure 7 – Effect of processing temperatures on the exfoliation on nanocomposites prepared from PE1 at a screw speed of 100RPM and comparison with PE1+1% clay only.

The melt flow index values of PE1 nanocomposites can be found in *Table 3* and it interesting to note that the viscosity of the recycled polymer composite is not significantly reduced by further addition of clay whereas by changing the amount of clay present in the virgin matrix the effect is more substantial. Following the trend of the PE:PE-MAH blends the PE2 nanocomposites exhibit a shear and temperature dependent rheology.

In terms of shear flow the composites were also characterized by capillary rheometry and their behaviour was broadly in line with the MFI results, as shown in *Figure 8*. The effect of the nanoclay is relatively small, within the high shear region, but would be expected to become more significant under conditions involving relatively low shear processes. The Cogswell method for the estimation of extensional flow behaviour (*Figure 9*) shows more significant differences between the prepared samples (up to 100RPM for each temperature), with samples containing up to 5% clay exhibiting an increased extensional viscosity notably in the low strain rate region of experimentation.

Figures 8 and 9 present the typical influence of clay addition at a certain mixing speed and do not discriminate the curves clearly, the sample with 1% clay being the one exhibiting higher extensional viscosity over a specific extension range. Compared to the Cogswell method, uniaxial, free-surface melt extension can be more discriminating, is often more informative in terms of rupture behaviour and assists in terms of correlating types of reinforcement with the preparation methods. In addition, extensional rupture behaviour from melt uniaxial extension provides different information, including characteristics relating to melt state elasticity, extensibility and deformational strain energy.

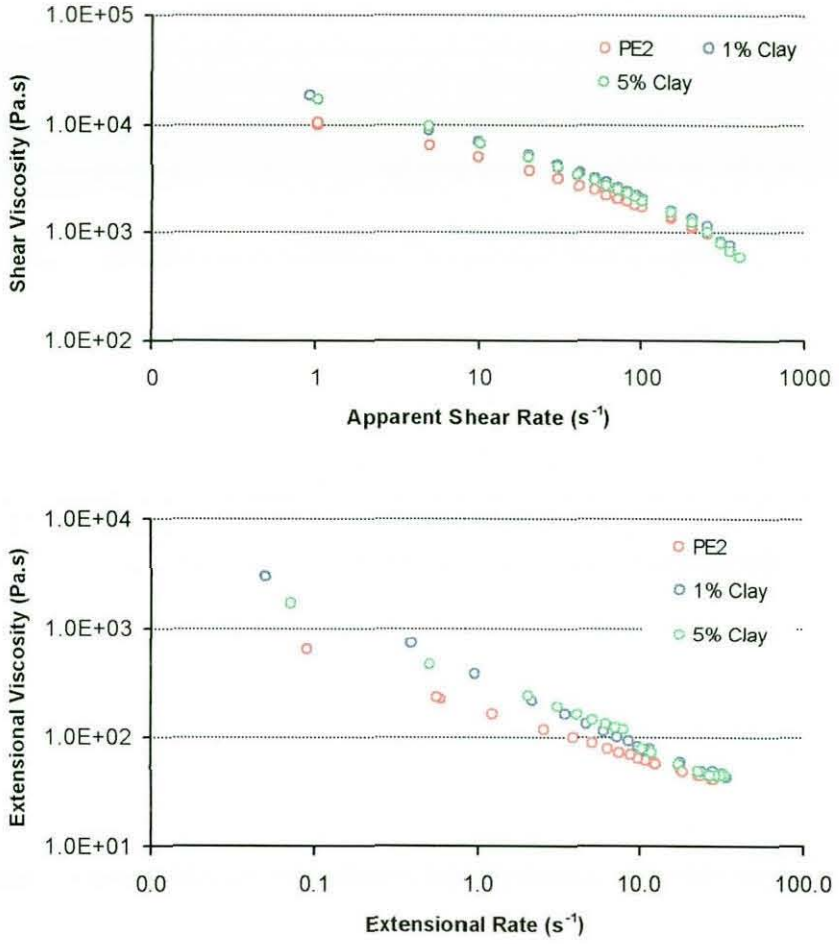

Figures 8 and 9 – Influence of clay addition to PE2 + 5% compatibiliser (mixed at 100 RPM and 150°C) on shear and extensional flow behaviour at 170°C in a the RH-7 capillary rheometer.

The addition of 5% PE-MAH to PE2, as seen in *Figure 10* promotes increased extensibility of the samples, and raises the yield stress, which results in a higher strain energy density; also in the case of the nanocomposites, the addition of 1% clay doesn't change the ductile response to load but increasing clay concentration to 5% leads to reduced extensibility, a significantly higher yield stress and a qualitatively different mode of melt rupture.

The influence of processing speed is represented in *Figure 11* where it can be seen that for the same clay loading for samples processed up to 100RPM show very similar curves with increased yield stress and lower extensibility when compared to PE2 or PE2:PE-MAH blend. When processed at higher shear rate the sample has a much lower yield stress but higher extensibility than the other composites. The loss of extensibility and ductility can be interpreted as a greater interaction and dispersion of the clay within the polymeric matrix. The difference in their preparation arises from shear stress generated at the mixing stage but also, some differences in mechanical (shear) heating profiles were also observed (2°C/min, 4.5°C/min and 6°C/min respectively, for 50RPM, 100RPM and 150RPM). Several process variables contribute to the rate and extent of diffusion of the polymer chains into the clay galleries, including localised shear stress and temperature variation, each of which will contribute to the viscosity of the molecular species penetrating the clay galleries.

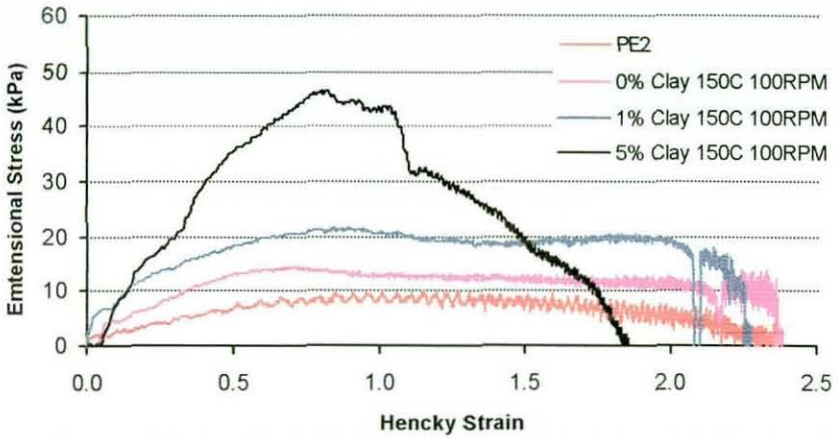

Figure 10 - Influence of clay addition to PE2 + 5%PE-MAH processed at 100 RPM and 150°C on extensional flow behaviour.

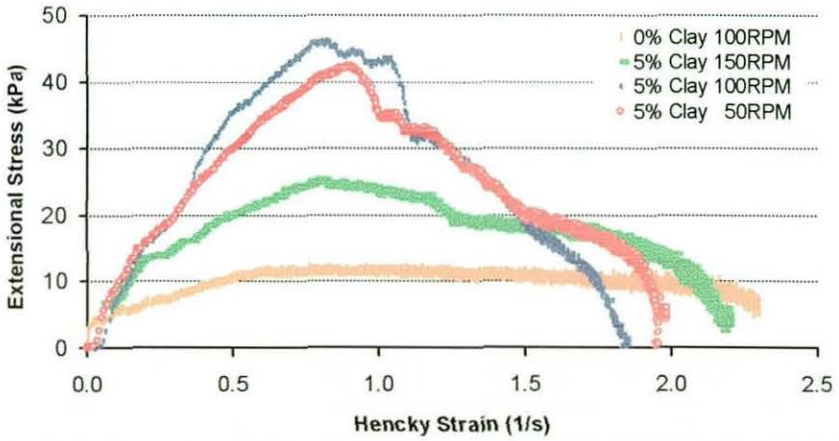

Figure 11 - Influence of processing conditions on the extensional flow of PE2 +5% PE-MAH nanocomposites mixed at 150°C.

When gas bubbles emerge from solution and bubble growth occurs in the melt state, a polymeric matrix needs to possess a certain degree of elasticity but it is also required to avoid rupture, so that therefore a combination of optimum deformation resistance, extensibility and strain energy absorption is desirable. A compilation of such results is presented in *Table 4* and indicate that after six minutes of mixing the highest strain energies are usually obtained at a mixing rotor speed of 100RPM. The recycled polymer organoclay hybrid prepared at 170°C containing 5% clay would appear to offer the optimum response for foaming. The recycled and virgin polyethylene nanocomposites seem to have similar properties, despite the differences in behaviour observed between the respective unmodified polymers.

No	Composition (PE/PE-MAH/Clay)	Mixing Temp. (°C)	Rotor Speed (RPM)	Extensibility (max $\dot{a}_H$)	Strain Energy Density (kPa)	MFI (g/10min; 5kg)
1	PE2 90/5/5	150	50	1.9	33	1.1
2	PE2 90/5/5	150	100	1.8	36	1.1
3	PE2 90/5/5	150	150	2.2	30	1.2
4	PE2 90/5/5	170	50	2.3	35	1.2
5	PE2 90/5/5	170	100	2.2	54	1.2
6	PE2 90/5/5	170	150	2.0	25	1.8
7	PE2 94/5/1	150	50	2.2	14	1.3
8	PE2 94/5/1	150	100	2.3	33	1.1
9	PE2 94/5/1	150	150	2.2	15	1.8
10	PE2 94/5/1	170	50	2.3	26	1.3
11	PE2 94/5/1	170	100	2.3	29	1.2
12	PE2 94/5/1	170	150	2.6	24	1.6
19	PE1 90/5/5	170	50	1.9	40	0.9
20	PE1 90/5/5	170	100	2.1	36	1.1
21	PE1 90/5/5	170	150	2.2	27	1.5

Table 4 –Shear and extensional flow properties of polyethylene nanocomposites.

3.3 Foaming of nanocomposites

In the majority of cases, the foamed nanocomposites exhibited a lower density and a more uniform and well-defined cellular structure than the main polymeric material alone. However the samples for which the highest strain energy data were obtained did not show the lowest densities but rather the samples processed at lower rotor speeds. This observation is true *(Table 5)* for samples produced at both mixing temperatures and for either grade of HDPE. Further work is required to fully characterise the microstructure of the foamed specimens, to understand the origin of this observation.

Composition (%) (PE/PE-MAH/Clay)	Mixing temp. (°C)	Rotor Speed (RPM)	Density (g cm^{-3})
PE2 90/5/5	150	50	0.36
PE2 90/5/5	150	100	0.40
PE2 90/5/5	150	150	0.48
PE2 90/5/5	170	50	0.40
PE2 90/5/5	170	100	0.43
PE2 90/5/5	170	150	0.50
PE1 90/5/5	170	50	0.50
PE1 90/5/5	170	100	0.48
PE1 90/5/5	170	150	0.52
PE2 100/0/0	-	-	0.53

Table 5 – Processing conditions and densities of the foamed samples.

4. Conclusions

1. Shear flow and extensional deformation of virgin and post-consumer recycled grades of HDPE are qualitatively similar, based upon practical data from capillary flow and free-surface measurements. Parameters for the 3-parameter Carreau model at 190°C have been evaluated for these materials and the differences observed are attributed to different molecular weight distributions.

2. Wall slippage effects were observed in post-consumer recyclate and slip velocity has been related to wall shear stress using a power law model.

3. The effect of processing conditions on the preparation of nanocomposites was analysed and it was observed that polyethylene / maleated polyethylene blends show a shear and temperature dependent behaviour (which was also found in the HDPE-clay nanocomposites prepared from virgin and recycled high-density polyethylenes), with both recycled and virgin nanocomposites exhibiting similar properties.

4. Free surface elongational measurements of the nanocomposites have been obtained and may be used to characterise deformation behaviour and thereby to assist in the prediction of foaming behaviour in extruded polymer melts.

5. The lowest free-foam densities were achieved in HDPE nanocomposites (5% clay) mixed at the lowest rotor speeds, for all mixing temperatures and for both grades of HDPE investigated.

5. References

1. Y. Kojima, A. Usuki, M. Kawasumi, A. Okada, T. Kurauchi, and O. Kamigaito, J.; *Synthesis of nylon-6-clay hybrid by montmorillonite intercalated with epsilon-caprolactam*, Polym Sci. Part A: Polym. Chem., 31, pp.983-6 (1993)
2. T. Lan, P. D. Kaviratna, T.J. Pinnavaia; *Nature of polyimide-clay hybrid composites*, Chem. Mater.,6 , pp.573-5 (1994)
3. P.B Messersmith, E.P. Giannelis; *Synthesis and barrier properties of poly(epsilon-caprolactone)-layered silicate nanocomposites*, J. Polym. Sci Part A: Polym. Chem, 33, pp.1047-57 (1995)
4. J. Zhu, C.A. Wilkie; *Thermal and fire studies on polystyrene-clay nanocomposites*, Polym Int., 49, 1158-63 (2000)
5. Alexandre, M.; Dubois, P.; *Polymer-layered silicate nanocomposites: preparation, properties and uses of a new class of materials*, Materials Science and Eng., 28, pp.1-63 (2000)
6. Vaia, R. A.; Giannelis, E. P.; *Polymer Melt Intercalation in Organically-Modified Layered Silicates: Model predictions and experiment*; Macromolecules, 30, pp.8000-8009 (1997)
7. Kwak, M., Lee, M., Lee, B-K, *Effects of processing parameters on the preparation of high density polyethylene/layered silicate nanocomposites*, SPE-ANTEC Tech. Papers, pp.2245-2249 (2002)
8. Dennis, H.R., Hunter, D.L, Chang, D., Kim, S., White, J.L., Cho, J.W., Paul, D.R, *Nanocomposites: the importance of processing*, SPE-ANTEC Tech. Papers, pp.428-433 (2000)
9. Lew, C.Y, Murphy, W.R., McNally, G.M., *Preparation and properties of polyolefin-clay nanocomposites*, Pol. Eng. Sci., 44, 6, pp.1027-1035

10. Arroyo, M.; Suárez, R.V, Herrero, B,; López-Machado, M.A.; *Optimisation of nanocomposites based on polypropylene/polyethylene blends and organo-bentonite*, J. Mater. Chem., 13, pp2915-2921 (2003)
11. Okamoto, M.; Nam, P. H.; Maiti, P., Kotaka, Hasegawa, N., Usuki, Arimitsu; *A house pf cards structure in polypropylene/clay nanocomposites under elongational flow*, Nano Letters, 1, 6, pp.295-298 (2001)
12. Nam, P.H.; Maiti, P.; Okamoto, M.; Kotaka, T.; *Foam processing of polypropylene/clay nanocomposites*, Pol. Eng. Sci, 42, 9, pp.1907-18 (2002)
13. Zeng, C.; Han, X.; James Lee, L.; Koelling, K.W.; Tomasko, D.L.; *Structure of nanocomposite foams*; SPE-ANTEC Tech. Papers, pp.1504-08 (2002)
14. Smoker, D.G.; *A study of the extensional flow behaviour of low density polyethylenes*, PhD thesis, Loughborough University of Technology, Loughborough, UK, (1984)
15. Cogswell, F.N.; *Measuring the extensional viscosity of polymer melts*, Transactions of the Society of Rheology; 16, No.3,1972, p.383-403 (1972)
16. Munstedt, H.; *New universal extensional rheometer for polymer melts. Measurements on a polystyrene sample*, J. Rheol, 23, pp.421-36 (1979)
17. Robert L., Demay, Y. Vergnes, B.; *Stick-slip flow of high-density polyethylene in a transparent slit die investigated by laser Doppler velocimetry*, Rheologica Acta 43:pp89-98 (2004)
18. Larrazabal, H. J.; Hrymak, A.N.; *Flow instabilities of linear PE in capillary dies*; International Polymer Processing 17, 1, pp44-8 (2002)
19. Mooney, M. Transactions of The Society of Rheology, 2, pp.210 (1931)
20. Scott Parent, J.; *Time and shear dependent rheology of maleated polyethylene and its nanocomposites*, Polymer, 45, pp.6595-6600 (2004)
21. Solomon , M. J., Almusallam , A. S., Seefeldt , K. F., Somwangthanaroj ,A., Varadan, P., *Rheology of Polypropylene/Clay Hybrid Materials*, Macromolecules, 34, 1864-1872 (2001)

Appendix II – Capillary Die Design

The standard L/D 16x1 mm flat entry die available is suitable to cover shear rates between 100-5000 s^{-1} using the recommended piston speeds by Malvern Instruments. However for lower shear rates the piston speed falls well below that recommendation which is about 10mm/min.
Therefore a new die had to be designed to perform the rheological characterization of the polymers up to $1s^{-1}$. The objective of this design was to:

- maximize the number of experimental points determined for each experiment,
- minimize the time of the experiment,
- achieve the lowest shear rates at a piston speed of 5mm/min
- achieve at least a minimum shear rate of $400s^{-1}$ with minimal material consumption
- have a total length smaller than 32 mm (barrel limit)

	Die Diameter	Die Radius	Min Shear Rate	Max Shear Rate	Length (mm) L/D 16
	0.7	0.35	437	7872	11
	0.8	0.40	293	5273	13
Velocity min	0.9	0.45	206	3704	14
5 mm/min	1.0	0.50	150	2700	16
Velocity max	1.1	0.55	113	2029	18
90 mm/min	1.2	0.60	87	1563	19
	1.5	0.75	44	800	24

Appendix III – RER Data Treatment

Calculation of the stress – strain curve from the force displacement raw data using the equations below.

$$\dot{\varepsilon} = \frac{Lt}{L - L_0}$$

$$\sigma_E = \frac{F_t L}{A_0 L_0}$$

L – sample length
L_0 – initial sample length
A_0 – initial cross-sectional area
F_t – measured force

Original sample length: 18mm
Initial cross-sectional area: 18 mm x 2 x (thickness) mm

For PR-HD4, with a thickness of 1.75mm. Test at constant velocity 50mm/s.

Displacement (mm)	Raw Signal (N)	Net signal (N)	time (s)	Area (mm2)	Stress (kPa)	Hencky Strain
0.025	0.436	0.054	0.003	24.466	2.19	0.00
0.029	0.439	0.051	0.006	24.461	2.07	0.00
0.054	0.443	0.047	0.009	24.426	1.92	0.00
0.127	0.466	0.024	0.012	24.328	0.97	0.01
0.237	0.512	0.022	0.015	24.181	0.91	0.01
0.380	0.568	0.078	0.018	23.993	3.26	0.02
0.538	0.630	0.140	0.021	23.789	5.88	0.03
0.699	0.695	0.205	0.024	23.584	8.67	0.04
0.853	0.775	0.285	0.027	23.392	12.16	0.05
1.014	0.858	0.368	0.03	23.194	15.87	0.05
1.164	0.956	0.466	0.033	23.012	20.24	0.06
1.314	1.033	0.543	0.036	22.833	23.80	0.07
1.457	1.104	0.614	0.039	22.666	27.07	0.08
1.607	1.182	0.692	0.042	22.492	30.75	0.09
1.753	1.251	0.761	0.045	22.325	34.07	0.09
1.900	1.308	0.818	0.048	22.161	36.91	0.10
2.043	1.346	0.856	0.051	22.003	38.90	0.11
2.193	1.379	0.889	0.054	21.839	40.72	0.11
2.339	1.414	0.924	0.057	21.682	42.60	0.12
2.493	1.434	0.944	0.06	21.519	43.85	0.13

Appendix IV – Raw Material Datasheets

Product Data Sheet

LANXESS

Buna® EP T 2070

Product Description Ethylene-propylene-rubber (EPM), low molecular weight, curable only by peroxide

Supply Form Bales

Raw Material Properties

Property	Nominal Value	Unit	Test Method
Mooney Viscosity ML (1+8) 100°C	35 ± 5	MU	ISO 289/ASTM D 1646
Ethylene content	68 ± 3	wt %	ASTM D 3900
Volatile matter	≤ 0.75	wt %	ASTM D 5668

Other Product Features

Property	Typical Value
Specific gravity	0.86 g/cm³
Total Ash	<= 0.5 wt % ASTM D 5667
Stabilizer	Non-staining
Packaging	34 kg bales in clear PE film (dispersable, Vicat A softening point max. 104 °C); pallets of 24 bales (816 kg)
Shelf-life	24 month from date of production at temperatures not exceeding 30 °C in dry conditions; exposure to light has to be avoided.
Product Safety	Relevant safety data and references as well as the possibly necessary warning labels are to be found in the safety data sheet no.823949.

These raw material properties are typical and, unless specifically indicated otherwise, are not to be considered as delivery specification.

Issue number: LX 02 / Date of issue: March 18, 2005 / Previous issue from 06.12.2004

basell
Polyolefins

Adflex Q 100 F

Advanced Polyolefin

Product Description

Adflex Q 100 F is a thermoplastic polyolefin, which has been developed for the extrusion of blown film. It is also suitable for sheet extrusion.

Q 100 F features very high softness and very low modulus. It does not contain any slip or anti-blocking agents. *Adflex* Q 100 F is ideal for the production of soft hygienic film and heavy duty film, as well as for the modification of LDPE or LLDPE to increase mechanical characteristics, puncture resistance, and to allow further downgauging. It can be easily processed on conventional LDPE or LLDPE blown film lines.

For Regulatory information, please refer to this product`s RAPIDS, which can be found on www.basell.com.

Product Characteristics

Status	Commercial: Active
Test Method used	ISO
Availability	Europe, North America, Asia-Pacific, Australia/NZ, Africa-Middle East, Latin America
Processing Method	Extrusion, Extrusion, Sheet, Film, Blown
Features	Flexibility, Good, Soft
Typical Customer Applications	Blown Film

Typical Properties	Method	Value	Unit
Physical			
Density	ISO 1183	0.89	g/cm³
Melt flow rate (MFR) (230°C/2.16Kg)	ISO 1133	0.6	g/10 min
Mechanical			
Tensile Stress at Yield	ISO 527-1, -2	5	MPa
Tensile Strain at Break	ISO 527-1, -2	400	%
Flexural modulus	ISO 178	80	MPa
Hardness			
Shore hardness (Shore D)	ISO 868	30	
Thermal			
Vicat softening temperature (A50 (50°C/h 10N))	ISO 306	55	°C

Notes

Typical properties; not to be construed as specifications.

Additional Properties

Elongation at Break, ISO 527 >400%.
Brittle/Ductile Transition, MTM 17238 = -55°C.

RIGIDEX® HD6007XA

INEOS Polyolefins (formerly Innovene) - *Polyethylene, High Density (MMW)*

General Information

Product Description

Rigidex HD6007XA is a medium molecular weight homopolymer grade supplied in pellet form for use in a wide range of blow moulding and extrusion applications.

General

Material Status	• Commercial: Active	
Availability	• Europe	
Test Standards Available	• ASTM • ISO	
Features	• Density, High • Homopolymer • Molecular Wt., Medium	• Processability, Good • Rigidity, High • Surface Finish, Good
Uses	• Containers, Thin-Walled	
Forms	• Pellets	
Processing Method	• Blow Molding • Extrusion	

ASTM and ISO Properties [1]

Physical	Nominal Value	Unit	Test Method
Melt Mass-Flow Rate (MFR) (190°C/2.16 kg)	0.6	g/10 min	ISO 1133
Enviro. Stress Crack Res (Condition A, BTT)	20.0	hr	ASTM D1693
Mechanical	**Nominal Value**	**Unit**	**Test Method**
Tensile Stress at Yield [2]	30.5	MPa	ISO 527-1, -2
Tensile Strain at Break [2]	1000	%	ISO 527-1, -2
Flexural Modulus	1700	MPa	ISO 178
Impact	**Nominal Value**	**Unit**	**Test Method**
Charpy Unnotched Impact Strength	8.00	kJ/m²	ISO 179

Additional Properties

Density, ISO 1872/1-1993: 962 kg/m³
Elongation at Break, ISO 527-1976, Type2, Speed D: >300%
Bottle Stress Crack Resistance, BP Chemicals' Method, 60°C: 1 hours
BTT Stress Crack Resistance, ASTM D1693-97a, F50 at 50°C: 20 hours

Notes

1 Typical properties: these are not to be construed as specifications.

2 Type 2

Appendix V – Flow 2000 Parameters

		PE-HD1	PR-HD4	PR-LD3	PR-PP1
Melt thermal properties	ρ_m (g/cm^3)	0.77	0.77	0.77	0.76
	Cp (J/kg/°C)	2500	2500	2300	2100
	k (W/m/°C)	0.18	0.18	0.24	0.15
Solid thermal properties	ρ_s (g/cm^3)	0.650	0.591	0.469	0.540
	Cp (J/kg/°C)	2500	2500	2300	1700
	k (W/m/°C)	0.4	0.4	0.28	0.22
	T_m (°C)	135.7	135.2	125.9	151.6
	T_c (°C)	116.9	122.6	112.5	117.8
	ΔH_f (J/kg)	224000	190000	148400	124200
Carreau model	η_0 (Pa s)	13226	10065	15940	6445
	t_1 (s)	0.95	0.55	0.97	0.373
	n	0.47	0.53	0.43	0.42

Appendix VI – HMS Daploy FTIR

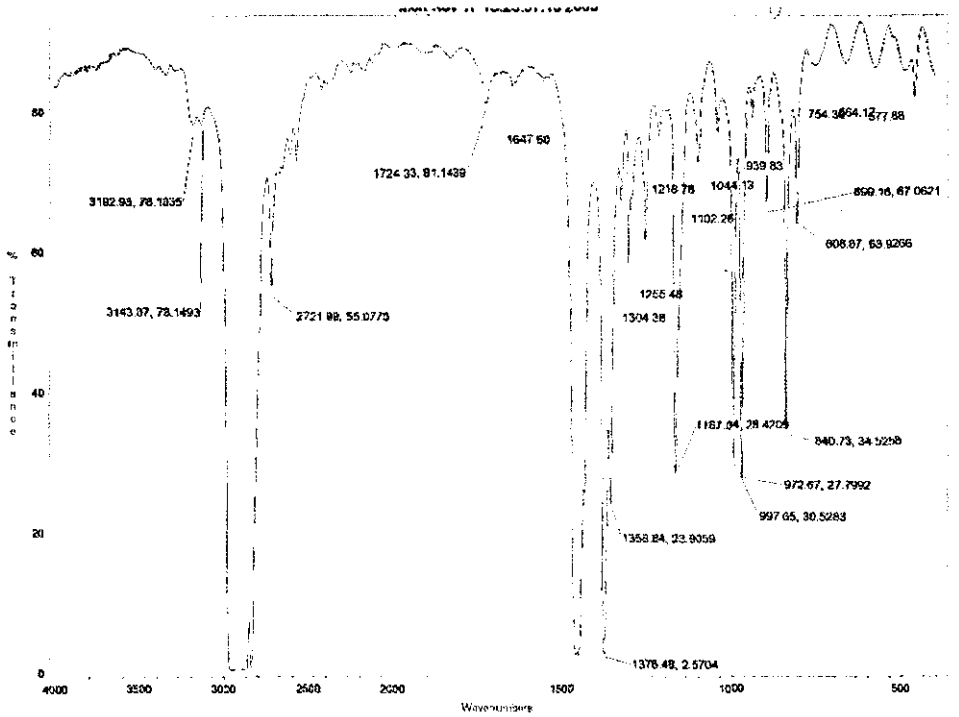

Fig – FTIR PO-PP1.

Appendix VXIII – Central Composite Design - PR-HD4

Central composite design used for the optimisation of PR-HD4 nanocomposite preparation.

TIME (min)	SPEED (rpm)	Compatibiliser (%)	CLAY ratio	MFI (g/10min)	STRESS (kPa)	ELONG (Hencky)	TOUGH (Pa)
1.5	50	5	1				
3.63	50	2	0.4	1.04	206	1.97	267
1.5	50	3	0.6	0.9	163	1.63	199
1.5	30	3	0.6	1.24	124	1.39	
1.5	50	1	0.2	0.9	154	1.65	187
5.75	30	5	1	1.05			272
10	50	1	0.2	1.28	172.6	1.83	273
10	30	3	0.6		140.2	1.63	
5.75	50	1	0.2	1.17	182.7	1.86	273
10	50	3	0.6	1.23	141.5	1.45	175
1.5	30	1	0.2	1.31	158.7	1.83	202
5.75	30	1	0.2				
5.75	50	0	0	1.38			
10	30	3	0.6		130	1.48	
5.75	50	5	1	1.05	149.5	1.7	253
10	50	5	1	1.14	100	1.17	112
10	30	1	0.2	1.35	109.9	1.55	164
3.63	30	2	0.4	0.99			272
5.75	30	3	0.6		190	1.91	
10	30	5	1	1.22	134.9	1.55	173
1.5	30	3	0.6	1.24	124	1.39	198
10	30	5	1	1.22	173.7	1.73	170
10	50	5	1	1.13	155.7	1.61	218
5.75	50	3	0.6	0.98	142.4	1.59	218
10	50	1	0.2	1.28	172.6	1.83	272
10	30	1	0.2	1.35	133	1.57	201
6	100	5	1	1.13	156.7	1.64	234
6	100	5	0.2	1.09	150.8	1.09	358
6	150	5	1	1.3	188	1.88	223
6	150	5	0.2	1.85	103	2.6	193
6	50	5	0	1.384			
6	100	5	0	1.483		2.1	134
6	150	5	0	2.218		3.1	220

Appendix XIII – Central Composite Design - PR-HD4

Central composite design used for the optimisation of PR-HD4 nanocomposite preparation.

TIME (min)	SPEED (rpm)	Compatibiliser (%)	CLAY ratio	MFI (g/10min)	STRESS (kPa)	ELONG (Hencky)	TOUGH (Pa)
1.5	50	5	1				
3.63	50	2	0.4	1.04	206	1.97	267
1.5	50	3	0.6	0.9	163	1.63	199
1.5	30	3	0.6	1.24	124	1.39	
1.5	50	1	0.2	0.9	154	1.65	187
5.75	30	5	1	1.05			272
10	50	1	0.2	1.28	172.6	1.83	273
10	30	3	0.6		140.2	1.63	
5.75	50	1	0.2	1.17	182.7	1.86	273
10	50	3	0.6	1.23	141.5	1.45	175
1.5	30	1	0.2	1.31	158.7	1.83	202
5.75	30	1	0.2				
5.75	50	0	0	1.38			
10	30	3	0.6		130	1.48	
5.75	50	5	1	1.05	149.5	1.7	253
10	50	5	1	1.14	100	1.17	112
10	30	1	0.2	1.35	109.9	1.55	164
3.63	30	2	0.4	0.99			272
5.75	30	3	0.6		190	1.91	
10	30	5	1	1.22	134.9	1.55	173
1.5	30	3	0.6	1.24	124	1.39	198
10	30	5	1	1.22	173.7	1.73	170
10	50	5	1	1.13	155.7	1.61	218
5.75	50	3	0.6	0.98	142.4	1.59	218
10	50	1	0.2	1.28	172.6	1.83	272
10	30	1	0.2	1.35	133	1.57	201
6	100	5	1	1.13	156.7	1.64	234
6	100	5	0.2	1.09	150.8	1.09	358
6	150	5	1	1.3	188	1.88	223
6	150	5	0.2	1.85	103	2.6	193
6	50	5	0	1.384			
6	100	5	0	1.483		2.1	134
6	150	5	0	2.218		3.1	220